



UNIVERSITÀ DEGLI STUDI DI BERGAMO

SCHOOL OF ENGINEERING

DEPARTMENT OF ENGINEERING AND APPLIED SCIENCES DOCTORAL

PROGRAMME IN ENGINEERING AND APPLIED SCIENCES

---

# **Structural issues in exoskeleton solutions for the integrated renovation of existing buildings**

Supervisor:

**Prof. Alessandra Marini**

Co-supervisor:

**Simone Labò, Ph.D.**

Doctoral dissertation of:

**Stefano Cademartori**

2022 – Cycle XXXV

UNIVERSITY OF BERGAMO

PhD Programme in *Engineering and Applied Sciences*

XXXV cycle

ICAR/09

UNIVERSITÀ DEGLI STUDI DI BERGAMO

Dottorato in *Ingegneria e Scienze Applicate*

XXXV ciclo

ICAR/09

Prof. Alessandra Marini (Coordinator)

*Author: Stefano Cademartori*

A handwritten signature in black ink, appearing to read 'Stefano Cademartori'.

*Title: Structural issues in exoskeleton solutions for the integrated renovation of existing buildings*

## **Abstract**

The renovation of the building stock has become a priority in recent decades. The deep renovation has been acknowledged as a successful and necessary strategy to foster a sustainable environment in response to emerging challenges and social needs. In Italy, approximately 80% of the existing building stock was constructed prior to 1980 and has exhausted its design service life, necessitating urgent seismic retrofitting, energy refurbishment, and architectural renovation.

The current building conditions and the need to achieve carbon neutrality in Europe by 2050 have increased attention on the construction industry, resulting in the development of novel sustainable retrofit solutions. The achievement of the ambitious goals established at the EU level will heavily rely on the implementation of holistic, high-performance interventions, to address the numerous and multifaceted emerging needs.

In response to these needs, this study examines the potential benefits and the limitations of adopting innovative exoskeleton solutions, conceived by applying the leading principles of structural life cycle engineering and designed using a multi-criteria performance-based approach. The solutions investigated in this work consist of prefabricated, dry-assembled, modular, and flexible timber shell exoskeleton, entirely assembled outside the building without any disruption of the building use, providing high performances in the operational phase, and ensuring demountability of the system at the end of its life, as well as the reuse and recycle of its components. Through the application of additional engineering layers, the analyzed structural exoskeletons can be easily integrated into holistic retrofit actions, that contextually target energy efficiency and functional and architectural restyling.

Inspired by the dissipative and adaptive systems recently developed for new buildings, this study examines the potential offered by extending these principles to the design of retrofit of an existing constructions, particularly to the design of innovative exoskeletons that modify their structural behaviour depending on the magnitude of the seismic event and that concentrate the induced damage within energy dissipative devices, developed and tested during the research activity, while preserving the structural integrity of other elements. The execution of two pilot interventions on real buildings, entailing their holistic and integrated renovation through the application of engineered exoskeletons, enabled investigating the feasibility, as well as the major drawbacks of the proposed solutions, resulting in their partial re-engineering with a view to simplify their implementation and foster their applicability.

## *Table of contents*

|             |   |           |
|-------------|---|-----------|
| <b>I.</b>   | <b><i>Foreword</i></b> .....  | <b>10</b> |
| <b>II.</b>  | <b><i>Introduction and Research Significance</i></b> .....                                    | <b>16</b> |
| 2.1.        | <i>Problem framing and Research Motivation</i> .....  | <b>16</b> |
| 2.2.        | <i>Current practice in the renovation of the existing building</i> .....                      | <b>21</b> |
| 2.3.        | <i>Holistic and Sustainable approaches for the renovation of the existing buildings</i> ..... | <b>25</b> |
| 2.4.        | <i>State of the art on the shell exoskeleton solutions</i> .....                              | <b>32</b> |
| 2.4.1.      | Examples of <i>cast-in-place</i> external retrofits.....                                      | 36        |
| 2.4.2.      | Examples of <i>prefabricated</i> external retrofits.....                                      | 39        |
| <b>III.</b> | <b><i>Assessment of existing buildings</i></b> .....  | <b>48</b> |
| 3.1.        | <i>Introduction</i> .....   | <b>48</b> |
| 3.2.        | <i>European buildings</i> .....   | <b>50</b> |
| 3.2.1.      | Location & seismic vulnerability of the European building stock                               | 50        |
| 3.2.2.      | Age .....   | 53        |
| 3.2.3.      | Building types and construction technologies .....  | 55        |
| 3.3.        | <i>Introduction to the main seismic vulnerabilities</i> .....                                 | <b>60</b> |
| 3.3.1.      | Reinforced concrete infilled buildings .....  | 60        |
| 3.3.2.      | Masonry buildings.....  | 66        |
| 3.3.3.      | Prefabricated RC industrial buildings .....   | 68        |
| 3.3.4.      | Lack of horizontal diaphragms .....   | 71        |
| 3.4.        | <i>Concluding remarks</i> .....   | <b>74</b> |

|            |  |            |
|------------|--|------------|
| <b>IV.</b> | <b><i>Structural retrofit strategies and solutions</i></b> .....                                     | <b>76</b>  |
| 4.1.       | <i>Introduction</i> .....  | 76         |
| 4.2.       | <i>A brief overview of traditional seismic retrofitting interventions</i> .....                      | 77         |
| 4.2.1.     | Examples of solutions for reinforced concrete buildings  | 77         |
| 4.2.2.     | Examples of solutions for masonry buildings .....  | 88         |
| 4.2.3.     | Examples of solutions for precast RC Buildings .....   | 96         |
| 4.3.       | <i>New trends in seismic retrofit and introduction to integrated interventions</i> .....             | <b>101</b> |
| 4.4.       | <i>Examples of integrated and holistic retrofit interventions</i>                                    | <b>105</b> |
| 4.4.1.     | <i>Integrated energy and architectural solutions</i> .....   | 105        |
| 4.4.2.     | <i>Integrated structural, energy, and architectural solutions</i>                                    | 111        |
| 4.5.       | <i>Research Needs</i> .....  | <b>115</b> |
| <b>V.</b>  | <b><i>Novel structural performances and design approaches</i></b> ..                                 | <b>116</b> |
| 5.1.       | <i>Introduction</i> .....  | <b>116</b> |
| 5.2.       | <i>Extension of the Life Cycle Structural Engineering concept</i>                                    | <b>117</b> |
| 5.3.       | <i>Multi-Criteria Performance-Based Approach and novel structural targets</i> .....                  | <b>119</b> |
| 5.4.       | <i>Introduction to novel design frameworks for sustainable retrofits</i>                             | <b>125</b> |
| 5.5.       | <i>Qualitative evaluation and pre-screening of the main structural retrofitting strategies</i> ..... | <b>130</b> |
| 5.6.       | <i>Research Needs</i> .....  | <b>134</b> |

|             |  |            |
|-------------|--|------------|
| <b>VI.</b>  | <b><i>Adaptive exoskeletons</i></b> .....  | <b>135</b> |
| 6.1.        | <i>Brief overview of exoskeleton</i> .....   | <b>135</b> |
| 6.1.1.      | Dissipative systems .....  | 140        |
| 6.1.2.      | High-strength elastic systems .....  | 142        |
| 6.2.        | <i>Adaptive exoskeletons</i> .....   | <b>144</b> |
| 6.2.1.      | Evolving structural behaviour .....  | 146        |
| 6.2.2.      | Response curve of the retrofitted system.....  | 150        |
| 6.2.3.      | Qualitative dynamic behaviour .....  | 152        |
| 6.3.        | <i>Conceptual design for adaptive exoskeletons</i> .....   | <b>160</b> |
| 6.4.        | <i>Structural design procedure</i> .....   | <b>166</b> |
| 6.5.        | <i>Numerical analysis of the dynamic behaviour</i> .....   | <b>179</b> |
| 6.5.1.      | Reference building .....   | 179        |
| 6.5.2.      | Structural design of the double-skin adaptive exoskeletons<br>181                                    |            |
| 6.5.3.      | Proportioning of the adaptive exoskeleton components for<br>varying alternative configurations ..... | 182        |
| 6.5.4.      | Numerical models .....   | 202        |
| 6.5.5.      | Ground motion .....  | 211        |
| 6.5.6.      | Analysis of results .....  | 215        |
| 6.6.        | <i>Concluding remarks</i> .....  | <b>222</b> |
| <br>        |  |            |
| <b>VII.</b> | <b><i>Development of the AdESA fuse</i></b> .....  | <b>225</b> |
| 7.1.        | <i>Introduction</i> .....  | <b>225</b> |
| 7.2.        | <i>Brief overview on Displacement-proportional Passive<br/>Energy Dissipation Devices</i> .....      | <b>226</b> |

|              |   |            |
|--------------|---|------------|
| 7.3.         | <i>Analysis of PEEDs characteristics from the Life Cycle Structural Engineering perspective</i> ..... | 239        |
| 7.4.         | <i>AdESA fuse</i> .....   | 240        |
| 7.4.1.       | <i>Description of the different configurations</i> .....  | 245        |
| 7.4.2.       | <i>Experimental test and results</i> .....  | 251        |
| 7.5.         | <i>Concluding Remarks &amp; Further Development</i> .....   | 262        |
| <br>         |   |            |
| <b>VIII.</b> | <b><i>Retrofit of an existing precast RC building with a hybrid-CLT exoskeleton</i></b> .....         | <b>263</b> |
| 8.1.         | <i>Introduction</i> .....   | 263        |
| 8.2.         | <i>Building description</i> .....   | 264        |
| 8.3.         | <i>Main deficiencies of the building in the as-is condition</i> ....                                  | 269        |
| 8.4.         | <i>Brief overview of the holistic intervention</i> .....  | 277        |
| 8.5.         | <i>Conceptual design of the retrofitting exoskeleton</i> .....  | 279        |
| 8.6.         | <i>Description of the structural intervention</i> .....   | 281        |
| 8.7.         | <i>Structural performance of the retrofitted system</i> .....   | 289        |
| 8.8.         | <i>Lesson learned &amp; partial re-engineering of the retrofit</i> ....                               | 298        |
| <br>         |   |            |
| <b>IX.</b>   | <b><i>Application of an adaptive exoskeleton to a post-World War II masonry building</i></b> .....    | <b>301</b> |
| 9.1.         | <i>Introduction</i> .....   | 301        |
| 9.2.         | <i>Building description</i> .....   | 302        |
| 9.3.         | <i>Assessment of the building in the as-is condition</i> .....  | 305        |
| 9.4.         | <i>Brief overview of the holistic intervention</i> .....  | 310        |
| 9.5.         | <i>Structural intervention</i> .....  | 312        |
| 9.6.         | <i>Critical analysis of the structural intervention</i> .....   | 317        |



|  |     |
|--|-----|
| 9.7. <i>Lessons learned and research needs</i> ..... | 328 |
| X. <i>Concluding remarks</i> .....                   | 331 |
| <i>References</i> .....                              | 335 |
| <i>Appendix A</i> .....                              | 367 |
| <i>Appendix B</i> .....                              | 374 |
| <i>Appendix C</i> .....                              | 400 |
| <i>Appendix D</i> .....                              | 414 |
| <i>Appendix E</i> .....                              | 426 |
| <i>Acknowledgements</i> .....                        | 434 |

# I. Foreword

The poor energy performance of the larger portion of the European building stock and the associated high environmental and economic impacts have been widely acknowledged in recent years, and major European roadmaps are attempting to reckon with the problem by enforcing ambitious sustainable development goals to be achieved in the next decade. Furthermore, more than half of the Italian building stock has exhausted its structural service life and is structurally deficient. Recent Italian seismic events have drawn attention toward the structural obsolescence of our construction heritage, which may have severe economic, environmental, and social consequences.

In response to this emergency, a systematic holistic renovation of the existing building stock is urgently required. Regardless of such a scenario, however, the traditional approach to renovation is to address the deficiencies of each building individually, often from an energy and architectural standpoint only, resulting in interventions that are ineffective and unsustainable when applied to buildings that are vulnerable to any type of natural hazard. In seismic-prone zones, thus in Mediterranean European regions and numerous other nations, the selection of energy-only or architectural interventions on structurally vulnerable buildings results in high-risk economic investments and an unsafe environment in terms of people's safety. Alternatively, only structural retrofit actions are undertaken, disregarding sustainability issues or even worsening the environmental impact of the building.

Demolition and reconstruction practices should be only carried out when mandatory and should not be extensively practised given their substantial environmental impacts associated with

waste production and raw material depletion. Moreover, from a social perspective, this option would necessitate the relocation of the inhabitants, as well as the downtime of the building use, for the duration of the operation, resulting in large economic and social costs.

More recently, isolated, and episodic efforts have been made to solve the problem of renovating the building stock holistically, acknowledging the integrated deep renovation as the only viable solution toward a truly sustainable built environment, in which ecoefficiency, as well as safety and resilience, are simultaneously pursued, extending the traditional concept of sustainability. As far as environmental sustainability is concerned, retrofit solutions may be conceived by addressing the principles of Life Cycle Thinking (LCT), which are aimed at minimizing the impacts and costs of the intervention and of the retrofitted building along its whole life cycle. In this perspective, the optimal solutions would consist of prefabricated, dry-assembled, modular, entirely assembled outside the building without any disruption of the building use, providing high performances in the operational phase, and ensuring demountability of the system at the end of its life, as well as the reuse and recycle of its components.

In such a scenario, this study investigates the potential benefits and applicability issues of exoskeleton retrofit solutions that are designed to be easily integrated into broader, holistic interventions that address energy, functional and architectural renovation needs contextually. To sustainably achieve the goals and facilitate their diffusion, these solutions must be designed according to the most advanced and stringent design standards and methodologies and according with LCT principles.

In this thesis, divided into ten chapters, starting with the identification of building needs and deficiencies, exoskeleton solutions are analysed in detail from both theoretical and applicative perspectives. The following is a synopsis of each chapter's content.

In the second chapter, the research significance is discussed. The urgent need to increase the built environment's sustainability necessitates coordinated research and action with the common goal of defining the multiple performances to be pursued and the design principles to be adopted to ensure the achievement of a broader sustainability concept, that combines eco-efficiency, safety, and life-cycle resilience. The widespread adoption of effective retrofit solutions necessitates the application of new conceptual and design frameworks that emphasise the use of long-term sustainable intervention techniques. The identification of holistic solutions suitable for the building under consideration requires first the evaluation of the potentials and limitations of each retrofit action in accordance with the predefined principles and objectives, followed by a thorough analysis of their implementation criticalities and a study of their potential re-engineering. This work aims to contribute to the exoskeleton shell technique, a retrofit solution that can be effectively integrated into a holistic intervention.

In the third chapter, a brief overview of the consistency of the European building stock considering their age, location, type and construction technology is presented. In the same chapter, the principal seismic vulnerabilities of the most common structural typology in the Italian scenario are discussed.

The first section of the fourth chapter provides a brief overview of traditional seismic retrofits for the strengthening of different

structural typologies, differentiating between local and global solutions, whilst in the second section new seismic retrofit trends are described and selected examples of integrated and holistic interventions are presented, focusing on their major potential and limitations.

The fifth chapter outlines the structural performance objectives for new and retrofitted structural systems. Focusing on retrofit design, the first section of this chapter analyses the potential associated with adopting a performance-based multi-criteria design approach capable of achieving high structural performance, while the second section introduces several innovative frameworks for the selection and design of a retrofit solution capable of accomplishing the desired performances.

The sixth chapter focuses on the study of exoskeleton solutions. In the first section of this chapter, the main advantages and drawbacks of both dissipative and elastic high-strength shear-wall and shell exoskeletons are examined. In the central section, novel adaptive exoskeletons are presented, that modify their structural behaviour in response to seismic intensity, dissipating a portion of the introduced seismic energy re-centring after an earthquake. Adaptive exoskeleton conceptual design and proportioning are also presented. The concluding section presents the results of a numerical study investigating the influence of several parameters and design choices on the dynamic response of adaptive exoskeletons and their ability to reduce residual displacement.

In the seventh chapter, a survey of passive displacement-dependent energy dissipation devices (PEDDs) is presented. PEDDs are the primary structural components of both adaptive exoskeletons. The first section of the chapter provides a brief overview of these devices, focusing on the definition of their

optimal characteristics from the life cycle structural engineering perspective, while the second section describes the characteristics of the *AdESA fuses*, the PEDDs developed during the research programme and applied to two real case studies.

In the final chapters of the thesis (VIII and IX), two real integrated retrofit interventions are illustrated, in which dissipative and adaptive exoskeletons were conceived (eighth and ninth chapters, respectively). The design of the retrofit was carried out with reference to the LCT-based framework developed by the research group, by considering the LCT-based performance objectives and related design targets and by addressing the design approach and procedures illustrated in this thesis. PEEDs and construction detailing as those developed in Chapter VII were implemented. The ex-post critical analysis of all the design stages, as well as of the construction site management and process, enabled identifying some critical issues that resulted in the partial re-engineering of some retrofit components, and in the identification of major research needs with a view to increasing applicability and feasibility of the proposed retrofit solution.

In particular, in the eighth chapter, the integrated renovation of an existing precast gym hall, entirely carried out outside the building, is presented. A dissipative hybrid CLT-steel shell exoskeleton, with horizontal arrangement of the CLT panels and passive displacement-dependent energy dissipation devices, is conceived for seismic strengthening, whilst further coating layers are applied to increase energy efficiency and fire protection and for the architectural finishes. The author, who is a member of the research team responsible for the project's design, has contributed in various areas. These include the conception of the structural system, the development of its

nonlinear numerical model, the experimental tests on novel dissipative components, and provision for assistance during the execution phase.

In Chapter IX the integrated renovation of an existing masonry residential building carried out from outside is presented. An adaptive CLT shell exoskeleton, with a vertical arrangement of the CLT panels and passive displacement-dependent energy dissipation devices, is conceived for the seismic strengthening, whilst further coating layers are applied to increase energy efficiency, and for the finishes. For this case study, the author collaborated on the analysis of the numerical model of the structural system while simultaneously exploring alternative schemes.

contains illustrative schemes of the contents of each chapter.

## **II. Introduction and Research Significance**

### **2.1. Problem framing and Research Motivation**

Recently, the London-based Institution of Structural Engineers and other built-environment organizations and professional bodies declared a climate and biodiversity emergency [1].

The construction sector is of critical importance to the European Union since it generates over 9% of the EU's gross domestic product and 18 million direct employments [2]. However, it is also one of the most environmentally damaging industries, accounting for around 50% of the depletion of raw materials, 35% of waste production, 35% of energy consumption, and 36% of greenhouse (GHG) emissions [3].

In the last several decades, many attempts to reduce the construction industry's environmental impacts have focused on reducing energy consumption and CO<sub>2</sub> emissions during building usage; according to a BPIE analysis [4], to achieve the aim of a climate-neutral Europe by 2050, building emissions must be reduced by 60% by 2030. This goal can only be met if the average rate of deep renovation (i.e., a renovation that cuts GHG emissions by 60%) increases from 1% to 4.4% in the decade between 2020 and 2030. Moreover, even if this ambitious goal were to be achieved, it would address just one of the major effects of the construction industry, since buildings would continue to create unsustainable impacts at all other phases of their life cycle, from material extraction to their end of life. New energy-efficient buildings have a larger embodied energy associated with their manufacturing and end-of-life



stages, which may impede the use-phase advantages [5]. Moreover, when just the energy restoration of a facility is performed without addressing its structural vulnerabilities, losses may occur in the event of natural disasters such as earthquakes, floods, etc., resulting in substantial environmental, economic, and social repercussions [6]. Many structures in Europe and especially in Italy are old and, in addition to being energy inefficient, vulnerable to seismic hazards. More than 40% of the Italian 11 million buildings are in an extremely poor state of preservation, according to a report on the country's building preservation [7]. In addition, more than 6 million structures, and 24 million people, are in regions with a high seismic risk where 70% of buildings were constructed prior to the implementation of seismic standards and 55% have already surpassed their 40-year service life.



Figure II.1 - Typical residential district built after WWII in Italian city peripheries. From [8].

Their seismic vulnerability, besides making them unsafe, implies a significant impact on the environment in terms of waste production and CO<sub>2</sub> emissions [6].

Although this condition is typical of the entire existing building stock, this study concentrates on buildings erected after World War II, a substantial portion of the overall building stock. Reinforced concrete buildings are the most representative of this period, they are generally clustered in degraded suburbs and characterised by anonymous architectural elements and living discomfort. They have substantial environmental implications, particularly in terms of energy use and waste production. In 2009, the average heating consumption reported by the energy assessments of these buildings indicates that are particularly energy-inefficient in comparison to the current regulations; more specifically, the average annual energy consumption of these buildings exceeds 200 kWh/m<sup>2</sup> [3]. Over the years, the only attempts to address the situations of this building stock have consisted of demolition and reconstruction or occasional non-integrated retrofits (Figure II.2), largely aimed at improving energy efficiency only. Both methods are highly inefficient from multiple perspectives. Unless required, the demolition and reconstruction process has a substantial influence on the environment and, even more so, on the functionality of the building. The concept of decoupled renovation, on the other hand, is not practicable because it is not sustainable from an economic, social, and environmental aspect. Additionally, in the worst-case scenario of strong earthquakes, the sole energy upgrading intervention on an unsafe structure may lead to the collapse of the building, with a resultant loss of investment, a significant impact on the environment, and, most importantly, the risk of loss of human life.



Figure II.2 - Traditional uncoupled refurbishment approach: the collapse of the solely-energy retrofit of an industrial warehouse renovated with photovoltaic panels after the Emilia-Romagna earthquake (2012) (left); solely structural retrofit: a typical seismic retrofit of an existent building through dissipative bracings (right). From [9].

In this situation, the reduction of the environmental impacts of the building, over its entire life cycle, must be pursued together with the reduction of its seismic risk; only in this way, true carbon neutrality can be achieved. According to the most recent European roadmaps [10] and directives, this goal could only be realized by contextually adopting three strategies:

- Increasing the renovation rate of the existing building stock.
- Applying integrated retrofit interventions to solve more building deficiencies, thereby fostering an enhanced concept of sustainability that includes eco-efficiency, safety, and resilience [11].
- Adopting a Life Cycle Thinking (LCT) and circular economy approaches.

To renovate in a truly sustainable way, a new definition of sustainable renovation of buildings was recently introduced. The SAFESUST commission has developed the framework for a "Roadmap for the improvement of earthquake resistance and

ecoefficiency of existing buildings and cities.” [11], coining the neologism “SAFESUST” (safety + sustainability), widening the notion of sustainable renovation to include safety and resilience [12], [13]. With this new definition, the role of structural engineering has been emphasized, which should enable the design of retrofit solutions, conceived with a “Life Cycle” perspective, able to reduce all possible life-cycle costs and environmental impacts. According to the UNEP/SETAC definition, "Life Cycle Thinking" is the consideration of the environmental, social, and economic impacts of a product throughout its entire life cycle and value chain, from “cradle to grave” [14]. Regarding the circular economy, it is recommended by EN15978 [12] that four main stages be considered: the product stage, the construction stage, the use stage, as well as the end-of-life stage, plus the potential life of the building components and material beyond the building’s life cycle, in the case of reuse, recovery, and recycling (Figure II.3).

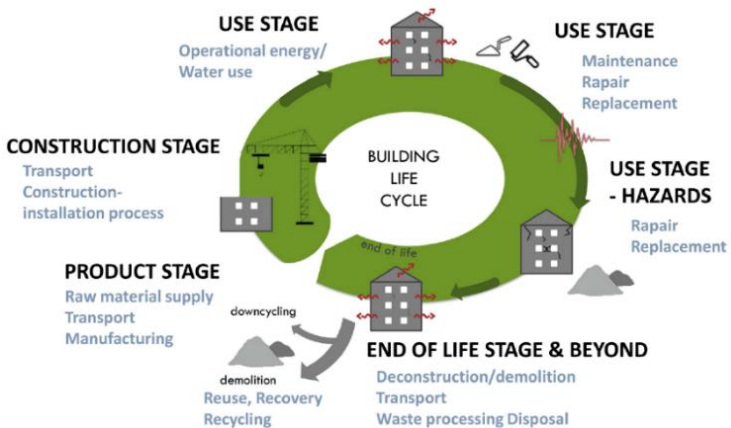


Figure II.3 - Building life cycle stages, according to EN15978 (2011). From [15].

This research aims to investigate the applicability of new seismic reinforcement solutions for the holistic and sustainable renovation of existing buildings, achieved using dry prefabricated retrofit techniques conceived according to the LCT principles and consisting of an externally engineered shell exoskeleton. The study focuses on their applicability to the Italian building stock, characterized by a wide variety of building types and uses. These solutions, when feasible, allow the combined achievement of global seismic reinforcement, energy refurbishment and architectural renovation [15].

## **2.2. Current practice in the renovation of the existing building**

The first step in the renovation design process is identifying the building's performance and weaknesses. In the past, buildings were designed to meet safety standards only for the construction phase, ignoring critical operational phase characteristics and never considering the end-of-life scenario (a) (Figure II.4). As analysed before, a building stock that consumes a lot of energy, emits a lot of CO<sub>2</sub>, and is prone to man-induced and natural disasters, like earthquakes, is the result of this approach. Today, the available solutions for building renovation can be roughly categorized into three main groups [16]:

1. Demolition and reconstruction, which has additional sustainability issues.
2. Uncoupled or partly coupled interventions, in which critical needs related to seismic resistance, resilience, energy refurbishment, indoor comfort and architectural renovation are resolved separately.
3. Holistic and Sustainable renovation, which is a relatively new concept that reckons with and tackles the

complex, multifaceted needs of an existing structure and considers the whole life cycle of the retrofitted building.

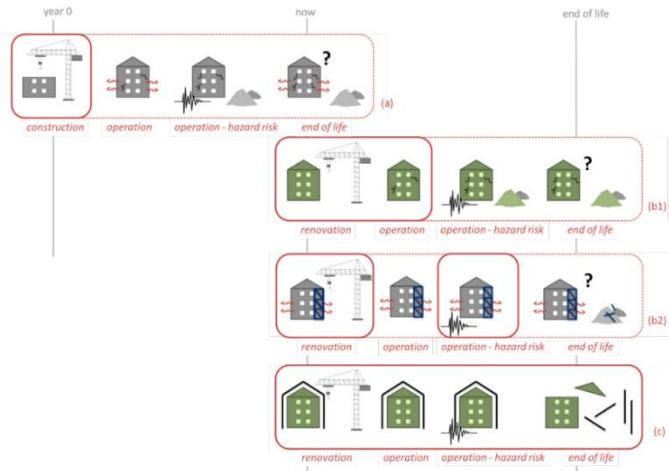


Figure II.4 - Different approaches for the design. (a) Design approach at the time of construction considering the sole construction phase. Current uncoupled design practice considering construction and operation phases; (b1) eco-efficient design of the energy retrofit; (b2) structural retrofit disregarding eco-efficiency; (c) next-generation LC-based design approach for the renovation, considering construction, operation, and end-of-life. From [16].

The adoption of the first approach, which contemplates the systematic demolition and reconstruction of the building stock, would be unsustainable in several aspects. This solution would create additional environmental impacts due to waste production and disposal, and in addition, users would have to be relocated during demolition, with potentially high social costs. This strategy should only be applied when it is mandatory [17] i.e. when seismic damage is so impairing and extended that the

structures cannot be repaired. Sustainability can only be achieved by significantly renovating the existing building stock.

Nowadays, the most common type of intervention is the uncoupled retrofit practice. Typically, the uncoupled interventions are solely energy (b1) (Figure II.4) or solely structural renovation (b2) (Figure II.4). Focusing on the construction and operating phases, solely-energy interventions partially consider the problems and critical issues that emerge throughout the life cycle of the building. When a building is upgraded based solely on its energy deficiencies (Figure II.5), it may still be vulnerable to hazards that could result in damage and collapse, posing additional risks to human life [18]. In the event of a building collapse, the environmental costs of these buildings are greater than those of non-renovated buildings due to the disposal of the energy upgrading system's components. In addition to failing in extending the building's structural service life, it is important to note that also near-zero energy buildings may be unsafe in the event of low-intensity earthquakes, resulting in unsustainable and non-resilient solutions. In this context, the goal of sustainability is partially achieved as it is mainly pursued through the choice of eco-friendly building materials and the reduction of energy consumption during operation.

Similarly, the solely structural intervention (Figure II.5), which is typically performed only in emergency situations, is designed considering only the operational phase, ensuring the safety of the structure in the event of severe seismic events. Usually, damage control, reparability after an earthquake, and end-of-life management are not considered during their design phase; as a result, the building may require extensive repairs after a seismic event, especially for non-structural components. Their

application can result in interventions that are safe and resilient, but not sustainable.

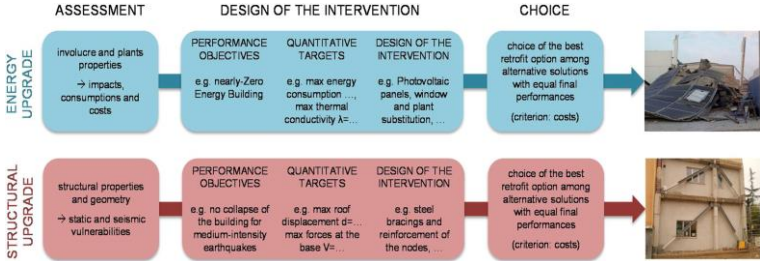


Figure II.5 - Example of the current approach to the design of the sectorial renovation and decision-making practice. From [12].

Recently, the concept of holistic integrated renovation has been established to solve the major shortcomings of uncoupled techniques. Holistic renovation (c) (Figure II.4) simultaneously addresses all structural defects or vulnerabilities and energy inefficiency, extending the service life of the structure while achieving safety, sustainability, and resilience. Such a renovation plan necessitates a novel and so far absent technique that ensures the effectiveness of the renovation measures, while also accounting for potential functional and mechanical interactions/interferences resulting from various retrofit operations. Such an extensive intervention can only be developed using a “Life Cycle” approach, where deep renovation actions are conceived considering the entire life cycle of the retrofitted building, including construction, operation, and decommissioning stages (c) (Figure II.4). The conceptual design of such interventions should address new principles, analysed in the following paragraph, and should assume the complete building life cycle as the reference time frame [12].



This research focuses on the study of the structural aspects of innovative holistic solutions adopted for the renovation of the Italian building stock, characterised by the presence of different building types with peculiar structural features and weaknesses.

### **2.3. Holistic and Sustainable approaches for the renovation of the existing buildings**

Commonly, the sustainable renovation of existing structures is defined as the implementation of green technology and eco-friendly materials. Recently, the concept has been broadened to include all the pillars of sustainability: environmental, economic, and social aspects; however, it rarely incorporates structural safety, so buildings renovated to be "more sustainable" may remain structurally unsafe and maybe even collapse during a low-intensity seismic event. The importance of integrating structural aspects into the design of the retrofit interventions also has direct repercussions on the environment; the possibility of damage or collapse caused by natural disasters is a major cause of extra impacts connected with waste disposal, and repair/reconstruction efforts [18], in addition to causing the potential loss of property. The preservation of human life through natural hazard risk reduction, including seismic reinforcement, should be among the social priority when considering sustainability in the building sector [19].

Interestingly, the requirement to "make cities and human settlements inclusive, safe, resilient, and sustainable" was included among the 17 objectives of the 2030 Agenda for Sustainable Development of the United Nations [20]. Recently, the EU Commission and Member States have granted funds and financial incentives for the renovation of existing buildings, emphasizing either energy efficiency or seismic resistance or

both, some examples are the Italian: "Ecobonus", "Sismabonus" and "Superbonus". However, this approach also exhibited significant shortcomings in two key aspects. First, in the renovation practice, important issues connected with structural safety, energy efficiency, comfort, and architecture are still handled in a sectoral and independent manner; Such a practice is the result of a quite sectorial technical culture that has been established and supported by sectorial standards, codes, and scientific literature, which has led, to date, to a renovation that largely disregards the building's needs and potential interferences between different types of interventions. After structural retrofits, safe buildings may be unsustainable or have worse environmental impacts; whereas a high-energy performing building may collapse during a low-intensity earthquake, demonstrating that significant public investments in energy improvements are lost when applied to structurally deficient buildings. The same is true for the design of acoustic upgrading interventions, architectural renovations, etc. Therefore, the uncoupled method is unsuccessful in promoting the sustainable transformation of existing structures. Second, by considering the existing low renovation rate, retrofit initiatives and legislation will hardly reduce CO<sub>2</sub> emissions unless they address the key renovation barriers. Some authors investigated the major technical, economic, and cultural/social barriers to the renovation, demonstrating that the major issues to be resolved are related to [21] [22]:

- The need for inhabitants to relocate and the downtime of the building during the intervention.
- High initial construction costs.
- Lengthy renovation works.
- Disruptive construction sites.

In this context, the scientific community has adopted different approaches to contribute to the sustainable building renovation.

Some authors developed an approach focused on the conceptual design of new sustainable solution sets and techniques for the improvement of the performance of existing buildings, while others focused on the development of optimization tools for the selection of the most sustainable solutions based on the assessment of the economic, environmental, and/or social sustainability. Both approaches can be further divided into four categories [19]:

- a. Methods combining environmental and economic sustainability.
- b. Methods combining safety and economic sustainability.
- c. Methods combining safety and environmental sustainability.
- d. Methods combining safety, environmental and economic sustainability.

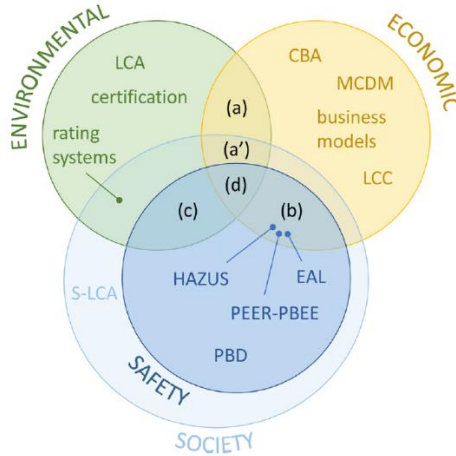


Figure II.6 - Environmental, economic, and social (here defined as safety or preservation of human life) are the three pillars of sustainability. Represented for each field are the tools used for the design and selection of the best solution. From [19].

As shown in the representation in Figure II.6 [19], few of the tools and frameworks analysed are conceived by adopting methods that consider all three pillars of sustainability including safety. Consequently, the adoption of these tools potentially leads to vulnerable, “sectorial” or uncoupled solution; moreover, many of these partially addressed the LCT criteria, without overcoming the main barriers to renewal. To address these research gaps, a novel concept of Sustainable Building Renovation (SBR) and an innovative LCT-based framework for the holistic design of sustainable retrofit treatments were developed [19].

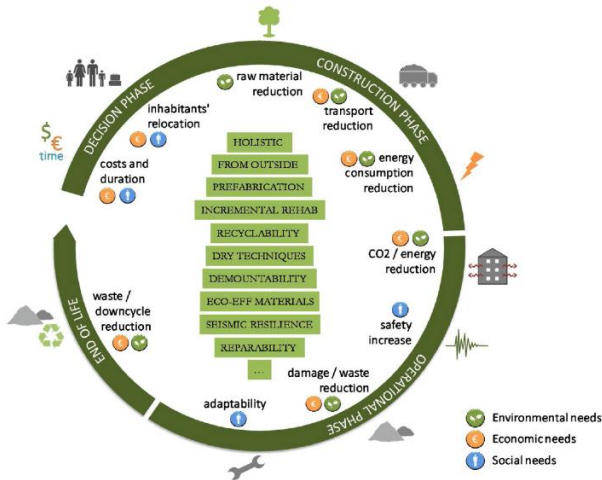


Figure II.7 - The new Sustainable Building Renovation (SBR) approach: environmental, economic, and social needs throughout the building's life cycle, and sustainable techniques to be incorporated into the design of retrofit interventions. From [19].

In this framework (Figure II.7), since the very beginning of the design process, LCT principles are considered to select and develop retrofits that minimize impacts across the building's whole life cycle.

These solutions are also imagined to overcome the key barriers to the renovation. To achieve this objective, sustainable solutions should encompass a few characteristics, such as:

- Holistic renovation interventions, able to solve contextually more than one building deficiency, maximizing the co-benefits.

- Retrofit from the outside, implemented adopting techniques installed/implemented/assembled exclusively from outside.
- Retrofit strategies inspired by incremental seismic rehabilitation [23], performed by initially carrying out the “minimal intervention” [24] and then by implementing an orderly series of discrete rehabilitation actions over an extended period of time (Figure II.8).

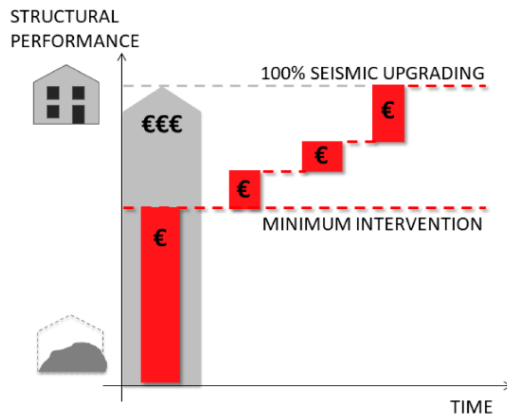


Figure II.8 - Concept of incremental seismic rehabilitation and minimum intervention. From [24].

And relevant criteria such as:

- Demountability of the renovation solution.
- Recyclability of the structural and non-structural components.

- Reparability of the retrofit, guaranteed by introducing sacrificial devices, concentrating the damage caused by seismic events.
- Prefabrication and standardization of the main components using dry techniques, to facilitate their dismantling and reuse at the end of life.

This new approach requires a multidisciplinary perspective, in which experts with different competencies should collaborate by adopting a common “Life Cycle Thinking” (LCT) approach (Figure II.9).

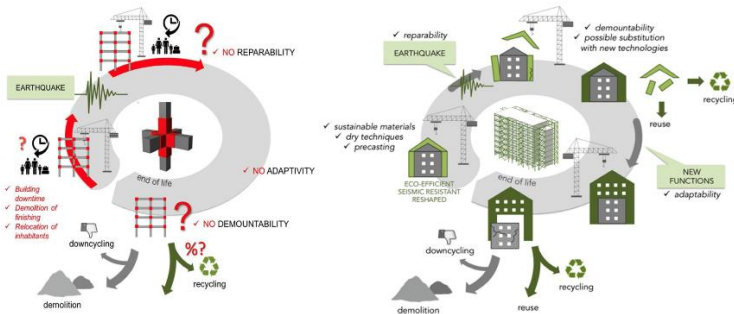


Figure II.9 - Application of the LCT principles to the preliminary evaluation of two retrofit options: strengthening the frame joints (left) and a comprehensive structural and energy exoskeleton (right). From [12] [16].

When adopting a life cycle perspective for the design of the renovation solution, all possible scenarios experienced by the building over its life cycle should be considered. Such scenarios differ based on the structure's typology, final use, and site; when assessing hazards and risks related to the building's location, all possible natural hazards must be carefully evaluated, both locally and regionally. Sustainability is a global goal, but efforts

to achieve it must be site-specific. In the case of buildings in Italy, for instance, the need to reduce/avoid environmental, economic, and social impacts associated with the possibility of earthquakes and floods cannot be ignored; to reduce losses due to hazards, new principles should be included in the retrofit's initial design phase.

The new technique for holistic and sustainable renovation of the existing building stock consisting of external shell exoskeletons, analysed in this research, overcomes the barriers to the renovation and contributes increasing the actual renovation rate. These external exoskeletons provide the global seismic reinforcement of the structure by triggering a global box-resisting mechanism. The target structural performance is achieved using prefabricated walls anchored to the existing building able to limit structural damage and concentrate it in replaceable and recyclable sacrificial devices. The demountability of the solution is guaranteed by the adoption of standardized precast elements, dry-assembled and made of recyclable and eco-friendly materials, which can be reused or easily recycled at the end of their useful life. In accordance with the principles of the SBR approach, this research will analyse solutions consisting of external wooden panels, coupled with sacrificial steel elements, applied to real buildings.

#### **2.4. State of the art on the shell exoskeleton solutions**

The innovative holistic and sustainable approach to building renovation requires new technologies and techniques or a new use/partial re-engineering of existing ones. In this perspective, the common approach for the seismic upgrading of residential buildings erected after the Second World War, typically made



of RC frames with masonry infills, based on local reinforcement of structural elements is not acceptable (Figure II.10). These techniques, focused on the reinforcement of frame portions and structural nodes, present several environmental, economic, and social problems. Damage to the finishing, which is necessary to reach the underlying elements, generates a great deal of waste; furthermore, interventions of this type often prove to be economically onerous, energy inefficient, and difficult to realize, also requiring the relocation of users during the operations (Figure II.10).



Figure II.10 - Partial finishing and non-structural elements demolition for an intervention of local strengthening of the columns. From [9].

The adoption of global reinforcement solutions overcomes the limitations of the traditional approach. The introduction of new external structural elements, linked to the pre-existing structure, enables the activation of global resistant mechanisms that meet the target structural performance, with lower environmental and social impacts. A preliminary classification of these structural solutions is proposed below, distinguishing between shear walls (a,b) and shell structures (c,d) (Figure II.11).

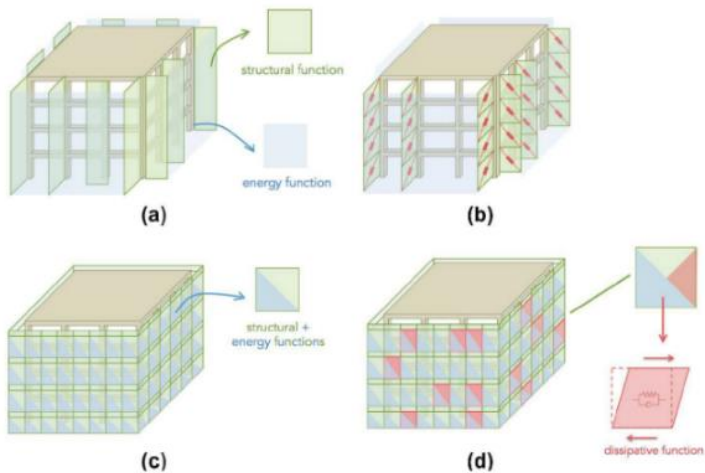


Figure II.11 - Retrofit solutions: (a) non-dissipative or (b) dissipative shear walls embedded in the external exoskeleton, (c) non-dissipative, or (d) dissipative shell structure with twofold use of the same encasing components. From [12].

As for the structural point of view, in the shear wall solutions, structural strength and stiffness, as well as seismic actions, are lumped into a few structural elements, while in the shell they are distributed in the structural elements along the façades, triggering the box structural behaviour. Exploit the extension of the new façade, shell structures allow reducing the cross-section area of each structural component and force a box structural behaviour [25] [26], resulting in reduced foundation overload and thinner exoskeleton components compared to shear walls solution.

Both solutions can be designed to be either over-resistant with respect to design actions or dissipative of part of the energy introduced by the earthquakes. Recently, to improve reparability and limit the damage, lumping of the energy dissipation into sacrificial elements was proposed, that could be

demounted and replaced, leading to the development of innovative dissipative systems (b), (d) (Figure II.11). From this perspective, a further subdivision of the external global retrofits is proposed by some authors [27], by classifying retrofit options according to the location of the dissipative devices in the structural system (Figure II.12).

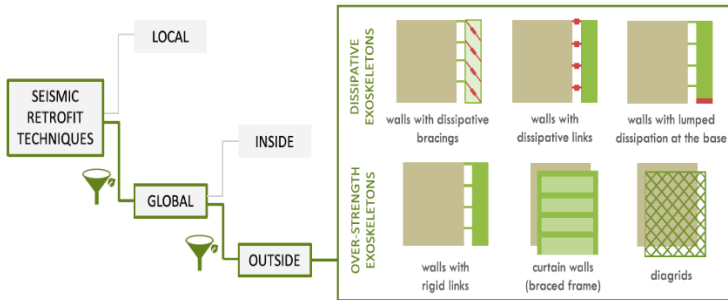


Figure II.12 – Preliminary classification of the global external seismic retrofit. From [27].

The dissipation devices can be an integral part of the structural retrofit system or serve as structural connections between the building and the retrofit, or between the retrofit and the foundations; when integrated into the retrofit structure, these devices can be lumped at the base or arranged in various combinations.

Both solutions can be connected to the existing structure using stiff or dissipative connections.

As for the energy efficiency, in shear wall systems is improved by the finishing curtain walls, the thermal insulation layer, or the ventilated façade technology that integrates the new walls, working in parallel. In this scenario, different technologies were proposed, from standard RC to steel shear walls, and solutions,

ranging from typical monolithic elements to innovative self-centring systems and hinged walls.

In the shell solution, the façade can be engineered to improve energy upgrading and structural strengthening by using the same elements. Due to the decreased stress level, the insulating panels can be engineered as seismic resistant elements, making the new skin a thermal insulating shell and an in-plane seismic resisting structure. As for the shear-walls solution, the dissipative devices can be installed in different layouts: they can be an integral part of the engineered façade, arranged in various configurations, or serve as structural connections.

Over the past decade, some authors and enterprises have focused on the development of various external solutions. The construction technologies proposed range from typical 'cast-in-place' solutions involving RC elements to more advanced 'precast' solutions involving the use of wooden or steel elements. Despite the continuous strive for achieving higher structural performance, few of the proposed solutions comply with the Life Cycle Thinking principles and succeed in clearing the barriers to renovation.

#### **2.4.1. Examples of *cast-in-place* external retrofits**

This type of integrated renovation solution generally involves the execution of cast-in-place external reinforced concrete elements and slabs, which do not offer the possibility of being dismantled and repaired or replaced in the event of seismic events-induced damage.

##### **2.4.1.1. *Geniale Cappotto Sismico* by Ecosism s.r.l.**

*Geniale Cappotto Sismico* (Figure II.13) is a proprietary solution of Ecosism s.r.l. consisting of a new RC skin able to

combine the seismic retrofit with the energy refurbishment and architectural renovation of RC and Masonry buildings [28].

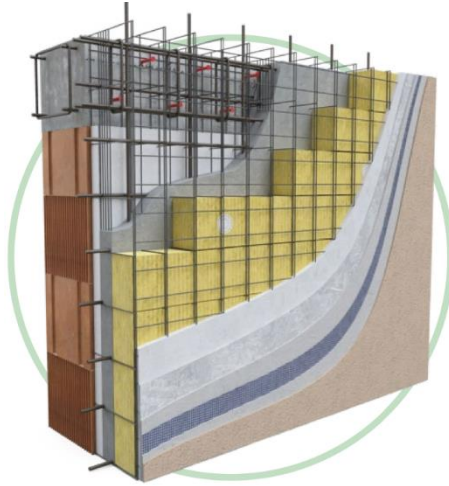


Figure IL13 - Representation of the different layers. From [28].

This solution can be classified as an over-resistant exoskeleton extended over the entire existing façade of the buildings. The cast-in-place RC structural layer, strengthened with galvanized steel reinforcement to ensure structural durability, is combined with two insulation panels to create the structural layer, which behaves as a shell and ensures the system's box behaviour. The connection between the RC exoskeleton and the existing structure is made possible by over-resistant steel dowels, which transfer seismic loads.

This holistic solution does not comply with the principles of Life-Cycle Thinking, provided that demountability, recyclability, and reparability of the RC shell are not guaranteed.

### 2.4.1.2. SismaCoat

SismaCoat is another property solution consisting of an RC shell installed from the outside that can combine seismic retrofit with energy renovation of existing structures (Figure II.14). This solution uses ‘wet’ technologies for the implementation of new over-strength skin, extended over the entire façades of the buildings, serving as a global strengthening for the structure. SismaCoat combines an insulation layer and a cast-in-place RC structural layer, situated between the building's façade and the insulation layer which serves as formwork [29].

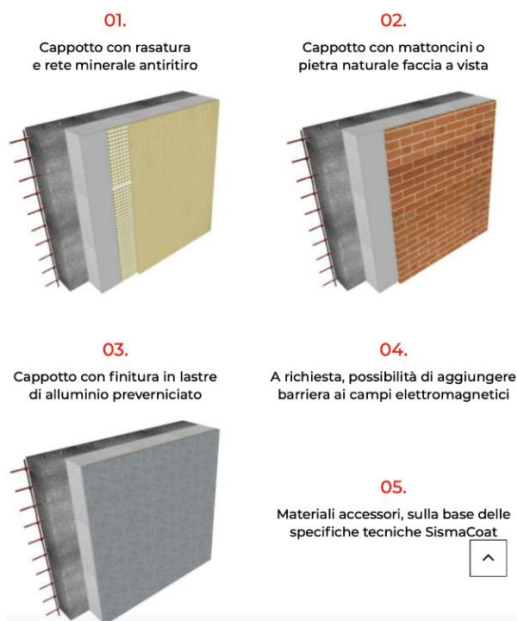


Figure II.14 - Representation of the different solutions. From [29].

The structural connection between the new skin and the existing building is made possible by over-strength steel dowels that are

bound to the building's façade. Earthquake-damaged structural components can't be easily repaired, demounted, or recycled.

## **2.4.2. Examples of *prefabricated* external retrofits**

For the execution of the external exoskeleton, a variety of construction technologies and materials can be used. 'Prefabricated' solutions are characterized by the adoption of prefabricated structural elements dry-assembled in situ to meet the requirements of the optimum holistic renovation intervention. The solutions analysed are distinguished using structural components that are recyclable and completely or partially demountable, such as environmentally friendly cross-laminated wood panels and steel frames.

### **2.4.2.1. *Resisto 5.9 il cappotto antisismico* by Progetto Sisma**

A *Progetto Sisma* property solution called *Resisto 5.9. il Cappotto AntiSismico* (Figure II.15) is a steel exoskeleton that is installed from the outside and that can combine seismic retrofit with energy renovation of Masonry buildings [30].



Figure II.15 - *Resisto 5.9* applied to a masonry structure. From [30].

This pre-assembled retrofit system, composed of over-strength steel frames and insulation panels, induces the system's box behaviour and prevent or limit the out-of-plane failure mechanisms of the walls. Over-strength injected bolts ensure the connection between the steel frame and masonry walls, the retrofit system only needs to be anchored to pre-existing masonry without the need for new foundations (Figure II.16).

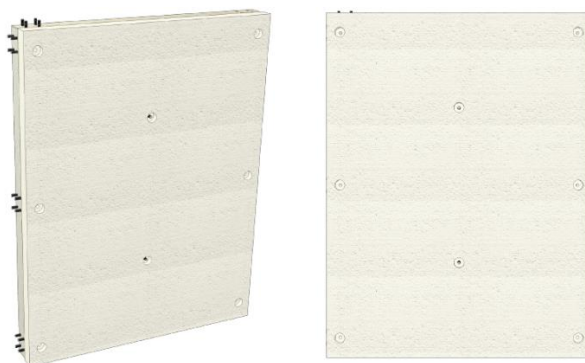


Figure II.16 - Steel frames combined with insulation panels. From [30].

The solution implements prefabricated steel components that are put together using dry methods cutting costs and execution time and avoiding disturbing the occupants. After severe seismic events, its reparability is not guaranteed and, in addition, the correct application of the system requires heavy demolition of the finishes.

#### **2.4.2.2. *Rhinoceros-Wall* by Wood Beton s.p.a.**

Rhinoceros-Wall, a proprietary product of *Wood Beton s.p.a.*, is a holistic solution consisting of a new over-strength exoskeleton installed from the outside, that enables seismic retrofitting,



energy refurbishment, and domestic system renovation of existing buildings without relocating occupants or interfering with daily operations. This global retrofitting system is composed of engineered walls extended over the entire existing façades of the buildings. This prefabricated double skin is available in two typologies, both of which use dry-fitted technologies: Rhinoceros-Wood (Figure II.17) and Rhinoceros-Steel (Figure II.18), each of them distinguished by the use of a different structural material.

The Rhinoceros-Wood Walls system, suitable for residential buildings up to three-storey, is made of precast shear walls composed of thermal insulation panels and environmentally friendly cross-laminated timber panels [31].

LEGENDA

- 1\_Edificio esistente
- 2\_Modulo prefabbricato
- 3\_Strato esterno isolante
- 4\_Intervallo verticale per impianti
- 5\_Mezzi di ancoraggio alla nuova fondazione
- 6\_Mezzi di ancoraggio metallici per cordolo esistente
- 7\_Plastra di regolazione al piede
- 8\_Modulo di tamponamento rimovibile

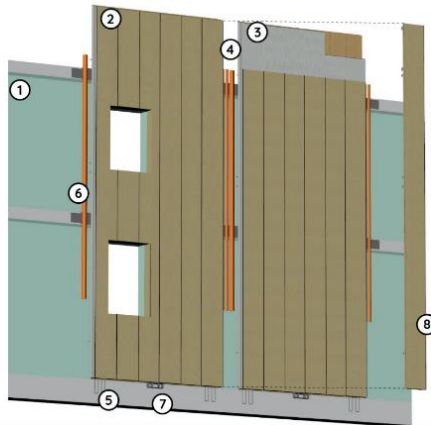


Figure II.17 - Rhinoceros-wood walls system. From [31].

Rhinoceros-Steel system extends the applicability of these exoskeletons to residential buildings up to 8 stories. This solution is made of recyclable steel frames combined with insulation and concrete panels [31].

**LEGENDA**

- 1\_Edificio esistente
- 2\_Modulo prefabbricato in calcestruzzo
- 3\_Telajo in acciaio
- 4\_Isolante di lana di roccia
- 5\_Interspazio verticale per impianti
- 6\_Mezzo di ancoraggio alla struttura esistente
- 7\_Giunto tra moduli prefabbricati
- 8\_Modulo di tamponamento rimovibile

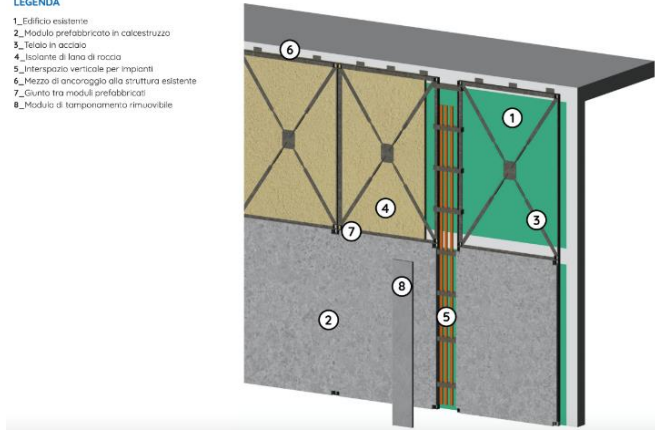


Figure II.18 - Rhinoceros-steel walls system. From [31].

In both solutions, the new pipes of domestic systems are placed in shafts located between shear walls. Retrofit components are supposed to be categorized as uncoupled shear walls, vertically arranged, and rigidly connected to their new RC foundation, preventing the possibility of structural repairs following seismic events. Over-strength dowels enable the connection between the exoskeleton and the existing structure. The retrofitting system is installed from the outside using prefabricated parts that are dry-fitted together, which speeds up installation and lowers costs without relocating the occupants.

Rhinoceros-walls contemplates the holistic renovation of the building by providing both seismic retrofitting, energy refurbishment, and domestic system renovation from a life-cycle perspective but without allowing it to be repairable.

### 2.4.2.3. Cross Laminated timber exoskeleton conceived by the University of Catania

The cross-laminated timber (CLT) exoskeleton proposed by the University of Catania is a retrofitting system based on the concept of cladding existing RC framed buildings with a new engineered skin comprised of pre-assembled and customizable wood panels, horizontally arranged and connected on each floor with an adjacent panel [32]. Assembled from the outside, this 'precast' technology system consists of adding CLT structural panels to the existing outer walls by connecting them to the RC beams using replaceable dissipative devices (Figure II.19). These devices are able to add stiffness to the system and dissipate seismic energy, thereby reducing the structural drift and earthquake-induced damage of the existing building. The CLT structural panels are combined with non-structural pre-assembled panels for insulation purposes, which are comprised of lightweight wooden frames coupled with bio-based materials.

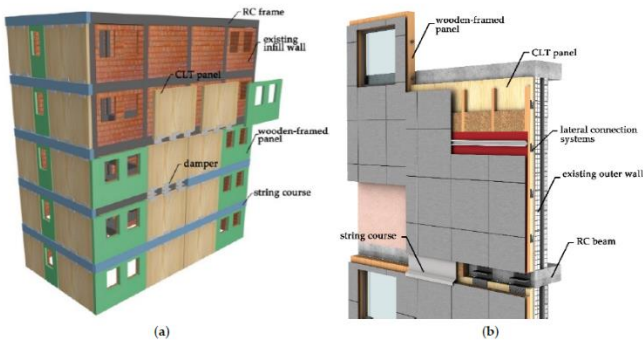


Figure II.19 - (a) Components of the proposed retrofitting system; (b) External installation of prefabricated panels. From [32].

The retrofit is completed by covering the RC beams with pre-assembled string courses to protect frictional dissipative devices (Figure II.20) and over-strength structural connections, chemically anchored to the pre-existence.

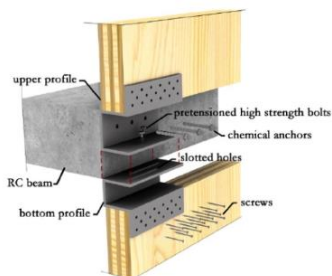


Figure II.20 - Proposed seismic energy dissipation devices. From [32].

The reinforcing elements of each level are able to slide horizontally over the same as the adjacent levels and dissipate part of the seismic energy introduced by severe earthquakes; new foundation system is required to resist the seismic loads collected by the reinforcement.

This holistic solution complies with the main LCT principles being demountable, recyclable, partially repairable and prefabricate but its applicability to the wide panorama of building types and technologies must be investigated.

#### **2.4.2.4. AdESA system conceived by the University of Bergamo**

The AdESA system is an innovative exoskeleton designed by the University of Bergamo [15]. This holistic solution, conceived in accordance with LCT principles, is realized using prefabricated and demountable elements dry-fitted. This system

is able to combine seismic upgrading with energy refurbishment and architectural restyling of existing buildings, without the need to relocate users and disrupt activities thanks to its limited construction time and the assembly from outside the building [15].

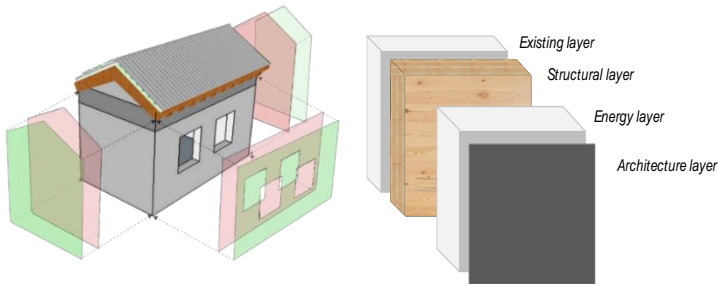


Figure II.21 - Different layers of the AdESA system. From [15].

The design of this system starts with the assessment of the vulnerabilities of the existing building and the identification of the expected structural performance, defining the minimum structural retrofit open to further incremental rehabilitation. The achievement of the defined performance targets is possible thanks to the design and application of an engineered multi-layer exoskeleton (Figure II.21), consisting of cross-laminated timber panels covered with insulation and finishing layers. The innovation of the system also consists of the adoption of the Life Cycle Thinking approach. Starting from the assessment of the building's vulnerabilities and energy requirements during its remaining 'service life', the adoption of this approach leads to the design of renovation systems made from environmentally friendly and recyclable materials.

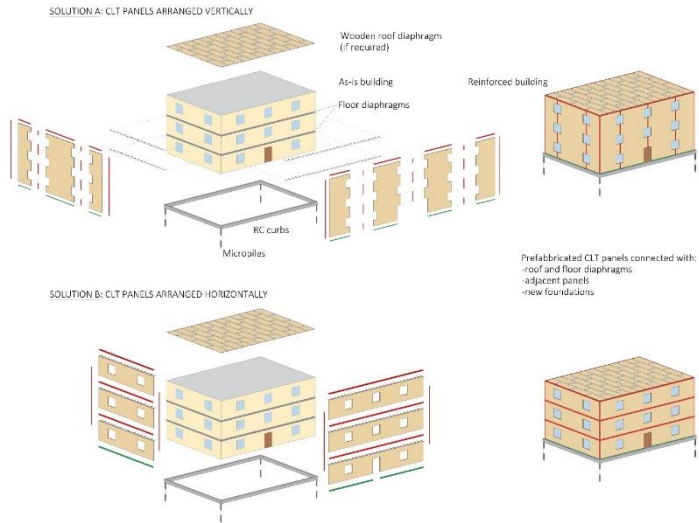


Figure II.22 - Different structural layer concepts of the AdESA system. From [15].

AdESA exoskeleton can be arranged in adherence to the existing façades or offset to create new user spaces, facilitating the architectural renovation. The seismic-resistant layer of the system can be arranged horizontally between two adjacent floors or vertically from the ground to the roof, ensuring the system's box-like behaviour, with both structural and energetical purposes (Figure II.22). Tangible long-term energy savings guaranteed by the coupling of the different layers can partially compensate the cost of the structural retrofit. The structural connections between the exoskeleton and the existing building are made of over-strength steel dowels while the energy dissipation is lumped in demountable and recyclable devices, allowing the reparability of the system after a severe seismic event. New RC foundations need to be realized to support the new self-supporting shell.

Stefano Cademartori

This retrofit solution will be analysed in detail in the following chapters by investigating its potential, applicability, and development possibilities.

## **III. Assessment of existing buildings**

### **3.1. Introduction**

It is critical increasing awareness of the state of preservation, the weaknesses, the relevant impacts, and the multifaceted needs of the existing building stock to fully understand the necessity for a holistic and sustainable renovation of European buildings. The location of the building, its age, and the construction techniques are key features, which are distinctive to characterize the stock being considered and can provide relevant preliminary information on its state of preservation, energy efficiency, and structural performance. Consequently, the first section (Section 3.2) of this chapter examines statistical data on the state of preservation of the European and Italian building stock [21] [33]. The second section (Section 3.3) introduces the primary seismic vulnerabilities of our buildings, whose recognition is essential for the concept and design of efficient renovation strategies.

As mentioned in the previous chapter, the focus is on Italian post-WWII buildings, mostly consisting of infilled reinforced concrete structures and masonry buildings in the case of residential buildings, and prefabricated RC industrial buildings. These buildings, which are commonly designed for gravity loads only and thus un-engineered against horizontal actions, have several structural deficiencies that affect their ability to withstand seismic actions:

- The main structural criticalities for reinforced concrete buildings are related to structural irregularities both in plan and elevation, poor detailing of the elements and



the joints, as well as the interaction between the main structural elements and the infills.

- The poor performance of masonry buildings is frequently correlated with poor quality of the masonry, the onset of local mechanisms, particularly out-of-plane overturning of the perimeter walls, as well as with the low resistance and deformation capacity of the walls, jeopardized by irregular distribution of the opening in elevation.
- Most precast reinforced concrete building vulnerabilities are due to the presence of a simple isostatic scheme, not designed against seismic actions and therefore lacking connections between structural components. These structures are commonly conceived to withstand sole vertical actions; their little resistance to lateral loads is usually offered by friction between structural elements.
- Regardless of the type of construction, the limited strength or even the lack of floor and roof diaphragms are one of the main seismic vulnerabilities. Assessing diaphragm capacity is fundamental for the vulnerability assessment and seismic retrofit conceptual design.

In Europe, most of our daily social and economic activities take place within buildings. Besides the fact that we spend a significant part of our income and live most of our lifetimes within them, they also consume a substantial portion of natural resources for their construction and operation. To meet the needs of the future a holistic, extensive, and sustainable renovation is required.

## 3.2. European buildings

The function, typology, and principal architectural and technological characteristics of European buildings differ considerably. Consequently, the renovation requirements of existing buildings can vary greatly based on their age, location, structural type, and material characteristics. Most of the statistical information presented in the first part of this chapter, essential for the identification of their main characteristics, was collected by Eurostat and analysed by BPIE (Building Performance Institute Europe) [21] and JRC (Joint Research Centre) [3].

### 3.2.1. Location & seismic vulnerability of the European building stock

According to estimates provided by BPIE [21], the EU-27, including Switzerland and Norway, had approximately 25 billion m<sup>2</sup> of usable land in 2011. Europe's North and West regions contain 50% of the estimated total area, while the South, including Italy, and Central regions contain 36% and 14%, respectively (Figure III.1).

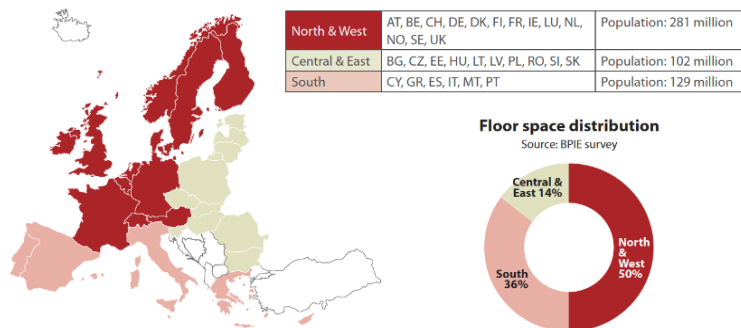


Figure III.1 - Subdivision of Europe into northern, central, and southern regions. From [21].

At the time of the census, annual growth rates of the residential sector are approximately 1%, while many countries have experienced a gradual decline in the rate of new construction in recent years. Consequently, most of the heritage was constructed in an earlier era.

Seismic activity threatens the European continent, particularly the southern parts of the Mediterranean region, where millions of people live. This activity can be classified as tectonic or non-tectonic, caused by human activities, particularly with gas extraction, and affects many European nations to varying degrees. As reported in the lower representation (Figure III.2), in terms of tectonic activity, Iceland and the southeastern regions of the continent have the highest probability of earthquakes. Specifically, the countries exposed to the highest risk are Italy, Greece, Turkey, Romania, and the Balkan region, whereas Spain, Portugal, France, Germany, and Belgium are European countries with lower hazards (Figure III.2) [34].

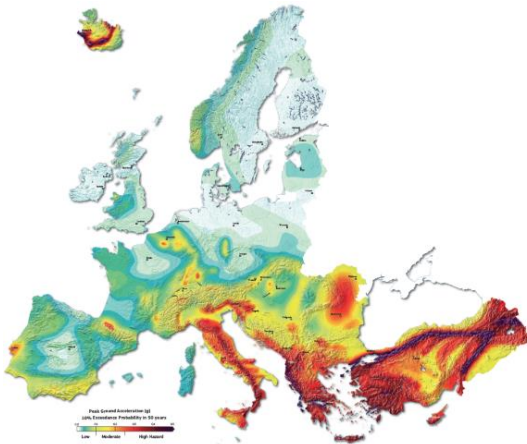


Figure III.2 - The ground motion that is estimated to be attained or exceeded with a 10% probability in 50 years is shown on the European Seismic Hazard Map. Yellow to orange colours

denote moderate hazards, yellow to blue colours denote relatively low hazards, and red colours denote high hazards. From [21].

The non-tectonic seismicity is another factor to be considered. The entire European Union is interested in this phenomenon even though the magnitude of the generated accelerations is lower than that caused by tectonic activity. The distribution of non-tectonic events reported in the Euro-Med Bulletin [35] is shown in Figure III.3. Non-tectonic activity is seen in spots, with concentrations in Finland, Netherlands, and Spain.

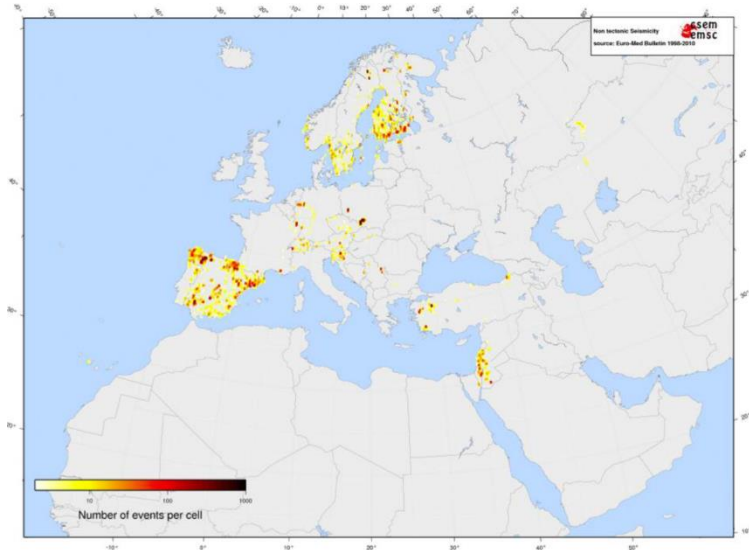


Figure III.3 - Distribution of non-tectonic activity. From [35].

Assessing the existing building stock's seismic vulnerabilities and considering seismic retrofitting should be prioritized to protect human life throughout the entire European continent.

To assess the vulnerability of existing European buildings, it is essential to identify specific building characteristics that may

affect their seismic behaviour. The fundamental and most important information concerns the building's structural type and construction period.

### 3.2.2. Age

The age of Europe's architectural heritage varies greatly and spans many centuries (Figure III.4). Such an indicator is critical for the structural assessment of the building stock because different construction technologies are associated with each construction time interval, and from this information first data on the expected main structural, seismic, and energy performances of buildings can be deduced.

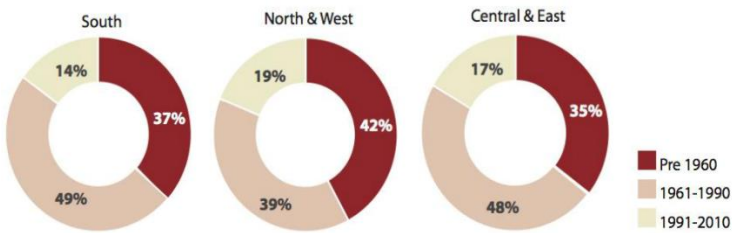


Figure III.4 - Age distribution of residential buildings in EU regions. From [21].

Furthermore, assuming a nominal design service life of 50 years, it is critical to assess the percentage of the building stock that has reached the end of its design service life and now requires structural assessment.

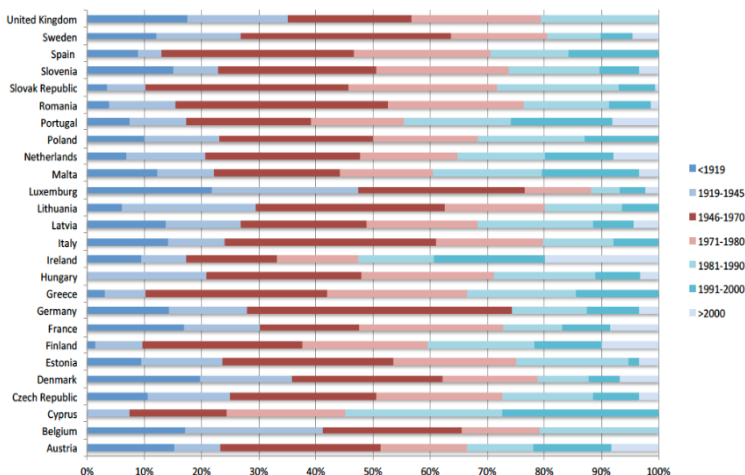


Figure III.5 - Estimated age distribution of the housing stock. From [36].

As shown in the representation above (Figure III.5), Luxembourg, Denmark, Belgium, France, and the United Kingdom have the highest number of historic buildings (erected before 1919) in the northern European region. The countries with the highest percentage of buildings constructed after World War II, built in the period from 1946 to 1970, are Germany, Romania, Sweden, Slovakia, and Italy, with a rate of approximately 40%. During this period of intensive construction, Italian standards did not account for the quantification of seismic actions nationwide (the seismic zonation was published in later years) and the structural concepts were compliant with capacity design principles.

The major distinction between buildings constructed during different time periods consists of the available technologies and the regional art of construction. In particular, the progressive switch from masonry construction to RC frames during the first

half of the 20th century is a significant turning point in the history of construction. The structural type is intrinsically linked to the potential challenges and vulnerability; therefore, its identification is crucial for the effective design of the intervention.

### **3.2.3. Building types and construction technologies**

To gain a better understanding of the structural, seismic, and energy performance of Europe's building stock, it is essential to examine the distribution of building and structural types, the characteristics of materials, and the macro-types of secondary elements and components, such as walls, finishes, and installations. One of the primary significant classifications of the European building stock is into residential and non-residential sectors, with each sector consisting of numerous types. Below are the results of a survey [21], which analysed the distribution of residential and non-residential useable floor areas for each country (Figure III.6).

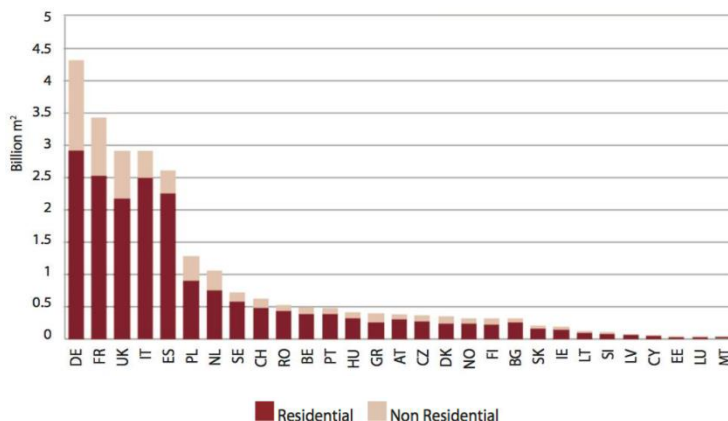


Figure III.6 - Usable floor area per each European country and division between residential and non-residential. From [33].

The residential building stock comprises 75% of the total building stock in the EU. Particularly in the southern region of the continent, a preponderant proportion of land is occupied by residential buildings (Figure III.7).

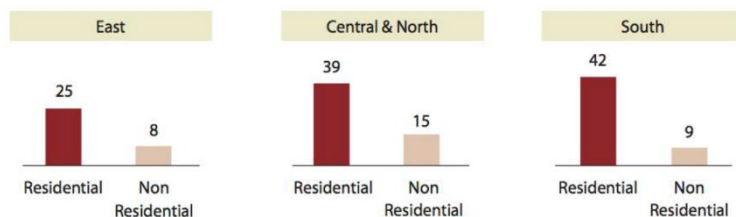


Figure III.7 - Surface area per capita in the three European regions in m<sup>2</sup>. From [33].

There are various types of dwellings within the residential sector, which can be primarily divided into single-family housing and apartment buildings. The proportion allocated to each of these categories varies significantly throughout Europe. The underlying representation (Figure III.8) of these data



illustrates the prevalence of single-family homes in the middle-to high-income countries, including Italy, where the proportion of single-family homes exceeds 70%.

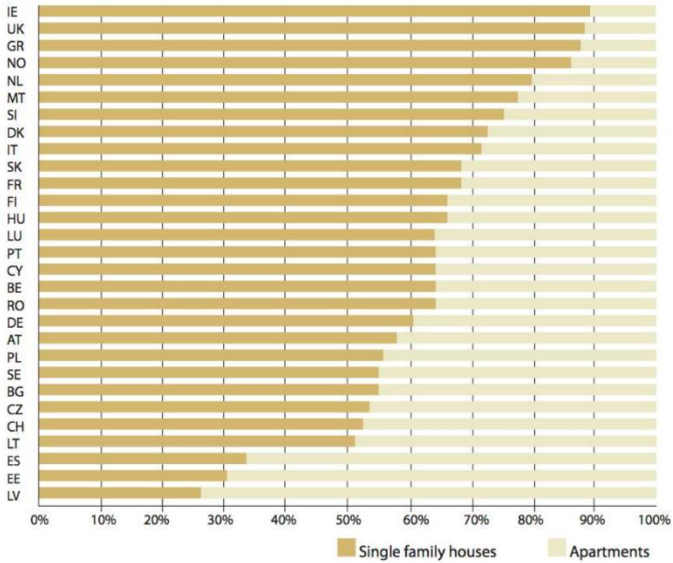


Figure III.8 - Single-family houses and apartment buildings in Europe. From [33].

To better comprehend the structural, seismic, and energy performance of the European building stock, it is also necessary to examine their structural type, material characteristics, and secondary element and component types at a deeper level. Recently, numerous European research initiatives, mostly focused on analysing the energy performance of buildings, examine a set of reference buildings to predict and estimate their energy use and include this type of information. In the TABULA Webtool project [37] the building stocks of 15 European nations were analysed, its 'Matrix of building types' provides an overview of building types for this project. The

columns of the matrix represent four building size classes, classified as: detached houses, terraced houses, multi-family houses, and apartment buildings, while the rows represent a series of building year classes. Individual cells of the matrix represent the "building types" of a European nation, each of them is represented by a photo, a description of typical construction materials used for the wall, floor, and roof sections, and information on the thermal envelope of a model building. This building is assumed to be representative of the particular building type, meaning that its characteristics are typically found in homes of the same age and size category (Figure III.9, Figure III.10).

















| Construction Year Class | Additional Classification | SFH<br>Single Family House   | TH<br>Terraced House  | MFH<br>Multi Family House  | AB<br>Apartment Block   |
|-------------------------|---------------------------|--|---|--|---|
| ... 1900                | generic                   | <br>IT.MdClim.SFH.01.Gen  | <br>IT.MdClim.TH.01.Gen  | <br>IT.MdClim.MFH.01.Gen  | <br>IT.MdClim.AB.01.Gen  |
| 1901 ... 1920           | generic                   | <br>IT.MdClim.SFH.02.Gen  | <br>IT.MdClim.TH.02.Gen  | <br>IT.MdClim.MFH.02.Gen  | <br>IT.MdClim.AB.02.Gen  |
| 1921 ... 1945           | generic                   | <br>IT.MdClim.SFH.03.Gen  | <br>IT.MdClim.TH.03.Gen  | <br>IT.MdClim.MFH.03.Gen  | <br>IT.MdClim.AB.03.Gen  |
| 1946 ... 1960           | generic                   | <br>IT.MdClim.SFH.04.Gen | <br>IT.MdClim.TH.04.Gen | <br>IT.MdClim.MFH.04.Gen | <br>IT.MdClim.AB.04.Gen |

Figure III.9 - Example of Building Type Matrix - classification of the Italian residential building stock erected before 1960. From [37].










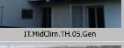






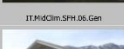



| Construction Year Class | Additional Classification | BFH<br>Single Family House  | TH<br>Terraced House   | MFH<br>Multi-Family House   | AB<br>Apartment Block  |
|-------------------------|---------------------------|---|--|---|--|
| 1946 ... 1960           |                           | <br>IT.MiClim.SFH.04.Gen | <br>IT.MiClim.TH.04.Gen | <br>IT.MiClim.MFH.04.Gen | <br>IT.MiClim.AB.04.Gen |
| 1961 ... 1975           | generic                   | <br>IT.MiClim.SFH.05.Gen | <br>IT.MiClim.TH.05.Gen | <br>IT.MiClim.MFH.05.Gen | <br>IT.MiClim.AB.05.Gen |
| 1976 ... 1990           | generic                   | <br>IT.MiClim.SFH.06.Gen | <br>IT.MiClim.TH.06.Gen | <br>IT.MiClim.MFH.06.Gen | <br>IT.MiClim.AB.06.Gen |
| 1991 ... 2005           | generic                   | <br>IT.MiClim.SFH.07.Gen | <br>IT.MiClim.TH.07.Gen | <br>IT.MiClim.MFH.07.Gen | <br>IT.MiClim.AB.07.Gen |
| 2006 ...                | generic                   | <br>IT.MiClim.SFH.08.Gen | <br>IT.MiClim.TH.08.Gen | <br>IT.MiClim.MFH.08.Gen | <br>IT.MiClim.AB.08.Gen |

Figure III.10 - Example of Building Type Matrix: classification of the Italian residential building stock erected after 1960. From [37].

The 2001 national census [38] revealed that 61.5% of the 6,903,982 Italy's residential buildings are load-bearing masonry structures, 24.7% (2,768,205) are reinforced concrete structures, and 13.8% (1,554,402) are other structures such as wood, steel or other. The proximity to other buildings and the number of storeys are two important factors that influence the seismic performance of existing structures. The data from the census indicate that 53.0% of the buildings are detached, while the remaining 47.0% are adjacent to other buildings on one or more sides. More buildings have a first floor than a ground floor only (52.9% versus 22.6%, respectively), 17.3% of buildings have a second floor, and only 7.2% have a third floor or higher.

### **3.3. Introduction to the main seismic vulnerabilities**

Numerous building features must be recognized to analyse the seismic behaviour of structures and define their vulnerabilities. The sections that follow provide a brief overview of the most common seismic vulnerabilities of reinforced concrete infilled buildings, masonry buildings, and precast reinforced concrete structures, which are frequently used to build industrial buildings.

#### **3.3.1. Reinforced concrete infilled buildings**

When assessing the seismic vulnerability of reinforced concrete structures, their structural performance is highly variable, making it difficult to propose general and exhaustive guidelines for predicting their seismic behaviour. Most of Europe's reinforced concrete building stock was designed and built without seismic safety standards or reference to a good seismic-resistant structural concept, resulting in extremely vulnerable structures.

From the end of World War II until the late 1980s, typical Italian RC structures consisted of reinforced concrete frames with masonry infill walls (Figure III.11).

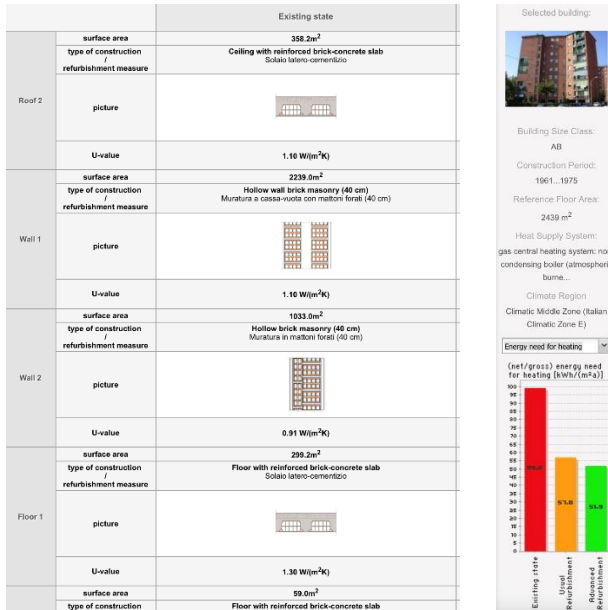


Figure III.11 - Example of Building Data for the Italian apartment blocks built between 1961 and 1975. From [37].

The interaction between the frame and masonry infills may severely impact the seismic vulnerability of existing reinforced concrete buildings. Infills increase structural stiffness and modify the intensity and distribution of the seismic action on the frame during a seismic event. The frame-infills interaction can have positive effects in the case of a regular distribution of infills for buildings in low seismicity areas; in these cases, the infill provides the seismic resistance needed to counteract the modest seismic actions. In highly seismic areas, the collapse of the infills often causes early RC frame collapse. A non-uniform distribution of masonry infills can introduce the plan and vertical irregularities into the structure, generating torsion or

stress concentration in some RC elements, and putting the building's safety at risk. Infills can trigger both global and local collapses, caused by local column damage or shear failure (Figure III.12) [39].

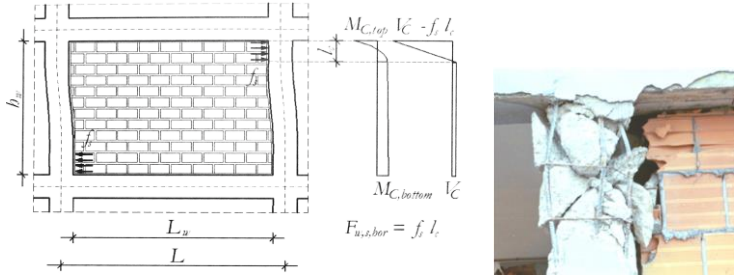


Figure III.12 - On the left side: Schematic representation of forces induced in RC columns by compressed diagonal struts of masonry infills. From [39]. On the right side: Example of Local column damage caused by infill corner crushing after the Molise earthquake, in 2002. From [40].

Recent earthquakes around the world have shown many examples of infilled frames damaged and collapsed. Focusing on the Italian territory and building stock, reference can be made to the recent reports redacted after the earthquake which targeted L'Aquila (2009) [41] [42], and Emilia (2012) [43] [44].

At the basement level of RC buildings, particularly in apartment blocks, a 'pilotis' floor for garages is commonly observed, resulting in significant vertical irregularity. This vulnerability is frequently caused by an uneven distribution of strengths, stiffnesses, and masses due to masonry infill configuration, which causes deformations to be concentrated at this level (Figure III.13). Consequently, stresses are concentrated at the ends of the columns located at this level, overloading the

structural joints, and resulting in permanent drift or collapse [45].

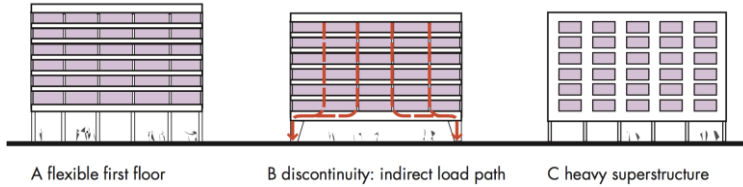


Figure III.13 - Vertical irregularities and soft storey vulnerability: a scheme of the main configurations that lead to a soft storey mechanism. From [45].



Figure III.14 - Example of soft storey mechanism at the first storey. From [33].

Another relevant example of a common vertical irregularity at the first level is the presence of short/squat columns. This type of irregularity is frequently caused by partial basement infills or strip windows. Such a configuration can result in the premature brittle shear failure of short RC columns, which may also lead to the global collapse of the building (Figure III.14). Figure III.15 illustrates a typical example of the short/squat column failure, in which an X-shaped shear failure occurred in the short columns between two adjacent basement ribbon windows.



Figure III.15 - Following the L'Aquila earthquake, a partial infill of the frame caused a typical brittle shear failure of squat columns. From [46].

In the aftermath of past earthquakes, many examples of these types of damage were observed in RC-infilled frames [47] [48] [49].

Plan irregularity is another relevant source of structural vulnerability, which consists primarily of the irregular shape of the building and the asymmetry of the structural frames, the eccentric positioning of the stair and lift cores, and the unbalanced arrangement of load-bearing structures along the perimeter. All these characteristics may result in a concentration of seismic actions in a few localized structural elements that were not designed to resist horizontal loads and may induce torsion forces in the building (Figure III.16). These effects may compromise the structural integrity of the building and result in an unexpected partial or total collapse.



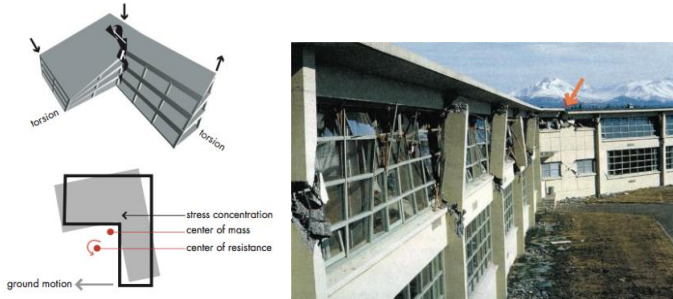


Figure III.16 - On the left side: Plan irregularity due to re-entering corners. On the right side: Effects of irregularity in the plan detected after the Alaska Earthquake in 1964 at West Anchorage High School. From [45].

Existing reinforced concrete structures in Italy, only designed for gravity loads, frequently feature unidirectional frames with inadequate seismic detailing (Figure III.17). The modest resistance provided by these structures in the secondary direction and the ineffective design of the structural elements and of the beam-column joints results in very low local and global ductility, and consequently, in low energy dissipation capacity [33].

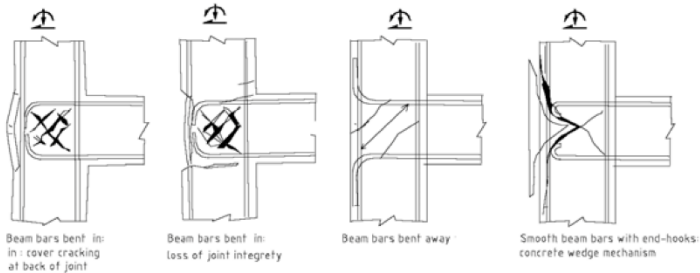


Figure III.17 - Typical anchorage details and collapse mechanisms for beam-column joints designed for gravity loads only. From [50]

The existing reinforced concrete walls, designed for vertical loads only and typically positioned along stairways and lift shafts, must always be considered when assessing the seismic response of a building. Due to the lack of reinforcement and properly designed structural detailing, their behaviour is comparable to that of masonry infill walls, as they contribute significantly to the overall system's stiffness. Due to their high stiffness, the seismic action transmitted to these elements is significant and can cause them to sustain severe damage prior to the activation of the reinforced concrete frame and the damage of secondary elements (Figure III.18).



Figure III.18 - Damage at the base of the staircase wall of an RC building caused by the 2012 Emilia, Italy, earthquake. From [44].

### 3.3.2. Masonry buildings

Ancient masonry structures, which were commonly composed of bricks or stones held together with lime-based mortar of low quality, were typically erected to resist only vertical loads. The seismic resistance of these structures depends on their three-dimensional structural layout. In these buildings, the existing

floors are usually not assimilable to the seismic-resistant floor and roof diaphragms, which are necessary to ensure the overall box-like behaviour and prevent out-of-plane overturning mechanisms (Figure III.19). Additionally, old wooden perimeter ties with steel anchors are frequently ineffective in restraining out-of-plane mechanisms due to the natural decay of the wood or the failure of the anchor-to-tie connection. Moreover, the irregularities in plan and elevation reduce the overall capacity of the building. These conditions frequently trigger local collapse mechanisms affecting portions of the structure.

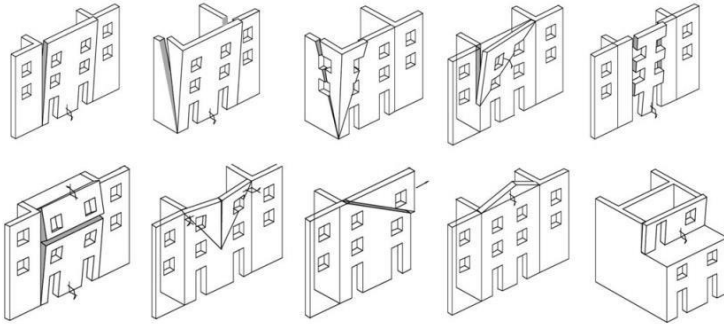


Figure III.19 - Kinematic out-of-plane failure mechanisms of unreinforced masonry buildings.  
From [51].

Unreinforced masonry structures comprised of bricks or concrete blocks are also extremely common in Italy [38]. These buildings typically have poor horizontal strength, which is primarily caused by the lack of an efficient connection between horizontal existing floors (not engineered to trigger a diaphragm action) and perimeter walls, allowing out-of-plane collapse mechanisms to occur; the number, size, and location of the openings heavily influence their vulnerability. Large openings, small columns, and long masonry walls without cross retaining

walls or stiffening elements contribute to further increasing the seismic vulnerability of these structures.

Most of the buildings built or renovated in Italy after WWII have reinforced concrete floors lightened by hollow clay blocks, as analysed in the following paragraph (Figure III.23). The level of constraint between horizontal floor and masonry must primarily be verified in the vulnerability assessment stage. As long as the floor can trigger adequate diaphragm action [52], adequate constraint between the vertical structural masonry piers and the floor can reduce these structures' seismic vulnerability to the sole activation of in-plane collapse mechanisms [53] [54], typically triggered by earthquakes of greater magnitude.

### **3.3.3. Prefabricated RC industrial buildings**

In Italy, prefabricated structures are widely employed, particularly in the industrial sector. This is due to the numerous advantages associated with their execution in comparison to conventional cast-in-place structures. By utilizing prefabrication, it is possible to provide faster construction times at a lower cost. Moreover, by standardizing the production process in the factory, greater quality control, safety, and sustainability can be achieved in production. Even though these characteristics are the greatest strength of this type of construction, the frequent poor engineering of the connections between the elements introduces severe weakness in terms of seismic action resistance (Figure III.20). Assembling the structure's components does not allow for monolithic connections like a continuous RC casting [55], so the main vulnerabilities of this type of construction are the poor detailing of the connecting elements.



Figure III.20 - Examples of damage and collapse of the reinforced concrete precast joint having the task of providing stability to the roof beam. From [56].

In fact, if cost reduction and production control allow having elements with great mechanical performance, the connections must be made by site operations, where control is more difficult. These prefabricated structures, which are typically designed to resist only vertical actions, exhibit little resistance to lateral loads, which is often attributable to the lack of connections engineered for this purpose and the reliance on frictional resistance between adjacent structural elements (Figure III.21).



Figure III.21 - Collapse of the horizontal closing panel and its structural connection. Form [56].

The type of connecting elements has a direct impact on both the static scheme and the seismic vulnerability. RC columns connected to roof beams typically resist horizontal loads, in some cases, these connections are made with pinned connections or by building braces to hold the beam in place [57] [58] [59]. In other cases, these elements are absent and horizontal forces are transmitted by friction alone, which may be particularly critical when the structure is hit by a near-fault earthquake, such as those typical in Italy, characterized by high vertical accelerations. The result of such assemblages is a structure with moderate lateral stiffness. The decreased stiffness causes the structure's natural period to increase, resulting in decreased loads with large displacements demand. Due to the typical earthquake response of these structures, and the inadequacy of structural detailing, this type of construction is among the most vulnerable during an earthquake (Figure III.22).



Figure III.22 - The effects of the Emilia-Romagna earthquake on some prefabricated industrial buildings. From [60].

In conclusion, the primary vulnerabilities associated with precast reinforced concrete buildings result from the lack of

connections and structural details designed for seismic actions. The modest resistance of these structures to lateral loads is typically provided by the friction between the primary and secondary structural and non-structural elements that contribute to the building's overall resistance.

Over the years, the scientific community has focused on this peculiar type of structure, looking deeper into the role of both primary and secondary structural elements as well as their connections [61] [62] [63] [64].

### **3.3.4. Lack of horizontal diaphragms**

Regardless of their relevance in the LFRS, the issue of the in-plane diaphragm and the in-plane capacity of existing floors has not been extensively investigated, with the exception of wooden floors in masonry buildings, for which some studies are available in the literature [65]. Diaphragms are always necessary to transfer the floor inertia forces to the lateral force-resisting system for all building types, regardless their structural typology.

In RC buildings, the seismic capacity of existing slabs is not the primary weakness associated with limiting the overall capacity of existing structures, which are frequently sensitive to greater vulnerabilities, but it can become so when an additional seismic resistance system is added.

In historic buildings with original wooden floors, loosely connected to the perimeter walls and lacking any in-plane stiffness and resistance, it is frequently necessary to place new seismic-resistant systems able to compensate for the lack of horizontal diaphragms.

In most buildings constructed in Europe after World War II, both in the case of RC frames and masonry buildings, the floors were made of horizontal reinforced concrete slabs. In some European countries, such as Italy, the concept of using hollow clay blocks to lighten diaphragms became popular at the turn of the twentieth century. At the time, the blocks had no structural function, but from the 1930s to the early 1970s [65], in areas with no recognized seismic hazard, special reinforced hollow bricks were introduced to contribute to the static strength of the floor alongside the cast-in-place RC elements (Figure III.23).

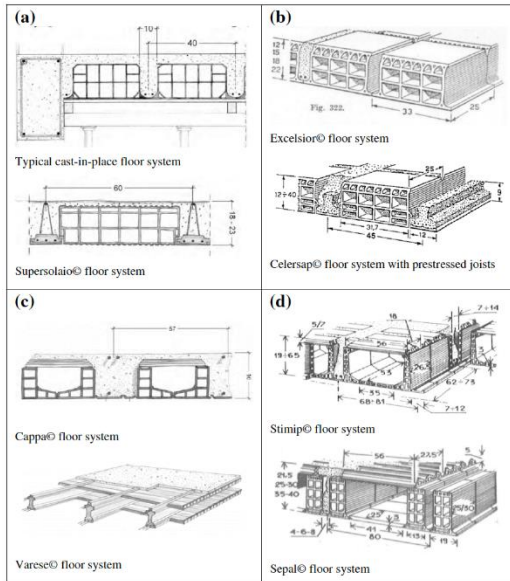


Figure III.23 - Beam and hollow-clay-block floor systems with (a) and without (b) concrete topping; beam and hollow-clay-block floor systems with blocks composed of different hollow-clay elements with (c) and without (d) concrete topping. From [66].

Recent studies indicate that only some beam and block floor systems have a reliable in-plane capacity, thanks to the



activation of a tied-arch resisting scheme, while others cannot act as diaphragm floors, particularly the *Varese* typology. When the action of diaphragms can be relied upon, they frequently exhibit stiff behaviour to the point of brittle failure [66].

In precast reinforced concrete structures and buildings, the roofing components have been identified as one of the major weaknesses. In the past, it was common practice to install roofs with no mechanical connections for horizontal force transfer. Friction alone ensured horizontal stress transmission, but its contribution was not quantified in depth. This method of assembling roofs, from a structural point of view, results in a high degree of roof flexibility, which is increased if the roof includes openings. Therefore, all concepts relating to the rigid deck and the distribution of seismic forces among the diverse seismic-resistant elements do not apply to these constructions. The inadequate connection between the elements carries the risk of excessive differential displacements between the various elements, which may lead to instability (Figure III.24).



Figure III.24 - Example of the collapse of the roof due to loss of support of its elements. From [56].

Estimating the diaphragm capacity is essential for both the vulnerability assessment of an existing building and the conceptual design of the seismic retrofit intervention.

### **3.4. Concluding remarks**

Analyses of the European building stock in terms of its primary characteristics, state of conservation, and potential vulnerabilities reveal the need to adopt a holistic and sustainable approach to renovation.

The survey in this chapter revealed that most European buildings, either residential or industrial, are old, technologically obsolete, and seismically vulnerable.

About 60% of the buildings in Italy were constructed prior to 1970; consequently, they have reached the end of their 50-year design service life, and the possibility of their continued use should be determined based on the results of a detailed structural assessment analysis. Moreover, their energy consumption is frequently quite high, their technological solutions are obsolete, and their building envelopes are consisting of outdated, low-performance materials.

In this scenario, in order to reduce waste and pollution, it is preferable, whenever possible, to renovate existing buildings by safely extending their useful life rather than demolishing and rebuilding. Promoting the achievement of the European objectives for material reuse and waste reduction.

The following chapter offers a brief review of the current state of knowledge on traditional and most common structural retrofit strategies and solutions, analysing their benefits and drawbacks, along with some innovative approaches, technologies, and

Stefano Cademartori

solutions that have the potential to promote the spread of holistic, integrated, and sustainable renovation solutions.

## **IV. Structural retrofit strategies and solutions**

### **4.1. Introduction**

This chapter provides a brief overview of the current state of structural retrofit strategies and the most common technical solutions, analysing their advantages and limitations, along with some innovative approaches, technologies, and solution sets for implementing integrated and holistic retrofit strategies.

The first section (Section 4.2) of this chapter provides a brief description of *traditional* retrofit solutions and a few selected key examples of best practices currently used to improve the seismic performance of various structural types, examining their principal limitations and potential.

In the subsequent section (Section 4.3), new trends in structural retrofitting and the integration of circular economy principles in the design of holistic solutions are examined. Adopting this new paradigm in the construction industry necessitates the application of integrated solutions that are both effective and sustainable to extend the useful life of existing structures, materials, and systems.

The final section (Section 4.4) presents significant examples of integrated rehabilitation projects that have been implemented to date, overcoming the limitations of *traditional* solutions, and providing insights into the effective integration of LCT and circular economy principles.

The pursuit of the EU's targets will soon require substantial effort. The unique characteristics, constraints, and renovation goals of each building determine the optimal solutions, which

should incorporate life cycle thinking and circular economy principles to achieve the set objectives. Exploring the challenges presented by renovations based on these innovative approaches may soon no longer be an option but a necessity.

## **4.2. A brief overview of *traditional* seismic retrofitting interventions**

Various techniques and solutions can be implemented for the structural retrofit of existing buildings; the following are a few significant examples of the most common solutions currently available.

The Italian panorama is characterised by a wide variety of structural and building types with specific requirements and vulnerabilities that deserve investigation to determine the *optimal solutions*. In the following sections, local and global retrofit solutions are categorised and analysed according to the structural type of the existing building, dividing them into solutions applicable to reinforced concrete, masonry, and industrial structures.

Although *traditional* solutions vary in technologies, materials, and concepts, they are characterized by the lack of an integrated and holistic design approach and the exclusion of the innovative principles of life cycle thinking and circular economy.

### **4.2.1. Examples of solutions for reinforced concrete buildings**

For the seismic retrofitting of existing RC buildings, two primary approaches have been employed traditionally:

- the “Local approach”, which consists of strengthening the main structural elements through local retrofit of

both joints and members of frames and walls (Figure IV.1).

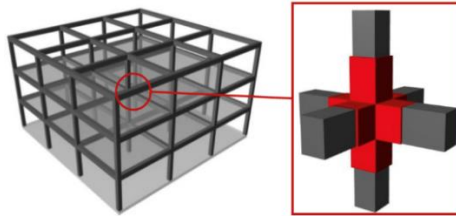


Figure IV.1 - Example of Local strengthening of existing RC frame joints. From [67].

- the "Global approach", in which the building is integrated with a new lateral force-resisting structure (LFRS), made of new structural elements or devices, designed to withstand the horizontal loads, or in which existing structural elements are strengthened to withstand the seismic action (Figure IV.2).

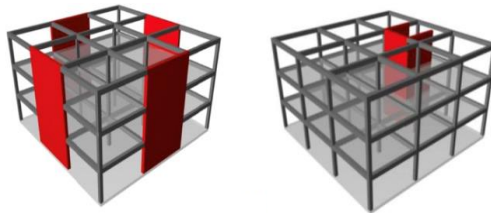


Figure IV.2 - Examples of Global interventions: On the left, new construction of a seismically resistant structure. On the right, the reinforcement of existing RC walls. From [67].

Occasionally, *mixed* solutions are also suggested [67], in which both global and local interventions are carried out contextually. This is the case, for example, of those retrofit solutions exploiting energy dissipation, which may require preliminary interventions to increase the ductility of the existing building. In such cases, additional local interventions may be

required, either on a portion of the existing structure or on some components, to locally increase their deformation capacity or to modify their failure mechanism.

#### **4.2.1.1. *Local interventions***

These interventions usually involve reinforcing the main structural RC elements such as beams, columns, and structural nodes using a variety of approaches [68] [69].



Figure IV.3 - Intervention of local strengthening of the columns requiring partial completion and demolition of non-structural elements and finishes. From [70].

Common methods of local reinforcement for frames include wrapping the elements and structural joints with a new reinforced concrete [71], steel (Figure IV.3) [72], FRP [73], or high-performance concrete [74] [75] jacket (Figure IV.4).



Figure IV.4 - On the left side: beam reinforced with a new RC layer. In the centre: RC column reinforced using CFRP jacketing. On the right side: column reinforced by introducing a steel sheet. From [76].

Reinforcement using steel jacketing has the advantage of strengthening the structural elements but also increases their volume, due to the external stratigraphy required for corrosion and fire protection, the building's mass, and the stiffness of the structure. Frames can also benefit from the external bonding of fibre-reinforced composite (FRP) materials, this solution offers a high strength-to-weight ratio, good corrosion resistance, speed of execution, and relative ease of application, but it is inadequate when it is necessary to significantly increase the axial resistance of the columns, and their exposure can cause fire resistance issues. High-performance fibre-reinforced concrete (HPFRC) thin layers are a great alternative for reinforcing the axial strength of columns, especially when the structure is made of low-resistance concrete [77].

Since local interventions frequently require the partial demolition of non-structural elements and building finishes, resulting in high renovation costs that can represent a significant portion of the total cost of the intervention, may not be the most effective for retrofitting. In addition, the efficacy of these local reinforcements is in some cases uncertain, and their benefits may be compromised further by operational challenges experienced during the construction phases. They also present the disadvantage of limiting the building's use to a variable



period and may not be effective for unidirectional frames because they cannot generate three-dimensional seismic-resistant systems [78].

#### **4.2.1.2. *Global interventions***

Several techniques aimed at integrating existing buildings with completely new earthquake-resistant systems (Lateral Force Resisting System, LFRS) are addressed in the case of global retrofit interventions. The basic interventions that can be carried out when implementing a conventional global strategy are the addition of new exterior shear walls or bracing systems, as well as the reinforcement of existing walls, such as elevator cores or perimeter walls, that were originally designed to resist only gravity loads.

The most common approach for reinforcing and stiffening structures includes creating new shear walls within the existing reinforced concrete frame or outside the building volume. As the new shear walls stiffen the structure, the existing frame's beams and columns experience less relative displacement and damage during ground motion and can therefore continue to support the competent gravity loads following the earthquake. The additional shear walls can also prevent the occurrence of *low-ductile* global mechanisms, such as *soft storey* while protecting *displacement-sensitive* components due to their high stiffness; typically, these solutions perform best for low-rise structures.

Multiple options and configurations are available for the introduction of the proposed walls, such as the addition of new steel bracing [79], cladding the existing concrete walls and cores with high-performance materials [80], and implementing new earthquake-resistant shear walls in individual bays of the frame

by removing the infill walls and casting a new RC panel, or filling the space between two adjacent columns (Figure IV.5, left).

Alternatively, the new walls can be cast outside of the volume of the building, though they would still need to be accurately connected to the existing frame (Figure IV.5, right).



Figure IV.5 - On the left side: construction of new earthquake-resistant shear walls between frame bays. From [81]. On the right side: construction of new external RC shear walls, adjacent to the pre-existence. From [79].

The addition of steel cross bracing is an efficient alternative to cast-in-place solutions, potentially feasible for all buildings not subject to restrictive architectural limitations (Figure IV.6). This type of bracing enables faster assembly and connection to the existing structures, hence potentially decreasing disruption and building downtime, which is typically less than what is required for cast-in-place systems.



Figure IV.6 - External steel bracing for seismic retrofitting of a hospital building. From [82]

In some cases, the introduction of these retrofit solutions may require local interventions on secondary- and non-structural elements, resulting in *mixed* solutions. These additional interventions consist mainly of increasing the strength or deformation capacity of the infills, commonly made of masonry brickwork in Italian buildings, with different techniques. Among the solutions reported in the literature, the main retrofit strategies encompass the reinforcement of infills, transforming them into shear-resistant walls, and the modification of the infills-RC frame interaction [83] [84]. Inspired by the vernacular architecture of earthquake-prone regions (Figure IV.7) [85], some downgrading solutions use sliding joints to increase the infill deformation capacity, while limiting damage and reducing infills-to-frame interaction (Figure IV.8). These additional interventions frequently necessitate the removal and refurbishment of finishes, as well as long downtime of the building.

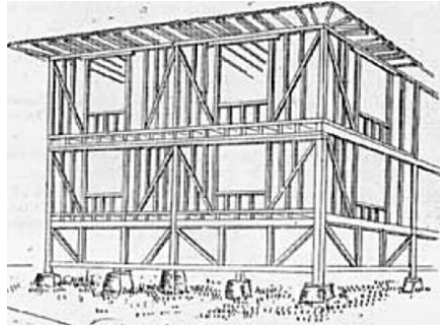


Figure IV.7 - Example of the vernacular architecture of earthquake-prone regions. From [85].

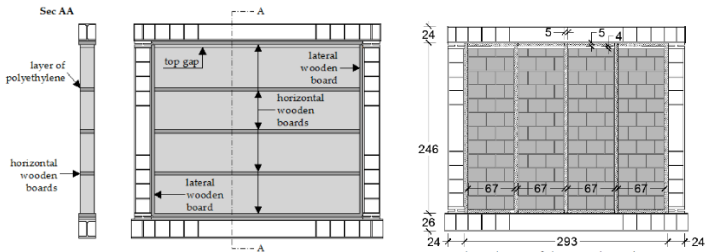


Figure IV.8 - Examples of masonry infills with horizontal & vertical sliding joints. From [86].

The primary structural limitation of the global *traditional* solutions just examined is the concentration of seismic actions on a small number of structural elements, such as new shear walls and additional bracing. Therefore, the foundations of these additional elements must be sufficiently stiff and resistant to withstand the forces transmitted to their bases, particularly in soils with poor mechanical properties.

Installing passive and active energy dissipation systems and implementing isolation systems [87] are interesting examples of novel global retrofitting, that partially overcome the obstacles and limitations of the solutions analysed above. Existing structures can benefit greatly from the implementation of

additional damping technologies because they permit a portion of the energy introduced by the earthquake to be dissipated, thereby limiting structural and non-structural deformations and damage. The first step in classifying these systems is to divide them into passive, active, hybrid, and semi-active categories [88].

Active, hybrid and semi-active control systems differ in the integration of force delivery devices with real-time sensors and the requirement to be powered by an external energy source.

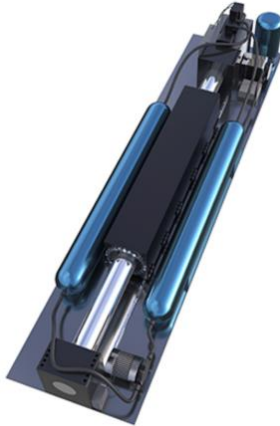


Figure IV.9 - Illustration of an active mass damper. From [89].

Their incorporation not only reduces the destructive effects of seismic excitation but can also potentially increase reliability and safety against wind and vibrations [88] through the intervention of externally powered actuators capable of applying additional beneficial forces to the structure [90]. The installation of these devices requires a careful evaluation of the structural capacity of the existing structural elements,

specifically the diaphragms and beams, to which they will be anchored.

Unlike their predecessors, passive dissipation systems [38] do not require additional energy sources to function. These energy dissipation systems can be divided into two main categories based on whether the dissipation depends on the relative displacement and deformation induced or on their deformation velocity [91].

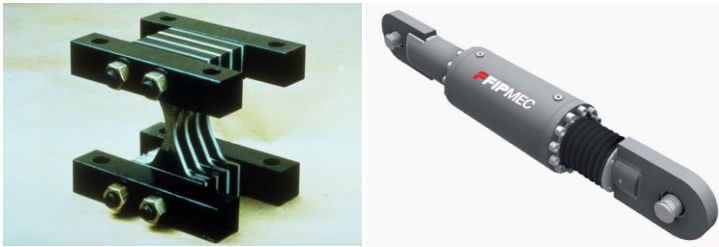


Figure IV.10 - On the left side: picture of ADAS hysteretic devices, one in which the energy dissipation depends on the deformation induced. From [92]. On the right side: example of fluid viscous damper, in which energy dissipation is also dependent on deformation velocity. From [93].

The various dissipation devices can be incorporated into a new lateral force-resisting structure in various configurations. They may be a part of the new system or serve as structural connections between the LFRS and the pre-existence [94] [95] [96]. In other cases, dissipators can be installed directly into an existing structure by designing dissipative bracing systems between two adjacent levels of the building's frame [97], although these applications may present significant disadvantages and limitations (Figure IV.11).



Figure IV.11 - example of retrofitted viscoelastic dampers in bracing configuration. From [93].

In the design of dissipative bracing systems, the deformation capacity of the existing building, the new load configuration after their installation, and the need to reinforce or build new foundations [98] must be assessed. New buildings appositely designed for the installation of these elements have sufficient ductility and deformation capacity to ensure their optimal functioning, and the main structural elements are designed to withstand the generated forces, whereas in existing structures these actions may cause severe structural damage, and the deformation demand on the pre-existing structure may significantly exceed its deformation capacity. Their implementation could also result in a substantial decrease in architectural value. To reduce the visual impact of these solutions, new bracing integrated with displacement-dependent dissipation devices, consisting of yielding steel or aluminium plates, can be added in a variety of configurations (Figure IV.12)

that restrict their installation within the spans of existing RC frames [99] [100] [101]. These dissipators are designed to serve as a controlled yielding fuse dissipating incoming seismic energy while protecting other components.

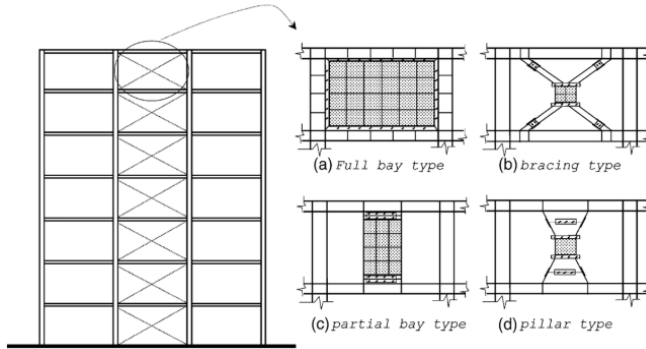


Figure IV.12 - Conventional configurations of steel displacement dependent devices in RC Frames. From [99].

#### 4.2.2. Examples of solutions for masonry buildings

The seismic vulnerability of masonry structures varies greatly based on a variety of endogenous factors. Recent medium- and high-intensity Italian earthquakes have primarily damaged historic structures due to the poor quality of the masonry and the lack of a lateral force-resisting system able to engage a global *box behaviour* for the building, resulting in the widespread onset of local out-of-plane failure mechanisms.

The priority seismic retrofit interventions for these buildings usually involve improving the walls' masonry quality to restore *monolithicity* and reduce their susceptibility to out-of-plane collapse mechanisms. Following the limitation of the most vulnerable mechanisms, a global retrofit of the building is



needed to activate a *box-global*-resistant mechanism. To ensure the activation of the global behaviour, the diaphragms' in-plane capacity and constraint with vertical resistant elements must be carefully assessed. In numerous historic structures, floor and roof diaphragms do not meet the requirements, requiring an intervention.

Depending on the building's structural vulnerability, requirements, and possible restrictions, various retrofitting techniques can be implemented. The different solutions, especially for historic structures, should be subject to a set of requirements or criteria to determine their effectiveness and compliance with recognised preservation principles. Whenever possible, reversible, replaceable, non-intrusive interventions involving minimal impairment and impact on the original structure should be favoured.

#### ***4.2.2.1. Improving the quality of the masonry***

When needed, the improvement of the masonry quality of the walls to restore their *monolithicity (unitarian behaviour)* can be regarded as the preliminary mandatory intervention for both the static and seismic retrofit of the buildings [102] [103]. Traditional methods and tools, as well as compatible materials, can be employed in several techniques for consolidating and improving the capacity of masonry elements with multiple poorly bonded leaves. Through-ties improving the interlocking of the wall leaves and providing confinement (Figure IV.13) [104], local dismantling and reconstruction of deteriorated masonry wall portions (Figure IV.14) [104] and the mortar injection [105] [106] fall into this category.

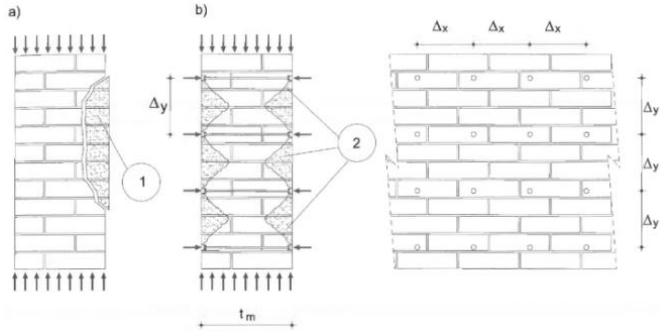


Figure IV.13 - Intramural tying scheme. From [104].

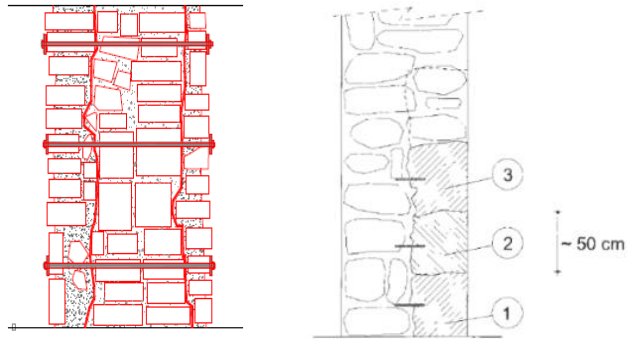


Figure IV.14 - On the left side: Masonry wall section with intramural steel ties. On the right side: Local dismantling and reconstruction example. From [104].

Several techniques that can be used for local reinforcement, however, necessitate the use of *modern* equipment and materials that, in some cases, can pose significant compatibility and reversibility issues. These solutions can involve the external jacketing of the masonry wall with a cast-in-place, high-performance structural plaster or the injection of incompatible mortars. Such an intervention can be applied to either one or both sides of the wall depending on accessibility. Typically, the

structural plaster consists of a thin layer of mortar (lime-based mortar for historic construction, cement based for modern masonry walls) strengthened with high-strength fabrics [107] or fibres [108] [109], whose adherence to the support is improved with thin through ties. When applied on both sides of the wall, these additional layers, together with thin through ties, introduce continuous confinement for the masonry wall, preventing it from disintegrating and increasing the wall's strength and stiffness. These solutions can also improve resistance to out-of-plane seismic actions by delaying the activation of the out-of-plane bending mechanisms.

#### ***4.2.2.2. Inhibition of local mechanisms***

The occurrence of local collapse mechanisms, frequently associated with the out-of-plane overturning of perimeter masonry panels or a significant portion of them (Figure IV.15, Figure IV.16), is typically caused by either the lack of an effective seismic-resistant system (often due to the lack of diaphragms) or the inadequacy of the restraint between the structural portion affected by the mechanism and the seismic-resistant systems [110] [111] [112] [113], consisting of the bearing walls oriented in the direction of the seismic action and seismic-resistant diaphragms. These collapse mechanisms commonly represent the primary vulnerability of the building, as they are triggered by seismic events with a lower intensity than those required to trigger global ones and may cause severe damage also to other elements supported by walls subject to overturning.

In many buildings, especially in historic buildings with original wooden floors, no diaphragm action can be relied upon, provided that the existing wooden planks cannot transfer in-plane shear forces, and the effectiveness of the restraint between

walls and the existing floor is frequently uncertain and determined by the friction between them, unable at inhibiting these mechanisms.

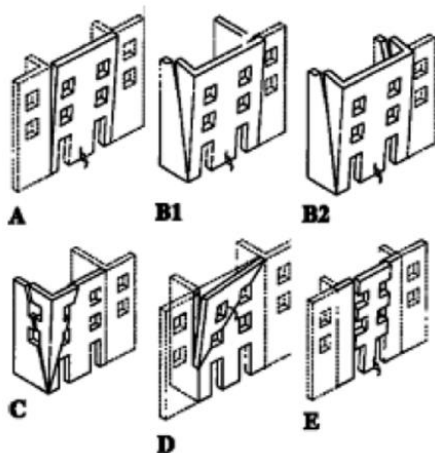


Figure IV.15 - Mechanisms for overturning failures of perimetral walls. From [110].

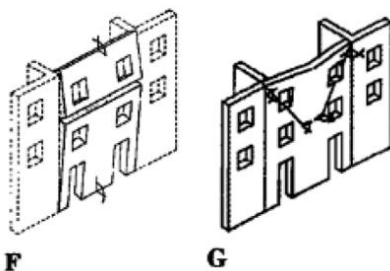


Figure IV.16 - Out-of-plane bending mechanisms of perimeter walls. From [110]

Steel ties, if their effectiveness has been preliminarily ascertained, or floor and roof diaphragms are often adopted to effectively inhibit these mechanisms.

The utilization of a timber strong-back systems [114] [115] [116] stems as a novel approach to preventing the activation of out-of-plane mechanisms, and to potentially enhance the performance of the corresponding elements for in-plane actions. These timber systems, which can be installed within buildings without architectural restrictions, permit the coupling of structural reinforcement with energy efficiency and architectural renovation measures.

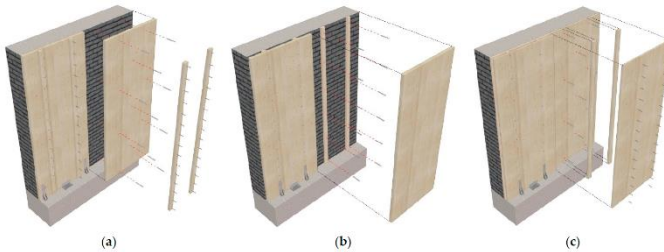


Figure IV.17 - Installation diagram of a strong-back Timber-based hybrid solution: (a) timber panels mounted to the wall and strong-backs applied to the panel surface; (b) strong-backs fixed to the wall and timber panels mounted to the strong-backs; and (c) timber panels linked to the wall and strong-backs and additional panels mounted to the first layer of panels. From [114].

#### **4.2.2.3. Box-Structural behaviour**

Despite the high quality of the materials and the monolithic behaviour of the masonry walls, the lack of a structural system that provides the building with a global *box-like* behaviour can result in severe seismic damage and collapse.

The installation of perimeter and/or vertical steel ties [117] [118] that activate a tied-arch mechanism [119] is one of the primary solutions that can be implemented to induce the activation of the global resisting mechanism and inhibit the activation of local mechanisms (Figure IV.18); the effectiveness of these mechanisms is however compromised by the presence

of slender walls, large wall openings, and chimney pipes within the thickness of the wall.

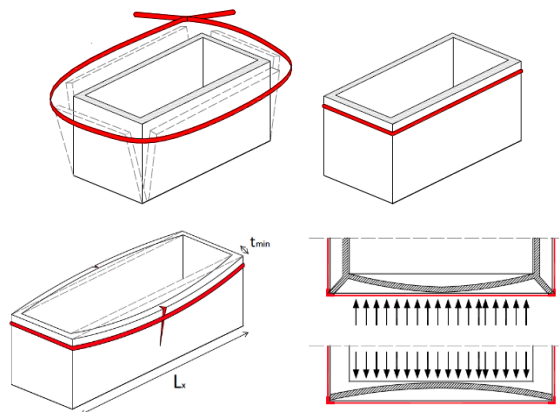


Figure IV.18 - On the top: Scheme of perimetral tying of masonry buildings without roof and/or floor diaphragms. In the bottom: In-plane masonry arch-resistant mechanisms. Representation adapted. From [119].

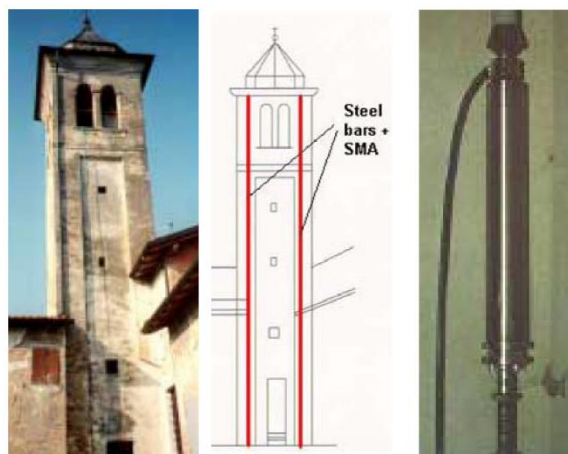


Figure IV.19 - Scheme of the retrofit of the bell tower of the Church of S. Giorgio in Trignano with SMA vertical wires in series with vertical prestressed steel ties. From [117].

Numerous existing floors and roofs are not designed to serve as seismic-resistant diaphragms and are ineffective in preventing out-of-plane wall detachment and overturning of the perimeter walls, especially in historic buildings with wooden floors. To compensate for the deficiencies, various techniques can also be adopted for their retrofit and connection to earthquake-resistant elements, using both *dry* and cast-in-place techniques (Figure IV.20) [25], [120] [113] [121].

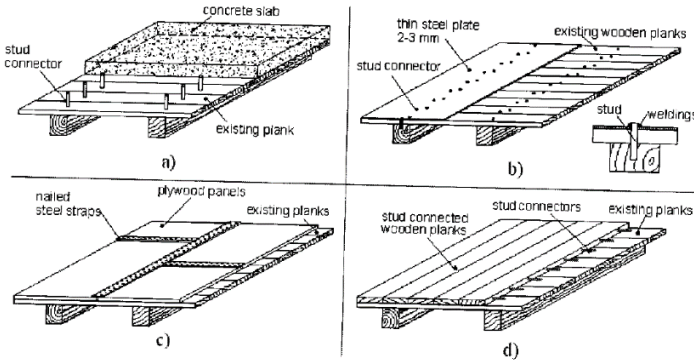


Figure IV.20 - Schematic illustration of wooden floor in-plane shear reinforcement via overlaying a) ordinary thin RC slab; b) thin steel plate; c) nailed plywood panels; and d) stud-connected wooden planks. From [25].

In buildings without horizontal floors, such as churches and theatres, reinforced roof diaphragms connected to the perimeter walls with steel dowels [25] [122] [123] [124] collect and transfer the actions gathered by the diaphragm to the vertical seismic-resistant elements, thereby preventing out-of-plane mechanisms of the transversally loaded walls (Figure IV.21).

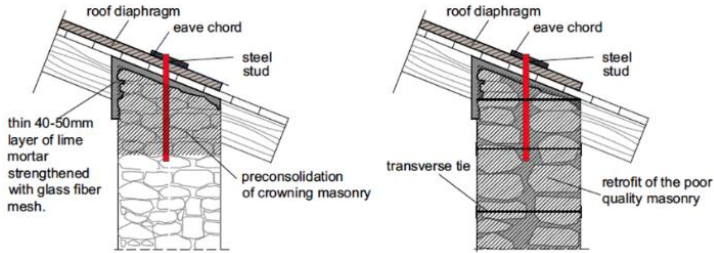


Figure IV.21 - Examples of masonry strengthening and introduction of metal dowels for the connection between masonry and roof diaphragm. From [122]

### 4.2.3. Examples of solutions for precast RC Buildings

In Italy, the majority of low-rise industrial structures built in the past sixty years are prefabricated constructions. Typically, these structures are characterised using primary prefabricated reinforced concrete structural elements and infill elements/cladding panels with no structural function.

Recent earthquakes in northern Italy have revealed the vulnerability and deficiency of these buildings, which were frequently designed and erected during eras in which seismic design recommendations were not part of the standards.

The absence of connections between vertical and horizontal structural elements, as well as the presence of external cladding elements that are inadequately anchored to the main structures, are the primary and most relevant seismic vulnerabilities exhibited by these buildings. Interventions for seismic retrofitting can be generally divided into two types of strategies: local retrofit interventions of individual structural elements and improvement of the structural connections, or global reinforcements with the introduction of new lateral force-resisting structures (LFRS).



In the following, a few representative examples of the numerous solutions that can be adopted for retrofitting precast RC structures are proposed. The interventions are those reported in the recently published retrofitting guidelines [125], which can be referred to for further information.

#### 4.2.3.1. *Improving the connection between elements*

In many cases, the ability of a prefabricated building to withstand seismic loads is jeopardized by the potential loss of support of structural elements, such as beams and roof elements, because of excessive relative displacements.

Several local interventions can be implemented to improve beam-column structural connections. Some include extending the base of the beam's support on the column while retaining the original sliding supports so as not to alter the original structural design. While others involve the addition of new mechanical connection devices between the two elements, consisting of steel bolted plates or connecting ropes that mutually constrain the elements (Figure IV.22), or energy dissipation devices designed to concentrate the damage while maintaining the column and beam's structural integrity (Figure IV.23).

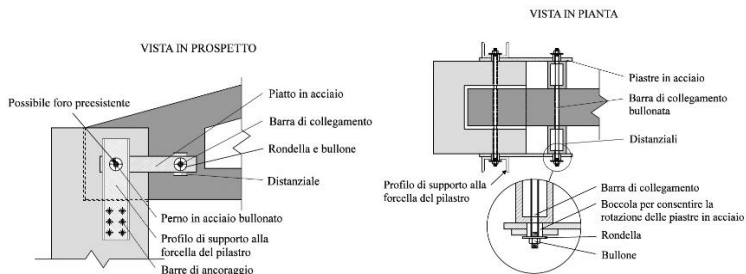


Figure IV.22 - On the left-side: representation of a beam-to-column connection improved by introducing a steel bolted plate. From [125].

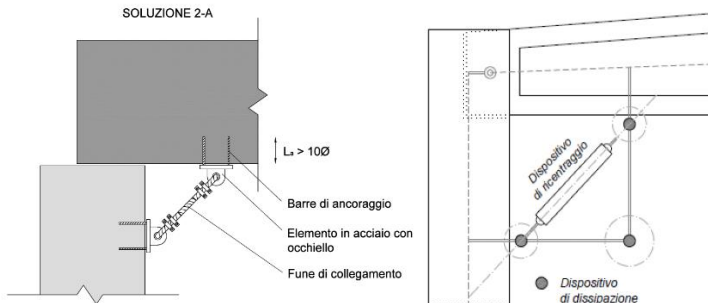


Figure IV.23 - On the left-side: representation of a beam-to-column connection reinforced by introducing a steel connecting rope. On the left-side: conceptual representation of the same structural joint reinforced by introducing an energy dissipation device coupled with a re-centring element able to limit residual displacement. From [125].

The same connection types used to improve the column-beam connection can also be used to enhance the beam-roof element connection. The introduction of new mechanical connection devices between these two elements, either rigid or dissipative, enables the limitation or elimination of their relative displacements. Introducing dissipative devices also reduces the building's displacement demand by dissipating a portion of the introduced seismic energy.

Another important vulnerability is frequently related to the failure of the structural connections between the external cladding panels and the RC structure resulting in the out-of-plane overturning of these elements, not designed to withstand seismic actions. Several intervention strategies and solutions can be adopted for the mitigation of this vulnerability. They can be divided into those solutions that only prevent out-of-plane overturning through the introduction of new structural connections resistant to seismic actions, designed not to alter the original static scheme of the structure, and those that, in addition to preventing overturning, take advantage of the resistance

resources offered by these elements due to the proper connection with the RC structure, thereby modifying the structure's original static design [15].

#### ***4.2.3.2. Global intervention - introduction of the new LFRS***

For the implementation of global retrofit interventions (Lateral Force Resisting System, LFRS) consisting of new earthquake-resistant systems, several techniques and solutions are available.

The same solutions involving the use of steel bracing/strengthening systems [79] [97] [101] that were analysed in the previous section on the global retrofitting of RC buildings, Paragraph 4.2.1.2, can be adapted for the reinforcement of precast structures. Recently, several authors [15] have proposed a novel approach, examined in detail in the following chapters, for the development of external resisting systems involving the use of exoskeletons in close proximity to and constrained to the building's facades, integrated into a solution able to simultaneously pursue energy and architectural renovation (Figure IV.24).

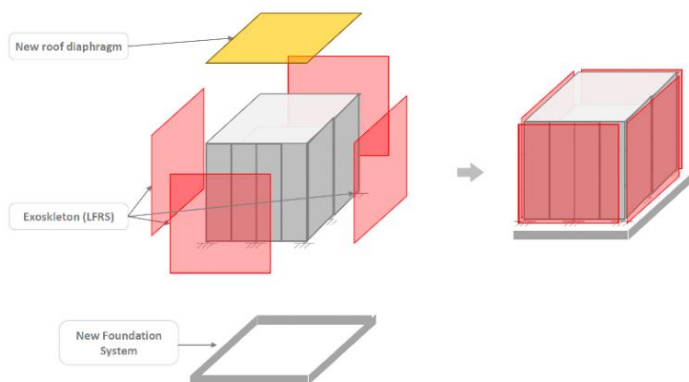


Figure IV.24 - Conceptual representation of the new system for the global retrofitting of precast RC building developed by some authors [15], which includes the introduction of a new external exoskeleton (in red) and a new covering diaphragm (in yellow).

As with the previously analysed building types, the seismic resistance of existing *unengineered* floors, which are frequently present only at the roof level, must be carefully evaluated, by paying special attention to the design of the connection systems with the existing building, which is necessary to transfer the seismic actions to the new LFRS. Frequently, this diaphragm is composed of isolated precast RC elements in simple contact or connected with steel dowels to the beams below, which restricts its seismic load-resistant capacity.

For the reinforcement of these crucial structural components, different techniques are available, including cast-in-place and dry solutions. The dry solutions include those analysed above for the reinforcement of existing floors in masonry buildings [25], which can be implemented using various technologies and structural materials, entailing the construction of an additional roof diaphragm above the existing one appropriately connected to both the existing one and to the new LFRS [15].

### **4.3. New trends in seismic retrofit and introduction to integrated interventions**

In recent years, new challenges have been posed to structural engineers; the emerging deficiencies in our buildings and societal requirements necessitate an intensive design effort to create new high-performance retrofit systems that protect our heritage, also integrable into solutions able to pursue simultaneously the energy and architectural renovation.

Promoting holistic building stock renovation is crucial to achieving a climate-neutral European Union by 2050 [10]. To attain the targets of energy efficiency, structural safety, and architectural renovation for European buildings, life cycle thinking, and circular economy principles must be incorporated from the initial phase of the interventions.

The potential impacts of applying ten strategic actions proposed by the European Environment Agency [126] for an efficient renovation of the built environment are presented in Figure 20. Efficient renovation is pursued by incorporating circular economy principles directly into the design of retrofit systems. Below, a *baseline* scenario assumes the continuation of current renovation rates and activities, separated into energy and non-energy renovations, until 2050, based on the available literature. A second *policy-compliant* scenario accelerates the rate of renovation in accordance with the EU ambitions. In a third, more *ambitious* scenario, renovations are accelerated so that the entire stock of buildings is renovated by 2050. The main limitations of the modelling proposed by the European agency stem from the sectorial nature of the analysis, which focuses solely on the technical aspects of the proposed solutions without considering the socioeconomic aspects of large-scale actions,

such as funding and incentive needs, required skills, people's priorities, or economic costs.

The first actions proposed in the documents are those that increase the service life of the building. In the following illustration, potential material and greenhouse gas savings are shown by favouring renovation measures (Figure IV.25).

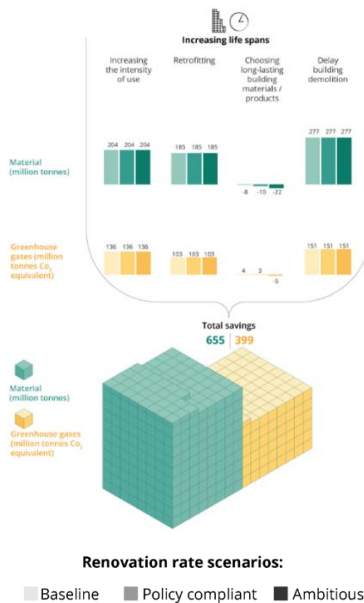


Figure IV.25 - Effects of building life span extension in terms of materials used and GHG emissions, estimated from now until 2050. From [126].

Extending the service life of the buildings reduces the demand for brand-new, *resource- and climate-intensive* construction, whereas investing in long-lasting materials presents challenges that must be carefully considered. The baseline scenario indicates a high net material consumption and cost in terms of

greenhouse gas emissions. This is because the production of the most durable materials results in a greater amount of greenhouse gases being released into the atmosphere. Nevertheless, this practice will aid in the preservation of natural resources because fewer replacements will be required in the future.

The selection of recycled products and the concept of solutions that comply with the design for disassembly principles should be encouraged during the conceptual design phase (Figure IV.26).

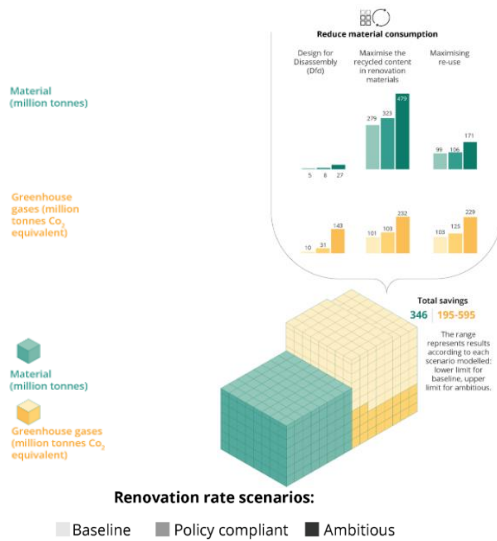


Figure IV.26 - Effects of the reduction of material consumption materials usage and GHG emissions, estimated from now until 2050. Adapted from [126].

The future reuse of the components, refitted in further interventions, will significantly reduce the demand for raw materials. In this perspective, different strategies should be adopted to optimise the reuse of systems, for example by

enabling easy selective removal and replacement of damaged or obsolete parts, while preserving the integrity and re-usability of other components.

In addition, according to a European study, the use of prefabricated facades in renovations, including finishing and insulation, results in average material savings of about 25% compared to non-prefabricated alternatives. In accordance with these actions, bio-based materials and products should be favoured whenever possible (Figure IV.27).

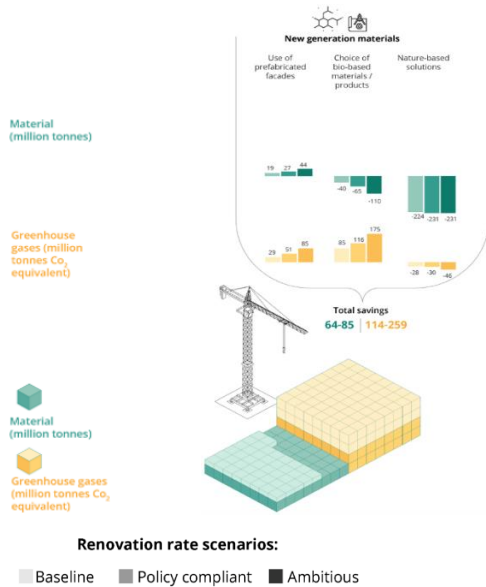


Figure IV.27 - effects of the employment of new generation materials on material consumption and greenhouse gas emissions, estimated from now until 2050. Adapted from [126].

Buildings play a crucial role in the climate and circular economy strategies of the European Union. Climate neutrality requires not only the reduction of the energy consumption of buildings



and the decarbonization of the used energy source but also the reduction of emissions from a life-cycle perspective.

Limiting the adoption of circular economy principles to the design of new buildings would not produce immediate benefits, but these would be realised over decades. To observe them in the short term, we also need to focus on increasing the lifespan of our building stock by renovating it in a holistic, efficient, and sustainable way.

#### **4.4. Examples of integrated and holistic retrofit interventions**

There have been numerous examples of urban and building renovations in Europe over the years, but few of them targeted the reduction of static or seismic structural vulnerabilities, and a restricted minority tried to tackle the multifaceted need of the buildings. The first exceptions to the widespread uncoupled solutions were those interventions coupling architectural and energy upgrading. Among such interventions, only a minority was conceived with a circular economy and life cycle approach. To demonstrate the effectiveness of holistic interventions from an urban, architectural, structural, and energy efficiency perspective, a selection of significant European examples of integrated solutions is provided below.

##### **4.4.1. *Integrated energy and architectural solutions***

The first European examples of external interventions with an integrated approach to energy and architectural refurbishment can be divided into *camouflage* and *remodelage* interventions. The former encompasses those interventions that aim at preserving the volumetric and internal layout and entail the application of a new technological layer; while the latter are

those that also propose a renewal of the volumetric and architectural composition.

*Camouflage interventions* usually involved applying external layered envelopes to the facades to improve energy efficiency and architectural value. This initiative typically entails the minimal intervention needed to bring existing buildings up to new energy standards, as recently incentivized by public funding. In contrast, the *remodelage* intervention is more intrusive because it involves reshaping part or all of the building to improve its performance, diversify housing types, and redesign common areas [127] These interventions are often part of larger urban redevelopment projects for neighbourhoods, with the building intervention as a subset [128].

Medium-rise multifamily dwellings are the focus of the case studies examined. These buildings were typically constructed in the decades after World War II in the suburbs and were frequently in a poor state of preservation when renovation projects were initiated. The primary objective of all these initiatives was to upgrade the performance of the buildings by modernising the technological systems and providing the occupants with new, environmentally friendly living spaces.

Several European countries initiated sustainable social housing redevelopment projects in the 1980s [129] [130] [131] [132] [133].

These early prototypical interventions were frequently incorporated into community-based renovations that included the creation of new shared spaces and green pathways, combining energy rehabilitation with urban and architectural restyling through double-skin solutions [8] or selective demolitions and additions.

Stefan Forster's 1996–1999 renovation of Germany's Leinefelde-Thüringen neighbourhood (Figure IV.28). offers interesting architectural lessons [134] and suggestions.



Figure IV.28 - On the left side: principal façade of the pre-existing buildings in the Leinefelde-Thüringen neighbourhood before renovation. On the right side: Render of the same façade after the intervention designed by Stefan Forster. From [134].

In this project, the residential units were combined to create garden-facing, energy-efficient duplexes. The existing loggias were converted into solar greenhouses, and the living spaces were expanded with the addition of new balconies along the facades. These new elements are supported by a new steel exoskeleton placed on its own foundation in close proximity to the façade; this additional structure was conceived to withstand the static loads only; but later enhancement of the solution proved the possibility to conceive such structures to seismically upgrade a variety of buildings in earthquake-prone areas [12].

The 2005 winner of the Paris Habitat Office for Public Housing renovation competition for a high-rise building was another intriguing example of the integration of different energy and architectural renovation solutions. The initial intention of the public administration was to demolish the large residential *Bois-Le-Prêtre* tower and replace it with a new one. However, the winning team led by Frédéric Druot and Lacaton & Vassal

Architects proposed an alternative solution in response to the emerging economic situation [135].

The existing 16-story building was designed in 1959 and renovated in 1990 with the adoption of an additional insulation layer on the facade to meet new technical requirements, but this reduced the size of the windows, thereby deteriorating the living conditions (Figure IV.29).



Figure IV.29 - On the left side: photo of the main façade at the end of construction, taken by the designer Raymond Lopez in 1959. On the right side: photo of the same façade after the first energy-efficient renovation, taken in 1990. From [135].

The architects demolished and rebuilt the facades introducing large glass panels so that residents could enjoy the Parisian urban landscape and enhance their living conditions. The project also renovated the apartments and added a three-meter-wide steel structure to the perimeter without relocating the residents. The addition produced a two-meter winter garden and a one-meter outdoor balcony (Figure IV.30). Despite far from the designers' intention, the additional steel exoskeleton could have

also served as a reinforcement system for this building and structural type.



Figure IV.30 - Render of the main façade after the renovation designed by Frédéric Druot and Lacaton & Vassal Architects. From [135].

This solution demonstrates the viability of effectively integrating structural reinforcement with architectural renovation and energy efficiency in high-rise buildings.

Following these precedents, other authors started to use external structural systems in integrated renovation solutions.

The project proposed in the research project *SuRE-FIT: Sustainable Roof Extension Retrofit for High-Rise Social Housing in Europe*, developed from 2006 to 2008 under the 6th Framework Programme [136] is another fascinating case study of energy refurbishment and architectural renovation, that offers interesting insights for the potential integration of the structural retrofitting system into renovation solutions (Figure IV.31). The proposed project entails the energy upgrading of a 4-storey

residential building from 1983, the removal of existing architectural barriers, and the addition of a few storeys to be placed on top of a self-supporting steel and timber exoskeleton supported by its own foundations (Figure IV.32). The expansion of interior spaces and the creation of new apartments, which can be accomplished by utilising the potential offered by exoskeletons, can be an interesting economic driver for these projects.



Figure IV.31 - On the top: main façade of the pre-existing buildings before renovation. In the bottom: the same facade after the intervention. From [136].



Figure IV.32 - Three-dimensional representation of the intervention concept: 1) existing building; 2) new staircase; 3) new slab above the existing building; 4) structural steel frames; 5) new timber apartments; 6) new common spaces and services; 7) "Small boxes" of volume extension in the façade. From [136].

#### **4.4.2. *Integrated structural, energy, and architectural solutions***

According to the author's knowledge, few research activities have focused on the study of external solutions capable of pursuing the seismic, energy, and architectural upgrading of existing buildings holistically.

One of the first interventions using this approach was carried out on an existing building in Japan (Figure IV.33). The intervention is acknowledged as a pioneering project for its time [137]. The 2009 intervention designed by Takeuchi, Yasuda, and Iwata was intended as the first example of holistic renovation in eastern Asia. The intervention entails the renovation of a 40-year-old building from seismic, energy, and architectural perspectives. The solution conceived by the designers for the building's structural retrofit encompassed the

installation of passive devices to dissipate seismic energy, namely Buckling Restrained Braces (BRBs), constrained to the perimeter ring beams of the building. This system has been incorporated into an *integrated facade* capable of simultaneously enhancing the building's energy efficiency and renovating its exterior.



Figure IV.33 - Midorigaoka 1<sup>st</sup> Building, Tokyo Institute of Technology: retrofitted building façade. From [137].

A new technological layer was incorporated directly between the elements of the structural reinforcement to increase its energy efficiency, consisting of glass panels installed at each floor's base and louvres installed at the top. In conceiving this intervention, the designers took the needs of the users into account by opting for a solution that could be implemented entirely from the outside, but without fully integrating the principles of life cycle thinking and the circular economy. During the nine-month-long renovation work, occupancy dropped to approximately 60%.



Other researchers have recently taken an interest in these topics. In past years, the AdESA system, a global solution for the integrated and holistic renovation of existing buildings, was proposed. This innovative system was developed by a joint consortium of industrial SMEs and research institutions, and first applied for the holistic retrofit of a precast gym hall built in the 80s [15] and more recently for the renovation of a masonry residential building erected in the 50s (Figure IV.34).



Figure IV.34 - on the left side: picture of the building's secondary façade before the start of the construction site, shot by the author. On the right side: render of the same façade after the renovation. From [138].

The AdESA system, whose application to the two case study buildings will be examined in detail in Chapters VIII and IX, demonstrates the potential of these *double skin* exoskeletons. This Innovative layered shell is composed of a structural layer made of cross laminated timber panels (Figure IV.35), thermal insulation layer for the energy efficiency improvement, and cladding finishing layer for the architectural restyling, all of which are implemented in a dry, modular, and flexible exoskeleton.



Figure IV.35 - picture of the installation of the structural layer in cross laminated timber panels, shot by the author.

Prioritizing eco-efficiency, safety, and resiliency, these solutions are founded on the Life Cycle Thinking principles that aim to reduce the environmental impact of the building from the moment of its conception until its dismissal. Using macro-prefabricated dry-assembled components and standardised connections, they are designed to be easily assembled and disassembled and to permit components to be reused or recycled at the end of their service lives. By introducing sacrificial, replaceable elements lumping and minimizing damage, it is possible to limit the amount of damage caused by a seismic event.

#### **4.5. Research Needs**

The approach and practices of the construction industry should evolve in response to ecological and social needs and challenges. Accelerating the transition to a circular economy should be a main priority, and this should be accomplished by extending the lifespan of existing structures, materials, and building systems. In this scenario, holistic renovation initiatives offer the greatest potential by overcoming certain renovation limitations and barriers inherent to *traditional* solutions that are still widely used. The application of circular economy principles and the adoption of Life Cycle Thinking throughout the entire process can significantly reduce their environmental impact and facilitate their implementation, but the effective application of these solutions requires raising structural standards, defining new design targets and adopting retrofit optimisation strategies that minimise structural damage resulting from seismic events and ensuring the demountability and reusability of its components.

## V. Novel structural performances and design approaches

### 5.1. Introduction

As mentioned in the previous chapters, the current global climate emergency and the ambitious European targets necessitate new strategies and approaches for both the structural design of new buildings and the retrofit solutions. These novel strategies must prioritise the safe extension of the building's service life, the reduction of the environmental impacts and the conscious management of the carbon embedded in building materials. In this scenario, *structural engineers* have the pivotal role of conceiving solutions that foster the transition to a sustainable built environment, combining safety and resilience with eco-efficiency and cost-effectiveness.

Achieving these objectives will largely rely on the systematic renovation of the existing building stock, which should be accomplished by fostering holistic, high-performance interventions that address the construction multifaceted needs. The accomplishment of these aims requires the expansion of the concept of *life cycle Structural Engineering*, attained by integrating the Life Cycle Thinking and circular economy principles and adopting the multi-criteria performance-based structural design. In this perspective, it is necessary to redefine structural standards and performance requirements that solutions should meet for the duration of their life cycle.

The combined application of all these novel approaches necessitates the development of new tools and frameworks for managing the resulting complexity and identifying the optimal

solution that ensures the target performance while minimising costs and environmental impacts.

## **5.2. Extension of the Life Cycle Structural Engineering concept**

Researchers have recently focused on incorporating the Life Cycle Thinking (LCT) approach and the concept of holistic solutions into structural engineering practices to define novel performance targets and design approaches that meet emerging needs.

The Safesust Roadmap [11] first expanded the concept of sustainable renovation to contextually include eco-efficiency, safety, and resilience, and recently the European Commission proposed the Level(s) framework [139] to promote the design and construction of sustainable buildings by taking the life cycle thinking and circular approach into account, but without focusing on the crucial aspect of structural safety. Both frameworks acknowledge the importance of structural engineering, but they lack a common methodology and tools for effectively translating their leading principles into the structural design. To overcome these limitations, *traditional* methods and approaches of structural engineering need to be revised and expanded.

In 2011, Cost Action C25 [140] introduced the concept of *Life-time Structural Engineering*, adding some novel performance targets for the design of new buildings and retrofits. This new concept supports the design of buildings that include eco-efficiency, durability, ease of maintenance and deconstruction, but does not provide tools or indicators for implementing LCT and fails to consider interactions between various maintenance interventions. Recent research [12] [19] has expanded and

redefined the concept of *Life Cycle Structural engineering* to present a broader perspective on the topic that attempts to effectively combine eco-efficiency and cost-effectiveness with structural safety and resilience in retrofits, thus overcoming the main obstacles. These studies once again highlighted the significance of renovating the existing building stock by adopting an integrated approach and provided guidelines that promote the adoption of incremental rehabilitation, to be pursued by working exclusively from the outside, and introduced additional new design principles and objectives, including:

- “Design for eco-efficiency”, which fosters the adoption of low environmental-impacting materials, possibly from the circular economy, as to reduce raw resources depletion, waste, and pollution;
- “Reparability” for the retrofit components, to effectively reduce damage, losses and the resulting environmental impacts generated by frequent seismic events and to ensure structural safety during extreme ones, pursued by introducing repairable/replaceable systems capable of concentrating structural damage;
- “Ease of maintenance and adaptivity to future needs” to contain costs/impacts and obsolescence rate in the use phase;
- “Design for dismantling” and for easy recycling and reusing of the different systems that compose the solution favouring the selection of dry techniques using standard and prefabricated connections and components, resulting in a reduction of waste generated by construction and demolition.

- “Durability” that enables effective sustainability of a solution throughout its entire life cycle by preventing deterioration.

Consequently, the extension and integration of *Life Cycle Structural Engineering* influence structural design at all stages, from the conceptual design phase, leading to new structural configurations, to design development and construction document phases, fostering the adoption of new design paradigms and tools, as well as novel solution sets and detailing are necessary.

### **5.3. Multi-Criteria Performance-Based Approach and novel structural targets**

Recent earthquakes in Italy have highlighted the necessity for innovative strategies and higher more demanding structural standards to improve the performances of both new construction systems and retrofit solutions. To achieve the design objectives and incorporate the principles of the *extended* life cycle structural engineering, it is necessary to *raise the bar* from the concept of *minimum* structural performance standards required by current regulations [141], by shifting the targeted goals from the commonly accepted *Life-Safety level* to the more demanding *damage-control* level [142].

In this perspective, recent research [6] has highlighted the need to promote the structural retrofitting of the building stock by showing the significant environmental and social-economic impacts associated with seismic risk and the potential need for extensive repair and reconstruction following earthquakes (Figure V.1). Projected at neighbourhood and urban scale, the findings of these studies become more alarming since structural vulnerabilities or inadequate structural retrofitting of entire

communities might compromise the efficacy of energy-saving measures with high economic costs.

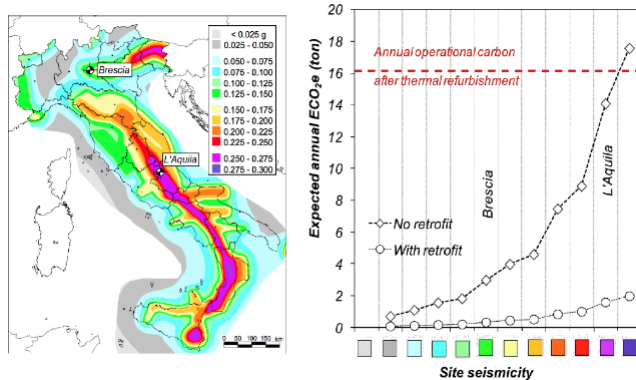


Figure V.1 - On the left is the seismicity of the Italian site with a comparison of the expected annual equivalent  $\text{CO}_2\text{e}$  emissions of unretrofitted versus retrofitted buildings at each site seismicity. From [6].

To reduce the costs and impacts of retrofitted systems over their extended service life, it is also essential to develop structural solutions mitigating the effects of both severe and frequent seismic events (Figure V.2), minimizing the damage to the pre-existing structure and concentrating the structural damage on easily repairable or replaceable (*fuse-like*) elements.



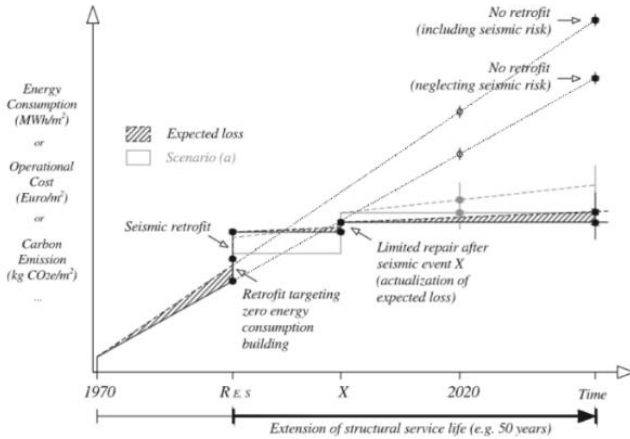


Figure V.2 - Impact of energy consumption, operating costs, and carbon emissions during the building life cycle for integrated energy and seismic retrofits. From [6].

To meet the new requirements, several concepts of Performance-Based Earthquake Engineering must be refined. According to some authors [142], the matrix of seismic performance design objectives established by SEAOC Vision 2000 [143] should be reconfigured (Figure V.3) to better match the requirements, with the basic-objective curve shifted toward a *damage-control* approach.



Figure V.3 - Rearrangement of the Seismic Performance Design Objective Matrix defined by the SEAOC Vision 2000 PBSE guidelines to match building tagging, and modification of the *basic objective* curve towards a *damage-control* approach (blue line). From [142].

Adopting a multi-criteria performance-based approach [144] from the early stages of the conceptual phase through the end-of-life phase enables the effective minimisation of losses, providing control and damage limitation of primary and secondary structural elements, non-structural elements, foundation systems, and equipment (Figure V.4). This novel approach requires the adoption of new performance objectives and targets, such as:

- Limiting the maximum interstorey drift for *displacement-sensitive* components to avoid damage to structural and non-structural elements, infills, thermal panels, windows, installations, etc.
- Limiting the maximum floor acceleration to ensure the integrity of *acceleration-sensitive* components, thereby

avoiding damage to floor diaphragms, equipment, and various sensitive non-structural components. Limiting the maximum stress in the stairwell to ensure the safe exit of occupants.

- Introducing *fuse* and *energy dissipative* elements and components lumping the damage generated by severe seismic events.
- Minimizing the residual displacements, which are key in determining the post-earthquake reparability of the structures and therefore affect the economic losses from earthquakes.
- Ensure the activation of a ductile resistant mechanism for both the existing building and the retrofit system during exceptional and unforeseeable seismic events.

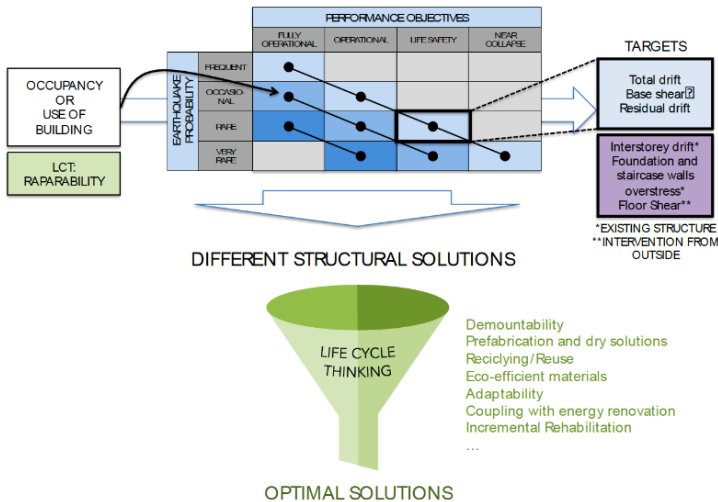


Figure V.4 - Schematic representation of the new multi-criteria performance-based design strategy. From [144].

Even though numerous approaches and strategies have been examined and developed in the last decades, the correlation between the direct and indirect costs generated by seismic events throughout a building's life cycle and measurable and tangible structural design parameters is *not well defined* [145]. To meet the novel structural requirements, the solutions developed and analysed in this study incorporate the principles of *extended Life Cycle Structural Engineering* adopting *challenging* structural objectives and targets, described above and *qualitatively represented* below in the rearranged *SEAOC Vision 2000* matrix of seismic performance design objectives (Figure V.5). Adopting this stringent standard prevent damage for more frequent seismic events by guaranteeing high-performance levels and *full building operability up to rare seismic events*, while *life-safety is ensured for even more rare events* with longer return times by activating ductile and dissipative resistant mechanisms for both existing building and retrofit system.

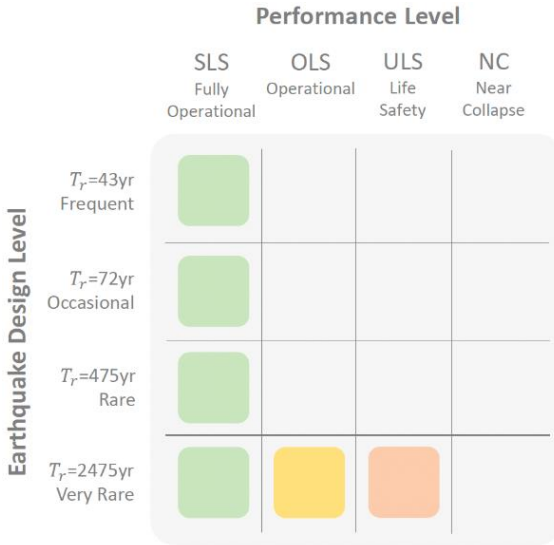


Figure V.5 - Revision of the matrix of Seismic Performance Design Objective established by the SEAOC Vision 2000 PBSE guidelines to meet the requirements of multi-criteria performance-based design.

### 5.4. Introduction to novel design frameworks for sustainable retrofits

Early approaches to integrating sustainability principles into the concept of retrofits were limited to assessing their compliance with the principles of sustainability and circular economy, with *ex post* life cycle tools and assessment typically used to calculate only costs and carbon emissions, often considering a cradle-to-gate timeframe.

In the last decade, an increasing number of studies have focused on methods and operational tools to improve the sustainability of buildings and retrofits, by contextually enforcing eco-efficiency, safety, and resilience. In this context, some

researchers have proposed novel conceptual design approaches for the design of new sustainable solutions and techniques, while others have developed decision-making tools to select the most sustainable solutions [19] based on their compliance with the three pillars of sustainability: economic, environmental, and social. However, few of these tools were designed with the LCT principles and all three pillars of sustainability, also accounting for safety and resilience, thus potentially resulting in sectoral, or decoupled solutions. To demonstrate the complexity of retrofitting when energy and structural issues are considered together, some authors [146] examined the literature on available tools, international sustainability protocols, and ad-hoc methods for the combined assessment of seismic safety and energy efficiency of buildings, highlighting their limitations and the need for additional research.

More recently, some authors [19] [147] proposed a novel LCT-based framework that can be addressed for the design of integrated sustainable deep renovation interventions (SBR). Such works proposed an inversion of the *traditional workflow* by introducing the principles of LCT at the beginning of the design process. This four-stage framework (Figure V.6) is intended to serve as both a pre-design assessment tool and a post-design comparative evaluation tool, based on the current Multi-Criteria Performance-Based design method.

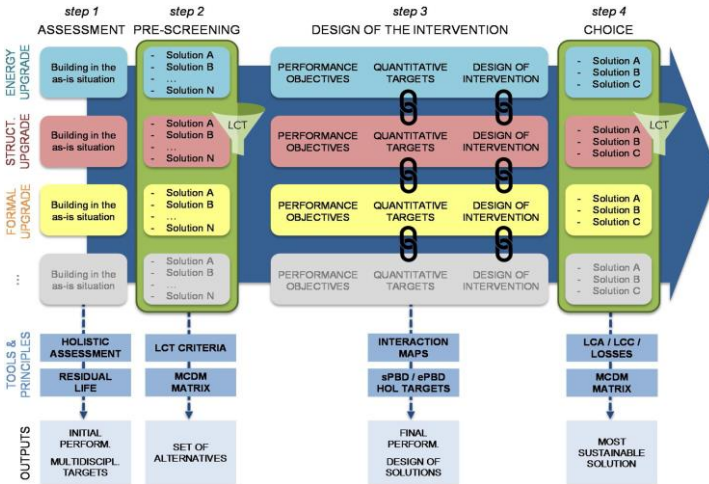


Figure V.6 - Framework for Sustainable Building Renovation Design. From [19].

The first step in the process entails evaluating the building's current situation and deficiencies in all *relevant areas*, including structural, energy, and architectural issues. This allows for the identification of the primary needs of the building from a holistic and multidisciplinary perspective, leading to the selection of the minimum performance objectives to be pursued in the renovation process.

After the assessment of the building in the *as-is condition*, the framework provides the *pre-screening* of potential eligible alternative solutions. According to the SBR approach, the suitability of potential structural, energy-related, or integrated solutions is determined by analysing their specific characteristics in relation to a set of requirements and constraints derived from the building's multiple needs, Life Cycle Thinking principles, and potential renovation obstacles. To accomplish this, a qualitative multi-criteria decision-making

can be adopted, in which the relevance of each criterion is determined based on the priorities indicated by owners and stakeholders, minimum performance targets, and national or international regulations. By comparing different solutions based on *qualitative estimates* rather than quantitative analyses, designers and decision-makers can quickly select the best set of alternatives and discard the unsuitable ones (Figure V.7).

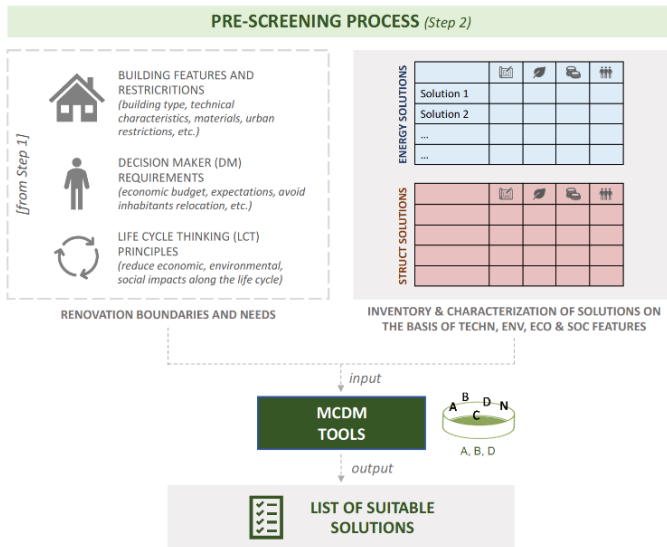


Figure V.7 - Workflow of the pre-screening procedure used to determine the best strategies. From [147].

In the third step, the design of iso-performance solutions derived from those identified in the previous phase follows the principles and guidelines outlined by performance-based multi-criteria design from a multidisciplinary and holistic perspective. Contrary to *conventional processes*, this framework requires the incorporation of LCT principles from the outset, compliance



with *stringent* pre-defined structural standards, and the analysis of potential interferences and limitations imposed by the integration of the structural retrofit with other interventions required to tackle the multifaceted needs of the building (particularly interferences with architectural restyling and energy amelioration measures). To accurately compare alternatives, the solutions defined at the conclusion of this phase must ensure that the retrofitted building achieves the same performance levels.

In the final step, the optimal retrofit option is chosen based on a multi-criteria comparative evaluation of solutions throughout the building's life cycle. To assess the environmental, economic, and social impacts associated with each solution at each stage of the building's life cycle, probabilistic Life Cycle Assessment and *expanded* Life Cycle Cost procedures should be adopted, considering losses caused by natural hazards, such as earthquakes, and the *expanded* Expected Annual Loss analyses should be conducted, taking into account damages to non-structural elements and indirect losses. To facilitate evaluation by various actors, the impacts and performance of each solution should be converted into synthetic indicators, with a weight assigned to each parameter, and the best solution should be determined by ranking the selected suitable alternatives (Figure V.8).

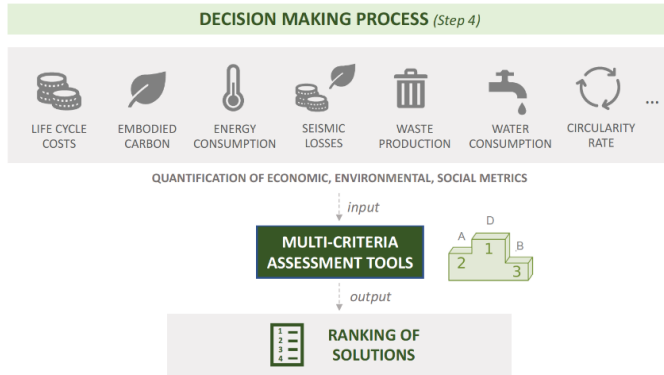


Figure V.8 - Flowchart of the decision-making procedure for selecting the optimal retrofitting option. From [147].

## 5.5. Qualitative evaluation and pre-screening of the main structural retrofitting strategies

Numerous structural retrofit strategies have been conceived and implemented for the different structural systems and building types characterizing the Italian construction heritage. This section provides a *qualitative analysis* from a structural perspective of their potential and limitations in relation to the stringent performance standards and objectives imposed by the adoption of the previously defined *extended* multi-criteria performance-based design approach.

Understanding and analysing the structural behaviour and effects of implementing different strategies are relevant prerequisites for evaluating alternative solutions. The following Figure V.9 is an effective conceptual representation of the structural behaviour of RC buildings retrofitted by implementing the main strategies proposed in the literature,

represented within an Acceleration-Displacement Response Spectrum domain [148].

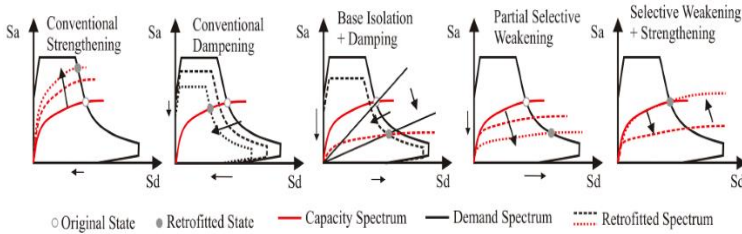


Figure V.9 - Acceleration-Displacement Response Spectrum diagrams illustrating various retrofit strategies, from left to right: a) strengthening; b) conventional damping; c) base isolation plus damping; d) partial selective weakening only; e) selective weakening plus strengthening. From [148].

One of the most widely employed strategies is the conventional global reinforcement, implementable using a variety of techniques and technologies including those described in Chapter IV. This approach entails a major increase of the stiffness of the retrofitted building and thus involves increasing the accelerations experienced by the reinforced system while decreasing the displacements, and thus the drifts, caused by seismic events of any magnitude, without introducing additional damping. The limitation of displacements and drifts for frequent seismic events effectively reduces damage and associated environmental and economic costs over their extended life cycle. For very rare seismic events, the increase in accelerations experienced by the existing structure may result in a significant increment of dynamic loads in *acceleration-sensitive* elements, such as floor diaphragms, stairwells, and installations, which might require significant local interventions. The overstrength of the new lateral force-resisting system conceived by applying this strategy may necessitate the design of elements with high resistance and stiffness and solid foundations.

The implementation of various active and passive dissipative devices [88] makes it possible to simultaneously reduce and limit the displacement and accelerations experienced by the reinforced system during earthquakes by introducing additional damping. The effectiveness of these devices depends on the characteristics and limitations of the existing structure. The installation of passive devices, either with *deformation-* or *velocity-dependent* energy dissipation [91], in an existing structure designed for gravitational loads requires the existing elements to endure quite *challenging* deformation and to resist the actions generated by these additional elements, with possible damage to structural and non-structural elements, resulting in significant environmental and repair costs even in the case of frequent seismic events. To enable optimal energy dissipation, preliminary local interventions may be required to increase the strength and deformation capacity of the existing elements.

Base isolation can reduce the accelerations experienced by the existing building, concentrating the displacement demand on the new additional systems; displacements can be effectively reduced through the integration of a dissipative system. Frequently, the application of these systems concentrates the intervention on an existing building, which consists of the installation of the selected insulation devices and the operation required for their installation, in structural elements and non-structural elements located in the lower structural portions of the building, thereby limiting the invasiveness on the other components and levels. The application of these systems permits the significant reduction of damage caused by seismic events and the resulting impacts over the building's extended life span. However, the implementation of these systems necessitates a detailed analysis of their compatibility with architectural and plant system components.

Selective weakening is a retrofit strategy that was originally conceived to improve the deformation capacity and ductility of RC frames to accommodate the displacements required by seismic events, while simultaneously reducing the experienced accelerations. This strategy involves the selective weakening of either the primary structural elements [148] to achieve a ductile failure mechanism and reduce the building's stiffness, or the secondary elements through local interventions [86], such as limiting or modifying the interaction between the RC frame and the secondary elements. The reduction of the displacement demand and the limitation of the resulting damage caused by seismic events can be accomplished by introducing an additional conventional strengthening system that allows the preservation of the deformation capacity, obtained upon completion of the selective weakening, at the expense of higher accelerations. The adoption of this strategy may necessitate the implementation of quite invasive interventions, requiring partial demolition of the finishes, which may require building downtime and generate significant economic and environmental impacts.

Each of the evaluated retrofit strategies has distinct benefits and drawbacks that should be evaluated during the *qualitative pre-screening* phase. For an accurate assessment of their suitability and effectiveness, a comprehensive preliminary evaluation of the building's potential structural limitations and vulnerabilities is required.

## 5.6. Research Needs

The pursuit of the European goals necessitates the adoption of new and innovative approaches, strategies, and tools for both the design of new buildings and, most importantly, for the implementation of efficient, sustainable, and high-performance retrofit solutions.

For their proper design, it is necessary to introduce and develop new design spectra and *measurable and tangible* design tools to control and limit damage to structural and non-structural components and to reduce direct and indirect losses and impacts resulting from earthquakes of varying magnitudes.

Meeting the stringent structural performance objectives and design targets introduced by the adoption of the *extended* multi-criteria performance design approach requires the development of innovative structural solution sets that, beginning with the re-engineering of conventional systems, integrate their strengths and overcome their limitations.

## VI. Adaptive exoskeletons

### 6.1. Brief overview of exoskeleton

Among possible retrofit measures, a growing attention has been paid to the adoption of exoskeletons lately, as a possible strategy to minimize disruption of the inhabitants and avoid or reduce building downtime. Exoskeleton are assembled exclusively outside the building and, depending on their structural scheme, they may extend over a limited or substantial portion of the building's surface. Often these retrofit structures are supported by an independent foundation system [149].

Through the introduction of different engineered layers, these retrofitting systems can be effectively adopted for the design of an integrated solution contextually improving the seismic resistance, the energy efficiency, the architectural upgrading of buildings, as well as the comfort of the inhabitants [12] [15].

When architectural and urban planning constraints are not an issue, depending on the building's needs and the choices made by the stakeholders, the different layers of the new external retrofitting involucre, each having specialised functions [150], can be installed on the structural exoskeleton in a variety of configurations:

- Exoskeleton *installed in close proximity* to the existing building. In this configuration, the engineered layers are installed in close proximity to the existing facade's, creating a *structural-energetic-architectural double skin*.
- Exoskeleton *placed at distance* to achieve volumetric expansion, introducing of new living spaces [15].

Regarding the architectural layout, the system enables varying degrees of morphological transformation, determined by the choice of the exoskeleton shape, extension and the distance from the facades of the existing buildings.

Regardless the global layout, the exoskeleton can be designed by addressing different seismic-resistant schemes, each with distinct features and structural behaviours [149] [12]. The appropriate scheme is determined not only by structural factors, but also by the morphological and distributive characteristics of the existing building and the amount of usable space along the building's perimeter. The first classification of exoskeletons was introduced by [149], and is based on the structural scheme and the type of resistant components:

- *Bi-dimensional elements, consisting of Shear-walls (Figure VI.1)*, in which the stiffness and seismic resistance of the new lateral force-resisting system (LFRS) is lumped into a series of discrete structural elements incorporated into the exoskeleton. This structural configuration is preferred when the full size of the facades cannot be exploited, because of regulatory constraints or architectural features, such as large and numerous openings in the facade, thereby limiting the dimensional extension of the structural retrofit.

Shear-walls can be arranged parallel or perpendicular to the existing façade [151]. Due to the concentration of seismic actions and the size of these systems, deep foundations are typically necessary to absorb the bending moment and shear at the base of the walls.

The other type consists of systems that are parallel to the facades. These systems may take advantage of the



dimensions of the existing building surface extension to reduce stresses in the structural elements and the load on the foundations.

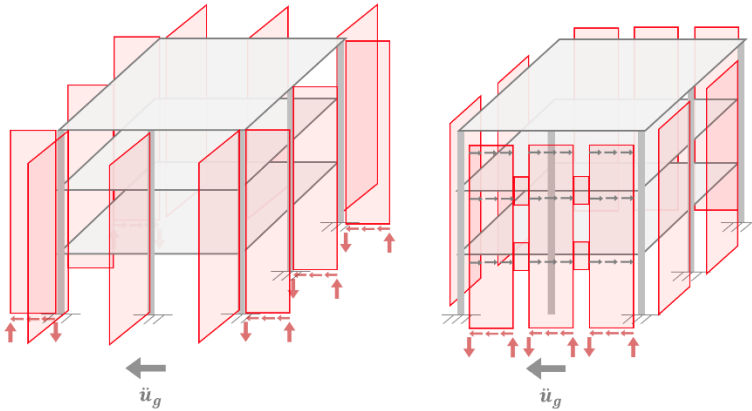


Figure VI.1 - Schematic representations of the resistance mechanisms triggered for the two different shear-walls schemes. On the left side: solutions with shear-walls arranged perpendicularly to the building facades. On the right side: solutions with shear-walls arranged parallel to the building facades.

- *Tri-dimensional structures*, consisting of *Shell-exoskeletons* (Figure VI.2), in which the new seismic resistant elements extend over the entire facades to activate a 3D box-like structural behaviour [25] [26]. Regardless of their orientation, these systems are capable of absorbing base shear in all directions due to their shell configuration [149]. These structural retrofits exploit the dimensions of existing building facades to reduce the size of structural components of the new lateral force-resisting system and to limit the foundation overload. The reduction of the stress level in the structural elements ensured by these scheme enables the pursuit of energy efficiency and the achievement of structural safety through the dual use of the same

elements: for instance, the thermal-insulating envelope could also serve as an in-plane seismic resistance structure.

Several structural solutions including diagrids [96] [152] [153], grid shells, and *traditional* curtain walls [46] can be engineered as shell structures.

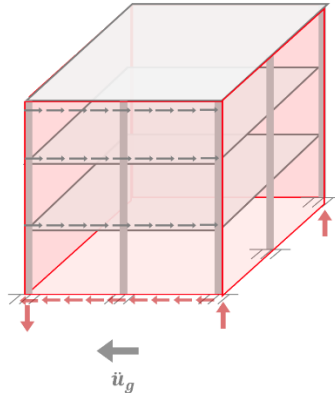


Figure VI.2 - Schematic representations of the resistance mechanisms triggered for shell-exoskeletons.

Both options require horizontal resisting diaphragms to collect and transfer the seismic loads from the existing building to the new structural exoskeleton. Fulfilling this requirement may be challenging if the existing floors and roof slabs are not designed to resist these actions, particularly for solutions in which the additional elements are arranged parallel to the facades. Due to the greater distance between the vertical elements of the new LFRS in solutions in which the additional elements are arranged parallel to the facades, the existing diaphragms must bridge a larger span and must ensure a higher capacity than in solutions with shear walls arranged perpendicular to the facades [66]. Consequently, when designing these solutions, especially the

shell systems, the preliminary assessment of the in-plane capacity of the existing floors and roof slabs is mandatory [66].

The exoskeletons also implement three distinct types of structural connections to ensure proper operation and to transfer the collected seismic loads, namely:

- *Connections between the components of the exoskeletons.*
- *Connections between the exoskeleton and the existing structure.*
- Connections between the exoskeleton and the foundation system.

Different devices can be selected, including either rigid or dissipative connections [154], with direct and significant effects on the structural behaviour of the retrofitted system.

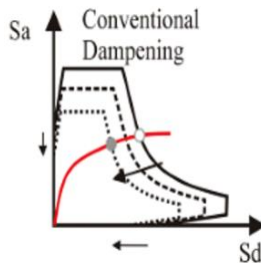
Exoskeletons can be designed to exhibit qualitatively different structural behaviours during a seismic event, depending on the characteristics of the new lateral force-resisting system, the features of the existing building, and the type of structural connections. The main solutions described in the scientific literature fall within two main categories [27] (Figure II.12).

- *Dissipative exoskeletons*
- *High-strength elastic exoskeletons*

Comparing the *structural behaviour* of retrofitted systems employing these retrofit solutions through the lens of the LCT, reveals that both have peculiar benefits and drawbacks. In the following, a brief qualitative analysis of their characteristics and compliance to the stringent structural standards outlined in the previous chapter are presented.

### 6.1.1. Dissipative systems

Dissipative exoskeletons control the seismic response by dissipating a portion of the seismic energy in *energy dissipation devices that may also be conceived as sacrificial fuse elements*. For earthquakes of any magnitudes, these systems reduce the accelerations experienced by the retrofitted structure, thereby reducing both the inertia forces, and the displacements demand on the retrofitted system by increasing the damping ratio while maintaining the same displacement capacity of the existing building [87] (Figure VI.3).



○ Original State ● Retrofitted State — Capacity Spectrum — Demand Spectrum ..... Retrofitted Spectrum

Figure VI.3 - Acceleration-Displacement Response Spectrum diagram conceptually illustrating the structural behaviour of dissipative exoskeletons. From [148].

By dampening the structural response, dissipative solutions allow to optimize the size of the exoskeleton's structural components, thereby reducing new material depletion. In addition, by concentrating the energy dissipation into a limited number of damping components, which are designed to avoid damage or to be easily disassembled and replaced after a high-intensity seismic event, the principles of reparability and adaptability are satisfied.

In the following, a preliminary classification of dissipative exoskeletons is made, which is based on the different types and

configurations of the damping system, the new lateral force-resisting system [155], and the structural connections:

- *Dissipative exoskeletons featuring high-strength elastic structural connections to the existing structure.*

In these solutions the dissipative elements, consisting of both passive or active devices and sacrificial *fuse* elements, may be configured as bracings or couplers between structural components and serve as primary structural elements of the new LFRS [27]. The incorporation of the energy dissipation devices into the exoskeleton, designed to function as the *weakest link in the chain*, and the introduction of high-strength elastic connections with the existing structure facilitate device repair, replacement, and maintenance operations.

Depending on the characteristics of the existing building, these systems can be designed for the retrofitted structure to either exhibit a linear lateral deformation profile, activating a global resistant mechanism for the existing building, or to concentrate deformations at one or more levels, activating a soft-storey mechanisms.

- *Elastic over-resistant exoskeletons with dissipative connections either to the existing structure or to the exoskeleton new foundations.*

When dissipative structural connections between the new lateral force-resisting system and its foundation [96] are adopted, a sort of isolated structure is obtained: the displacement demand is lumped at the exoskeleton base and the action transferred to the foundation is limited. In this case, preliminary interventions for

increasing the ductility of the vertical structures of existing building ground floor may be necessary.

Dissipative devices can as well be adopted as structural connections between the high-strength elastic exoskeleton and the existing structure. In such a case they limit the seismic action transferred to the exoskeleton at each floor. During the design phase, particular attention must be given to ensure the reparability and replacement of these elements.

The selection of dissipative devices and *fuse* elements directly affects the structural behaviour of both types of dissipative exoskeleton. Dampers, particularly passive ones, typically require a significant displacement or adequate relative velocity between their fixed ends to perform properly and dissipate a significant amount of energy, potentially entailing challenging deformation and large global ductility demand for existing structure, which may necessitate preliminary interventions to ensure adequate performances [27]. Moreover, in the aftermath of a seismic event, residual displacements, and deformations of both the energy dissipation devices and the existing structure may be significant due to the absence of a self-centring behaviour of the new lateral force-resisting system.

### **6.1.2. High-strength elastic systems**

The elastic exoskeletons accomplish the required performance objectives by introducing stiff and resistant structural elements that limit the displacements and the drift of the existing building. These retrofit components (exoskeleton and connections) provide sufficient strength to withstand the seismic actions while remaining essentially elastic until collapse. The permanence of the retrofitted building within the elastic range

for design actions makes it possible to minimise and potentially avoid any further intervention on existing structure.

However, such a peculiar structural behaviour increases the accelerations and inertia forces experienced by the reinforced system during earthquakes of any magnitude, necessitating careful assessment of the capacity of the *acceleration-sensitive* components (Figure VI.4).

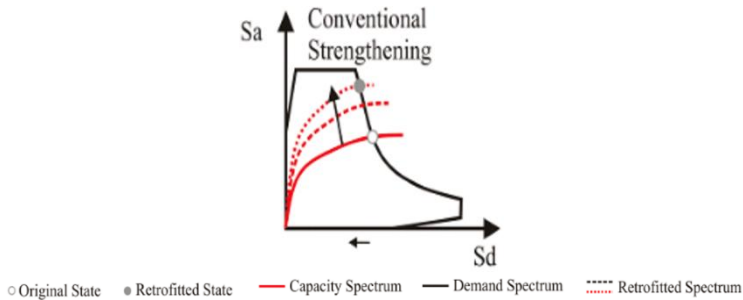


Figure VI.4 - Acceleration-Displacement Response Spectrum diagram conceptually illustrating the structural behaviour of High-strength elastic exoskeletons. [148].

Adopting these systems for the strengthening of RC buildings may result in the proportioning of exoskeletons with one-to-six times the initial RC structure stiffness, resulting in large and resistant LFRS, which may require the introduction of massive new foundations [27]. Many useful criteria for estimating their stiffness and resistance are reported in literature [96] [156] [157].

## 6.2. Adaptive exoskeletons

Recently some authors have introduced the concept of *responsive retrofit* (Figure VI.5), a new type of solution designed to enhance the structural performances, contain the retrofit dimensions, increase its effectiveness, and boost the adaptability and repairability even further [12]. Like responsive facade systems and bio-inspired kinetic structures [158], which adapt their behaviour as climatic conditions change, shear walls- and shell-solutions can be re-engineered to adapt their structural behaviour based on the magnitude of the earthquake. For the frequent low-intensity earthquakes these systems can be designed to avoid potential damage, while for rare stronger seismic loads the evolution of their static scheme may enable the onset of a ductile failure mechanism with controlled, possibly lumped, damage. *Passive responsive structure* can be designed by incorporating sacrificial fuse elements or passive energy dissipation devices acting as structural connections and couplers between the main structural elements; these elements can also be replaced by active devices resulting in *active responsive structures*. In both solutions, these important devices are designed to be the *weakest link in the chain* while preserving the integrity of the other elements, components, and connections. Nevertheless, despite their high structural performance, these systems are deficient in controlling and limiting residual deformations and drifts after a high-intensity seismic event.



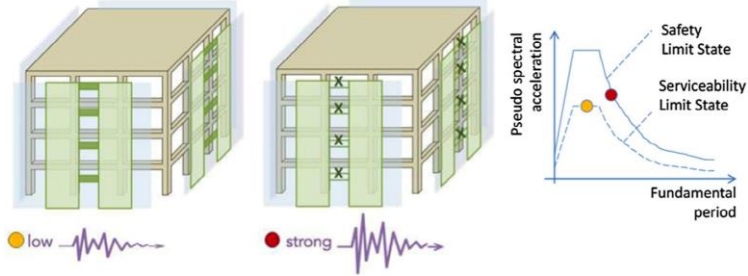


Figure VI.5 - Schematic illustration of responsive structures comprising dual-wall solutions with specially designed coupled elements. From [12].

An innovative and interesting design approach for the construction of new timber buildings with high structural performance, defined as Pres-Lam system [159], has recently been proposed. *Adaptive exoskeletons* enhance the *responsive wall* concept accounting also for the residual drift and displacement control by exploiting the rocking mechanisms of CLT shear-walls [160] [161] (Figure VI.6).



Figure VI.6 - Image of the two-story CLT prototype structure being tested on a shaking table at the USDC during the summer of 2017. From [160].

As the responsive walls, these innovative controlled rocking system *adapts their structural behaviour* based on the *earthquake's magnitude*. During frequent low-intensity earthquakes, the rocking mechanism is prevented, whereas for high seismicity events, the rocking mechanism is activated thus allowing for a localized and controlled damage.

Thanks to such an innovation, compared to responsive systems, adaptive exoskeleton enables the realisation of *damage-controlled* retrofits; they may also allow for dissipation energy thanks to the yielding of couplers located between rocking walls and other sacrificial components located at their base, while preserving the structural integrity of the remaining elements.

In the following sections, the *adaptive exoskeletons are described and analysed*.

### **6.2.1. Evolving structural behaviour**

The innovative concept behind these exoskeletons consists in their capacity to *adapt, evolve, and restore* their structural behaviour and static scheme depending on the magnitude of the seismic events. When a predefined dynamic load level is reached (*i. e.  $\ddot{u}_{g,limit}$* ), these exoskeletons meet the established performance objectives by altering their resisting mechanisms (Figure VI.7).

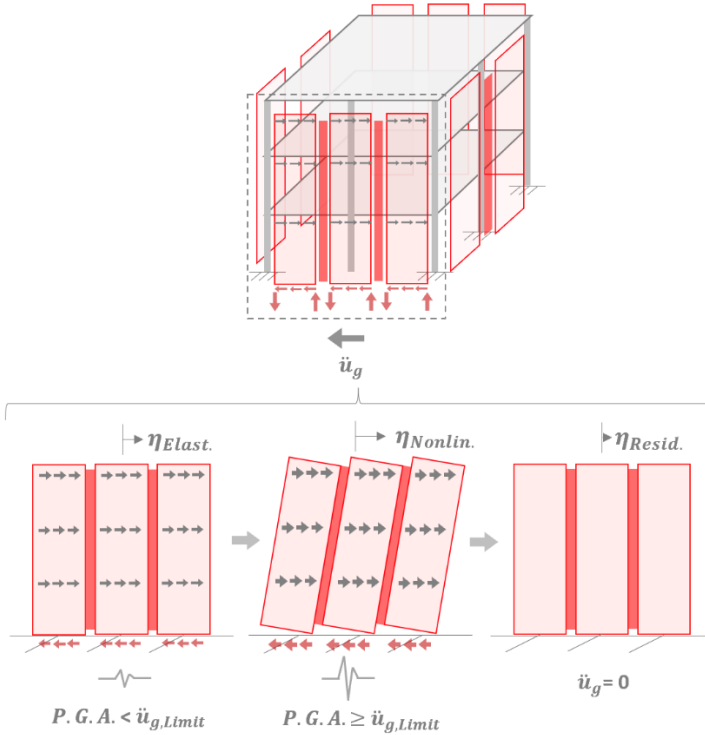


Figure VI.7 - Conceptual representation of the adaptive behaviour of an exoskeleton façade in response to the magnitude of the ground acceleration. For seismic events with peak ground acceleration (P.G.A.) below the design threshold ( $\ddot{u}_{g,Limit}$ ), the exoskeleton facade exhibits linear elastic behaviour with limited deformations, whereas when the threshold is exceeded, the resistant mechanism evolves in the nonlinear field and then restores its initial configuration after the earthquake.

The control of total drift, inter-storey drift and residual displacement and the restoration of the initial structural scheme obtained through specific devices enabling a self-centring behaviour. In the following, the conceptual structural behaviour of the solutions investigated in this study is briefly described:

- *High-stiffness elastic behaviour*, manifested for frequent seismic events with a return period of up set at 475 years, this intensity threshold defines the peak ground acceleration (P.G.A.) above which the resistant mechanism evolves ( $\ddot{u}_{g,limit}$ ) (Figure VI.7, left).

For *low-intensity* seismic events, the stiff exoskeleton limits structural damage to *displacement-sensitive* components and enforces a linear profile to the lateral deformation of the retrofitted system, at the expense of increased accelerations and inertial forces. Conceptually the solution behaves like *conventional high strength retrofit* solutions.

- *Nonlinear behaviour and energy dissipation* are triggered for very rare seismic events with a return period exceeding the set 475 years (Figure VI.7, central).

Upon overcoming such intensity levels, the exoskeleton's structural behaviour changes qualitatively in response to *high-intensity* seismic events. The evolution of the static scheme allows to reduce the retrofit stiffness, thus limiting the increase in accelerations and inertia forces experienced by the retrofitted system, at the expense of potentially greater displacements and drift.

The introduction of an energy dissipation systems within the exoskeleton, designed to act as the *retrofit's weakest link* while preserving the integrity of the other structural elements and connections, limits damage and maximum drift preventing the collapse of the existing building. The introduction of self-centring systems and devices ensures the control of drift and residual

displacement, thereby enhancing the performance of the exoskeleton.



Figure VI.8 - Matrix of the seismic performance design objectives for adaptive exoskeletons, indicating conceptual structural behaviour for each earthquake design level.

Enforcing an elastic behaviour for frequent up to rare seismic events entails the limitation and possible avoidance of damage on the existing building, thereby reducing/avoiding direct costs and economic, environmental, and social impacts associated with possible repair works as well as indirect losses. On the other hand, the *damage-control* for very rare seismic loads and the possibility of re-centring the new lateral force-resisting system entail possible reparability after the seismic event. Such a performance objective (Figure VI.8) requires the introduction and design of an adequate dissipation system, containing displacements below predefined thresholds, that must be defined according to the building's characteristics, and the

implementation of structural details capable of limiting residual drifts after the seismic event.

### 6.2.2. Response curve of the retrofitted system

In the following, the optimal response-curve of an adaptive structure is described from a conceptual and qualitative perspective to highlight both the potential and the challenges of applying adaptive solutions.

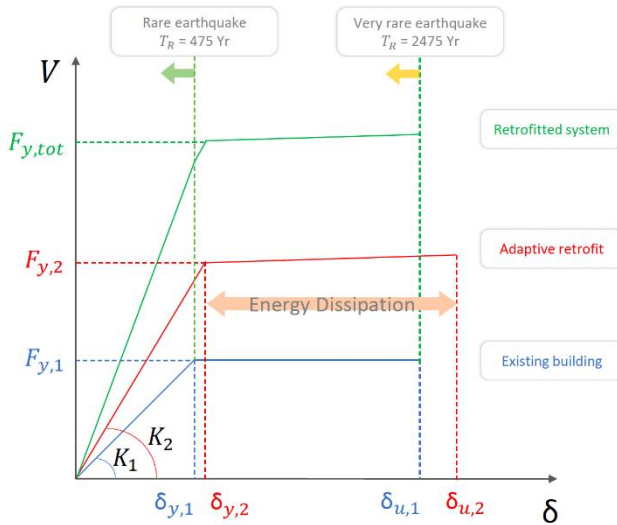


Figure VI.9 - Qualitative representation of the optimal system response curve with the bilinear elastic-plastic curve of the existing building in blue, that of the adaptive retrofit in red and the retrofitted system in green. The area covered by the hysteretic cycle of passive dissipative devices is highlighted in red.

The following assumptions underlie the definition of the response-curve (Figure VI.9) :

- The exoskeleton and the existing **building are modelled** as single-degree-of-freedom (SDOF) systems.
- The *existing building* is represented by an equivalent bilinear elastic-plastic response-curve. The elastic response branch, defined by the elastic stiffness  $K_1$  and limited at the attainment of the yielding force  $F_{y,1}$ , ideally represents the displacement range where no damage occurs. Beyond the yield displacement  $\delta_{y,1}$ , the extension of the *plastic range* is dependent on the characteristics of the analysed structure and on its global ductility, determining the ultimate displacement  $\delta_{u,1}$ .
- The *adaptive exoskeleton (responsive exoskeleton with re-centering behaviour)* is also represented by an equivalent elastic-nonlinear dissipative curve. Its elastic stiffness  $K_2$  and yielding force  $F_{y,2}$  should be defined according to the performance objectives and related design targets established for the existing building subjected to seismic events with 475 years return period. Several useful simplified models are available in the literature for estimating these quantities [96] [156]. The integration of energy dissipation devices into the exoskeleton ensures that the displacements of the retrofitted system are contained within the plastic field of the existing building ( $<\delta_{u,1}$ ). The requirement of limiting accelerations and inertia forces suggests the selection of devices with low post-yield stiffness and

adequate dissipative and deformation capacity, capable of dissipating a substantial portion of the energy introduced at target displacements.

This investigation focuses solely on the applicability and potential of passive dissipative systems that operate without an external energy source; in this section, the analysis is restricted to a qualitative definition of their constitutive model, whereas in the subsequent sections of the thesis, their mechanical properties are defined and thoroughly analysed.

- The *connections* between *the exoskeleton and the existing structure* and between *the exoskeleton and the new foundation* are conceptually represented by indefinitely elastic and rigid links.

The actual stiffness of these elements, designed to remain in the elastic field for the design loads, would also play a role in the system's global response; however, in this paragraph, their elastic stiffness is assumed to be infinite, and focus is made on the influence of the other parameters can be better underlined.

In the following section, the dynamic behaviour of new dissipative structural systems is analysed qualitatively and their potential integration into adaptive exoskeletons is explored.

### **6.2.3. Qualitative dynamic behaviour**

A brief literature survey is presented, with a few selected references on the design and analysis of the dynamic behaviour of new self-centring structural systems that base their resistant mechanism on *dissipative controlled rocking behaviour*. Such



structural systems partly inspired the development of adaptive exoskeletons.

The low-damage self-centring seismic resisting systems were initially introduced at the end of the last century, in the 1990s, for the development of innovative precast reinforced concrete structures as part of the US PRESSS program [162] [163]. Their novel lateral-force resisting mechanism, based on *controlled rocking* behaviour, is similar to an *internal isolation system*, resulting in limited- or negligible-damage to the structural elements [164].

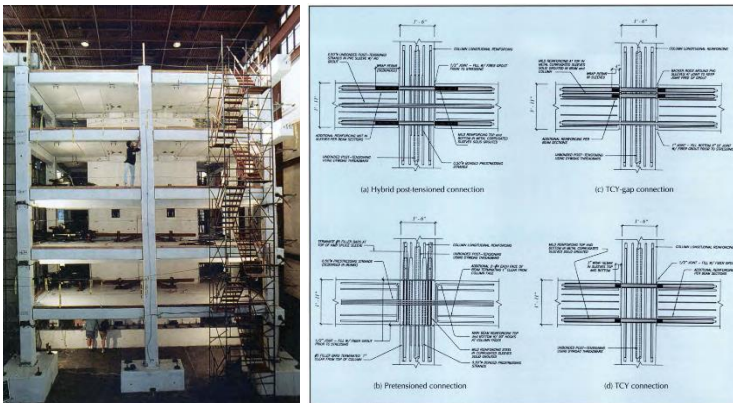


Figure VI.10 - On the left-side: Tested five-story structure in PRESSS program. On the right-side: Types of seismic frame connections. From [163].

Numerous studies and researches, including significant contributions from New Zealand [165] [166] [167] and the United States [168] [160] [161], have substantially contributed to the development of these innovative *low-damage technology*, significantly enhancing their structural performance and extending their applicability to timber [159] [169] [170] [171],

referred to as the Pres-Lam system, and steel structures [172] [173].

The original concept of these innovative systems is based on the use of ductile structural joints, to which structural elements are connected through different types of unbonded post-tensioned tendons or bars that generate moment-resistant structural connections, relying on the *simple* rocking behaviour to withstand the seismic actions. Subsequently, numerous researchers proposed diverse implementations of the original configuration by adding different devices and energy dissipation systems.

Initial studies and applications of these energy dissipation devices entailed their introduction within rocking elements, using for instance mild-steel reinforcement bars [174], which could make their repair or replacement challenging; later, damping devices were installed externally in many different configurations [165] [166], overcoming some of the limitations of the earliest versions.

In the following, some of the configurations in which coupled- and single-dissipative rocking walls can be realised are schematically illustrated, showing the various locations of the energy dissipative or sacrificial *fuses* elements. These elements may be installed at the base of the walls, coupled with the re-centring elements, or serve as coupling elements between adjacent walls [175] [173].

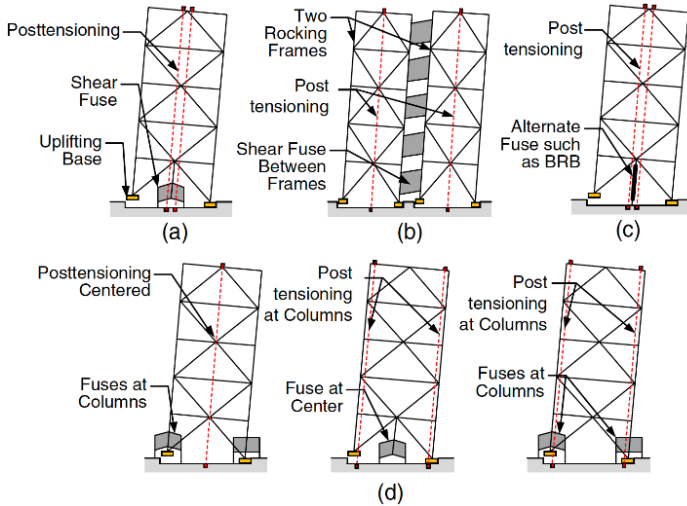


Figure VI.11 - Conceptual and schematic illustrations of some of the configurations and schemes in which dissipative coupled and single steel rocking walls can be designed. From [173].

The high structural performance provided by the most advanced version of these systems, designed using the most recent design guidelines [176], enables achieving the previously defined multicriteria performance targets. Compliance with the most recent PBEE recommendations [177] can be also guaranteed, including the control and limitation of deformations and residual displacements.

The adaptability of controlled rocking systems has been a focus of research since their conceptual design. These systems, which employ a multi-level performance approach, are suitable for both design and retrofit purposes. They can maintain the point of decompression, which refers to the full non-cracked section, up to an earthquake service level. Following this, the controlled rocking starts, allowing for high performance tuning at various intensity levels.

The dynamic behaviour of the *advanced* rocking systems and their response curves are directly affected by the configuration and typology of the energy dissipation devices. Numerous studies [176] [178] have highlighted the distinctions and peculiarities in the adoption of different passive device types, preliminary classified as *velocity-dependent* and *displacement-dependent* [154] energy dissipators. Regardless the typology of the self-centring system, conceptually represented by a bilinear-elastic curve, the *dissipative self-centring structural systems* can be classified based on the type and arrangement of their passive energy dissipation devices, with different structural features [176], qualitatively analysed in the following:

- *Flag-Shape (FS) systems* incorporate *displacement-dependent* devices, typically combined in parallel with the self-centring systems (Figure VI.12).

The constitutive model and the mechanical properties of these energy dissipation elements depend directly on their typology and specific features. Preliminary, they can be modelled with an elastic-plastic skeleton curve with variable stiffnesses, yield strength, and ductility.

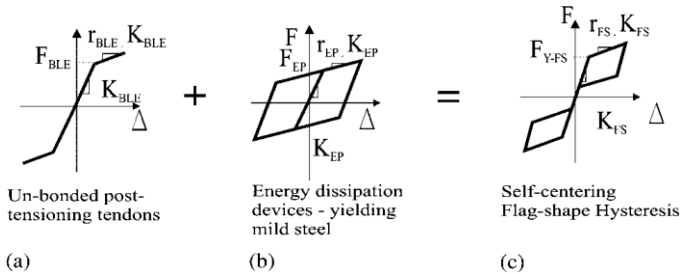


Figure VI.12 - Representation of the response curve of an ideal flag-shape system in which: (a) represents the re-centring system consisting of un-bonded post-tensioning tendons (b) represents the dissipative system consisting of yielding mild-steel (c) represents the hysteresis of the FS system. From [176]

Potentially, these solutions *well conform* to the previously defined structural characteristics and ideal response curve of adaptive exoskeletons. To limit accelerations and residual deformations, it is required to select *displacement-dependent* energy dissipators with reduced post-yielding stiffness and calibrated yield strength.

- *BiLinear Elastic Velocity-dependent energy dissipation (BLEV) systems* incorporate *velocity-dependent* energy dissipation devices, combined in parallel with the self-centring systems (Figure VI.13).

The characteristics of the dissipators largely affect the behaviour of the system; the adoption of certain types of dampers, such as linear viscous damping systems, in which the resistance offered is directly proportional to the excitation velocity, could present obstacles that could limit their applicability in adaptive exoskeletons. Several studies demonstrated that the energy dissipation of these systems may be limited for high-cycle excitations with low velocity, which are typical of *far-field earthquakes*, whereas the damping forces and accelerations experienced by the adapted system may be excessively large for low-cycle seismic events with high velocity [176], which are typical of *near-fault earthquakes* [179].

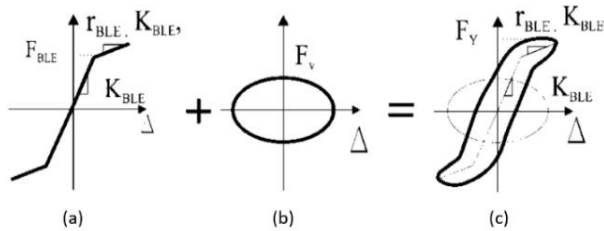


Figure VI.13 - Representation of the response curve of an ideal BLEV system in which: (a) represents the re-centring system consisting of un-bonded post-tensioning tendons (b) represents the dissipative system consisting of linear viscous dampers (c) represents the hysteresis of the BLEV system. From [176]

Moreover, even for *frequent low-intensity seismic events*, their functioning may necessitate *challenging* relative displacements for the existing building, as previously mentioned for dissipative exoskeletons [27].

- The *Advanced Flag-Shape (AFS) systems* combine different energy dissipation mechanisms in parallel and/or in series with the self-centring devices.

These systems partially address the limitations posed by the *BLEV* solutions; the *displacement-dependent* damping can potentially provide adequate energy dissipation and resistance for low-velocity excitations, while the inherent benefits of *velocity-dependent* damping can reduce displacement demand for high-velocity earthquakes.

The reduction of maximum displacements for near-fault seismic events can be accomplished by combining different types of dissipators in parallel (Figure VI.14) experiencing a potential increase in accelerations for rare high-velocity earthquakes.

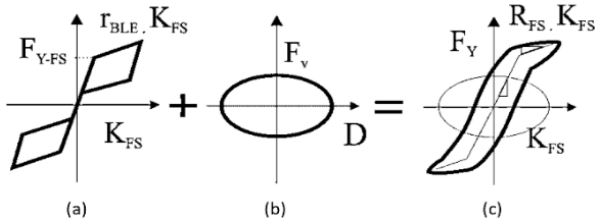


Figure VI.14 - Representation of the response curve of an ideal AFS system with dissipators combined in parallel, in which: (a) represents the response curve of FS systems (b) represents the dissipative system consisting of linear viscous dampers (c) represents the hysteresis of the analysed BLEV system. From [176]

Combining these devices in series (Figure VI.15) allows for the limitation of the maximum force expressed by *linear viscous* velocity-dependent devices.

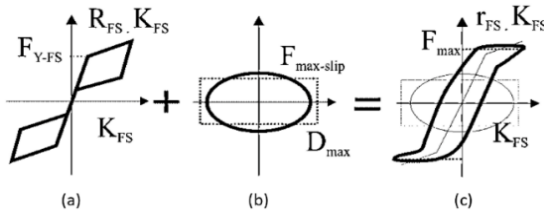


Figure VI.15: Representation of the response curve of an ideal AFS system with dissipators combined in series, in which: (a) represents the response curve of FS systems (b) represents the dissipative system consisting of dampers (c) represents the hysteresis of the analysed BLEV system. From [176]

As for BLEV systems, the introduction of several types of velocity-dependent devices could limit their applicability due to the requirement for *significant* relative displacements even for *frequent low-intensity seismic events*, when adaptive exoskeletons should ideally exhibit *high-stiffness elastic behaviour*.

The different innovative solutions analysed offer specific benefits and limitations, in addition to numerous insights for their integration into exoskeletons. The preliminary qualitative analyses conducted suggest the development of *adaptive*

*exoskeletons* with nonlinear dissipative behaviour comparable to that of *Flag-Shape systems*, in which passive displacement-dependent energy dissipation devices are combined in parallel with self-centring systems. These conceptual solutions well conform to the optimal structural features and ideal response curve previously defined (see Section 6.2.2), partially overcoming the limitations associated with the introduction of some types of *velocity-dependent energy dissipation devices*. Several numerical studies [176] [180] [181] have also observed the *good* structural and dissipative behaviour of the flag-shape systems when subjected to far-field seismic events, as well as the *satisfactory* behaviour when subjected to near-fault seismic events, albeit with *lower-than-expected* energy dissipation, especially for tall and flexible buildings.

It is important to note that the conceptual solutions analysed above, were primarily conceived for the design of *new buildings*, which have significantly different characteristics than those of *structural retrofit systems* for existing buildings. The incorporation of these novel concepts into the structural retrofit solutions necessitates their revision and integration, as well as the adoption of new structural design procedures that enable their efficient application to different buildings having different needs, peculiarities, and structural features.

### **6.3. Conceptual design for adaptive exoskeletons**

This section investigates the structural properties and applicability of *adaptive exoskeletons* composed of either coupled shear-walls arranged in parallel to existing facades, or tri-dimensional shell-structures. The main structural components of these exoskeletons, whether shear walls- or shell-solutions, can be arranged in two distinct configurations [15] that are distinguished by the different orientation of the



structural panels and dissipators/couplers. The two configurations investigated in this study are characterized by the presence of:

- *Structural panels* and *passive energy dissipation devices (PEDDs)*, also functioning as *couplers* between adjacent panels, **arranged vertically** and spanning from ground to roof level (Figure VI.16, Figure VI.17). The retrofit energy dissipation capacity is primarily concentrated in the devices that couple the rocking walls, while the system's re-centring is ensured by the introduction of unbonded elastic steel bars resisting tensile stress only, placed within the structural panels constrained at their top and at the foundation level.

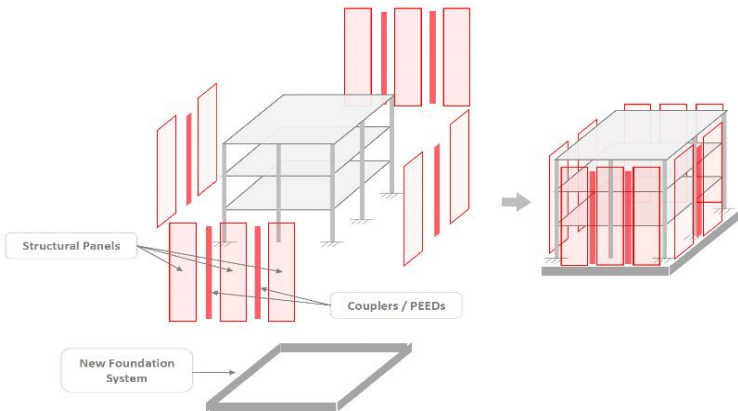


Figure VI.16 - Conceptual representation of the vertical structural arrangement of adaptive exoskeletons.

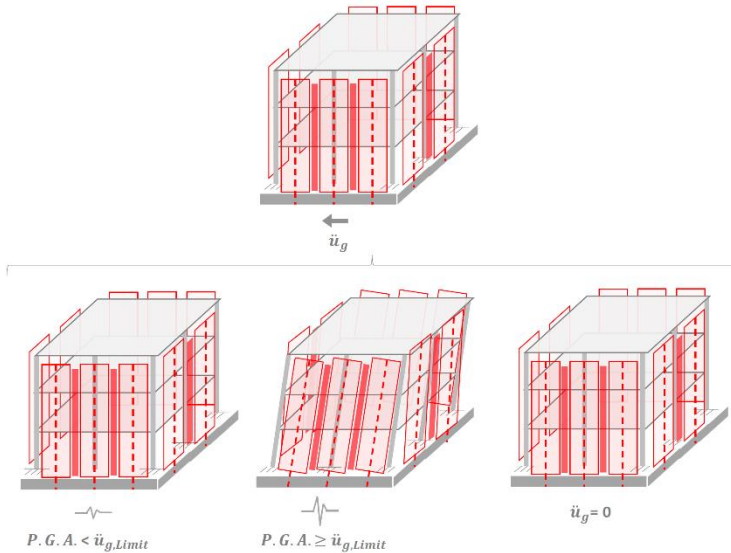


Figure VI.17 - Conceptual representation of the vertically arranged adaptive exoskeleton in response to the magnitude of ground acceleration. For seismic events with peak ground acceleration (P.G.A.) less than the design threshold ( $\ddot{u}_{g,limit}$ ), the exoskeleton exhibits linear elastic behaviour with limited deformations, whereas when the threshold is exceeded, the resistant mechanism evolves to dissipative coupled rocking and then restores the initial configuration at the end of the earthquake.

- *Structural panels and passive energy dissipation devices (PEDDs) also serving as couplers between panels, arranged horizontally* and spanning between two adjacent floors (Figure VI.18). In this configuration, the couplers are placed along a horizontal strip between the ground floor and first floor panels, lumping the displacement demand in the nonlinear field at this level. This results in the activation of a soft-storey mechanism at the ground floor of the existing building for those seismic events with peak ground

acceleration exceeding the threshold set for the yielding of the couplers (Figure VI.19). The inability of the horizontal configuration to actively reduce residual drift following a severe seismic event is one of the key differences between this exoskeleton configuration and the one described previously.

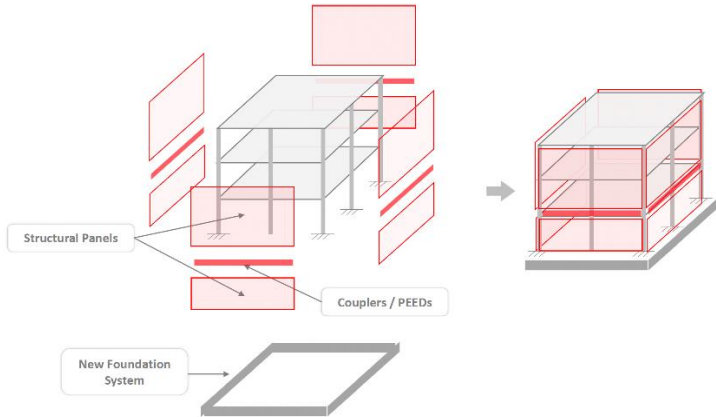


Figure VI.18 - Conceptual representation of the horizontal structural arrangement of adaptive exoskeletons.

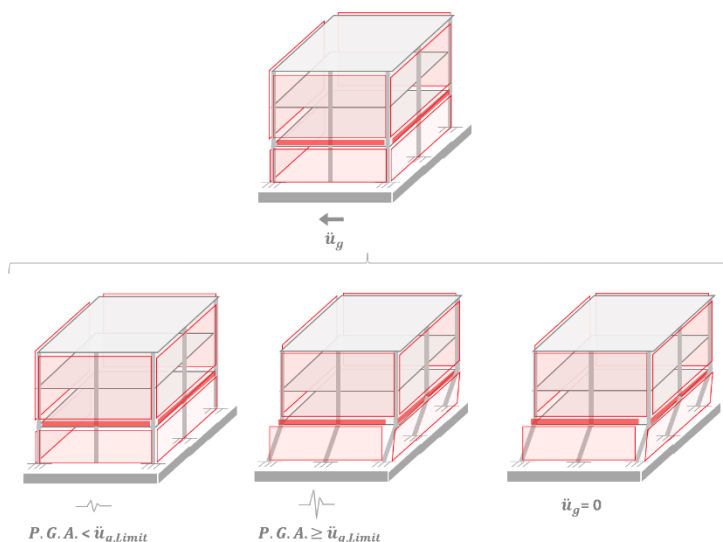


Figure VI.19 - Conceptual representation of the *horizontally arranged* adaptive exoskeleton in response to the magnitude of ground acceleration. For seismic events with peak ground acceleration (P.G.A.) less than the design threshold ( $\ddot{u}_{g,limit}$ ), the exoskeleton exhibits linear elastic behaviour with limited deformations, whereas when the threshold is exceeded, the couplers yield resulting in the activation of a soft-storey mechanism. At the end of the seismic event, the retrofit is unable to reduce the residual drifts induced.

The arrangement of the main structural components is a design choice that directly affects the dynamic behaviour of the retrofitted system and its capacity to limit damage by minimising the residual drift after a seismic event. Several factors, including the structural characteristics of the existing building, the architectural and regulatory constraints, the stakeholder preferences, and the potential construction complexities determine its selection.

These systems can be designed using different *construction materials*, including precast reinforced concrete, steel and engineered timber or CLT panels, and various types of *displacement-dependent energy dissipation devices*. The case

studies and the models described and analysed in this study focus on the use of *prefabricated, dry-assembled CLT panels* with *standardised devices and connections* that guarantee a high level of adaptability and fast assembly.

The distinctive structural features of the different exoskeleton solutions analysed in this chapter, having either vertical or horizontal arrangements of the panels, are summarised in the following sections (Sec. 6.4.1, and 6.4.2), whereas the characteristics shared by all analysed models are listed below:

- The primary structural elements are assembled using *cross-laminated timber (CLT) panels*. From a life cycle thinking perspective, the selection of eco-friendly timber panels increases the potential reuse rate at end-of-life (85% -90%), as the large elements are readily adaptable to further processing and reuse [15]. Furthermore, the adoption of renewable materials such as CLT panels increases eco-efficiency of the solution.
- The adoption of *displacement-dependent passive energy dissipation devices (PEDDs)* that do not require external energy sources for operation and that are easily removable and replaceable after a severe seismic event.
- The adoption of *high-stiffness elastic structural connections* between the exoskeleton and the existing building and between the exoskeleton and the new foundations, designed to behave elastically even for severe seismic event.

The implementation of R.C. foundations under the exoskeletons, which at this stage of the research are envisioned as infinitely resistant and rigid elements to maintain the focus

on the exoskeleton's characteristics. It is acknowledged that the design of the exoskeleton should account for the relevant soil-structure interaction issue. Such a topic, which is outside the scope of this thesis, is currently being investigated in a parallel research project.

#### **6.4. Structural design procedure**

The design of these retrofit systems represents for structural engineers a *fascinating challenge* that is quite different from those posed by the design of new buildings.

The *design procedure for adaptive exoskeletons proposed* in this study is composed of *two main steps*: the first one involves the preliminary definition of their principal structural characteristics in the elastic range, while the second focuses on the nonlinear dissipative response of the solution by conceptually defining its dissipative behaviour and by assessing its compliance with the structural performance objectives and related design targets.

In the *first step*, the optimal stiffness and strength required to guarantee the expected structural performance during frequent low-intensity up to rare earthquakes are determined by adopting design spectra conceived for external elastic retrofits [156] [157].

In the *second step*, conformity with established design standards is evaluated by adapting and integrating the procedures proposed for the direct design of both new high-performance timber seismic resisting systems [170] [182] and post-tensioned retrofit systems [50] [183] based on the *Displacement-Based Design Retrofit methodology*. It is worth noting that the second step focuses only on the design of adaptive exoskeletons

characterised by the vertical arrangement of structural panels and couplers.

#### **6.4.1. Elastic behaviour**

The elastic behaviour of the retrofit for frequent low-intensity up to rare events could reduce displacements and damage to the existing building, thereby reducing damages and related costs and environmental and social impacts.

For earthquakes with peak ground accelerations exceeding the design threshold, the resistant mechanism of the exoskeleton evolves to protect the main structural elements from damage. The adaptation of the resisting mechanism to seismic intensity is ensured by the yielding of the couplers, which are designed to serve as the *weakest elements*, thereby limiting the increase in seismic loads and stresses in other structural elements. In the following, a schematic representation of the ideal system response curve and the acceptable displacement interval for earthquakes with a return period up to 475 years are presented (Figure VI.20).

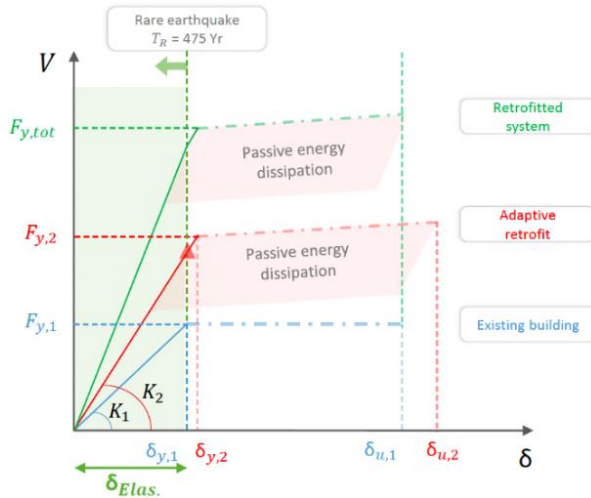


Figure VI.20 - The range of acceptable displacements  $\delta_{Elas.}$  in the linear elastic range is highlighted in green on the schematic representation of the system's ideal response curve. The red triangle along the retrofit response curve represents the coupler yielding point.

The design of the optimal characteristics of the retrofits in their elastic range up to yielding ( $K_2$ ,  $F_{y,1}$  in Figure VI.22) both structural arrangements, can be made with reference to the design spectra presented in [156] [157]. Such spectra are derived from the results of a series of non-linear time history parametric analyses performed on simplified numerical models representing the retrofitted system, in which the interaction between the elasto-plastic retrofit system and the existing building is modelled. The existing building and the retrofit system are represented by a simplified two-degree-of-freedom (2DOF) model in which the responses of the systems are respectively described by degrees of freedom  $u_1$  (DOF1) and  $u_2$  (DOF2).



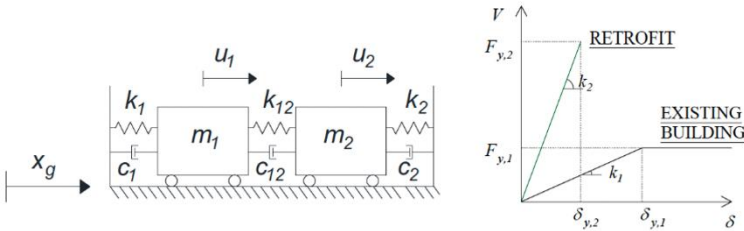


Figure VI.21 - Schematic representation of the simplified 2DOF model, showing a) the simplified 2DOF system; and b) the response curve of the retrofitted building with 2 degrees of freedom (2DOF) operating in parallel. Adapted from [156].

In general, the applicability of this simplification is acceptable if the elastic stiffness of the retrofit is significantly higher than the stiffness of the existing building or if the ratio of the exoskeleton's mass ( $m_2$ ) and the mass of the existing building ( $m_1$ ) ranges between 1/20 and 1/10 (which is reasonable for the considered cases) [46]. In certain instances, in relation to the set performance objective, a retrofit stiffness that is comparable or potentially lower in magnitude might be adequate.

The fundamental parameters used to describe the simplified model are the ones presented in the following:

- The *structural response of the existing building (element 1)* is described by its fundamental period ( $T_1$ ), effective mass ( $m_1$ ), initial elastic stiffness ( $k_1$ ), constant damping coefficient ( $c_1$ ) and yielding force ( $F_{y,1}$ ).
- The *structural response of the adaptive exoskeleton (element 2)* is described by the initial elastic stiffness ( $k_2$ ), defined as a function of the existing building's elastic stiffness ( $k_1$ ), the yielding force ( $F_{y,2}$ ), and the constant damping coefficient ( $c_2$ ).

- The *rigid structural connection* between the *existing structure and the exoskeleton system* is represented by a general link connecting the two masses  $m_1$  and  $m_2$ , described by its stiffness ( $k_{12} \rightarrow \infty$ ). Based on this assumption  $\tilde{k} = k_2$
- The target *elastic damage parameter*  $\mu_{Elast.}$ , representative of the *ductility demand* for the existing building in the retrofitted conditions. This design parameter is defined as the ratio of the target elastic displacement  $\delta_{d,Elast.}$  experienced by DOF1, during a seismic event with threshold intensity ( $T_R = 475$  years) with respect to its yielding displacement  $\delta_{y,1}$ :

$$\mu_{Elast.} = \frac{\delta_{d,Elast.}}{\delta_{y,1}} \leq 1$$

By adopting the design spectrum of the construction site, defined for earthquakes with a return period of 475 years, which determines the seismic intensity threshold for triggering the nonlinear dissipative behaviour of the retrofit, the suggested procedure determines the following design parameters:

- The *strength parameter*  $\eta$ , representative of the yielding force of the existing structure ( $F_{y,1}$ ) adimensionalized in terms of the existing building effective mass ( $m_1$ ) multiplied by the site spectral acceleration  $Sa(T_1)$  with return period set at 475 years:

$$\eta = \frac{F_{y,1}}{[m_1 Sa(T_1)]}$$

Following the process [156], it is possible to derive the design spectra for the analysed building and define the retrofit a-dimensional parameters:

- The *stiffness ratio*  $\tilde{\lambda}$ , representative of the ratio of the equivalent elastic stiffnesses of the retrofit ( $\tilde{k}$ ) to the elastic stiffness of existing building ( $k_1$ ).

$$\tilde{\lambda} = \frac{\tilde{k}}{k_1} \xrightarrow{k_{12} \rightarrow \infty} \frac{k_2}{k_1}$$

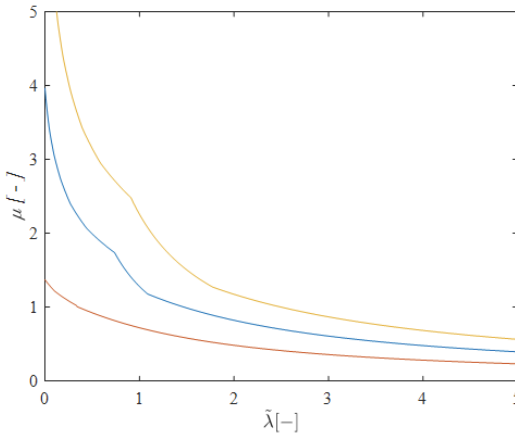


Figure VI.22 - conceptual illustration of three different design spectra for the same building obtained by varying only the *strength parameter*  $\eta$  from 0.85 (yellow line) to 0.50 (blue line) to 0.30 (orange line).

The equivalent elastic stiffness and strength of the adaptive exoskeleton in each of the building's principal directions can be preliminary defined as follows:

- The *Minimum equivalent elastic stiffness of the retrofit* ( $k_2$ ) is defined by multiplying the response parameter  $\tilde{\lambda}$  with initial elastic stiffness of the existing building ( $k_1$ ):

$$k_2 = \tilde{\lambda} k_1$$

- The *Minimum required base shear for the retrofit* ( $V_{Rd,min.}$ ) is defined by multiplying the effective mass of the existing building ( $m_1$ ), increased by 10% to account for the mass of the exoskeleton, with the site spectral acceleration of the retrofitted system  $Sa(T_{1,retrofitted})$  and subtracting the resistance offered by the existing structure ( $k_1 \delta_{d,Elast.}$ ):

$$V_{Rd,min.} = 1.1 m_1 Sa(T_{1,retrofitted}) - k_1 \delta_{d,Elast.}$$

The *minimum required global resistant moment* ( $M_{Rd,min.}$ ) can be calculated multiplying the required base shear by 2/3 of the total building height ( $H_{building}$ ):

$$M_{Rd,min.} = V_{Rd,min.} \frac{2}{3} H_{building}$$

By enforcing stringent limits to the maximum displacements of the existing building ( $\delta_{d,Elast.}$ ), and consequently to the drift, results in the design of adaptive exoskeletons with a high elastic stiffness, capable of linearizing the lateral deformation of the retrofitted system.

#### 6.4.2. Nonlinear dissipative behaviour

Nonlinear dissipative behaviour potentially limits damage and maximum drifts during major earthquakes, preserving the load-bearing capacity of the existing structure and preventing its collapse. During rare high-intensity earthquakes, in which the peak ground acceleration exceeds the predetermined design threshold, the induced displacements are expected to be contained by the energy dissipation partly provided by the yielding of the couplers. Below is a schematic representation of the conceptual system response curve and acceptable

displacement range  $\delta_{Nonlin.}$  for seismic events with a return period greater than 475 years (Figure VI.23).

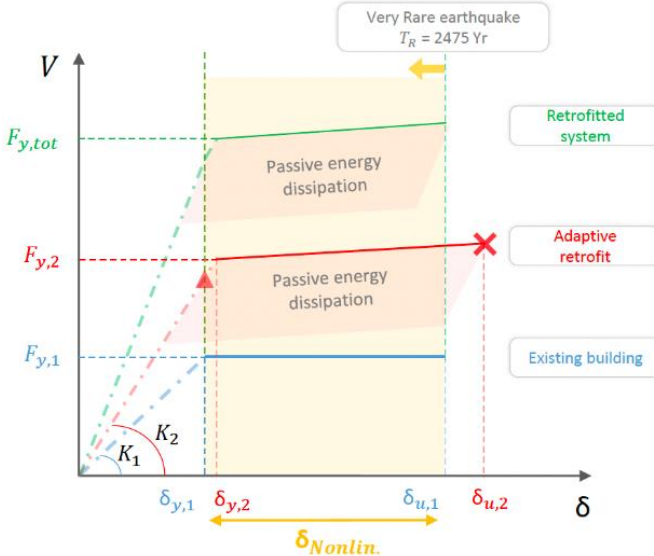


Figure VI.23 - The range of acceptable nonlinear displacements  $\delta_{Nonlin.}$  in the dissipative range is highlighted in yellow in the schematic representation of the system's ideal response curve. The red triangle represents the coupler yielding point, while the red cross represents the adaptive exoskeleton's maximum deformation capacity.

This second step of the procedure is focused on the design of adaptive exoskeletons with a *vertical structural arrangement* that exploit *controlled and dissipative rocking* to guarantee the envisioned structural performances, including the reduction of the residual drift after the seismic event.

Recently, several authors have proposed adopting Displacement-based design approaches [184] for the direct design of external retrofit systems (DBDR) exploiting the controlled rocking of R.C. [50] and timber [183] walls for the seismic reinforcement of existing reinforced concrete frame

buildings. Starting from the minimum required performance in terms of stiffness ( $\tilde{k}$ ) and strength ( $\mathbf{V}_{Rd,min.}$  ;  $\mathbf{M}_{Rd,min.}$ ) defined in the *previous design step*, in this *second step* the *DBD approach* is extended and integrated.

The following steps are suggested:

- Definition of the *target displacement* of the existing building in the nonlinear range  $\delta_{d,Nonlin.}$  for the set seismic intensity level.

$$\delta_{y,1} < \delta_{d,Nonlin.} < \delta_{u,1}$$

This target displacement depends on both the characteristics of the existing building and the predefined performance objectives.

- Definition of the *nonlinear ductility demand*  $\mu_{Nonlin.}$  for existing building (Figure VI.24), defined as the ratio between the target displacement for the existing building in the nonlinear range  $\delta_{d,Nonlin.}$  and its yielding displacement  $\delta_{y,1}$ .

$$\mu_{Nonlin.} = \frac{\delta_{d,Nonlin.}}{\delta_{y,1}} > 1$$

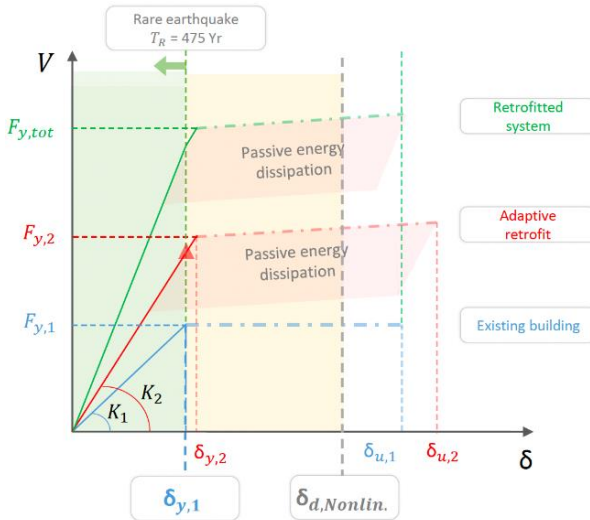


Figure VI.24 - Conceptual representation of potential nonlinear ductility demand for existing building

- Characterization of the *optimal energy dissipative capability* of the adaptive exoskeleton.

In *flag-shape systems* employing controlled and dissipative rocking, the total resisting moment provided by the system ( $M_{tot,R}$ ) can be considered as the sum of two contributions, the contribution of the individual walls ( $M_{wall,i}$ ) and the contribution provided by the coupling effect ( $M_S$ ) [170] [182].

$$M_{tot,R} = \sum_i M_{wall,i} + M_S$$

The contribution guaranteed by the individual wall is the sum of the contribution provided by the post-tensioning ( $M_{PT}$ ) plus eccentricity of the axial force ( $M_N$ ). In adaptive exoskeletons, in order to guarantee

elastic behaviour in the first stage, up to the defined threshold (i.e. earthquakes having a return period of 475 years - red triangle in Fig. 25), the total resisting moment must equal the minimum required resisting moment defined at the conclusion of the first step of the procedure ( $M_{Rd,min.}$ ):

$$M_{tot,R} = \sum_i (M_{PT} + M_N)_i + M_S = M_{Rd,min.}$$

The relative weight of each contribution can be defined preliminarily by requiring the exoskeleton to recentre at the end of the seismic event. To this end the coupling contribution must be limited [182]:

$$\beta_{CB} = \frac{M_S}{M_{tot,R}} < 0.5$$

- Definition of the *equivalent viscous damping ratio* for the retrofitted system  $\xi_{Retrofitted}$ .

By applying DBDR principles, the damping of the retrofitted system is evaluated based on a weighting in proportion to the base shear provided by the existing building and the exoskeleton [50], calculated using the simplified and conservative approach as follows:

$$\xi_{Retrofitted} = \frac{V_{Rd,min.}}{V_{Rd,min.} + F_{1,y}} \xi_{Esosk.} + \frac{F_{1,y}}{V_{Rd,min.} + F_{1,y}} \xi_{Exist.Build.}$$

The equivalent viscous damping of the existing building ( $\xi_{Exist.Build.}$ ) must be evaluated based on the building's specific structural features, whereas the equivalent viscous damping of the adaptive exoskeleton ( $\xi_{Esosk.}$ )



can be evaluated preliminary using the following formulation [182]:

$$\xi_{Esosk.} = \xi_{el} + \xi_{hys}; \xi_{hys} = \frac{2 \beta_{CB} (\mu_{Nonlin.} - 1)}{\pi \mu_{Nonlin.} (1 + r(\mu_{Nonlin.} - 1))}$$

The rate of equivalent elastic damping ( $\xi_{el}$ ) can be assumed conservatively to be 2% and the coefficient  $r$  to be 0.06 [182].

After defining the dissipative characteristics of the exoskeleton and determining the potential equivalent viscous damping, it is possible to determine whether the defined characteristics meet the requirements imposed in the nonlinear field by calculating the *minimum base shear required* by applying the *Displacement Based Design Retrofit* approach ( $V_{Rd,min.,DBDR}$ ):

$$V_{Rd,min.,DBDR} = 4 \pi^2 \frac{1.1 m_1}{T_{eff,Retrofitted}^2} \delta_{d,Nonlin.} - F_{1,y}$$

The effective period of the retrofitted system ( $T_{eff,Retrofitted}$ ) is calculated using the design displacement spectra of the site [184], damped by introducing the previously calculated equivalent viscous damping ratio ( $\xi_{Retrofitted}$ ).

The adaptive exoskeleton meets the requirements and the design procedure ends if the minimum required base shear defined at the end of the first step ( $V_{Rd,min.,design-spectra}$ ) is greater than- or equal to- the minimum required base shear calculated using the DBDR methodology ( $V_{Rd,min.,DBDR}$ ):

$$\frac{V_{Rd,min.}}{V_{Rd,min.,DBDR}} \geq 1$$

If this condition is not met, the design process becomes iterative by gradually increasing the structural standards in the exoskeleton's elastic range.

The containment of residual drift for the existing structure also requires that the contribution provided by the walls, sum of the contribution provided by the post-tensioning ( $M_{PT}$ ) plus eccentricity of the axial force ( $M_N$ ), exceed the resistance offered by the existing building.

$$\sum_i (M_{PT} + M_N)_i > F_{y,1} \frac{2}{3} \mathbf{H}$$

## **6.5. Numerical analysis of the dynamic behaviour**

In this chapter, the procedure previously described is applied to the design of alternative configurations of adaptive exoskeleton walls for the seismic retrofitting of a reinforced concrete reference building, representative of a residential building typology widespread in Italy.

After defining the elastic and dissipative structural properties of the alternative solutions, some representative configurations, both with vertical and horizontal arrangement of the primary structural elements, are designed and analysed.

The final section presents and discusses the results obtained from the nonlinear time history analyses of the finite element models of the analysed configurations.

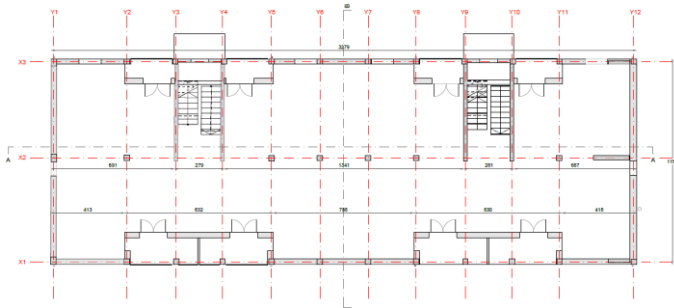
### **6.5.1. Reference building**

The reference building selected for the design of the adaptive exoskeletons is representative of a residential building typology that was widespread in northern Italy in the 1980s, whose structure consists of one-way reinforced concrete frames partly infilled with masonry (Figure VI.25).



a)

*Pianta piano tipo - Stato di fatto*  
Scala 1:100



b)

Figure VI.25 – Typical post WWII RC building: a) Pictures of a reference building; b) plane geometry

Based on findings of a research carried out by the university of Bergamo, which had the aim of classifying from a structural point of view hundreds RC social housing buildings [185], and according to [96]<sup>1</sup>, the input parameters were introduced to represent the ordinary post Second World War RC structures

---

<sup>1</sup> Reference geometry of post WWII RC building are summarized in Appendix B.

(Table 1). Further information can be found in the technical report [186].

Table 1 – Equivalent SDOF system parameters.

| Equivalent SDOF |       |         |
|-----------------|-------|---------|
| $m_I$           | 1118  | [kN/g]  |
| $k_I$           | 73.81 | [kN/mm] |
| $F_{y,I}$       | 1219  | [kN]    |
| $T_1$           | 0.77  | [s]     |

### 6.5.2. Structural design of the double-skin adaptive exoskeletons

The following characteristics must be possessed by the adaptive exoskeleton in order to meet the performance requirements, assuming the building location in Brescia, a province in northern Italy in medium-high seismic zone ( $a_g=0.233g$  [141]). For further details on the retrofit design steps, refer to the .

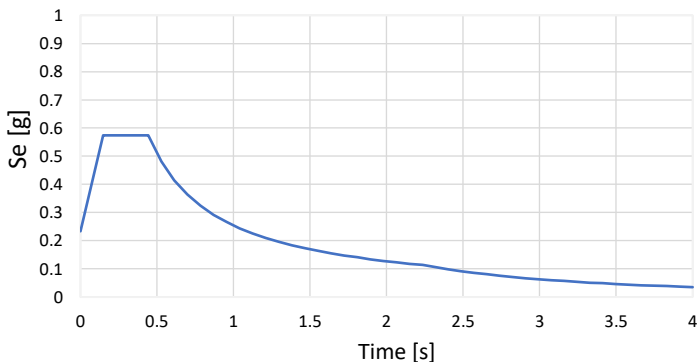


Figure VI.26 - Elastic design spectrum of the site at life-safety limit state (LSLS). From [141].

Following the design procedure in Sections 6.4.1 and 6.4.2, the *minimum required base shear* ( $V_{Rd,min.}$ ) for the retrofit to be able to limit the building drift under 0.5% at the Life-Safety Limit State (Figure VI.26) is equal to:

$$V_{Rd,min.} = 1.1 m_1 Se(T_{1,retrofitted}) - F_{y,l} = 3417\text{kN}$$

while the *minimum equivalent elastic stiffness* of the exoskeleton ( $k_2$ ) to limit displacements and damage to displacement-sensitive components is:

$$k_2 = 46.5 \frac{\text{kN}}{\text{mm}}$$

By applying the previously described nonlinear design parameters in the nonlinear range and adopting a coefficient  $\beta_{CB}$  equal to 0.45, it is possible to limit the building drift at NCLS under 0.8%. For the reference case study building, the *minimum base shear required* at near-collapse limit state ( $V_{Rd,min.,DBDR}$ ), defined by applying the *Displacement Based Design Retrofit* approach, is lower than the *minimum required base shear for the retrofit* ( $V_{Rd,min.}$ ) previously defined to satisfy the structural requirements in the elastic range.

$$V_{Rd,min.,DBDR} = 4 \pi^2 \frac{1.1 m_1}{T_{eff,Retrofitted}^2} \delta_{d,Nonlin.} - F_{1,y} = 978\text{kN}$$

$$< V_{Rd,min.} = 3417\text{kN}$$

### 6.5.3. Proportioning of the adaptive exoskeleton components for varying alternative configurations

Starting from the design parameters introduced in the previous section (Section 6.5.1), this section describes the geometrical

and technological features of the components of the adaptive exoskeleton, namely: the CLT panels, the couplers, and the re-centring systems.

Differentiating between vertical and horizontal structural arrangements, the alternative layout options are described in the two sections that follow. For the sake of simplicity, the numerical analyses focus on single coupled rocking systems extracted from the *adaptive exoskeleton* are analysed.

#### **6.5.3.1. Vertical arrangement of the panels**

The design of adaptive exoskeletons with the vertical arrangement of the primary structural elements, composed by dissipative coupled rocking systems, requires the definition of specific performance points (Figure VI.27), namely: *Couplers*

yielding, full plasticization of the CLT compressed toe, Re-centring system yielding.

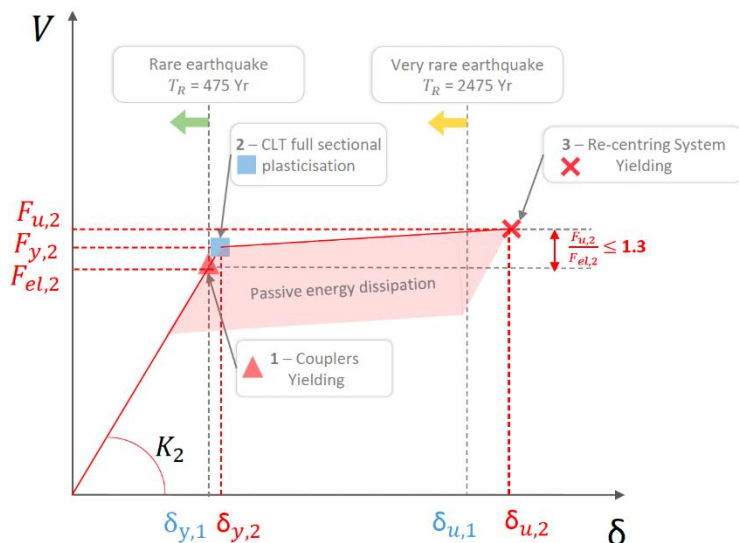


Figure VI.27 - Conceptual representation of the response curve of the adaptive exoskeleton with design performance points displayed: 1,2,3.

### 1. Couplers yielding

The couplers are assumed to yield when the conventional yielding displacement of the existing building ( $\delta_{y,1}$ ) is reached; this way damage to CLT panels is avoided and elastic steel bars is guaranteed (Figure VI.28). The underlying design assumptions are:

- Linear distribution of compressions at the base of the CLT panels, ensured by limiting the axial load to less than half the maximum load, and the achievement of elastic compression limit ( $f_{cd}$ ) for the most stressed timber fibre.



- The axial load in the re-centring steel bars, given by the sum of the pre-tension load ( $N_{PT}$ ) and its increase due to the elastic deformation of the retrofit ( $T_{PT}$ ), is smaller than yielding load ( $N_{yd}$ ). To ensure the proper operation of the re-centring system and to prevent its premature yielding, the maximum load in each steel bar ( $N_{PT} + T_{PT}$ ) has been limited to approximately two-thirds of the yielding load, therefore.

$$N_{PT} + T_{PT} = \frac{2}{3} N_{yd} < N_{yd}$$

- At this performance point the action in the retrofit is defined as  $F_{el,2}$ .

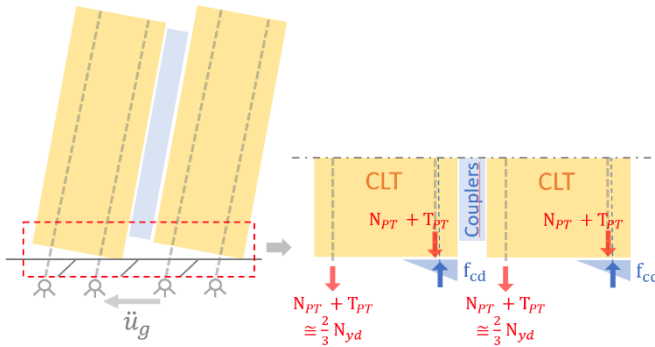


Figure VI.28 - Conceptual representation of the distribution of compressions at the base of CLT panels of coupled-rocking walls systems at couplers yielding.

## 2. Full plasticization of the CLT compressed toe

Further increase in displacement induces the progressive plasticisation of the compressed base section and the progressive decrease of the retrofit stiffness until complete sectional plasticisation is attained (Figure VI.29), which is associated with the

conventional exoskeleton yield strength ( $F_{y,2}$ ) and displacement ( $\delta_{y,2}$ ). The elastic behaviour of the re-centring elements beyond the activation threshold of the dissipators guarantees the self-centring response of the system.

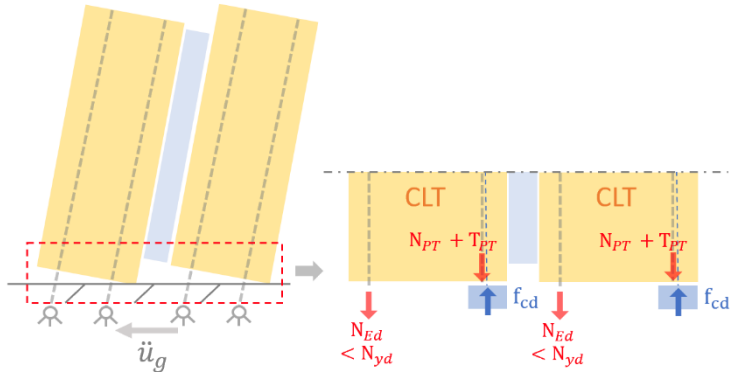


Figure VI.29 - Conceptual representation of the distribution of compressions at the base of CLT of coupled-rocking walls systems when reaching full sectional plasticization.

### 3. *Re-centring system yielding:*

The ultimate capacity of the exoskeleton ( $F_{u,2}$  ;  $\delta_{u,2}$  ) is associated with the yielding of the re-centring bars (Figure VI.30).

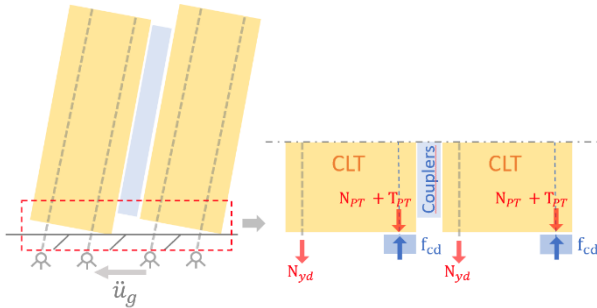


Figure VI.30 - Conceptual representation of the distribution of compressions at the base of CLT of coupled-rocking walls systems when reaching re-centring yielding.

The seismic action in the nonlinear range is capped by limiting the ratio between the base shear at the first performance point ( $F_{el,2}$ ) and the ultimate force ( $F_{u,2}$ ), with the aim of limiting the total accelerations experienced by structural and non-structural sensitive elements:

$$\frac{F_{u,2}}{F_{el,2}} \leq 1.3$$

The configurations described below were conceived by assembling *commercial-sized CLT panels* [187] [188] and *Dywidag Gewi S670/800-Plus continuous threaded steel bars* [189]. The technological properties and details are described below. Refer to for an in-depth description of the design process.

The geometry of the various configurations was determined by assuming compliance with the architectural limitations imposed by the arrangement of windows and doors in existing reference residential buildings (Section 6.5.1). To facilitate transport, the base width of the CLT panels comprising the systems was

restricted to about 2.5 metres, and to simplify the construction process, it was decided to concentrate the couplers in the centre of the horizontal timber strips, so that they are only subject to shear loads, whilst bending moment is resisted by the timber spandrel panel.

The two principal configurations, from which all others are derived, are described in the following:

- A) *CLT coupled rocking walls with post-tensioned steel bars*, referred to as “*configuration A*” (Figure VI.31) in the following.

This configuration is distinguished by the presence of two unbonded post-tensioned steel bars for each vertical CLT panel; these re-centring systems are constrained at the top of the panels by an anchorage system that transfers compressive loads to the timber section and is conceptually hinged in the underlying foundation.

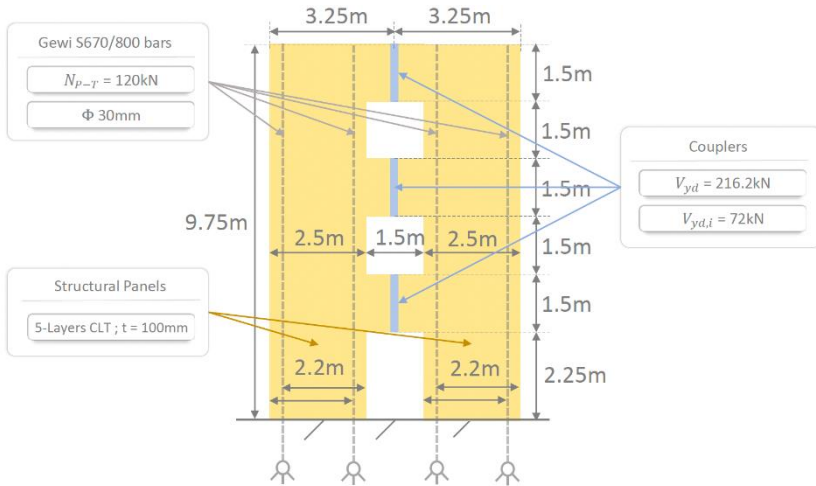


Figure VI.31 - Conceptual representation and synthetic description of the *configuration A*.

The solution features:

- Bars diameter:  **$\Phi 30\text{mm}$**
- 5-Layers CLT Panels:  **$t = 100\text{mm}$**
- Post-tensioning load for each steel bar:  **$N_{pT} = 120\text{kN}$**
- Shear yielding force for each of the 3 vertical stripes of couplers:  **$V_{yd,i} = 72\text{kN}$**
- Elastic base shear resistance:  **$F_{el,2} = 295.7\text{kN}$**
- Ultimate base shear resistance:  **$F_{u,2} = 380\text{kN}$**

B) *CLT coupled rocking walls with passive steel bars*, referred to as “*configuration B*” (Figure VI.32) in the following.

Unlike *configuration A*, in *configuration B* no initial post-tensioning is applied to the steel bars.

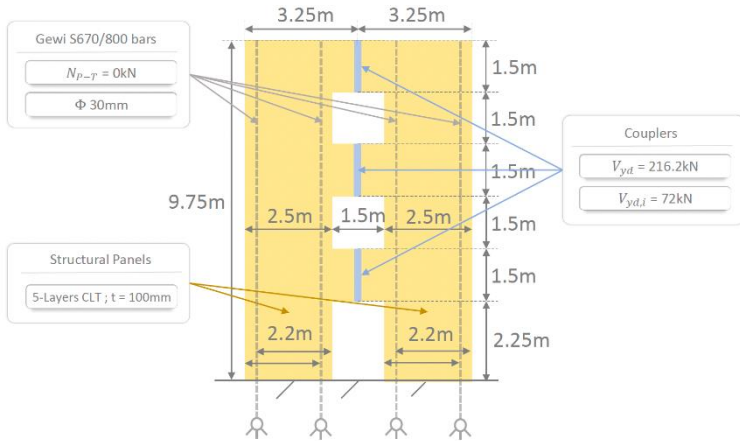


Figure VI.32 - Conceptual representation and synthetic description of the *configuration B*.

The solution features:

- Bars diameter: **Φ30mm**
- 5-Layers CLT Panels: **t = 100mm**
- Post-tensioning load for each steel bar:  **$N_{p,T} = 0\text{kN}$**
- Shear yielding force for each of the 3 verticals stripes of couplers:  **$V_{ydl,i} = 72\text{kN}$**
- Ultimate base shear resistance:  **$F_{u,2} = 380\text{kN}$**

Recently, some authors have proposed several structural solutions that further raise the level of reparability of the rocking solutions thanks to the introduction of replaceable sacrificial and energy dissipative elements at the base of the walls [161]. These innovative elements, consisting of timber (LVL) crushing blocks (Figure VI.33) designed to serve as the *weakest link* in the wall, make it possible to limit the damage to the CLT panel sections at the base, thereby reducing the need for repairs by concentrating the damage primarily in them, while increasing the system's energy dissipation capacity.

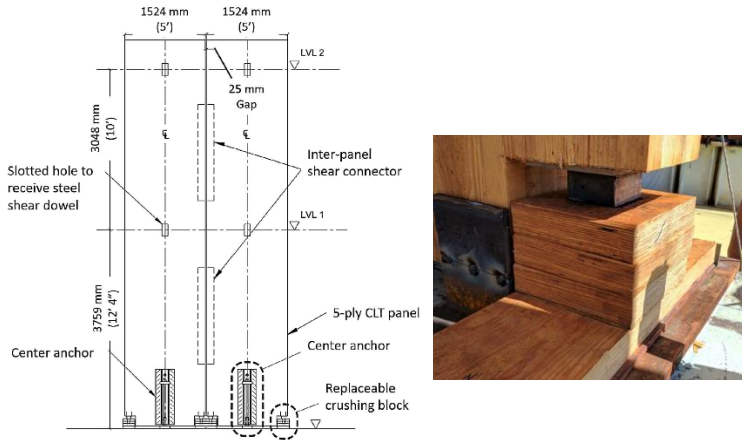


Figure VI.33 - On the left-side: Coupled rocking-wall dimensions, detailing, and design arrangement. On the right side: photo of the screw-Reinforced LVL crushing toe block. From [161]

Taking inspiration from these solutions, two additional configurations (C and D in the following) are conceived by integrating replaceable *sacrificial fuse elements* into the two principal solutions (*configurations A and B*), which are represented conceptually by compression-only, displacement-dependent, energy dissipation elements.

C) *CLT coupled rocking walls with post-tensioned steel bars (like Configuration A) with additional sacrificial fuse elements at the wall toe (Figure VI.34), referred to as configuration C in the following.*

At this stage of the research, these dissipative devices are conceptually represented by a rigid-plastic constitutive model.

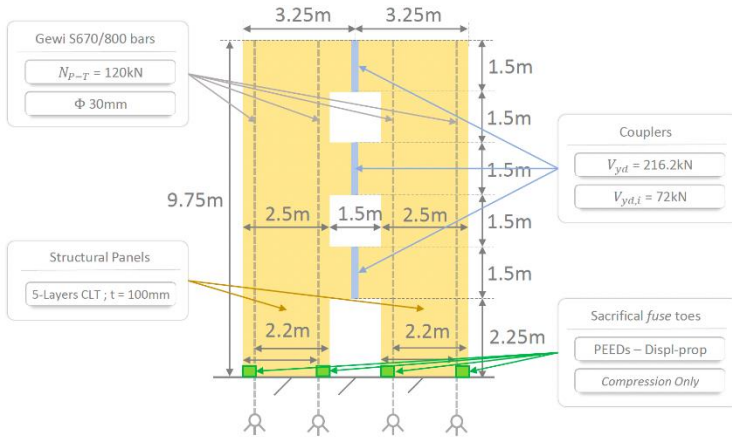


Figure VI.34 - Conceptual representation and synthetic description of the *configuration C*.

The solution features:

- Bar diameter: **Φ30mm**
  - 5-Layers CLT Panels: **t = 100mm**
  - Post-tensioning load for each steel bar:  **$N_{PT} = 120\text{kN}$**
  - Shear yielding force for each of the 3 verticals stripes of couplers:  **$V_{yd,i} = 72\text{kN}$**
  - Elastic base shear resistance:  **$F_{el,2} = 295.7\text{kN}$**
  - Ultimate base shear resistance:  **$F_{u,2} = 380\text{kN}$**
- D) *CLT coupled rocking walls with passive steel bars (like Configuration B), with additional sacrificial fuse elements at the wall toes (Figure VI.35), referred as configuration D in the following.*



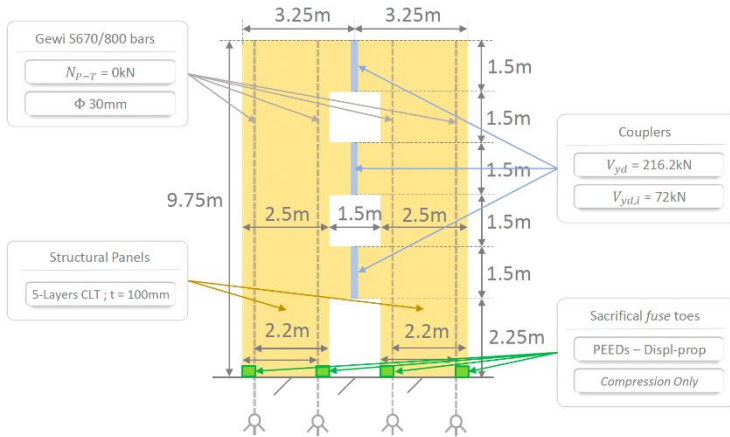


Figure VI.35 - Conceptual representation and synthetic description of the *configuration D*.

The solution features:

- Bar diameter: **Φ30mm**
- 5-Layers CLT Panels: **t = 100mm**
- Post-tensioning load for each steel bar:  **$N_{PT} = 0\text{kN}$**
- Shear yielding force for each of the 3 vertical stripes of couplers:  **$V_{yd,i} = 72\text{kN}$**
- Elastic base shear resistance:  **$F_{el,2} = 295.7\text{kN}$**
- Ultimate base shear resistance:  **$F_{u,2} = 380\text{kN}$**

Due to the geometry of the facades and the arrangement of the openings, the existing building's architectural constraints frequently necessitate the installation of hybrid systems consisting of coupled rocking walls combined with metal end-profiles. The addition of these end elements, which are coupled

to the structural panels via couplers and dissipators that repropose the resistant scheme of composite structural systems with incomplete interaction [190], increases the resisting moment guaranteed by the coupling effect.

The *PreWEC* systems, an acronym for *Precast Wall with End-Columns*, are an additional hybrid system for enhancing the dissipation capacity and resistance of coupled rocking walls [168]. Several comparable systems that employ the coupling between Pres-Lam panels and steel end-columns (CWC systems), incorporating UFP-type couplers and dissipators [191], have been documented in literature and executed in recent constructions in New Zealand [192].

In these solutions, the shear-walls are connected to steel end columns anchored to the foundation through a vertical stripe of hysteretic dissipators, thereby increasing both the system's energy dissipation capacity and its total resistant overturning moment. Such structural solution, originally conceived for hybrid systems with prefabricated RC rocking walls and steel columns, have recently been implemented using only timber materials, such as CLT panels for the walls and glulam for the columns [193].

Two additional configurations were conceived to test the effectiveness of hybrid, PreWEC-like, solutions. To this end, the two primaries' configurations (A and B) were equipped with end-steel-columns, made of structural steel S235, connected to the CLT walls by means of *displacement-dependent passive energy dissipation devices*, like those introduced as couplers for the CLT panels. Configurations E and F were obtained.

E) CLT coupled rocking walls with post-tensioned steel bars and Steel end-columns (Figure VI.36), referred as configuration E in the following.

In addition to configuration A, two S235 steel end-columns connected to CLT walls were introduced, using displacement-dependent passive energy dissipation devices conceptually represented by a rigid-plastic constitutive model, and hinged to RC foundation.

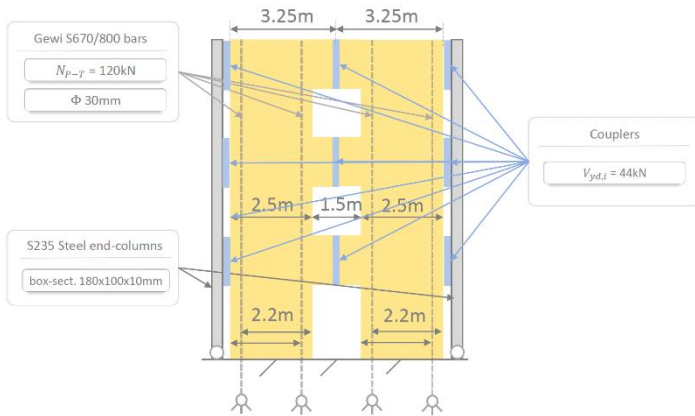


Figure VI.36 - Conceptual representation and synthetic description of the configuration E.

The solution features:

- Bar diameter:  **$\Phi 30\text{mm}$**
- 5-Layers CLT Panels:  **$t = 100\text{mm}$**
- Post-tensioning load for each steel bar:  **$N_{PT} = 120\text{kN}$**
- Shear yielding force for each vertical stripe of couplers:  **$V_{yd,i} = 41.5\text{kN}$**
- Elastic base shear resistance:  **$F_{el,2} = 295.7\text{kN}$**
- Ultimate base shear resistance:  **$F_{u,2} = 380\text{kN}$**

F) *Coupled rocking walls with passive steel bars and Steel end-columns (Figure VI.37), referred as configuration F in the following.*

In addition to configuration B, two S235 steel end-columns connected to CLT walls were introduced, using displacement-dependent passive energy dissipation devices conceptually represented by a rigid-plastic constitutive model, and hinged to RC foundation.

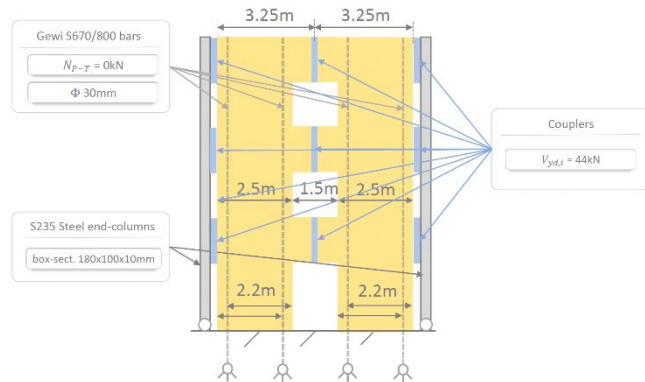


Figure VI.37 - Conceptual representation and synthetic description of the *configuration F*.

The solution features:

- Bar diameter: **Φ30mm**
- 5-Layers CLT Panels: **t = 100mm**
- Post-tensioning load for each steel bar:  **$N_{PT} = 0\text{kN}$**
- Shear yielding force for each vertical stripe of couplers:  **$V_{yd,i} = 41.5\text{kN}$**
- Ultimate base shear resistance:  **$F_{u,2} = 380\text{kN}$**

### 6.5.3.2. Horizontal structural arrangement

In this study, the analysis is limited to only two configurations characterized by a horizontal structural arrangement in order to highlight the major structural differences between the two macro-typologies (those featuring vertical and horizontal arrangements, respectively). Both the structural configurations evaluated in this section localise energy dissipation in *displacement-proportional PEDDs* placed between the structural panels at the first floor level. For this typology, the response curve and performance points are qualitatively different (Figure VI.38).

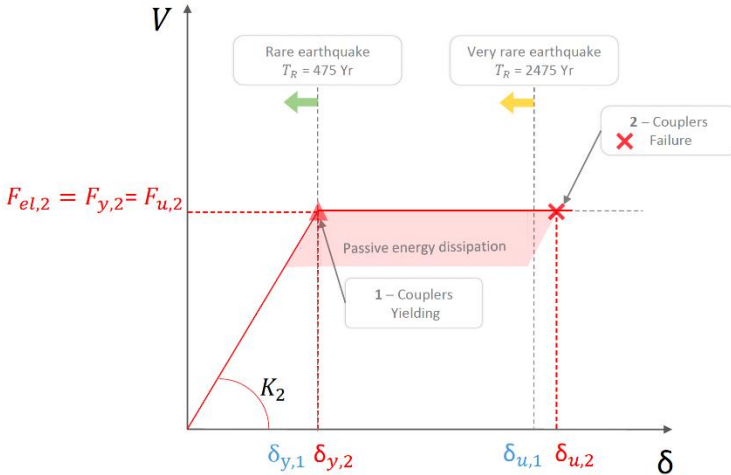


Figure VI.38 - Conceptual representation of the response curve of the adaptive exoskeleton with design performance points displayed: 1,3

#### 1. Couplers yielding

The couplers are assumed to yield when the conventional yielding displacement of the existing building ( $\delta_{y,1}$ ) is reached; limiting the stress acting on CLT panels preventing damage.

## 2. *Couplers failure*

The second performance point is reached ( $F_{u,2}$ ;  $\delta_{y,2}$ ) when the couplers reach their maximum deformation. In these systems, by introducing only displacement-proportional passive dissipators with a rigid-plastic constitutive model, it is possible to limit seismic actions while keeping all other elements in the elastic range. For these retrofits, the elastic limit resistance ( $F_{el,2}$ ), yielding strength ( $F_{y,2}$ ) and ultimate resistance ( $F_{u,2}$ ) coincide.

In the displacement interval between the first and second performance points, the displacement demand is primarily concentrated in the couplers, the residual drifts are not actively limited by the exoskeleton due to the absence of re-centring devices. Further research should prioritize the development of specific re-centring mechanisms adapted to the horizontal panel arrangement.

The analysed configurations are briefly described in the following:

- G) *CLT shear-walls with post-tensioned steel bars and horizontal couplers* located between the structural panels of the ground and first floors (Figure VI.39), referred to as *configuration G* in the following.

This configuration is characterized by the presence of two unbonded steel post-tensioned bars for each vertical timber shear-wall at the ground floor; unlike configurations A-F, the structural panels and the steel bars are designed to prevent rocking behaviour.

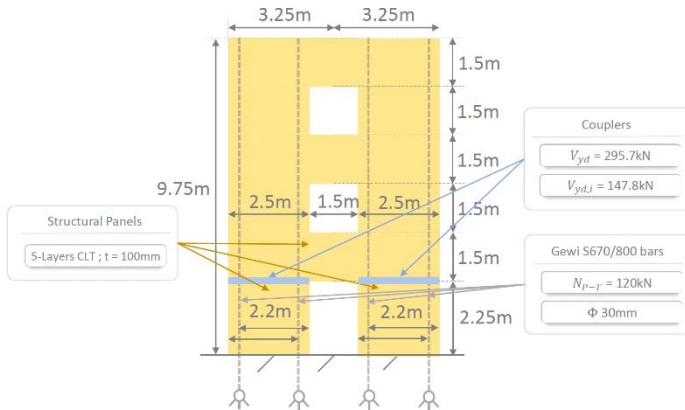


Figure VI.39 - Conceptual representation and synthetic description of the *configuration G*.

Both solutions are designed to attain the same base shear resistance as that of the solutions with vertical structural arrangement.

The solution features:

- Bars diameter:  **$\Phi 30\text{mm}$**
- 5-Layers CLT Panels:  **$t = 100\text{mm}$**
- Post-tensioning load for each steel bar:  **$N_{pT} = 120\text{kN}$**
- Total design shear yielding force of the horizontal couplers:  **$V_{yd,i} = 295.7\text{kN}$**
- Shear yielding force for each of the 2 horizontal rows of couplers:  **$V_{yd,i} = 147.8\text{kN}$**
- Base shear resistance:  **$F_{el,2} = F_{uiy,2} = F_{u,2} = 295.7\text{kN}$**

H) *CLT shear-walls with passive steel bars and horizontal couplers* located between the structural panels at the first floor level (Figure VI.40), referred to as *configuration H* in the following.

The only difference between this configuration and the previous one (*configuration G*) is the presence of passive steel bars with no initial post-tensioning.

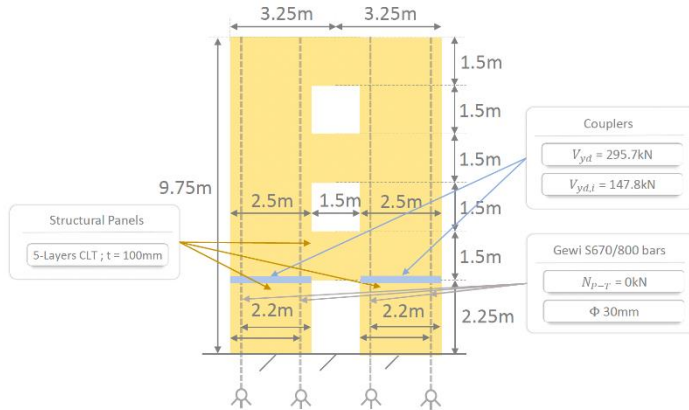


Figure VI.40 - Conceptual representation and synthetic description of the *configuration H*.

The solution features:

- Bars diameter: **Φ30mm**
- 5-Layers CLT Panels: **t = 100mm**
- Post-tensioning load for each steel bar:  **$N_{PT} = 0\text{kN}$**
- Total design shear yielding force of horizontal couplers:  **$V_{yd,i} = 295.7\text{kN}$**
- Shear yielding force for each of the 2 horizontal rows of couplers:  **$V_{yd,i} = 147.8\text{kN}$**
- Base shear resistance:  **$F_{el,2} = F_{uy,2} = F_{u,2} = 295.7\text{kN}$**

For the strengthening of the reference building, the number of retrofits represented by the analysed coupled-walls to be placed along each of the longitudinal facades is defined by dividing the required global shear strength defined at the end of structural design procedure ( $V_{Rd,global}$ ) by the elastic base shear



resistance of each retrofitting system ( $F_{el,2}$ ). The number of the analyzed coupled walls to be placed along each longitudinal facade is equal to:

$$n^{\circ} \text{ retrofits} = \frac{V_{Rd,global}}{2 F_{el,2}} = \frac{3417kN}{2 \cdot 295.7kN} \cong 5.8 \rightarrow 6$$

It is worth noting that single coupled-shear walls can be further coupled to obtain larger shear walls, as it will be discussed in the case study presented Chapter IX.

Post-tensioned bar solutions also effectively contain the residual drift of the existing structure when the sum of the post-tensioning contribution ( $M_{PT}$ ) and the eccentricity of the axial force ( $M_N$ ), calculated relative to the first performance point, exceeds the building's resistance. The sum of these contributions, as reported in the , is equal to:

$$M_{PT} + M_N \cong (N_{PT} + T_{PT}) Z_{el}$$

$$\rightarrow M_{PT} + M_N = 305.5kN \cdot 1.73m = 528.5kNm$$

Therefore, the minimum number of retrofits to be placed along each longitudinal facades, is approximately equivalent to:

$$n^{\circ} \text{ retrofit} = \frac{F_{y,1} \frac{2}{3} H}{2 (M_{PT} + M_N)} = \frac{1219kN \frac{2}{3} 9.75m}{2 \cdot 528.5kNm} \cong 6$$

### 6.5.4. Numerical models

This section briefly describes the features of the finite element models that are representative of the reference coupled shear walls described in the previous section [194].

The analysed configurations are represented numerically by *simplified 2D multi-axial springs models* (Figure VI.41) [159] employing the same types of one-dimensional finite elements.

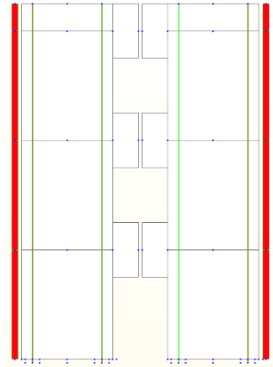


Figure VI.41 - Screenshot of the graphical representation of the numerical model of configurations E and F, created using the software [194].

A schematic representation of the numerical model containing the largest number of elements, which represents configurations E and F illustrated in Figure VI.42.

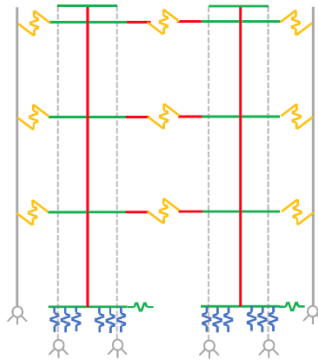


Figure VI.42 - Schematic representation of the numerical model of the configurations E and F, containing the greatest number of elements, in which each colour represents a different one-dimensional finite element.

With reference to the model described in Section 6.5.3, the main characteristics of the finite elements modelling configuration A to H are listed in the following:

- *5-Layers CLT structural panels* are represented using *beam elements*. The elasticity modules of these elements are described in and summarised in the table below taken from the software (Figure VI.43).

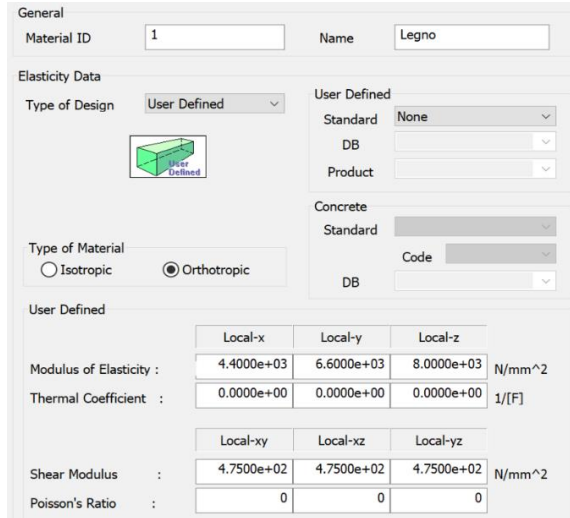


Figure VI.43 - Screenshot of the mechanical properties attributed to the beam representing CLT panels, taken from the software interface.

- Nonlinear properties of CLT panels of the configurations with vertical structural arrangement, from A to F, are represented using compression-only general links with a rigid-plastic constitutive model (Figure VI.44), denoted by the blue springs at the base of the timber walls, in order to concentrate the elastic timber deformations in the beam elements described above*

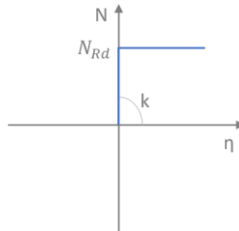


Figure VI.44 - Schematic representation of the rigid-plastic constitutive model of the compression-only general links modelling nonlinear CLT properties of the configurations from A to F.

Consequently, solely the axial properties were modelled:

- Elastic stiffness:  $K \rightarrow \infty$
- Post-yielding stiffness  $\cong 0$
- Compressive resistance  $N_{Rd}$ :

$$N_{Rd} = i_{G-link} t_{CLT} f_{cd,CLT}$$

$$N_{Rd} = 200\text{mm} \cdot 1000\text{mm} \cdot 8.69\text{MPa} = \mathbf{173.8\text{kN}}$$

- The *nonlinear properties of timber structural panels of the configurations with horizontal structural arrangement, G and H*, are represented using rigid-plastic with *simple bilinear* constitutive model (Figure VI.45), denoted by the light blue springs at the base of the timber walls.

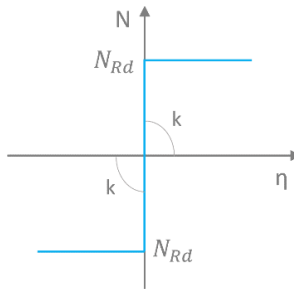


Figure VI.45 - Schematic representation of the rigid-plastic simple bilinear constitutive model representing nonlinear CLT properties of the configurations G and H.

In order to model the ideal contact area between the timber and the underlying foundations, three vertical nonlinear general links located at each bottom end of the vertical panels, with a 20 cm spacing ( $i_{G-link}$ ), are introduced. These elements, located at the centre of the contract area, are compression only elements. Accordingly, only the axial properties modelled:

- Elastic stiffness:  $K \rightarrow \infty$
- Post-yielding stiffness  $\cong 0$
- Compressive resistance  $N_{Rd}$ :

$$N_{Rd} = i_{G-link} \cdot t_{CLT} \cdot f_{cd,CLT}$$

$$N_{Rd} = 200\text{mm} \cdot 1000\text{mm} \cdot 8.69\text{MPa} = \mathbf{173.8\text{kN}}$$

- *Rigid elements without masses* are used to connect the different finite elements (green barycentric lines of the sections). These elements have the same sectional geometric properties as the vertical CLT panels and were introduced to properly represent the models designed.
- *Vertical steel bars made of Dywidag gewi S670/800 plus*, introduced as re-centring devices. These components are modelled with *truss elements*, having an elastic-plastic tension-only response (Figure VI.46). They possess the same sectional mechanical properties and post-tensioning load as the bars described in the previous section.

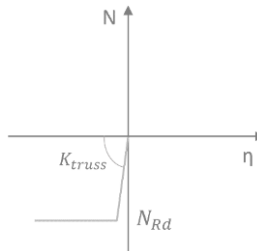


Figure VI.46 - Schematic representation of the elastic-plastic constitutive model of the tension-only truss modelling Dywidag Gewi steel bars.

The properties of these elements are as follows:

- Elastic modulus:  $E_s = 210000\text{MPa}$
- Sectional area:  $A_s = 707\text{mm}^2$
- Design yielding strength:  $f_{yd} = 645\text{MPa}$
- Tensile resistance:

$$N_{Rd} = f_{yd} A_s = 645\text{MPa} \cdot 707\text{mm}^2 = \mathbf{456\text{kN}}$$

- *Rigid horizontal elastic springs* are introduced to transfer the ground motion to the resisting systems.
- *Rigid plastic general links* (Figure VI.47), transferring *shear forces only* are introduced to model the couplers between adjoining elements (displacement-proportional passive energy dissipation devices, yellow springs).

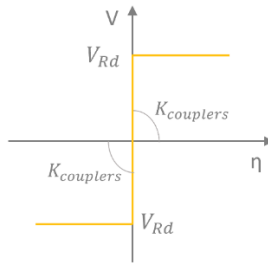


Figure VI.47 - Schematic representation of the rigid-plastic constitutive model of the vertical couplers.

The following mechanical properties are adopted:

- Elastic stiffness:  $K \rightarrow \infty$
- Post-yielding stiffness  $\cong 0$
- Shear resistance  $V_{Rd}$  varies according to the configuration considered as described in the previous section.

- *Steel end-columns* are modelled as *beam elements* (continuous grey barycentric lines). S235 structural steel and the geometric and sectional characteristics described in the previous section were adopted.

*Configurations C* and *D* are characterized by the presence of *sacrificial fuse systems*. These devices are conceptually modelled as compression-only elements and exhibit a compressive strength lower than that of the CLT section they are connected to, thereby preserving the timber integrity and concentrating damage. These elements enable decreasing the resistance of the four end-general links at the base of the CLT panels (grey vertical elements at the base, in Figure VI.48).



Figure VI.48 - Schematic representation of vertical general links at the base of CLT panels for configurations C and D. The end elements representing the sacrificial fuse toes are highlighted in grey.

To prevent damage in the CLT element without affecting the overall resistance of the system, the axial resistance of the fuse-elements is smaller than that of the equivalent CLT section:

$$N_{Rd} = 170\text{kN} < 173.8\text{kN}$$

*Configurations G* and *H*, characterised by the horizontal arrangement of both panels and couplers, were modelled with identical one-dimensional finite elements (Figure VI.48, Figure VI.49).



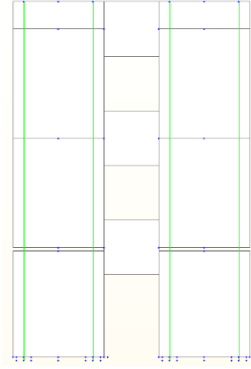


Figure VI.49 - Screenshot of the graphical representation of the numerical model of configurations G and H, created using the software [194]

Unlike the vertical arrangement configurations, the horizontal configurations feature two general links above the base panels, that simulate the rows of horizontal couplers (Figure VI.50).

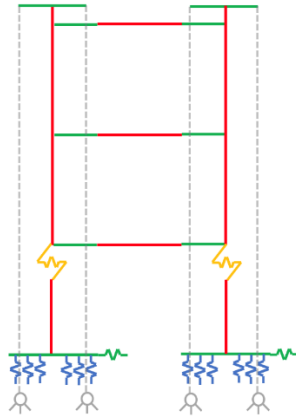


Figure VI.50 - Schematic representation of the numerical model of the configurations G and H, in which each colour represents a different one-dimensional finite element.

These elements are modelled by introducing rigid-plastic *general links representing the horizontal rows of couplers* with the shear resistance defined in the previous chapter:

$$V_{Rd} = 147.8\text{kN}$$

In all conceived models, the potential kinematic incompatibility between adjacent structural panels subjected to horizontal actions is inhibited as it is ideally avoided by the presence of horizontal diaphragms.

The existing building was modelled by introducing inertial masses at the floor level and constrained to the nodes of the coupled shear wall. The pertaining mass for each coupling shear wall ( $m_{tot-FEM}$ ) was calculated by dividing the building's total mass ( $m_{tot-building}$ ) by the minimum number of coupling shear walls to be arranged along each longitudinal direction to ensure minimum base shear resistance, as previously defined (Section 6.5.3):

$$m_{tot-FEM} = \frac{m_{tot-building}}{12} \cong \frac{1.1 \frac{1118\text{kN}}{g}}{12} \cong 102.5 \frac{\text{kN}}{g}$$

To represent the spatial distribution of the building's masses, each coupling shear wall pertaining mass ( $m_{tot-FEM}$ ) was divided into lumped masses ( $m_i$ ) introduced in the numerical models as shown in Figure VI.51.

$$m_i = \frac{m_{tot-FEM}}{6} = \frac{102.5 \text{ kN/g}}{6} \cong 17.1 \frac{\text{kN}}{g}$$

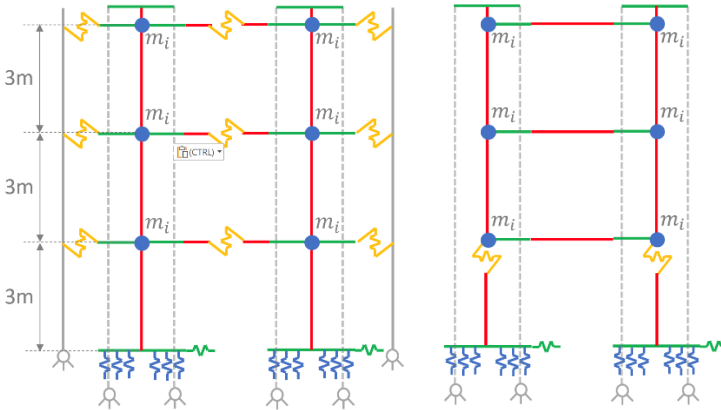


Figure VI.51 - Schematic representation of the numerical models modelling the vertically arranged solutions on the left and horizontally arranged ones on the right. The inertial masses located at the level of each existing slab are represented by the blue dots.

The damping ration introduced in the numerical models is mainly representative of the energy dissipated by the system in the elastic range, set equal to 2%.

### 6.5.5. Ground motion

The dynamic effects and severe damage caused by major near-fault earthquakes on different structural typologies, ranging from *traditional* seismic-resisting systems [180], to innovative high-performance [195] [196] [197] [198], and self-centring systems [176] [199], have received increasing attention and have been widely studied by many researchers [200] [201] [202] [203] [181] [204]. These studies highlight the peculiar characteristics and structural impacts of such ground motions. This *class* of earthquakes is characterized by the presence of *fling-step* and *forward-direction inputs* [181] [205] [206], as

well as by *low-cycles* and *high ground velocity* [176], generating large deformation demands for a wide range of structures.

In the past, several authors have summarised the main characteristics of these events by proposing few *simple mathematical models* [179] for representing their *peculiar principal characteristics*, such as few wavelets or various harmonic waves [181], series of pulses [207] and double impulse [204] [208] [209].

In this preliminary study of the qualitative structural and dynamic behaviour of adaptive exoskeletons, a *symmetrical double impulse* ground motion was selected for the nonlinear time history analyses. One of the primary goals of these analyses is to examine the energy dissipation capacity of the adaptive systems exposed to very rare, high-intensity earthquakes triggering the nonlinear behaviour. The selected ground motion enables a simple and direct investigation of the behaviour of the conceived systems subject to cyclic actions, the behaviour of these systems undergoing ground motion records of major near-fault earthquakes will be analysed in future research development. The characteristics of the selected ground input are described in the following:

- The double impulse period is 0.4 seconds, which falls within the typical period-range characterizing the *Italian earthquakes*, which varies between 0.3s for rigid soils, and 0.6s for more deformable soils [210].
- The peak-ground acceleration (P.G.A.), reached at the positive and negative peaks, is equal to 0.3g. The selected P.G.A. is significantly greater than the expected ground acceleration at the reference site for

seismic events with a return period of 475 years, which is estimated to be 0.222g, as well as that expected for much rarer and more intense earthquakes with a return period of 970 years, which is estimated to be 0.276g (Figure VI.52), to observe relevant nonlinear displacements and significant couplers deformations.

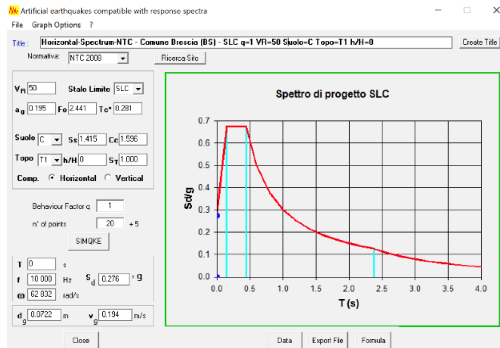


Figure VI.52 - Representation of the reference design spectrum for the site calculated for a return time of 970 years. Defined using [211].

- The time extension of the ground motion is approximately 0.4 seconds, the residual deformations are considered as those deformations recorded after 20 seconds past the double impulse (Figure VI.53, Figure VI.54).

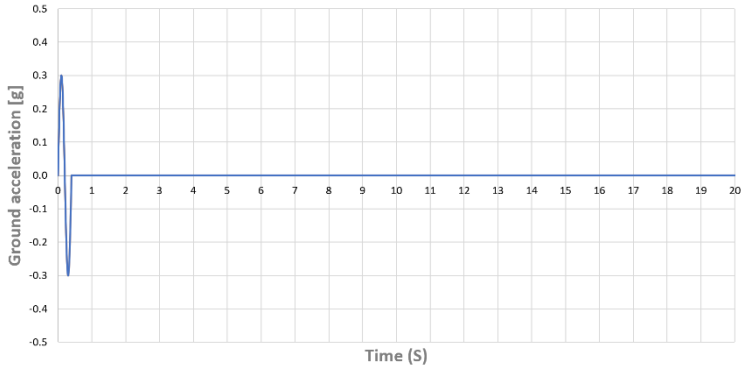


Figure VI.53 - representation of the *total extension* of the ground motion.

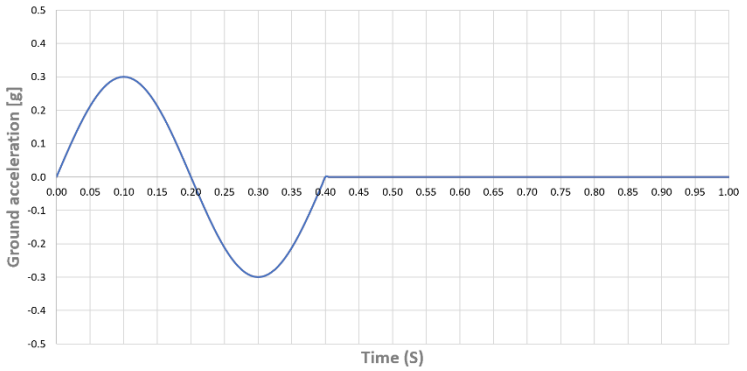


Figure VI.54 - Representation of the *characteristic principal part* of the ground motion showing the path and characteristics of the symmetrical double impulse.

### 6.5.6. Analysis of results

To allow for an easier discussion of the results, the analysed cases described in Section 6.5.3 are summarized in Table 2. To evaluate the influence of the amount of the post-tension, case A was evaluated by varying the post-tension amount by  $\pm 25\%$ .

Table 2 – Overview of the analysed cases in the parametric analyses.

| <b>Configuration</b> | <b>Description</b>  |
|----------------------|---|
| <b>A</b>             | <b>With</b> post-tension and <b>vertical</b> couplers   |
|                      | <b>A (-25%)</b> post-tension is reduced by 25%  |
|                      | <b>A (+25%)</b> post-tension increased by 25%   |
| <b>B</b>             | <b>Without</b> post-tension and <b>vertical</b> couplers                                      |
| <b>C</b>             | <b>With</b> post-tension, <b>vertical</b> couplers and <b>fuse</b> at the base                |
| <b>D</b>             | <b>Without</b> post-tension, <b>vertical</b> couplers and <b>fuse</b> at the base             |
| <b>E</b>             | <b>With</b> post-tension, <b>vertical</b> couplers and <b>steel profile (Hybrid walls)</b>    |
| <b>F</b>             | <b>Without</b> post-tension, <b>vertical</b> couplers and <b>steel profile (Hybrid walls)</b> |
| <b>G</b>             | <b>With</b> post-tension and <b>horizontal</b> couplers                                       |
| <b>H</b>             | <b>Without</b> post-tension and <b>horizontal</b> couplers                                    |

The top displacements experienced by the walls in the non-linear time history analyses are plotted in Figure VI.55, and their maximum and residual displacements are reported in Figure VI.56 (a), respectively.

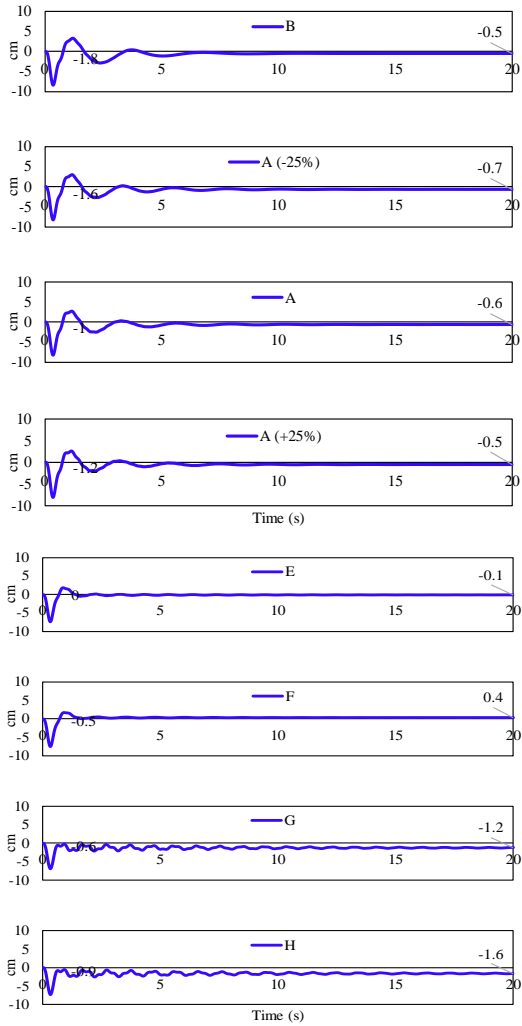


Figure VI.55 – Top displacement as a function of the analysis time for each of the analysed cases.



Considering **configuration A** as the reference case (which experienced a maximum top displacement equal to 8 cm - about 0.9% drift), it can be seen that the top displacement reduces by 12% when a hybrid system (**configurations E, F**) or horizontal couplers are considered (**configurations G, H**), while it does not significantly vary for the other cases. In **configuration B** the top displacement does not significantly vary due to a) the low influence of the post-tension when high diameter bars are implemented, b) the elastic target displacement imposed (0.5%). In particular, if a lower target displacement would be imposed (e.g., 0.25%), the post-tension would be more influencing (see Chapter IX). As for **configuration C** and **D**, the top displacement does not vary due to stiffness and strength were designed to be the same of **configuration A** and **B**, respectively. The reduction in the case of the hybrid system may be associated with the high capacity and stiffness of the walls when steel profiles are added while for the **configurations G** and **H** the reduction may be associated with the *simple bilinear* behaviour of the *general links* at the base (instead of the *compression only* behaviour introduced for all the other cases). The hybrid systems allow also for a residual drift reduction (-83% for **configuration E** and -33% for **configuration F**). Conversely, as expected, when horizontal couplers are introduced, the residual displacement always increases, provided that no re-centring capability is implemented in these models; furthermore, the residual displacement doubles when the post-tension is applied (**configuration G**) and increases by 2.6 times in the case without post-tension (**configuration H**).

As for **configuration A** the maximum displacement is not affected by the amount of the applied post-tension, while the residual displacement decreases by increasing the post-tension. Such a trend cannot be extended for **configuration B** in which

passive bars were introduced. The reason may be associated with a lower non-linear deformation at the wall toe experienced in **configuration B** in the absence of initial post-tension (Figure VI.57), resulting in a lower residual displacement. The maximum non-linear compression displacements of the *general links* at the base of each wall are plotted in Figure VI.57; in particular, the displacements of the six *general links* (three to the left and three to the right of the vertical centroid axis) of each of the coupled wall (left-L and right-R) are plotted. The maximum non-linear deformation increases for increasing the post-tension; it increased by 1 cm in the case without post-tension (**configuration B**), and by 1.4 cm in **configuration A (+25%)**. The non-linear deformation at the wall base decreases when a hybrid solution is adopted (**configurations E, F**) while it increases when horizontal couplers are implemented (**configurations G, H**). The steel profiles of the hybrid system slightly unload the panels which experienced a lower deformation. The increase in the **configurations G and H** may be associated with the *simple bilinear* behaviour introduced to allow for the couplers activation. From Figure VI.57 it can also be observed that in the cases with vertical couplers (**configurations from A to F**), the walls behave coupled (the two walls exhibit a global coupled behaviour), walls while such behaviour cannot be observed when horizontal couplers are introduced (**configurations G, H**). **Configurations C and D** are plotted with **configurations A and B** since no variations were observed for the same reason provided for the top displacement. This is reasonable since the fuses were designed to localize damages without changing the behaviour of the walls; consequently, the maximum fuse capacity was set very close (slightly lower) than that of the panels.

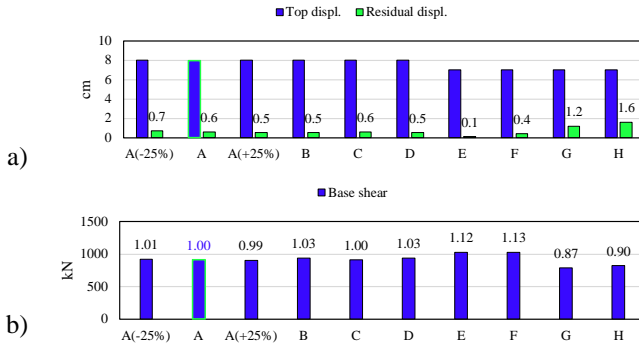


Figure VI.56 – Top displacement (blue) and residual displacement (green) experienced by the wall in the non-linear time history analyses. The reference case A is plotted with a green edge.

In Figure VI.56 (b) the maximum base shear is plotted. The post-tension does not significantly affect the base shear which increases by 12 % and 13 % when a hybrid solution with and without post-tension are adopted, respectively; the result agrees with those observed previously. When horizontal couplers are introduced in post-tensioned and non-post-tensioned walls, the base shear reduces by 13 % and 10 %, respectively. The results may be associated to a high global dissipated energy provided in these cases (Figure VI.58).

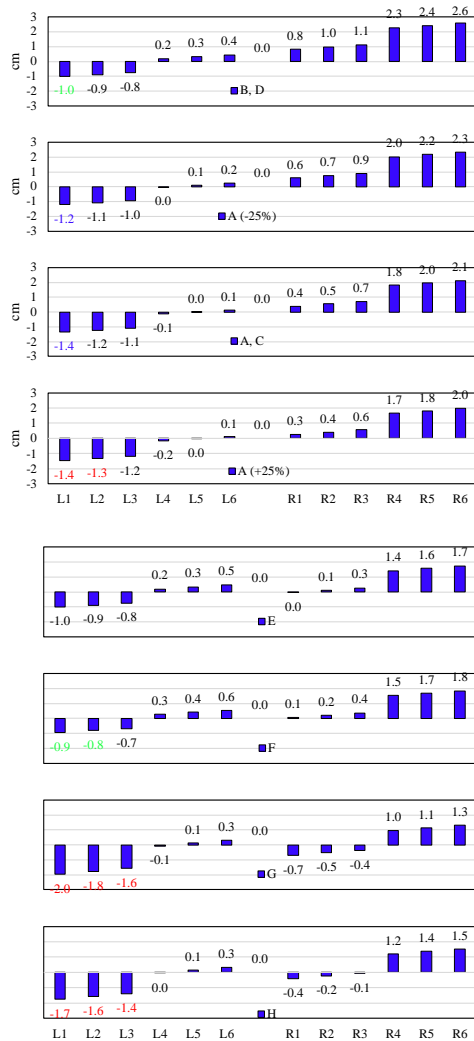


Figure VI.57 – Non-linear deformation of the general links at the base of the coupled walls. Six general links were placed at the base of each walls (three to the left and three to the right of the vertical barycentric axis). L and R refer to the left and right wall, respectively.

In Figure VI.58 the total dissipated energy normalized with respect to **configuration A** is plotted for each case (see the blue line histogram referring to the subtended area of the base shear-top displacement curve), while the share of the dissipated energy in the base *general links* and vertical and horizontal couplers are plotted in red and blue, respectively. Note that the percentages plotted for the general links at the base (red) and couplers (blue) refer to the single case considered.

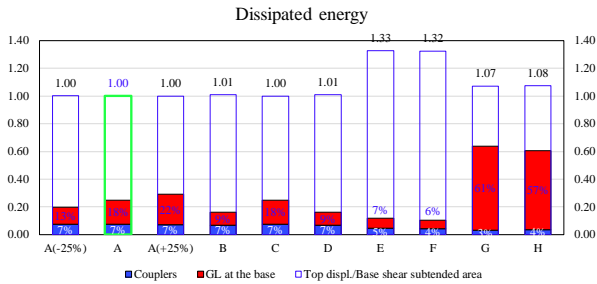


Figure VI.58 – Dissipated energy observed for each case is plotted; in particular, with a blue edge is plotted the subtended area of the base shear-top displacement graph while in red and blue are plotted the base general links, and vertical and horizontal couplers dissipated energy, respectively.

From Figure VI.58 it emerges that the subtended area of the base shear-top displacement curve increases by more than 30% when hybrid solutions are adopted and by about 7% to 8% when horizontal couplers are introduced. The dissipated energy of the couplers doesn't significantly vary in all cases; the reduction observed in **configurations G** and **H** may be associated with a lower number of couplers adopted (two instead of three). The base *general links* dissipated energy increases while increasing the post-tension; such a result agrees with the non-linear deformation trend observed in Figure VI.57. According to the results, the influence of post-tension in the examined models is limited; additional analyses and research will be conducted by

varying the characteristics of the case studies in order to analyse its influence in greater depth.

## **6.6. Concluding remarks**

In this chapter, the potential benefits offered by adaptive exoskeletons for the retrofit of existing buildings and their limitations were analyzed, and a design procedure was proposed to enable design professionals to easily calibrate performance objectives and related design targets. Simplified static models were also proposed allowing for a *hand calculation and thus a hand control* of the system response, and to preliminarily assess the relative influence of the involved parameters.

From a structural point of view, adaptive exoskeletons may be designed to guarantee quite challenging performance objectives, according to a Life Cycle Thinking (LCT) approach. For example, for frequent to rare events, they can be designed to guarantee full usability and no damage; this can be obtained by forcing an elastic behavior of the retrofitted building. On the other hand, for very rare events, they can be designed to ensure easy reparability of the building, limited damage and no residual displacements, by introducing energy dissipation systems and by guaranteeing the recentering behavior of the structure. Reparability may also be guaranteed by lumping the damage into few sacrificial and replaceable dissipative devices, ensuring the possible replacements of the damaged components through mindful design of the construction detailing, with particular reference to their connections to the structural system and their accessibility. Such LCT-based performance objectives allow the minimization of costs and impacts (both direct and indirect) associated with earthquakes and with the possible retrofit works.

The limits of applicability of the adaptive exoskeletons as a seismic retrofit technique are related to the structural system and the seismic response of the existing building in the as-is condition. According to the studies carried out in the present chapter, the adaptive exoskeletons are effective for the enhancement of the seismic behaviour of those existing buildings characterized by an elastic-plastic response curve; in this case, the proportioning of the retrofit components and the dissipative behavior of the retrofitting system are calibrated according to the actual ductility of the existing building with the aim of controlling the maximum displacement capacity. On the other hand, this type of retrofit is unsuitable for brittle constructions and with unreliable ductility, such as those discussed in Chapter IX, featuring poor quality masonry. In the cases of buildings featuring an elasto-fragile behaviour, adaptive systems could only be implemented upon completion of preliminary corrective interventions aimed at increasing ductility of some portions of the existing structure, and thus at controlling the collapse mechanism.

A few main lessons were also learnt from the numerical analyses; however, it should be considered that such remarks are strictly contextualized to the hypotheses adopted in this preliminary study investigation and that much research is required to further investigate the structural solution and to extend the validity of the obtained results. Limited to the hypotheses range, it has been noted that the post-tension does not significantly affect the results when high diameter bars are adopted and/or when high drift targets are imposed. It is expected that post-tension would be more influencing for low diameter bars and low drift target (see Chapter IX). High post-tension levels may lead to high nonlinear deformation at the wall

toes and to the yielding of the post-tensioning bars which results in high residual displacements.

In addition, considering the analyzed case study, it is worth noting that it would be realistically better to couple the six adaptive walls thus exploiting the whole façade dimension, thus significantly increasing stiffness and strength and allowing for a foundation stress reduction. However, the parametric analyses had the objective to make preliminary considerations about the influence of the main adaptive system components on the structural behavior. It is worth noting that in the case of coupling a series of adaptive walls (as in the case discussed in Chapter VIII and IX), the same design procedure can be adopted.



## VII. Development of the *AdESA fuse*

### 7.1. Introduction

Preliminary investigation of *adaptive exoskeletons* reported in the previous chapter highlighted the potential of integrating *displacement-proportional passive energy dissipation devices* (PEDDs) both as couplers between the primary structural elements, and as dissipative elements. This chapter extends the analysis by examining these *key elements* from a *technological perspective*.

The first section of this chapter provides a brief overview of the energy dissipation devices, as well as a description of some selected examples reported in the vast scientific literature. Then, the optimal structural performances of these devices are defined in compliance with the Life Cycle Structural Engineering perspective, which integrates life cycle thinking and circular economy principles and extends their assessment from structural to environmental and economic perspectives.

In the second section, the characteristics of the *AdESA fuse* [15], a displacement-proportional PEED that not requires special manlabor for production nor installation, specifically conceived considering construction site issues related to procurement and installation, as well as to reduce costs while guaranteeing performance, are described; experimental results, obtained from laboratory tests on different configurations are commented.

## 7.2. Brief overview on Displacement-proportional Passive Energy Dissipation Devices

Numerous authors from all around the world have proposed and developed various dampers and couplers that exploit the inelastic deformation of ductile metal sections to dissipate a portion of the input seismic energy.

A pioneering example of these devices is represented by the *UFP couplers* (Figure VII.1) [191], which were initially developed in New Zealand in the 1970s and subsequently further analysed and reengineered by many researchers. These devices consist of a curved steel plate coupling the structural elements to which it is connected and dissipating a portion of the input seismic energy by flexural yielding.

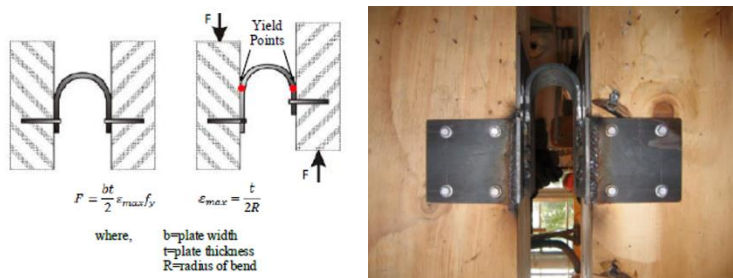


Figure VII.1 - Representation of UFP dampers. From [212].

Produced by hot-bending metal plates to form a U-shaped element (UFP), they can be designed for a wide range of displacements and forces, with variable plate thickness, depth, and radius of curvature.

Over the last few decades, other hysteretic metal dampers were proposed, that take advantage of the energy dissipation provided

by the yielding of the elements subjected to torsional and flexural actions [213] [214].

The X-shaped dampers known as *Additive Dampers And Stiffness (ADAS)* [215] [216] [217] [218] [219] are one of the distinguished example of the many hysteretic devices designed for both new structures, as well as for the retrofit of existing buildings. These devices are made of a series of steel plates with a distinctive X-shape (Figure VII.2) that allows for the development of a diffuse sectional yielding along the entire height of the plates when loaded out of plane by the earthquake-induced shear loads, resulting in a stable dissipative behaviour (Figure VII.3) [216].

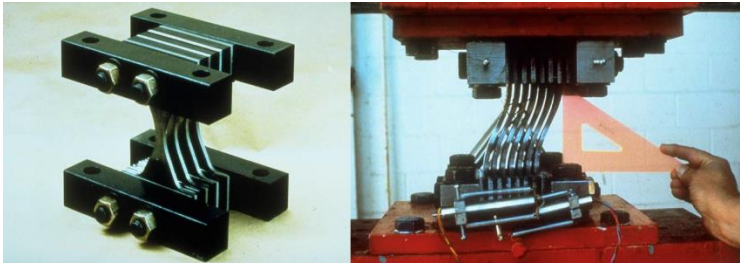


Figure VII.2 - Images of ADAS devices before (left) and during the laboratory test (right). From [214].

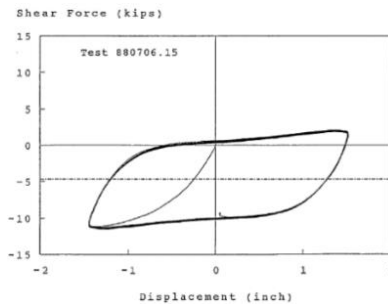


Figure VII.3 - Representation of the experimental curve obtained from laboratory tests. From [216].

The ADAS devices are also highly adaptable, as their strength and stiffness can be calibrated by varying the size, thickness, and number of the steel plates. One interesting alternative layout entails the replacement of the vertical X-shaped plates with triangular steel plates and the substitution of inferior end-fixed support with a pin (Figure VII.4), ideally downgrading it to a hinge support (*T-ADAS*) [214] [220].

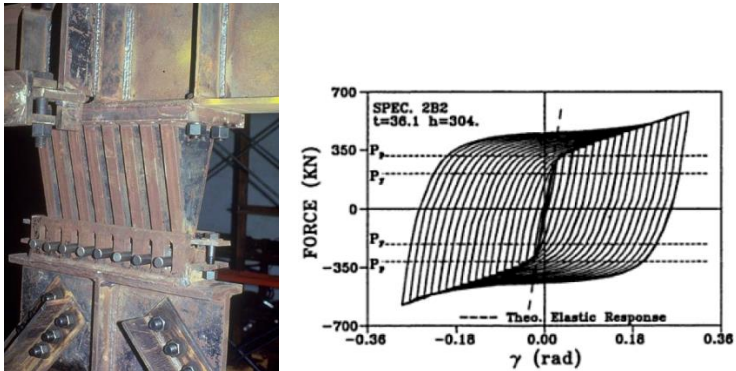


Figure VII.4 - On the left-side: image of T-ADAS devices before laboratory tests. From [214].  
On the right-side: results of the cyclic experimental tests. From [220].

A further example of a recently developed dissipator exploits the resistance mechanism of ADAS by basing energy dissipation on the activation of localised plastic hinges, which is ensured by the peculiar shape of the dissipative plates [13]. This prefabricated and standardised device is designed to accommodate various design specifications. Its replaceable dissipative elements, which consist of the pre-shaped steel plates, are inserted into the pre-cut slots in the connecting plates and subsequently welded to these elements (Figure VII.5). It is possible to calibrate its global resistance and stiffness by varying the number of steel plates or by modifying their sectional properties. However, its reparability is limited by

residual deformations in the dissipative plates, which inhibit their replacement.

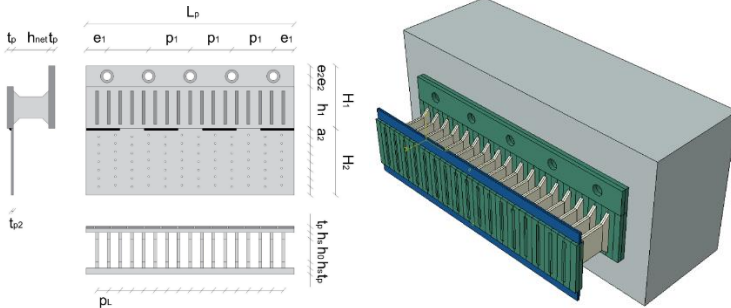


Figure VII.5 - On the left-side: 2D representation of the devices. On the right-side: 3D representation of the same devices. From [221].

Other researchers have proposed a variety of interesting hysteretic devices made of commercial steel beams. An intriguing example is the device developed in the 1990s to serve as a coupler and energy dissipator consisting of a square steel tubular section with two sides appositely shaped to reduce the cross-section (Figure VII.6), thereby localizing the plastic hinge [222].

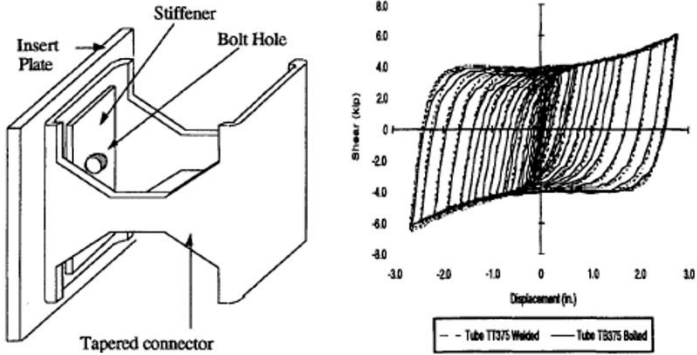


Figure VII.6 - On the left-side: representation of the devices. On the right-side: results of the cyclic experimental tests. From [222].

The use of a commercial tubular profile eliminates the need for welding and bolting between the weaker slitted plates and the other elements, preventing the formation of heat-altered zones that could jeopardize the dissipating capacity, or the reduction of the flexural stiffness due to bolt loosening. The strength and stiffness of these devices can be calibrated by modifying the sectional properties of the slitted plates.

Other authors have conceived hysteretic devices from commercial steel beams, such as the *Steel Slit Damper (SSD)* [223] [224]. This damper, made from a commercial profile and characterized by the slits in the web, manufactured with rounded edges to reduce stress concentration at the corners (Figure VII.7), eliminates welding and all uncertainties and alterations associated with such a process.

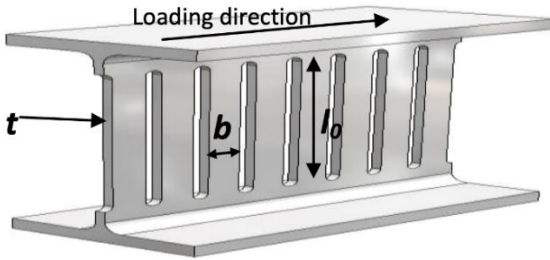


Figure VII.7 - Schematic representation of the Steel Slit Damper. From [224].

When the device is subjected to severe earthquake-induced shear loads acting in the main direction of the original steel beam, the flexural yielding of the web resisting elements dissipates portion of the seismic energy; the results of the experimental test demonstrated their large dissipative capacity (Figure VII.8, Figure VII.9) [223]. The disassembly and reassembly of the device is facilitated by the presence of four holes drilled in the flanges, which allow the device to be bolted to the structure.

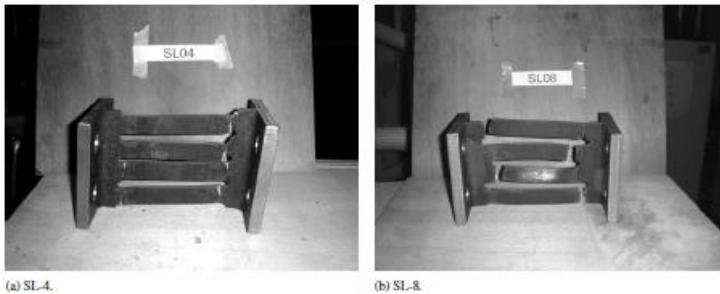


Figure VII.8 - Images of specimens at the end of the experimental cyclic tests. From [223].

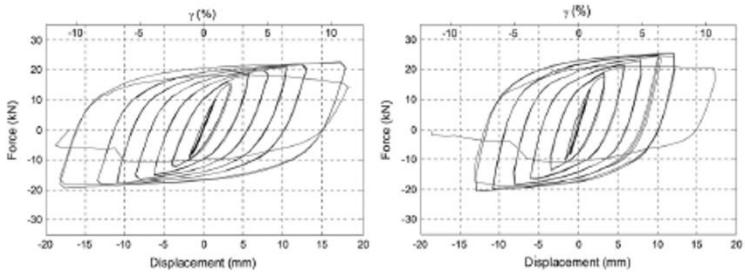


Figure VII.9 - Results of the cyclic experimental tests. From [223].

The same authors later proposed the *TSSD* [223], which stem as an optimization of the Steel Slit Damper (Figure VII.10). *TSSD* exhibits an increased dissipation capacity, that is obtained by changing the shape of the web slits, while limiting the increase in strength associated with steel hardening.

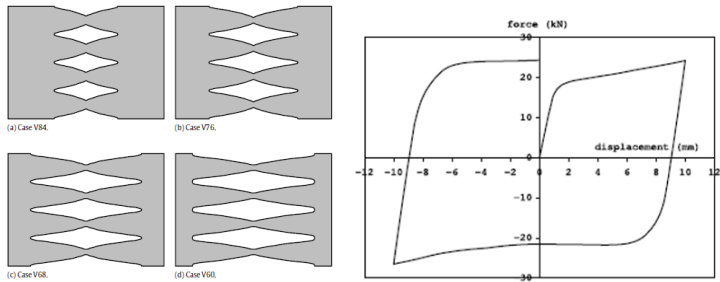


Figure VII.10 - On the left-side: representation of the *TSSD*. On the right-side: results of the cyclic experimental tests. From [223].

The same structural resisting mechanism and configuration were adopted by other researchers to create dissipative couplers to be used in timber rocking walls in light-weight structures. Such devices were realized by appositely cutting thin steel plates (Figure VII.11) [161].



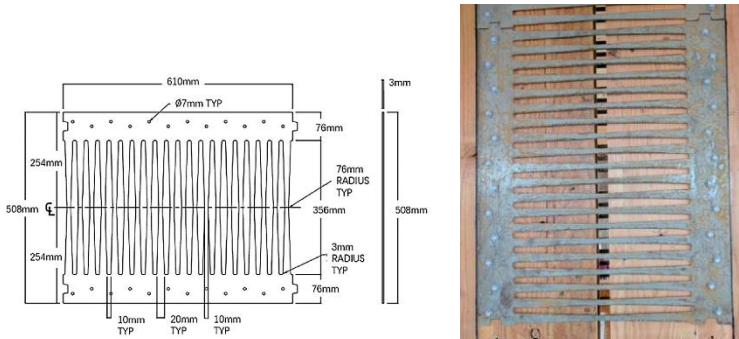


Figure VII.11 - On the left-side: representation of the devices. On the right-side: image of the specimen. From [161].

Another interesting typology of displacement-proportional dissipators exploits *inelastic axial deformation to dissipate energy*. Early examples of these devices include the *buckling restrained brace (BRB)* (Figure VII.12), developed in the 1980s [225] [226].

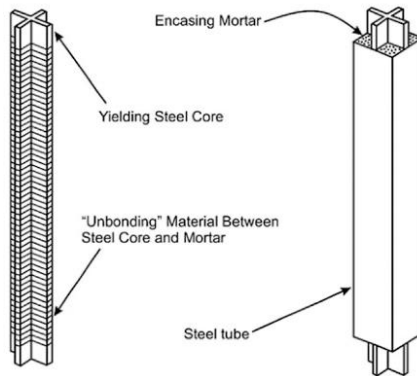


Figure VII.12 - Schematic representation of the BRB devices. From [225].

These dampers are made of a steel brace with circular or cruciform cross-section, inserted into a stiff steel tube; the gap between the two profiles is filled with a concrete-like material [225]. Because of the confinement provided by the concrete-filled tube, the brace can withstand compressive loads without buckling; BRB behaves essentially in the same way when subjected to either tension or compression. These devices can be used either as the main component of a dissipative frame system, or as couplers between steel-truss rocking walls by constraining them to their structural joints [227].

In recent decades, considerable effort has been devoted to the development of external, easily replaceable, cost-effective, and compact energy dissipators. The *Plug&Play fuse devices* (Figure VII.13) [165] [166] [228], which *incorporate* the functional principles of BRB, are an intriguing example. When these innovative devices are integrated within the rocking systems, they enable the design of a dissipative and repairable resisting system with replaceable sacrificial fuses connections, designed to serve as the *weakest link in the chain* according to capacity design principles [164].

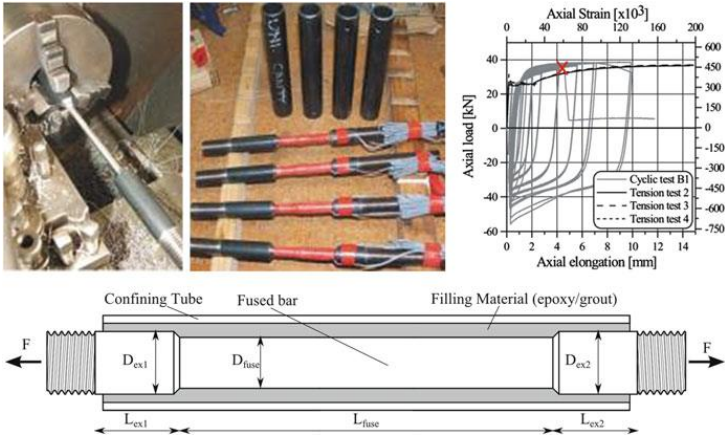


Figure VII.13 - On the top-left: production process of *Plug & Play* devices. On the top-Right: results of the experimental tests. In the bottom: schematic representation of geometry and element composition. From [164].

Another example of external, compact, and cost-effective device is the *high force/volume lead-extrusion damper (HF2V)* (Figure VII.14), an easily replaceable devices that can be installed to dissipate a significant amount of energy [229] [230]. The dissipative mechanism employed by these devices is based on exploiting the resistive forces provided by the plastic extrusion of the lead they contain through an annular restriction.

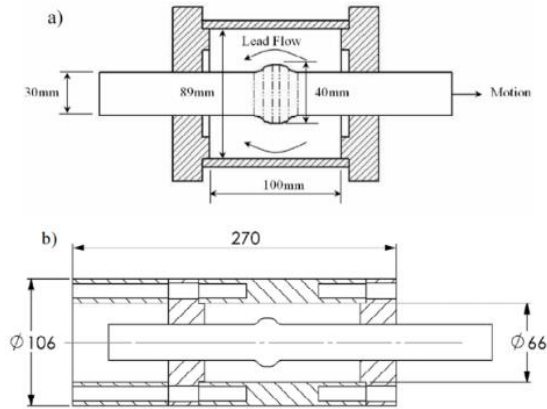


Figure VII.14 - Cross-Sectional views of different lead-extrusion damper configurations. From [230].

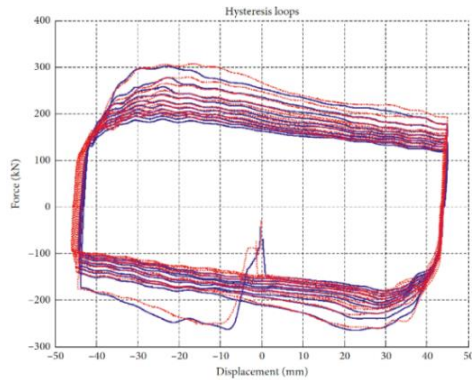


Figure VII.15 - Experimental results of the devices subjected to 10 fully reversed, near full-stroke displacement cycles. From [231].

Experimental tests demonstrated their robustness and reliability and highlighted the *weak relationship* between their response and the input velocity [231]. As shown in Figure VII.15, the hysteretic cycles obtained from the tests are stable also for high-

velocity input, and are characterised by a high initial stiffness. These devices are suitable with coupled rocking systems comprised of steel trusses that can effectively counteract the large, concentrated transferred loads [231].

Unlike the *hysteretic metal dampers*, *friction dampers* exploit friction developed between two solid bodies in contact that slide towards one another to dissipate energy, preventing any structural damage. During the seismic excitation, these devices slide for overcoming a design load and provide the desired energy dissipation by transforming part of the seismic input into heat, potentially exhibiting the stable hysteretic behaviour of the metallic devices [225].

In recent years, significant advancements have also been made in the further development of this type of friction devices. *Limited Slip Bolted (LSB) joints* (Figure VII.16) [232] developed in the 1980s, were one of the first dissipative connections designed to exploit friction.

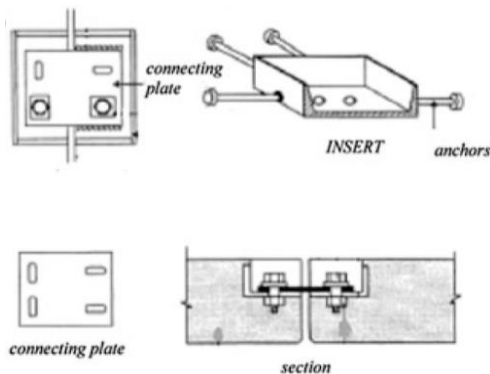


Figure VII.16 - Schematic representation of geometry and element composition. From [225].

Improved versions of these devices were obtained by enhancing stability and dissipative capacity under cyclical loads [233]. The frictional energy dissipation was later integrated into the bracing of frame structures [234] and for the construction of interesting dissipative structural elements, including *Sumitomo friction damper* (Figure VII.17) and the *Energy Dissipating Restraint (EDR)* [235].

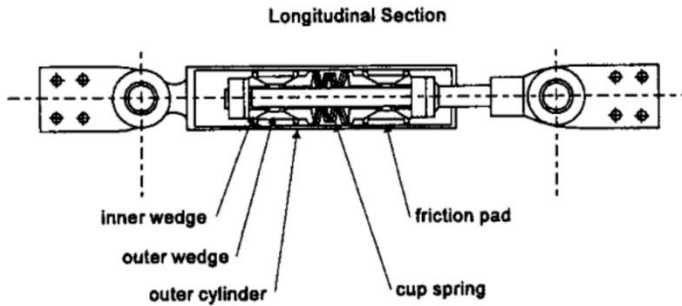


Figure VII.17 - Cross-Sectional views of the Sumitomo friction damper. From [236]

Frequently, these devices feature a constitutive model characterised by a high initial stiffness up to the activation of the dissipative mechanism. In the plastic range the response curve shows very limited stiffness, particularly for seismic inputs with moderate velocities [225]. However, several factors limit their application in the adaptive retrofits analysed in this study, including the need to monitor and maintain constant both the contact pressure between sliding surfaces, and their friction coefficient, directly affecting the structural behaviour of the retrofitted system. Maintaining their performance over time requires the design of special construction details preventing aging effects, such as the onset of corrosion and the change in the surface roughness. Detailed scheduling of maintenance interventions is thus required.

### **7.3. Analysis of PEEDs characteristics from the Life Cycle Structural Engineering perspective**

After focusing on the qualitative evaluation of the potential and limitations of some selected examples of *displacement-proportional passive energy dissipation devices* (PEEDs) reported in literature, this section defines their optimal features by analysing these elements compliance with both the life cycle thinking and circular economy principles.

Achieving the desired high structural performance for the retrofit requires the adoption and extension of the innovative *Life Cycle Structural engineering principles* (Chapter V), for the design of dissipative devices and couplers to be integrated into adaptive exoskeletons. Some key features that PEEDs must possess to ensure high structural performance while minimising environmental and economic impacts can be obtained by enforcing:

- “Design for damage limitation”. These devices should be designed to serve as the system's weakest link; lumping damage through their yielding thereby preserving the integrity of other structural and non-structural components.
- “Design for ease of disassembly and assembly” to facilitate their replacement after severe seismic events. The mindful design of the connections of the PEEDs to the structure, as well as their size and weight, may be critical as to enable replacement.
- “Design for reusability”. To this end, these elements should be standardized and pre-assembled preferring

the adoption of commercial elements and components to reduce costs and facilitate their supply.

- "Design for eco-efficiency," as for other retrofit components, the adoption of recyclable materials with a low environmental impact, preferably from circular economy, should be preferred. As opposed to active devices, the adoption of passive devices reduces the environmental impacts of the retrofit related to the production and storage of energy required for their operation.
- "Design for durability". Such a principle fosters effective sustainability of the retrofit system by preventing its deterioration. Therefore, ensuring durability also entails guaranteeing consistency in structural performance avoiding the influence of aging, and limiting extraordinary maintenance interventions.
- "Design for economic sustainability", the diffusion of the dissipative retrofit systems can be facilitated by the containment of the PEEDs production costs. To this end, their possible standardization, the use of commercial profiles, and the simplification of the manufacturing process should be attentively considered.

#### **7.4. AdESA fuse**

This section defines the characteristics of PEDDs developed within and industrial research project AdESA (Energy efficiency amelioration, seismic retrofit, and architectural restyling of existing building), carried out by the University of



Bergamo and Brescia and by a consortium of SMEs [15]. The fuse was specifically conceived to mitigate major construction site issues related to special material procurement and installation, as well as to minimize costs along the life cycle, while guaranteeing the envisioned performance.

This innovative *displacement-dependent passive energy dissipation device* exploits the energy dissipation provided by the activation of localised plastic hinges within ductile steel elements, dissipating part of the input seismic energy in the retrofit by accumulating damage. Starting with the definition of the ideal characteristics for this typology of devices, the *AdESA fuse* was designed to be potentially compatible with all structural retrofit types and to meet quite high-performance objectives.

Similar to *ADAS* elements, this coupler and dissipation device consists of a series of vertical steel plates connected to the retrofit. Unlike those devices described in the literature, the *AdESA fuse* does not exhibit a diffuse sectional yield when the peak ground acceleration (P.G.A.) exceeds the defined limit acceleration threshold ( $\ddot{u}_{g,Limit}$ ), but rather it envisions the activation of two plastic hinges located at the end of each steel plate (red dots and lines in the Figure VII.18). Such a design choice entails a reduction of the dissipation capacity but simplifies the design procedure, the key performance control and the production.

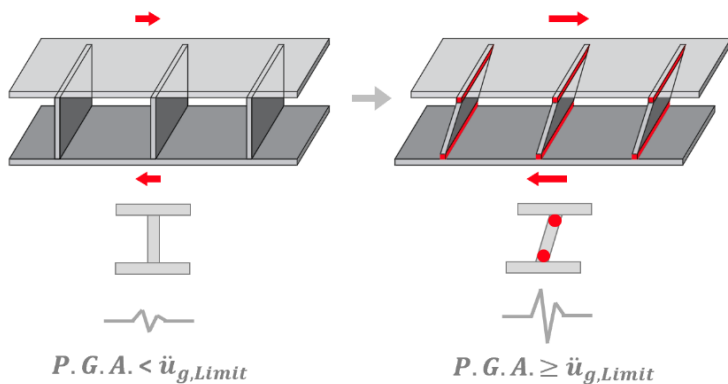


Figure VII.18 - Schematic representation of the functioning of AdESA devices. On the left-side: qualitative representation of the device for seismic events with P.G.A. below the limit  $\ddot{u}_{g,Limit}$ , with maximum stresses below the elastic limit and no activation of the plastic hinges. On the right-side: qualitative representation of the device for seismic events with P.G.A. above the limit  $\ddot{u}_{g,Limit}$ , where activation of plastic hinges at the ends of the vertical plates is observed.

In the previous chapter, the principal structural characteristics of couplers were conceptually analysed by considering and modelling these devices with an ideal rigid-plastic constitutive model. In this chapter the structural characteristics of the *AdESA fuse* are defined from a technological standpoint with reference to a more appropriate elastic-linear strain hardening constitutive model [225].

The conceptual response curve of the *AdESA fuse* (Figure VII.19) is defined by three performance points characterized by progressive deformation and activation of the plastic hinges.

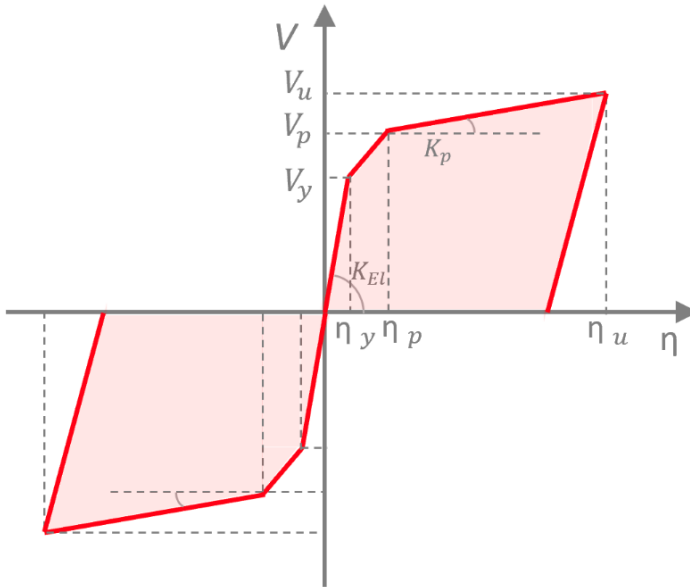


Figure VII.19 - Conceptual representation of the hysterical cycle of the AdESA fuses.

The performance points are qualitatively defined as follows:

1. *Attainment of yield strain.*

The first performance point corresponds to the attainment of the yielding strain and stress ( $f_y; \epsilon_y$ ) in the most stressed fibre at the end-sections of the vertical dissipative elements ( $V_y; \eta_y$ ). A linear distribution of the normal stress is assumed.

2. *Attainment of complete sectional yielding.*

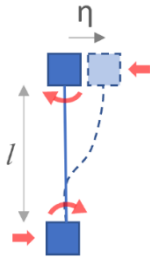
The second performance point corresponds to the complete sectional yielding ( $f_y; \epsilon_y < \epsilon_u$ ) with

the activation of two plastic hinges at the ends of each resisting elements ( $V_p ; \eta_p$ ).

3. *Attainment of the ultimate deformation of plastic hinges*  
The third performance point occurs when the ultimate deformation ( $\epsilon_u$ ) of the plastic hinges is reached ( $V_u ; \eta_u$ ). At this point, it is assumed that the steel has reached its maximum tensile strength ( $f_t$ ).

Several authors observed the effect of the couplers stiffnesses on the global response of the coupled rocking systems, suggesting the adoption of devices with high elastic stiffness ( $K_{El}$ ) to enhance the coupling effect between shear-walls [237]. On the other hand, the limitation of seismic actions following the yielding of couplers suggests the introduction of devices with limited post-yielding stiffness ( $K_p$ ), to enable accommodating the nonlinear deformations required by severe seismic events.

The AdESA device elastic stiffness ( $K_{El}$ ) and strength ( $V_{yd}$ ) can be easily calibrate to achieve quite different performances, satisfying the structural requirements set. The initial elastic stiffness of the vertical plates can be preliminary defined by assuming that their end sections are fixed (Figure VII.20, left), while their resistance can be modulated by locally reducing the resistant section, as illustrated in the following.



$$K_{El} = \frac{12 EJ}{l^3};$$

E = Young steel module  
J = Moment of inertia of the sections  
L = length of the steel plate

Figure VII.20 - On the left-side: schematic representation of the static scheme that can be adopted to define the elastic stiffness of steel plates. On the right-side: calculation formula.

### 7.4.1. Description of the different configurations

This section defines the geometrical characteristics and main structural properties of the steel prototypes representative of the various configurations designed for this device. For the sake of clarity, the characteristics of a single structural component of the AdESA device (Figure VII.21) are described in the following.

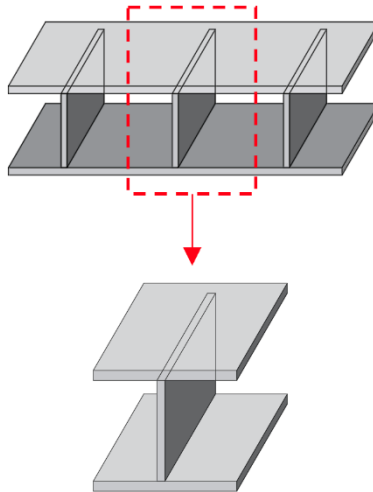


Figure VII.21 - Schematic representation of a single resisting and dissipative steel plate component of the AdESA device.

The first configuration of the AdESA device, referred to as *configuration I* (Figure VII.22), involves vertical dissipative plates made of S275 and S355 steel welded to other transverse plates. However, their simple and easily reproducible manufacturing process generates heat-altered zones close to the sections where the plastic hinges are located, which compromises their structural performances.

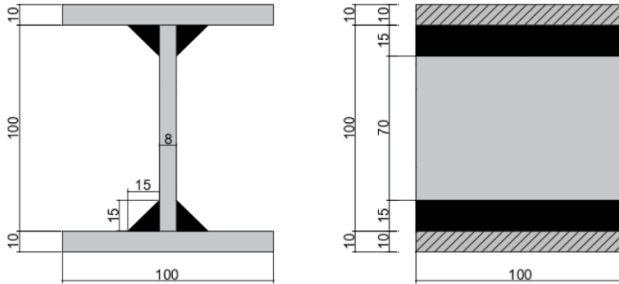


Figure VII.22: On the left-side: sectional view of the configuration I, in which the steel sections are coloured in grey and the welds in black. On the right-side: side view of the same device.

In order to avoid these issues, the *configuration II* (Figure VII.23) was derived from the first (*configuration I*) by introducing slits in the vertical plates, that localize the activation of plastic hinges at a distant from the weld lines and the heat-altered zones. Two variants have been designed for this configuration, one employing S275 steel with sharp-edges slits (Figure VII.24, left) and another using S355 steel with rounded-edges (Figure VII.24, right) to reduce local stresses in the proximity of sharp corners [223].

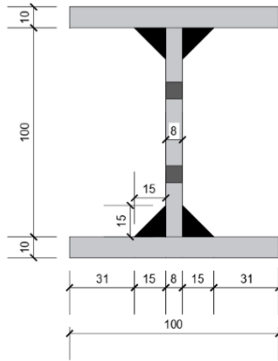


Figure VII.23 - Sectional view of the configuration II, in which the steel sections are coloured in grey and the welds in black.

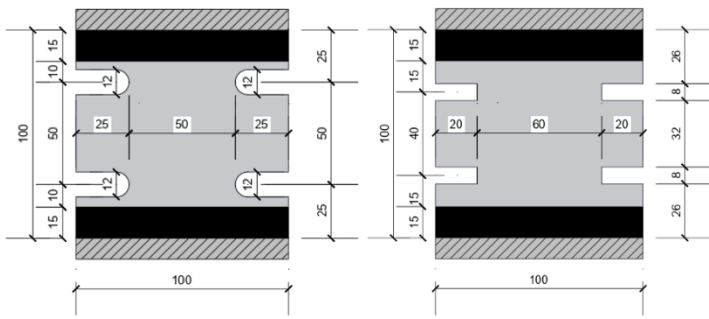


Figure VII.24 - Side views of the same device with rounded-edges (left) and sharp-edges (right).

In the final *configuration III*, the device is composed by a series of commercial HEB100 profile segments, welded together as shown in Figure VII.25, made of S355 structural steel. This way, the potential alterations and the imperfections associated with the welding process are overcome. In *Steel Slit Damper (SSD)* and the *TSSD devices* [223] [224] the steel H-beams with slitted webs are loaded in the main direction of the H-beam resulting in the yielding of the web resisting elements between two



adjacent slits. In the AdESA fuse proposed in this study, an effort is made to simplify the manufacturing process by reducing costs and facilitating the device supply and its applicability. Unlike SSD and TSSD, no CNC machine but rather simple circular saw blades are required for the fuse production. The resistance is provided by the H-beam sections (Figure VII.26) subjected to shear loads applied in the transverse direction of the steel H-beam and the energy dissipation is triggered by out-of-plane bending of its web with the onset of two localised plastic hinges at its ends.

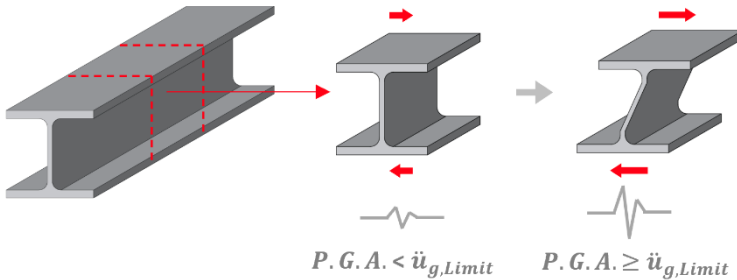


Figure VII.25 - Qualitative representation of the adaptive structural behaviour of the device, obtained by *slicing* a HEB100 beam, subjected to earthquakes of varying intensities.

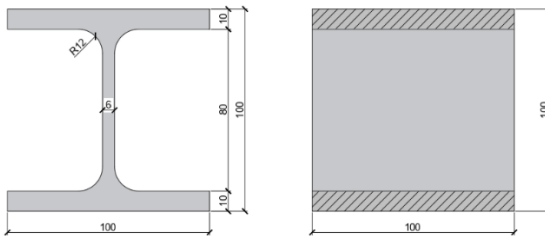
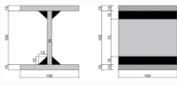
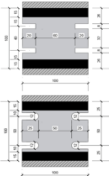
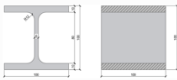
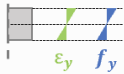
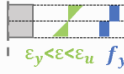
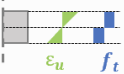


Figure VII.26 - On the left-side: sectional view of the fifth configuration obtained by slicing a HEB100 beam. On the right-side: side view of the same device.

The main geometrical and mechanical properties of the conceived prototypes, related to the 3 performance points, are shown in the Table 3; refer to for further information.

Table 3 - Summary of the main features of the three conceived configurations.

| Configurations  | I  | II   | III   |
|---|--|--|---|
| Geometry & Dimensions   |   |   |  |
| Steel (Elements)  | S275 – S355<br>(Plates)  | S275 (Sharp-Edges)<br>S355 (Rounded-Edges)   | S355 (HEB100)   |
| Distinctive features  | Welded plates<br>→ Heat-Altered zones  | Slitted plates<br>→ Plastic-Hinges<br>Localization   | H-Beams<br>→ High performances<br>& Cost Effectiveness                            |
| First Performance Point<br>- Yielding resisting Moment ( $M_y$ ) & Shear ( $V_y$ )<br>   | $M_y = 0.293\text{kNm}$ (S275)<br>- $0.378\text{kNm}$ (S355)<br><br>$V_y = 8.4\text{kN}$ (S275)<br>- $10.8\text{kN}$ (S355)  | $M_y = 0.176\text{kNm}$ (S275)<br>- $0.189\text{kNm}$ (S355)<br><br>$V_y = 7.3\text{kN}$ (S275)<br>- $7.6\text{kN}$ (S355)   | $M_y = 0.234\text{kNm}$<br><br>$V_y = 8.4\text{kN}$                               |
| Second Performance Point<br>- Plastic resisting Moment ( $M_p$ ) & Shear ( $V_p$ )<br> | $M_p = 0.44\text{kNm}$ (S275)<br>- $0.568\text{kNm}$ (S355)<br><br>$V_p = 15.2\text{kN}$ (S275)<br>- $19.58\text{kN}$ (S355) | $M_p = 0.264\text{kNm}$ (S275)<br>- $0.284\text{kNm}$ (S355)<br><br>$V_p = 13.2\text{kN}$ (S275)<br>- $11.4\text{kN}$ (S355) | $M_p = 0.35\text{kNm}$<br><br>$V_p = 14.95\text{kN}$                              |
| Third Performance Point<br>- Ultimate resisting Moment ( $M_u$ ) & Shear ( $V_u$ )<br> | $M_u = 0.688\text{kNm}$ (S275)<br>- $0.816\text{kNm}$ (S355)<br><br>$V_u = 23.7\text{kN}$ (S275)<br>- $28.1\text{kN}$ (S355) | $M_u = 0.41\text{kNm}$ (S275)<br>- $0.408\text{kNm}$ (S355)<br><br>$V_u = 20.6\text{kN}$ (S275)<br>- $16.3\text{kN}$ (S355)  | $M_u = 0.495\text{kNm}$<br><br>$V_u = 21\text{kN}$                                |

### 7.4.2. Experimental test and results

Several experimental cyclic tests were performed on portions of the *AdESA fuse in several configurations* to assess their structural and dissipative behaviour.

For configurations I to III, the specimens were assembled with six dissipative steel plates, having the geometric and mechanical properties described above, arranged in parallel and welded to a rigid, over-resistant steel frame designed to concentrate yielding and energy dissipation in the six central elements (Figure VII.27, Figure VII.28).

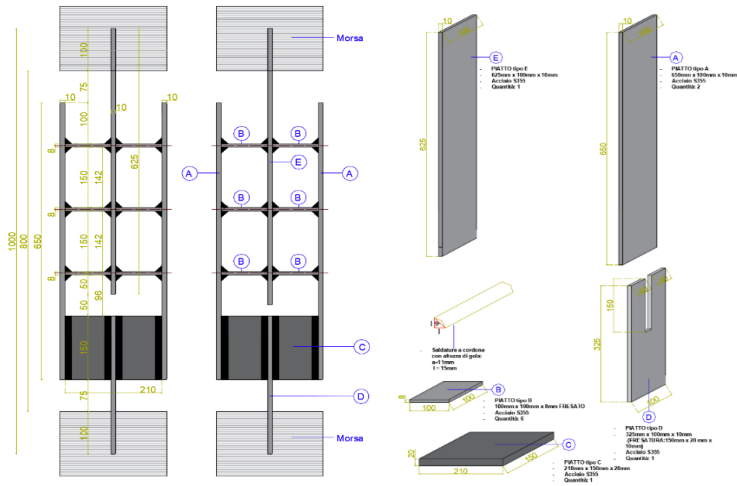


Figure VII.27 - Shared geometric dimensions of the metal samples.

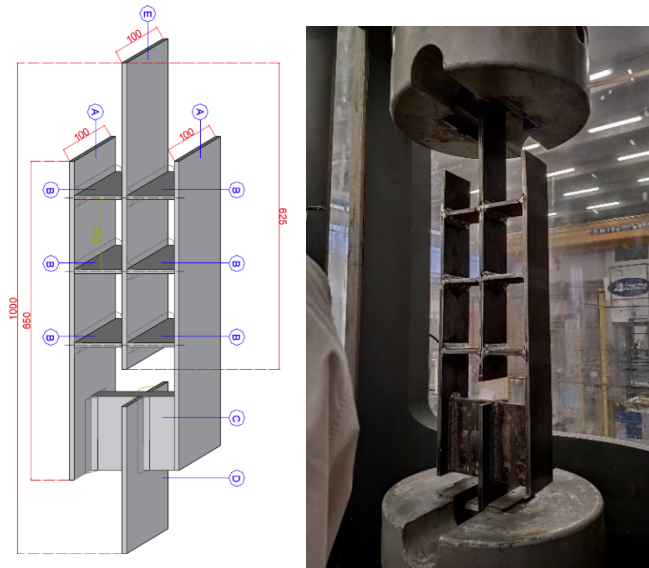


Figure VII.28 - On the left-side: three-dimensional view of the specimen representing the configuration I. On the right-side: view of the same specimen in the test machine.

The specimen representative of the configuration III, featuring the HEB100 H-beam profiles, are illustrated in (Figure VII.29). The same testing machine and testing bench were used in the test.

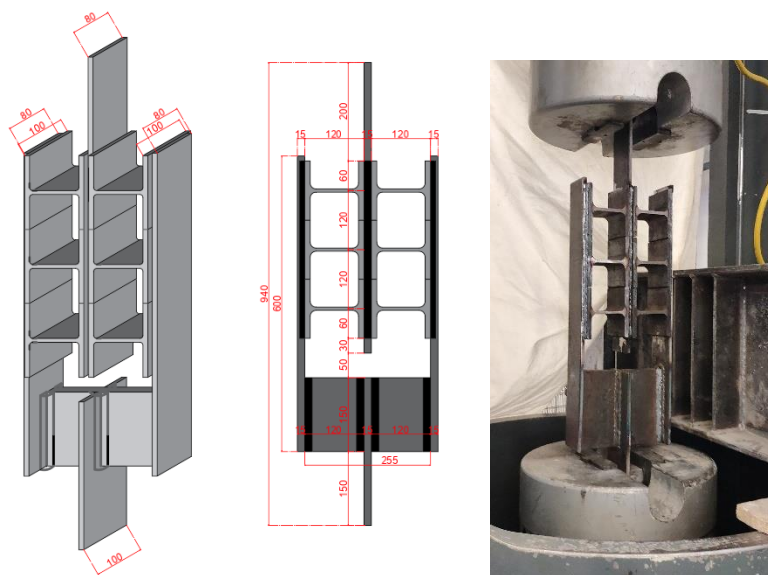


Figure VII.29 - On the left-side: geometric dimensions of the metal samples. On the right-side: view of the same specimen in the test machine.

Dissipative capacities and structural behaviour of the alternative configurations were investigated by conducting a series of cyclic tests under displacement-control in the BRT universal testing machine, installed at the laboratories of the Department of Engineering and Applied Science of the University of Bergamo.

The applied displacement history was characterised by cycles of increasing amplitude (Figure VII.30). The displacement was applied at a 0.2mm/s rate.

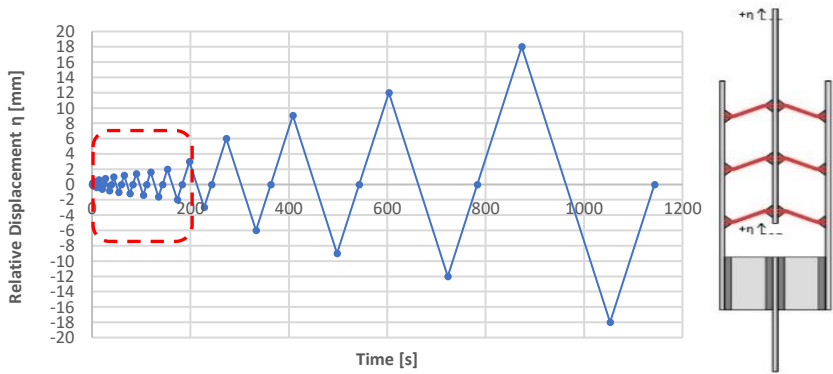


Figure VII.30 - History of relative displacement imposed to the specimen with the Schematic representation of the specimen during the test.

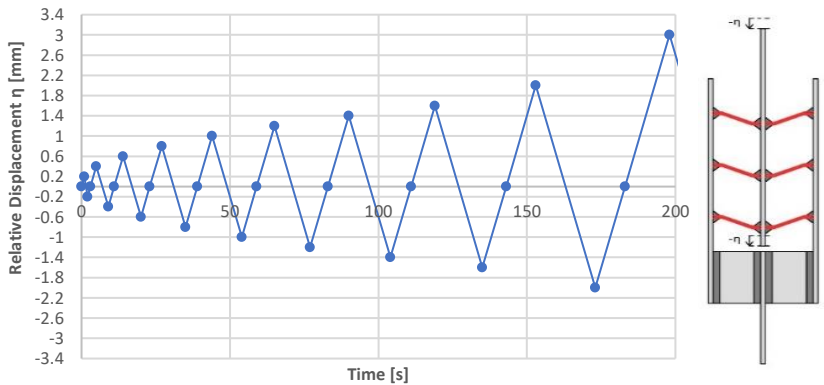


Figure VII.31 - First 200 seconds of the loading history.

The shear resistance ( $V$ ) of the single plate was determined by dividing the total load by the number of dissipative elements.

In the experimental response curves the second performance point, corresponding to the full section yielding and the

activation of the plastic hinges ( $V_p ; \eta_p$ ), is marked with a green square, while the third performance point, corresponding to the specimen's failure for overcoming the maximum deformation capacity ( $V_u ; \eta_u$ ) is represented by a red cross.

The initial elastic stiffness of the specimen ( $K_{El}$ ) is approximated by correlating the plastic shear strength of each resisting element ( $V_p$ ) with the relative displacement measured ( $\eta_p$ ) during the test:

$$K_{El} = \frac{V_p}{\eta_p} \text{ [kN /mm]}$$

Similarly, the specimen's post-yielding stiffness ( $K_p$ ) is defined:

$$K_p = \frac{V_u - V_p}{\eta_u - \eta_p} \text{ [kN /mm]}$$

- **Configuration I: welded steel plates**

Experimental tests conducted on specimens representing the characteristics of the *first AdESA fuse configuration*, which differ only by the type of structural steel used, demonstrate a good correlation between the analytically estimated plastic and ultimate shear resistances and the experimental results.

The shear-displacement curve obtained from testing the first specimen representing *configuration I* is shown in Figure VII.32.

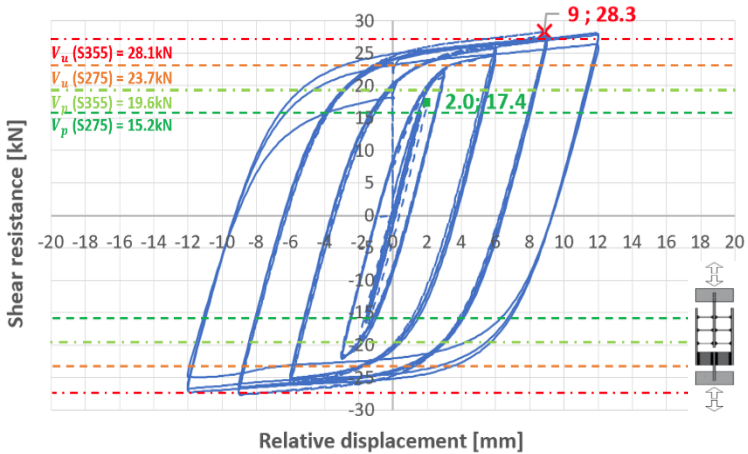


Figure VII.32 – Shear-displacement curve for the AdESA-Config. I: the dashed blue curve represents the specimen made of S355, while the continuous blue curve represents the S275 steel specimen. The green square represents the attainment of the first performance point while the red cross the attainment of the third point. The dotted horizontal lines indicate the theoretical resistance predictions reported in .

Both specimens exhibited similar behaviour and comparable stiffnesses, defined in the following by considering the S275 steel specimen.



$$K_{El} = \frac{V_p}{\eta_p} = \frac{17.4kN}{2mm} = 8.7kN/mm ;$$

In this reference case the elastic stiffness is about six times greater than the post-yielding stiffness ( $K_p$ ).

$$K_p = \frac{V_u - V_p}{\eta_u - \eta_p} = \frac{28.3 kN - 17.4kN}{9mm - 2mm} = 1.56kN/mm$$

The specimen failure occurred in the heat-altered zone in the proximity of the weld lines.

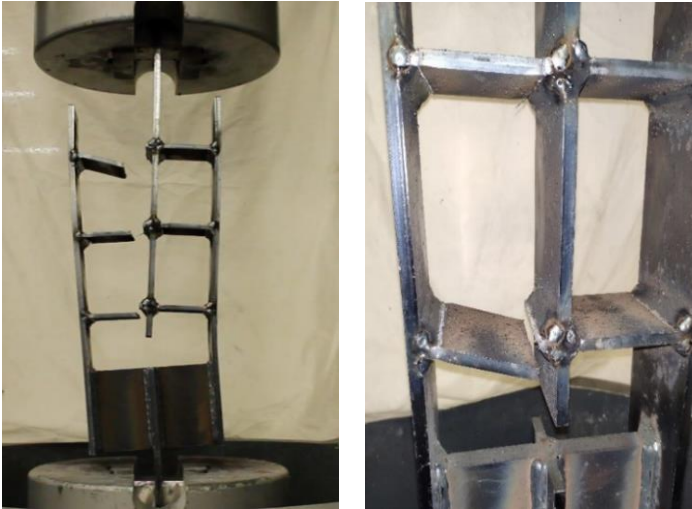


Figure VII.33 – Pictures of the test specimen of configuration I within the testing machine when failure is accomplished.

- ***Configurations II: welded steel plates with reduced sections***

Tests conducted on specimens with slitted plates that locally reduce their cross-section, representing *configuration II*,

demonstrated their ability to concentrate inelastic deformations and localise the activation of plastic hinges distant from the heat-altered zones. The comparison between experimental curves obtained from the different specimens characterised by slits with rounded- and sharp-edges are shown in Figure VII.34.

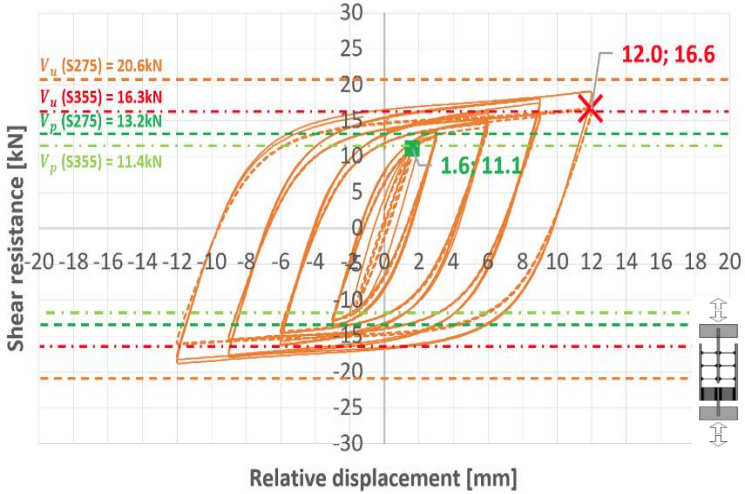


Figure VII.34 - The dashed orange curve represents the shear-displacement relationship obtained from the specimen of configuration II with rounded-edges, while the continuous orange curve represents the relationship obtained from the sharp-edges specimen. The green square represents the attainment of the first performance point while del red cross the attainment of the third point. The dotted horizontal lines indicate the theoretical resistance predictions reported in

Also in this configuration, both specimens exhibited similar behaviour, stiffnesses, and deformation capacity. Laboratory tests reveal a moderate decrease in both elastic stiffness and post-yielding stiffness compared to *configuration II*.

$$K_{EI} = \frac{V_p}{\eta_p} = \frac{11.1kN}{1.6mm} = 6.93kN/mm ;$$

$$K_p = \frac{V_u - V_p}{\eta_u - \eta_p} = \frac{16.6 \text{ kN} - 11.1 \text{ kN}}{12 \text{ mm} - 1.6 \text{ mm}} = 0.53 \text{ kN/mm}$$

As observed by visual inspection, the failure of the sharp-edged slits specimen was caused by the onset and propagation of several cracks that originated in the corners of the slits and then extended along the reduced section of the plates with a deflection towards the weld lines (Figure VII.35).



Figure VII.35 - On the left-side: Image of crack propagation from the corners of the slits. On the right-side: Image of the fracture of the reduced section at the end of the test.

- **Configuration III: device consisting of H-beam sections made of S355 structural steel**

Experimental and theoretical results well conform also in the case of *Configuration III*, which exhibited a significantly higher

deformation capacity than all other configurations (Figure VII.36).

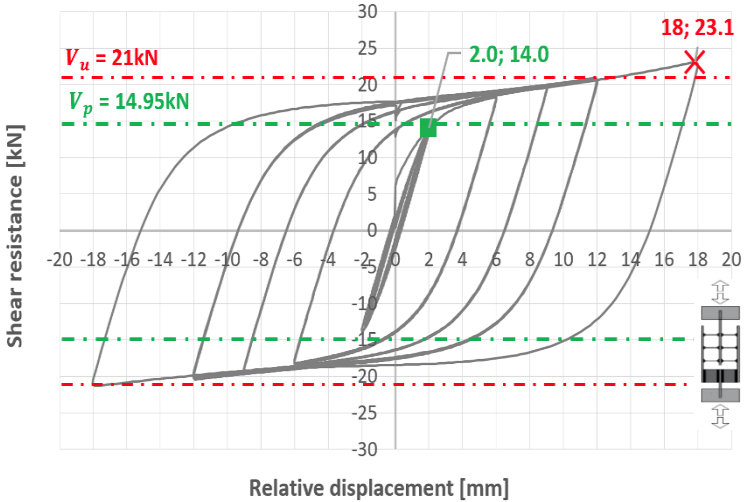


Figure VII.36 - Shear-displacement curve obtained from the sample of configuration V, consisting of I-beam sections made of S355 structural steel. The green square represents the attainment of the first performance point while del red cross the attainment of the third point. The dotted horizontal lines indicate the theoretical resistance predictions reported in

This specimen corresponds well in terms of elastic stiffness to the previously analysed configuration characterised by the presence of reduced cross-sections, whereas its post-yielding stiffness is the lowest of all the devices examined.

$$K_{El} = \frac{V_p}{\eta_p} = \frac{14 \text{ kN}}{2 \text{ mm}} = 7 \text{ kN/mm} ;$$

$$K_p = \frac{V_u - V_p}{\eta_u - \eta_p} = \frac{18 \text{ kN} - 14 \text{ kN}}{18 \text{ mm} - 2 \text{ mm}} = 0.25 \text{ kN/mm}$$

The specimen fails for overcoming the maximum rotation capacity of the plastic hinges for large inelastic deformations,

for a relative displacement of 18mm equal to 50% more than *configuration II*.



Figure VII.37 - Pictures of the test specimen of configuration III within the testing machine when failure is accomplished.

## 7.5. Concluding Remarks & Further Development

Experimental tests conducted on specimens of the various configurations of the *AdESA fuses* demonstrated their satisfactory dissipation and coupling capacities, these devices exhibit a good capacity to withstand large plastic deformation relative to their dimensions and to effectively limit the maximum shear transfer. Besides structural performances, the need for simplifying the production of the dissipative elements, as well as the need to speed up the construction process, emerged as quite relevant features to take into account in the design of these elements. In such a scenario, Configuration III, obtained by assembling steel H-beam portions, exhibited the most interesting characteristics among the tested configurations, making it suitable for adoption into the case studies analysed in Chapter VIII and IX.

In the future step of the research focus will be made on the further development of the *AdESA fuses* and on the experimental testing of the *sacrificial fuse toe* for achieving effective damage-control in adaptive exoskeletons, as well as on the standardization of the connection to the existing building.

## **VIII. Retrofit of an existing precast RC building with a *hybrid-CLT exoskeleton***

### **8.1. Introduction**

This chapter describes the structural retrofitting of a real case study building with the *AdESA* system, the innovative technique for the holistic and sustainable renovation of the building stock described in Section 8.4, that was developed by a consortium of SMEs and universities within an industrial research project [15] [238]. This case study implements the LCT design principles introduced in Section 5.3, the proportioning procedures illustrated in Section 6.4, and the *AdESA fuses* described in Chapter VII. In this first application, the structural CLT panels and the energy dissipators were arranged horizontally due to the architectural constraints, better described in the following.

A hybrid version of the *AdESA* system, was first applied for the retrofit of a 1980s prefabricated RC gymnasium in Brescia. The retrofit solution consists in a dry assembled, modular, and flexible exoskeleton that is applied to the existing building and is composed by multiple layers with distinct structural, energy, and architectural functions. This global structural-energy-architectural intervention increases the sustainability of the system by simultaneously fostering eco-efficiency, safety, and resilience. In addition to coupling structural and energy measures to reduce operating costs, this solution is designed in compliance with the principles of Life Cycle Thinking and Circular Economy to reduce impacts over the extended life of the retrofitted building. Using CLT structural panels, macro-

prefabricated components, and standardised structural connections, this adaptive retrofit is conceived to be easily assembled and disassembled from outside without disruption in the building use, allowing its components to be reused and recycled at the end of their service life. The achievement of the structural performance objectives imposed by the adoption of life cycle structural engineering principles is ensured by the enforcement of quite severe design targets for the proportioning of the hybrid shell exoskeleton. The introduction of *AdESA fuses* (Section 7.4), concentrating structural damage induced by severe seismic events and limiting the actions in the exoskeleton, as well as the exploitation of the controlled rocking of the cladding panels, protect the integrity of other structural and non-structural components of retrofit and existing building, limiting the extension of structural intervention.

As anticipated, the author, who was a member of the research team in charge of the design of the retrofit intervention, collaborated to the conceptualization of the structural system, and was responsible of the creation of its non-linear numerical model, the execution of experimental tests on the novel dissipative components, and the implementation of site control measures.

## **8.2. Building description**

The reference building selected for the first application of the *AdESA system* is a precast RC gymnasium (Figure VIII.1) owned by the Municipality of Brescia, a city in northern Italy classified as moderate-high seismic zone ( $a_g=0.168g$  [141], and climate zone E, HDD=2410 [15]).





Figure VIII.1 - Images of the case study building before renovation. From [239].

This building, erected between 1980 and 1981 using only prefabricated elements, features a rectangular plan (25.34x13.34 m<sup>2</sup>) and a height of 7.5m. The gymnasium hall hosts a full-height sports area at the ground floor and a loft area with an intermediate floor for the changing rooms, a storage area, and a technical room, which are connected by an internal staircase that is part of the RC prefabricated system.

The principal structure is composed of perimeter 38x38cm<sup>2</sup> RC columns with a 6m spacing. Mid-height corbels support the intermediate edge RC beams, which are responsible for supporting the cladding panels through structural bayonet connections to prevent in-plane and out-of-plane displacement of the external panels. The roof is composed of precast RC double tees beams with 12m span, a total height of 47cm, 3.5cm thickness of the upper flange, and lacking the RC topping. The roofing elements are supported by edge beams with an inverted T section that rest on the head of the RC columns and serve as

retainers for the cladding panels with the same connection devices as the intermediate beams.

The loft area has a  $5.7 \times 12.9\text{m}^2$  floor plan and is divided into two 6m wide main bays (Figure VIII.2). The intermediate floor slab (Figure VIII.3) is composed by precast RC double tee beams with a gross height of 50cm and an upper RC flange thickness of 3.5cm, supported by inverted T-beams that rest on the intermediate corbels of the perimetral RC columns. The slab stratigraphy is completed with a cast in situ 7cm thick RC overlay (gross height of 50cm), and additional reinforcement at the beam-column joint. This intermediate level is partly supported by a central RC column, shorter than the perimeter ones.

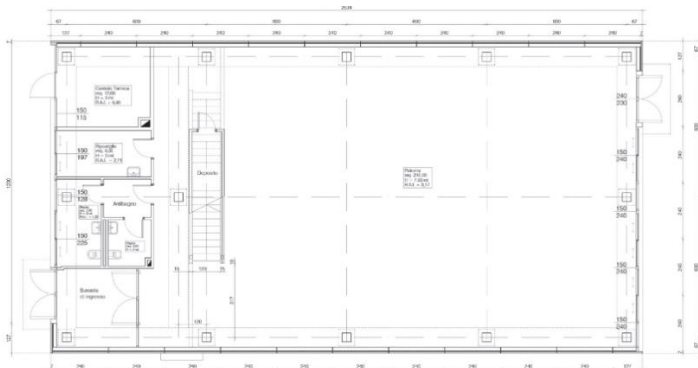


Figure VIII.2 - Ground floor plan. From [239].

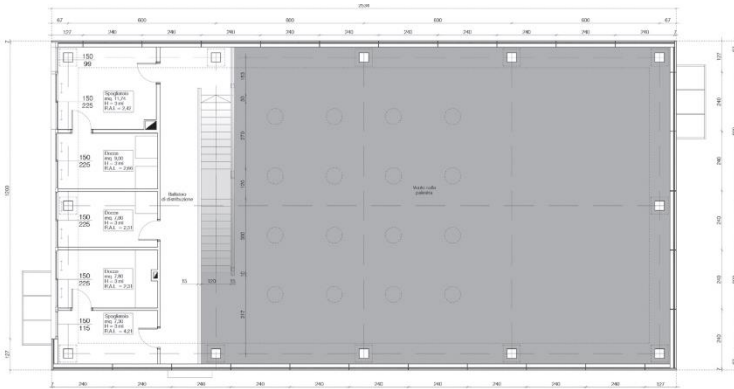


Figure VIII.3 - Intermediate floor plan. From [239].

Foundations are made of RC pockets connected by a 20cm-thick cast-in-place RC grade slab and by a perimeter inverted beam.

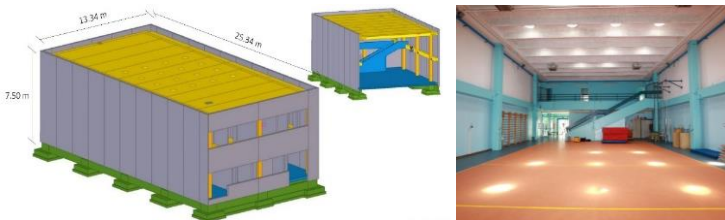


Figure VIII.4 - As-Is condition: Laser-scanner-generated 3D model (left) and interior view of the southern portion of the building with the intermediate floor (right). From [15].

The perimeter facades are composed of 22cm-thick prefabricated sandwich cladding panels, with two outer RC layers of 6 and 12cm and an inner 4cm insulation layer. Cladding panels are connected to the primary structure at two levels. Along the longitudinal facades, these panels ( $2.4 \times 8.1 \text{ m}^2$ ) are arranged vertically, with no openings (Figure VIII.5). Along

the transverse façades, given the presence of ribbon windows, cladding panels are arranged horizontally (Figure VIII.6).

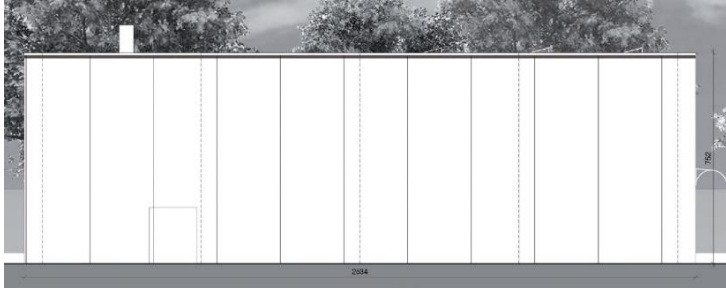


Figure VIII.5. - As-Is condition: representation of the east longitudinal side. From [239].



Figure VIII.6. - As-Is condition: On the left-side: representation of the short southern façade. On the right-side: representation of the short northern façade. From [239].

The earthquake-resistant system of the building in the as-is conditions consists primarily of the precast RC frame, fixed at the base, with the edge beams hinged to the columns.

Neither the roof, made of double tees beams connected only to the perimeter beams with metal dowels, nor the partial intermediate floor are engineered to behave like floor diaphragms. Furthermore, the limited extension and eccentric position of the intermediate floor is expected to potentially

influence the overall seismic response of the building by generating torsion effects.

In the longitudinal direction the presence of the cladding RC panels, which were designed as infill elements, is expected to play a crucial role in the response of the building. The cladding panel's high masses, stiffness, and the limited capacity of the mechanical fasteners to the frame can significantly impact the building's overall seismic response.

Additional information on the structural system of the existing building in the as-is condition is available in [15] [238] and [3].

### **8.3. Main deficiencies of the building in the as-is condition**

The structural static and seismic vulnerabilities of the building were evaluated by performing nonlinear static analyses of two 3D numerical models of the structure, having different level of refinement, implemented in a finite element software [194]. The elastic design spectrum of the site at life-safety limit state (LSLS) is reported in Figure VII.7 .

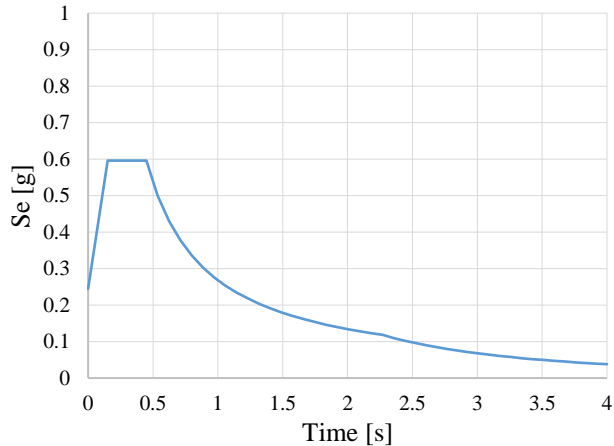


Figure VIII.7 - Elastic design spectrum of the site at life-safety limit state (LSLS). From [141].

These models, representing the building in the as-is condition, were developed by considering the geometric features surveyed through laser scanner, and derived from the construction documents, as well as the mechanical properties of the structural elements and connections derived from the available documentation and checked by sample. In the basic numerical model, *mesh A* (Figure VIII.8), only the primary structural components of the building were modelled, consisting of the

reinforced concrete frame, while secondary elements were only modelled as masses.

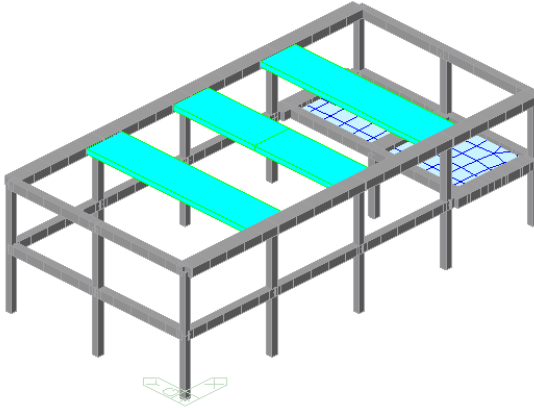


Figure VIII.8 - 3-D representation of the basic model called mesh A, extracted from the software, in which the RC frame is represented by the grey vertical elements and the roof elements are represented by the blue horizontal elements. From [15].

In mesh A, the perimeter columns were modelled using one-dimensional beam elements with lumped plasticity fixed to the ground, their moment curvature relationship as well as the moment axial force domains were automatically calculated considering the P-M interaction.

The intermediate and upper edge beams were modelled as single-bay elastic elements pinned to the columns. The roof elements were modelled as truss elements connected to the upper edge beams, whereas the intermediate RC slab was modelled with elastic plate elements to simulate its in-plane stiffness granted by the cast-in-place structural section. The potential interaction between the precast reinforced concrete staircase and the perimeter columns at mid-storey height was

modelled by imposing an absolute constraint on the horizontal translation at that point.

In the second model, referred to as *Mesh B* (Figure VIII.9), the basic model (Mesh A) was complemented with the prefabricated cladding panels. The external panels were modelled with one-dimensional beam elements pinned to the ground and connected to the frame by general-link characterized by an elastic-plastic behaviour. To calibrate the general link, the position, stiffness, and resistance of the structural connections were considered.

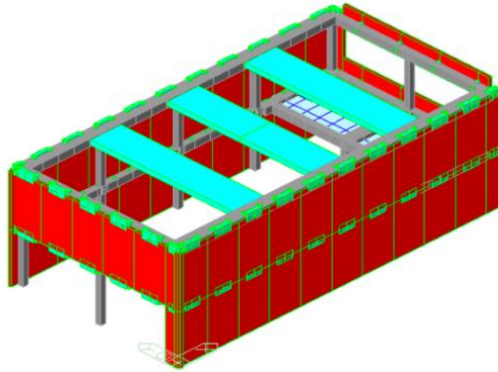


Figure VIII.9 - 3-D representation of the second model called mesh B, extracted from the software, in which the RC cladding panels are represented by the vertical red elements. From [15].

These connections play a critical role in the seismic response of the building. They consist of horizontally arranged anchoring devices linking the edge beams and RC pillar corbels with the external panels (Figure VIII.10). More about the evaluation of their mechanical features can be found in the and in [240].



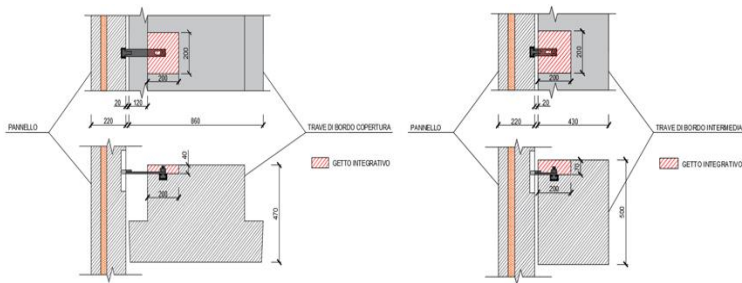


Figure VIII.10 - On the left-side: detail of the structural connection between intermediate edge beams and cladding panels. On the right-side: detail of the structural connection between roof-level edge beams and cladding panels. From [3].

As expected, the comparative analysis of the capacity curves obtained from the nonlinear static analyses emphasizes the influence of the cladding panel on the global structural response of the building. The capacity curves obtained for the two models differ quite substantially in terms of stiffness, deformability, and failure mode, thus the seismic vulnerability change remarkably based on the modelling assumptions. The potential for out-of-plane overturning of panels due to the failure of structural connections between panels and frame is a limit condition for the entire structure, regardless of the state of the other elements. The central role of cladding panels becomes evident when

comparing the capacity of the building to the seismic demand in the longitudinal direction, as shown in Figure VIII.11.

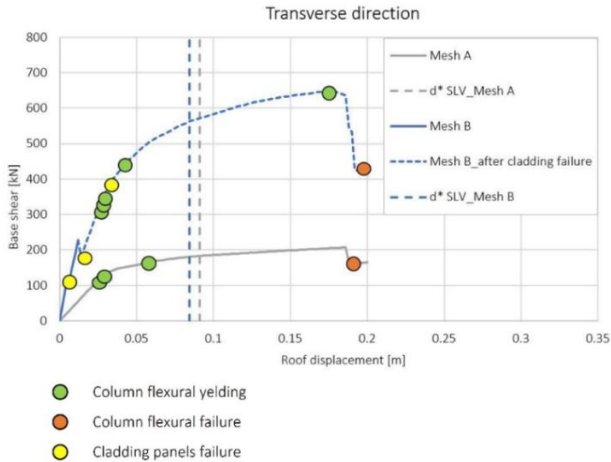


Figure VIII.11 - Capacity curve of the building in the transverse direction. The continuous grey line represents the mesh A capacity curve, while the blue line is the curve of the mesh B. From [15].

In *mesh A*, a diffuse yielding at the base of the RC columns is observed for roof displacements of 2.5 cm, which corresponds to a total drift of approximately 0.33%, until the ultimate flexural deformation (ultimate building drift of 2.5%) of the columns near the north façade is reached (Figure VIII.12). Such columns are more stressed due to the in-plan and in-elevation irregularity of the building, with particular emphasis on the torsional effect caused by presence of the intermediate partial slab. In this configuration, considering only the RC frame elements characterized by a high deformation capacity, the building satisfies the LSLS displacement capacity requirement.

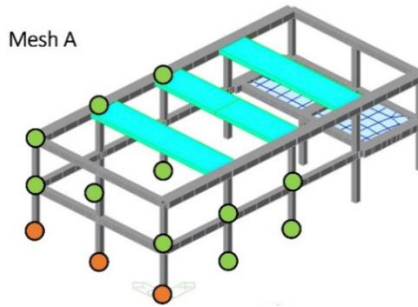


Figure VIII.12 - Performance of the structure, represented by mesh A, upon reaching ultimate deformation. From [15].

The capacity curve of *mesh B*, on the other side, demonstrates that the high deformability of the RC columns is incompatible with the capacity of the connections constraining the cladding panels. The presence of cladding panels with rigid structural connections results in the early failure of the connections on the north side for a very limited roof displacement of about 12mm, corresponding to a 0.16% drift, followed by the out-of-plane overturning of the panels. After this point, the building's capacity curve continues (dashed line in Figure VIII.11) until the ultimate flexural capacity of the first floor RC columns on the south side is reached.

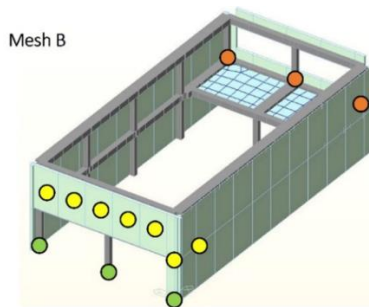


Figure VIII.13 - performance of the structure, represented by mesh B, upon reaching ultimate deformation. From [15].

It is worth noting that the dashed portion of the response curve is conventional, and significant from a numerical point of view only, provided that the building's capacity is limited by the failure of the structural connections and by the overturning of the cladding panels. In mesh B, the LSLs displacement demand is not met, and the building safety index before the intervention is equal to 0.14.

The main energy deficiencies of the building were identified by analysing the envelope, plants, and building management in terms of heating/cooling and air ventilation. Regarding the envelope, highly dispersive surfaces were identified both in the facade, which consists of RC sandwich panels insulated with 4 cm of rockwool, and in the roof, which is insulated with 5 cm of expanded cork. Concerning the thermal demand for winter heating and summer cooling, accurate dynamic analyses of a numerical model realized with Trnsys® software were performed to evaluate the building's behavior for each hour of the year under specific use conditions [15]. The analyses estimated a peak thermal load of 50 kW and an annual thermal load of approximately 63000 kWh for winter heating, and during the summer period a peak thermal load of 29 kW and an annual thermal load of approximately 21000 kWh related to cooling (Figure VIII.14).

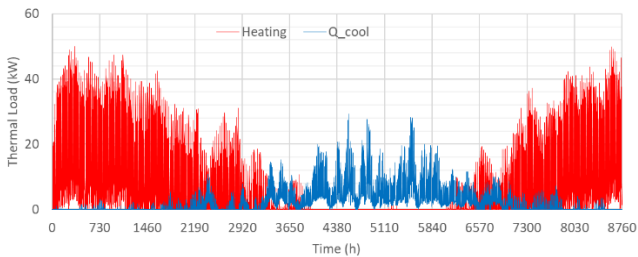


Figure VIII.14 - Energy performances of the building in the pre-intervention condition.

The building was also in a precarious state of architectural deterioration and required both aesthetic and functional renovations.

#### 8.4. Brief overview of the holistic intervention

The building was renovated by designing and implementing the AdESA system, a new solution for the structural, energy, and architectural retrofitting of existing suburban building stock. This system employs innovative technologies and virtual BIM design systems and is based on the application to an existing building of a layered envelope consisting of an internal structural layer, consisting of a shell exoskeleton made of CLT panels covered with a fireproof layer; an intermediate energy layer consisting of a thermal insulating coating; and an external architectural layer, which encloses the previous layers (Figure VIII.15).

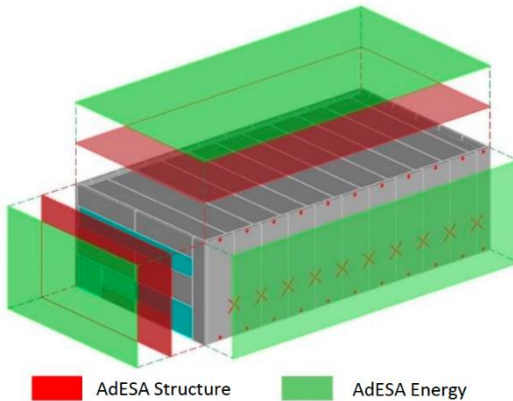


Figure VIII.15 - Concept of the AdESA intervention. From [3].

The energy upgrading (Table 4) was carried out by applying, over the structural shell, an insulation layer for improving thermal efficiency (8cm of EPS), as well as a finishing plaster

for the architectural renovation. The fire protection of the construction is guaranteed by the application of a protection layer underneath the insulation layer over the timber panels (12.5mm of *acquapanel*s) and of intumescent paints on the steel frame. The installation of new photovoltaic panels on the roof increased the building's sustainability by increasing its use of renewable energy sources. The results of the energy intervention (Figure VIII.16), as estimated by dynamic simulations, are depicted in the figure below for monthly heating and cooling demand and in Figure VIII.16 for thermal transmittance; with respect to the as-is condition, a annual heating energy saving of 50.51% are obtained in the post retrofit condition [15].

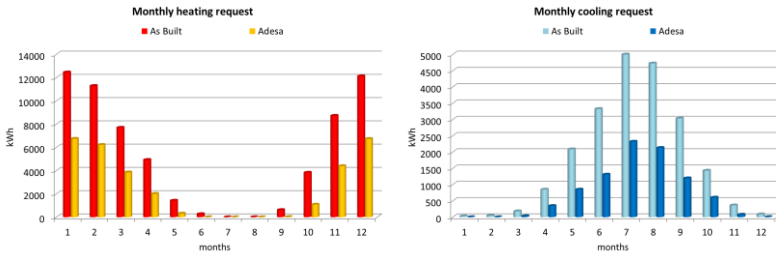


Figure VIII.16 - Energy performance prior to and subsequent to the energy intervention. From [15].

Table 4 - Results of the energy intervention's dynamic analyses. From [15].

| Insulation system |                          | Transmittance<br>[W/m <sup>2</sup> K] | Max Transmittance<br>[W/m <sup>2</sup> K] |
|-------------------|--------------------------|---------------------------------------|---|
| Transversal short |                          |                                       |   |
| walls             | CLT 10 cm + EPS 8 cm     | 0.24                                  | 0.28                                      |
| (Noth and South)  |                          |                                       |   |
| Longitudinal long |                          |                                       |   |
| walls             | EPS 10 cm                | 0.25                                  | 0.28                                      |
| (East and West)   |                          |                                       |   |
| Roof              | Plywood 3 cm + PIR 10 cm | 0.23                                  | 0.24                                      |

The gymnasium was painted white on the north and west sides and red on the south and east sides. As longitudinal elements located at the top and bottom of the facades and defining two horizontal red lines, the new window and door frames were also painted red (Figure VIII.17).



Figure VIII.17 - Views of the gymnasium at the end of the renovation process. From [15].

### 8.5. Conceptual design of the retrofitting exoskeleton

The *AdESA system*, conceived for the retrofit of RC and masonry structures, has been adapted to the specific characteristics of this building, to reckon with its morphological and architectural constraints.

The case study building, characterized by full-height RC cladding panels in the longitudinal facades, the ribbon windows along the short sides, and an internal intermediate partial floor, requires the adaptation of the shell exoskeleton in order to meet

the architectural features. The resulting structural shell consists of:

- a new plywood seismic roof diaphragm,
- hybrid shear walls with a horizontal arrangement of the structural panels along the short sides of the building, made of CLT panels and steel frames where the ribbon windows are located, supplemented with the *AdESA fuses (type I, Section 7.4.1)*;
- re-engineered RC cladding panels on the long sides, structurally behaving either as extended wall or like coupled rocking shear walls for the design or exceptional seismic events, respectively.

The structural concept of AdESA system as an external shell connected to the existing structure was maintained despite the partial re-engineering. In compliance with the principles of life cycle structural engineering (Section 5.2), design for damage control was performed. Earthquake-induced damage to the existing structural component and to the retrofitting system is limited by adopting quite demanding performance objectives: full functionality of the building at the Life-safety Limit State (LSLS), with limited deformation of the dissipators along the short sides and controlled rocking along the longitudinal direction; and a ductile failure mechanism for exceptional seismic events.

The performance objectives at LSLS were enforced by limiting the maximum inter-storey drift for the RC frame to 0.5%, by limiting the maximum shear load in the shell facades to 600kN, and by triggering the rocking behavior of the re-engineered cladding panels system. The concentration of damage caused by severe earthquakes and the limitation of seismic-induced loads is ensured by the introduction of passive energy dissipation



devices, the fuses illustrated in Section 7.4.1 (type I), within the exoskeleton. The horizontal arrangement of the energy dissipators and of the structural panels, combined with the lack of re-centering devices and systems, precludes the active reduction of the residual drift.

### **8.6. Description of the structural intervention**

The introduction of new seismic-resistant elements composing the shell along the perimeter of the building enable a box-like behaviour, significantly limiting the seismic actions on the existing structure and controlling its deformability, solving those vulnerabilities identified in the pre-intervention condition. The structural components of the exoskeleton, which are described in detail below, were dimensioned using *simplified design models* and linear static analyses with reference to the LSL. The hybrid resisting system in the transverse direction was proportioned based on the simplified models with horizontal structural arrangement analyzed in Section 6.3, while the re-engineering of the cladding panels is based on the models for the vertical arrangement, in which no recentering devices are introduced. Additional details are provided in .

#### **- *Timber roof diaphragm***

The new roof diaphragm was assembled on top of the existing RC roofing elements, considering the technology and specifics described in literature [25]. This structural element was dimensioned considering the analogy with bi-dimensional cords-and-panel structures, decoupling the structural functions between the components with the perimetral steel chords resisting the bending moment, and the timber web panel resisting to shear stresses (Figure VIII.18).

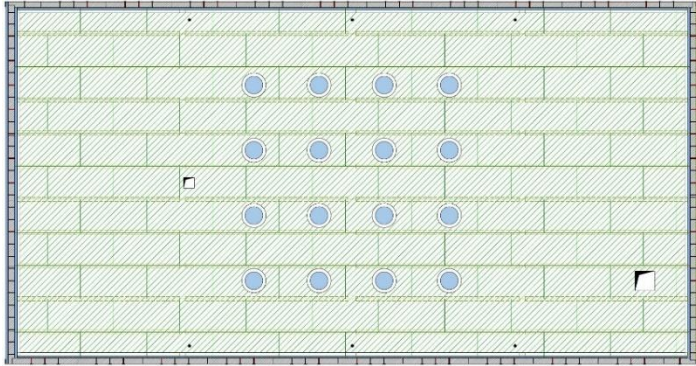


Figure VIII.18 - Roof plan following structural intervention. From [3].

Diaphragm shear panels are composed of 3cm thick plywood panels, connected with nailed steel flanges (nails  $\Phi 4 \times 2/5$  cm; flange:  $s=2$  mm) transferring the shear stress between panels and to the perimetral seismic resistant walls by means of steel studs ( $\Phi 22/45$  cm); steel tie rods prevent out-of-plane overturning of the cladding panels. Additional L-shaped ( $150 \times 100 \times 10$  mm) steel perimetral profiles were introduced as diaphragm chords (Figure VIII.19). The introduction of tie rods in the corners of each plywood panel, connected to the existing roof elements, prevented the thin timber web from buckling.

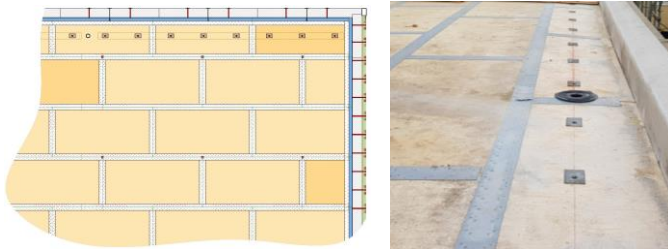


Figure VIII.19 - On the left-side: concept of the roof diaphragm. On the right-side: realization prior the introduction of the L-shaped perimetral elements. From [15].

- **Hybrid walls along the short facades**

Along the building's short side, new earthquake-resistant hybrid walls were installed in adherence to the existing facades. Architectural constraints related to the presence of ribbon windows and the stakeholder choices imposed the installation of timber structural panels and *AdESA fuses* arranged in the horizontal direction, coupled with seismic-resistant steel frames installed around the windows (Figure VIII.21), precluding the possibility of actively reducing residual drift.

Using simplified design models (Figure VIII.20) that account for the shear stiffness of the timber panels, the bending stiffness of the steel frames and the axial stiffness of the end-columns, the dimensions of the additional walls were determined.

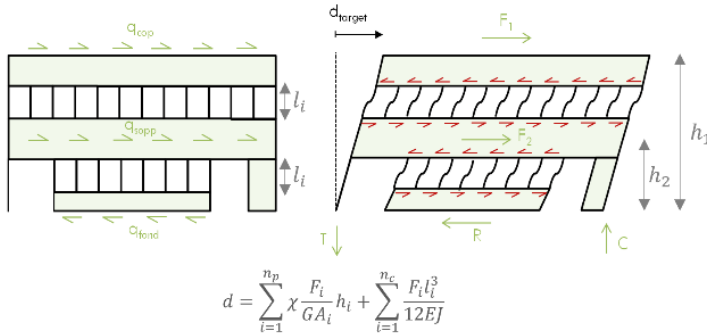


Figure VIII.20 - Conceptual representation of the simplified dimensioning model. From [15].

The hybrid walls are composed of horizontally arranged 5-layers CLT panels with a thickness of 100mm, connected with nailed steel flanges (nails  $\Phi 4 \times 2/5$  cm; flange:  $s=2$  mm), alternated with steel frames with rectangular tube profiles, consisting of 220x120x10mm horizontal elements and 180x120x10mm vertical elements (Figure VIII.21).

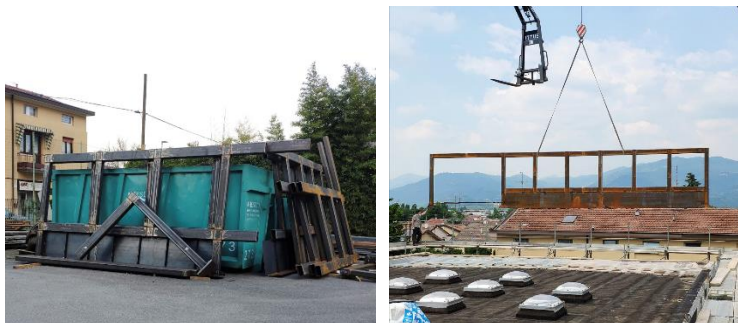


Figure VIII.21 - Pictures of frame installation, taken by the author.

The adoption of the steel frames, resulted in a hybrid version of the AdESA structural exoskeleton, which was originally envisioned as consisting of CLT panels only. The presence of horizontally arranged *AdESA fuses*, designed to offer a shear resistance of 15kN for each dissipative element, allows for the limitation of shear loads transmitted to the lower structural portion, thereby limiting seismic actions, and concentrating the nonlinear deformations at this level. This intervention introduces the second layout of the *fuses* analysed in Chapter VII, which is characterised by the presence of slits with rounded edges in the vertical steel plates.

The elevation of the south facade before and after structural intervention is depicted in Figure VIII.22. This representation includes the CLT panels in orange, the steel frames in dark gray, the structural connection to the roof and intermediate diaphragms consisting of rectangular plates, the dissipative *AdESA fuses* located between the steel frame on the ground floor and the intermediate timber panels (Figure VIII.23), and the new foundation system consisting of the RC curb and drilled piles.



Figure VIII.22 - Representation of the structural intervention along the short facades of the building, showing some structural details: 1) steel dowels summit connectors between exoskeleton and pre-existence; 2) steel dowels intermediate diaphragm connectors; 3) detail of AdESA fuses; 4) structural connections of the new foundation. From [15].



Figure VIII.23 - On the left-side: picture of the AdESA fuses installed along the southern façade. From [15]. On the right-side: detail of the dissipative connection. Picture shot by the author.

New RC foundation curbs were cast beneath the additional transverse walls to transfer the horizontal seismic loads collected by the shell exoskeleton facades and transfer them to the existing RC slab through steel dowels. It is worth noting that, as opposed to traditional shear-wall solutions, in which a relevant number of micropiles is required to resist the seismic bending moment, in the shell solution, by exploiting the extension of the shell exoskeleton facades, the lever arm of the axial forces balancing the seismic bending moment at foundation level increases remarkably, thus the number of the micropiles can be substantially reduced. In this application only 2 piles placed at the ends of the foundation curb in the transverse direction were adopted (4 micropiles total).

- *Longitudinal facades strengthening*

Along the building's longitudinal facades, the lateral force resisting system (LFRS) was created by re-engineering the existing cladding panels, thereby avoiding the introduction of a new structural layer (Figure VIII.24). To increase the in-plane stiffness and resistance of the building longitudinal facades, mechanical couplers, consisting of 10mm X-shaped S355 steel plates and (8+8)  $\Phi$ 20mm steel studs (Figure VIII.25, Figure VIII.26), were introduced between adjacent RC cladding panels to enforce panel coupling, exploiting the resistant resources offered by the extended structural façade, and relying on rocking activation for severe seismic events.

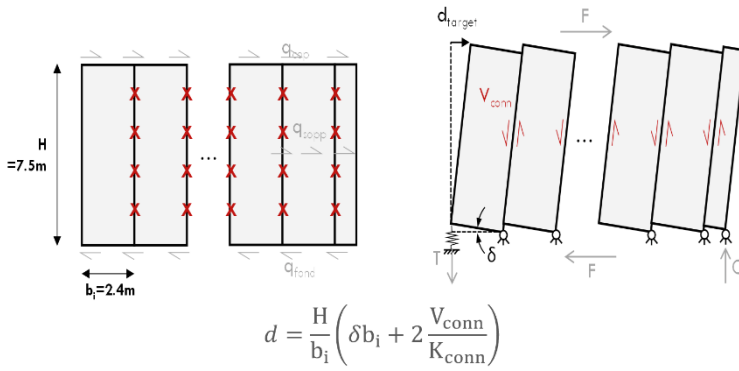


Figure VIII.24 - Conceptual representation of the simplified dimensioning model. From [15].

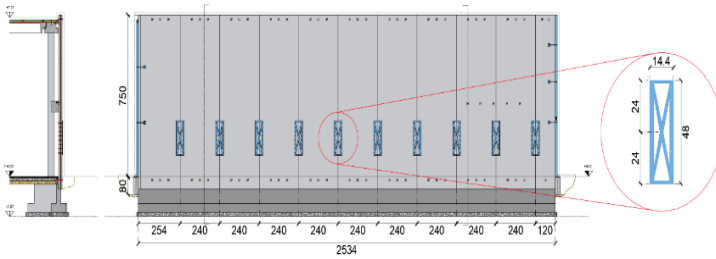


Figure VIII.25 - Representation of the structural intervention along the longitudinal facades of the building. From [15].



Figure VIII.26 - pictures of the mechanical coupling elements installed between the adjacent RC cladding panels. From [15].

To transfer the shear loads generated by the seismic actions to the existing foundation, 3 over-resistant  $\Phi 22$  S355 steel studs were installed at the base of each panel and a couple of  $\Phi 20$  steel dowels were also used to connect the roof diaphragm to the new LFRS at the top level. In addition, steel anchors were installed to secure the structural facade to the roof diaphragm and to prevent out-of-plane overturning.

- ***Intermediate slab strengthening***

The only interventions to be performed inside the building are the installation of three steel tie-rods at the intrados of the intermediate slab (Figure VIII.27), in the direction parallel to the TT tiles, for the re-engineering of the existing floor as a seismic diaphragm; and the realization of a horizontal *seismic separation joint* at the base of the internal precast staircase to avoid detrimental interactions during a seismic event.



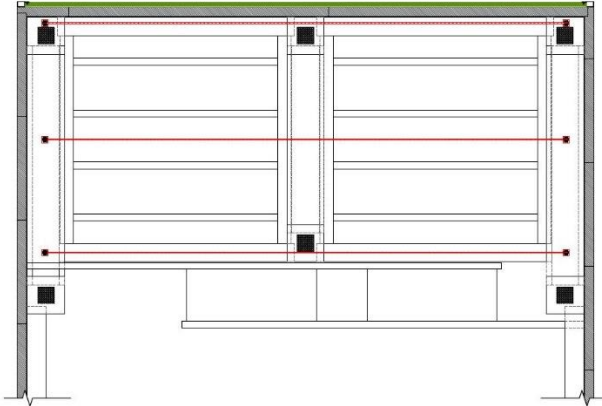


Figure VIII.27 - Plan of the intermediate floor after the structural intervention, viewed from the bottom up, with the tie rods highlighted in red. From [3].

### 8.7. Structural performance of the retrofitted system

The structural performance of the retrofitted building was investigated by performing nonlinear dynamic analyses. *Mesh C*, was created by implementing the exoskeleton components in *Mesh B* (Figure VIII.28). For the sake of clarity, only the main characteristics of the model are presented in this chapter, while details of the numerical model (geometry of each component, and mechanical properties) are presented in .

The strengthening elements installed along the longitudinal facades were modelled by adding general-links to simulate the new mechanical coupling connections between adjacent cladding panels, whereas the AdESA hybrid walls installed in adherence to the short facades were modelled with elastic plane-stress elements for the CLT panels, one-dimensional beam elements for the steel frames, and elasto-plastic general links for the structural connections between the new walls and the existing structure. At the roof level, to reduce the computational

effort associated with the large number of model nodes, a rigid diaphragm was implemented to account for the contribution of the seismic wooden diaphragm. The structural validations of the diaphragm were conducted using the total accelerations determined by the time history analyses.

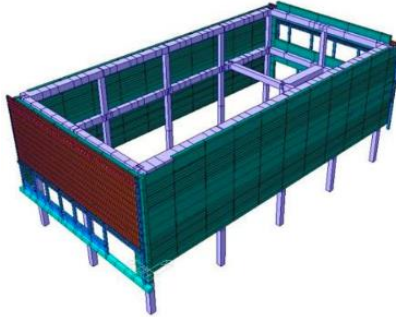


Figure VIII.28 - 3D representation of the numerical model of the retrofitted building, mesh C, extracted from the software. From [15].

The main properties of *mesh C* components are presented in Table 5 (adapted from [1]), further details can be found in .

Table 5 - Principal characteristics of the retrofitted building model, Mesh C. From [15]. Detailed descriptions of each component, including the adopted geometric and mechanical properties, are reported in .

| North & South Hybrid walls | Element Typology   | Finite Element Modeling           | Notes |
|----------------------------|--|-----------------------------------|-------|
| Steel Frames               | Hollow square profiles & plates in structural steel<br>S355:<br>220x120x10mm (horizontal elem.)<br>and 180x120x10mm (vertical elem.) | 1-dimension Elastic Beam elements | -     |

# Stefano Cademartori

|  |  |                                    |  |
|--|--|------------------------------------|--|
| CLT panels   | 5-layers 100mm   |                                    | Design compression strength:   |
|  | CLT structural   | 2-dimensions                       | $f_{cd,CLT} = 8.69\text{MPa}$  |
|  | panels:<br>13x2.5m   | Elastic plane-<br>stress elements  | Design shear strength:<br>$f_{vd,CLT} = 1.9\text{MPa}$   |
|  | commercial<br>elements   |                                    | Out-of-plane design bending resistance:<br>$M_{Rd} = 24\text{kNm / m}$   |
| 'Over-resistant'<br>Structural<br>connections                    | Steel dowels   | Elastic general<br>links           | Cladding panels - Intermediate RC beams:<br>$K = 1676.8\text{kN/mm}, V_{Rd} = 7.3\text{kN}$  |
|  | $\Phi 20/22$ in S355 steel   |                                    | Cladding panels - Roof-level RC beams<br>$K = 5.81\text{kN/mm}, V_{Rd} = 7.3\text{kN}$   |
|  |  |                                    | Cladding panels – Intermediate column corbels<br>$K = 9.23\text{kN/mm}, V_{Rd} = 7.3\text{kN}$   |
| <i>AdESA fuses</i>   | Steel dissipative<br>plates in structural<br>steel S275                  | Elasto-plastic<br>beam elements    | Maximum shear resistance for each<br>dissipative plate : $V=15\text{kN}$ .   |
| <b>East &amp; West<br/>longitudinal facades</b>                  | <b>Element Typology</b>  | <b>Finite Element<br/>Modeling</b> | <b>Description</b>   |
| Mechanical<br>coupling elements<br>between RC<br>cladding panels | 10mm plates in<br>mild steel S355 and<br>(8+8) $\Phi 20$ steel<br>dowels | Elasto-plastic<br>general links    | Equivalent elastic stiffness<br>$K_{conn} = 123.4\text{kN/mm}$ ,<br>Shear resistance referred to a row of 8 dowels<br>$V_{conn} = 130\text{kN}$  |
| 'Over-resistant'<br>connections                                  | Steel studs in S355  | Elastic general<br>links           | Cladding panels - Roof diaphragm<br>$K = 444\text{kN/mm}$<br>Cladding panels - Existing foundation<br>$K = 548\text{kN/mm}$<br>Cladding panels – Intermediate slab<br>$K = 72\text{kN/mm}$ |
| <b>New roof<br/>diaphragm</b>                                    | <b>Element Typology</b>  | <b>Finite Element<br/>Modeling</b> | <b>Description</b>   |

|  |   |                 |                 |
|--|---|-----------------|-----------------|
| Timber shear panels & L-shaped steel longitudinal profiles | 30mm thick structural plywood panels & L-shape steel profile in mild steel S355 | Rigid diaphragm | Rigid diaphragm |
|--|---|-----------------|-----------------|

Nonlinear time history analyses were carried out by considering seven Italian seismic events, compatible with the site's LSLS elastic spectrum [141], selected from the earthquakes with the highest peak ground velocity (P.G.V.). The selection constraint based on the P.G.V. was introduced with the intention of studying the relationship between this peak parameter and the induced damage and selecting the most severe seismic events for dissipative and re-centering structural systems. Rexel software was adopted (Figure VIII.29) [241].

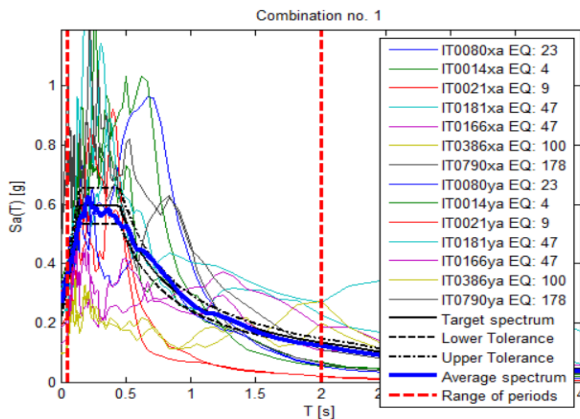


Figure VIII.29 - Set of 7 spectrum-compatible Italian seismic events obtained from Rexel software.

The results obtained from these analyses are respectful of the design target selected in the preliminary design phase. Widespread yielding of the *AdESA fuses* installed in the

transversal hybrid walls for the majority of the introduced seismic events can be observed, whereas the seismic-resistant steel frames and CLT panels remain in the elastic range. In the longitudinal direction, rocking activation of the precast RC panels is observed in all the performed analyses.

Specifically, in the transverse direction, the average maximum drifts achieved by the steel frames at the ribbon window level at the first floor of the south wall are roughly 0.52% (Figure VIII.30), as enforced during the design stage; other frames experience significantly lower drifts.

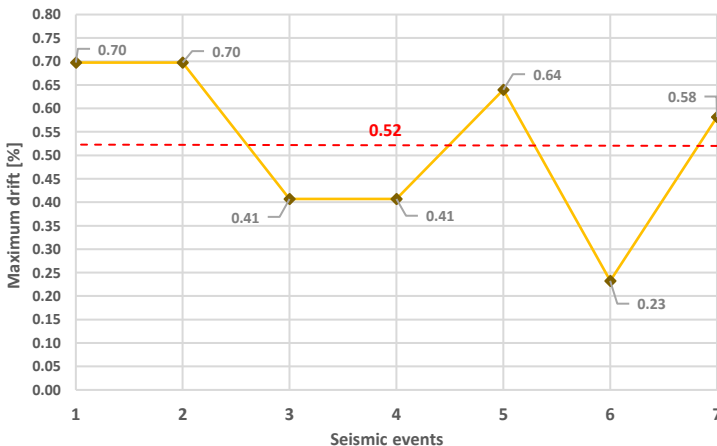


Figure VIII.30 - Maximum drifts achieved in the steel frame installed at the ribbon window level on the first floor of the south wall for the selected seismic events.

The average maximum drifts of the hybrid retrofitting walls is 0.36% for the south façade (Figure VIII.31) and 0.28% for the northern one (Figure VIII.32), resulting in a building maximum drift below the 0.5% threshold.

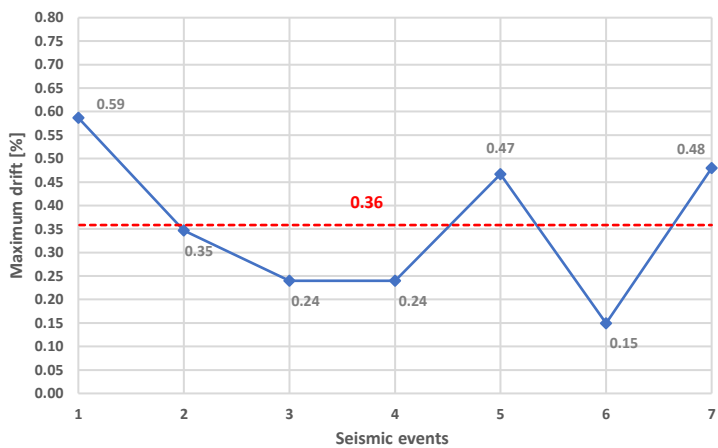


Figure VIII.31 - Maximum drifts achieved by hybrid walls placed along the south façade.

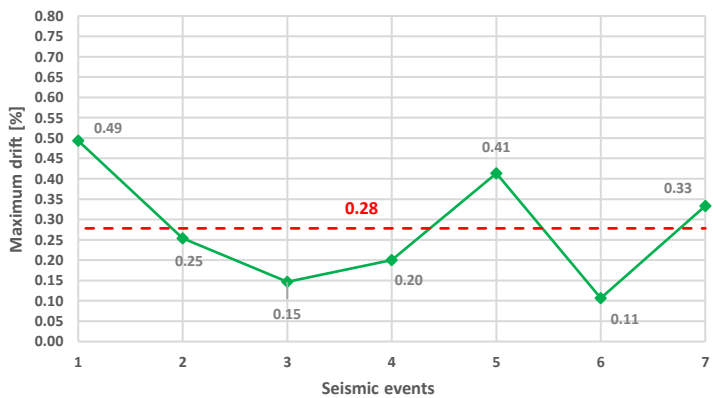


Figure VIII.32 - Maximum drifts achieved by hybrid walls placed along the north façade.

The *AdESA fuses* present large inelastic deformation for most seismic events, ensuring the limitation of the seismic loads below 600kN. The maximum drifts for these dissipative elements, (measured as maximum displacement over the height of the vertical steel plates), are 17% for the *fuses* placed along the north façade, corresponding to a relative displacement of approximately 1.2cm (Figure VIII.33), and 13% for the other; their residual drift at the end of the seismic event varies depending on the ground motion characteristics (with an average value of approximately 0.6cm).

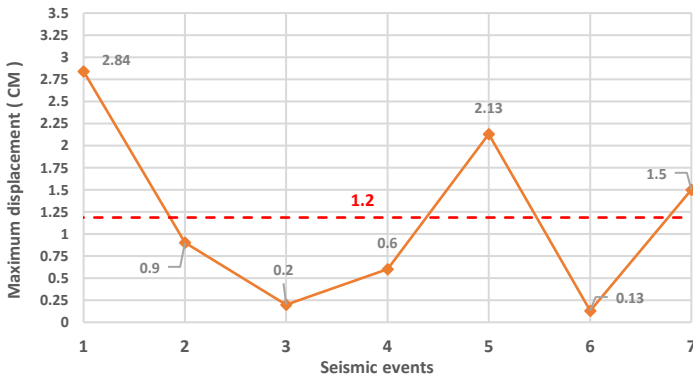


Figure VIII.33 - Maximum displacement over the height of the vertical steel plates achieve by the AdESA fuses placed along the north facade.

The lateral coupling elements between the longitudinal cladding panels enable the onset of controlled rocking behaviour, thanks to the yielding of the installed steel dowels, while maintaining the integrity of the X-shaped steel plates. The average maximum drift achieved by the cladding panels is approximately 0.12% (Figure VIII.34), with a residual drift close to zero.

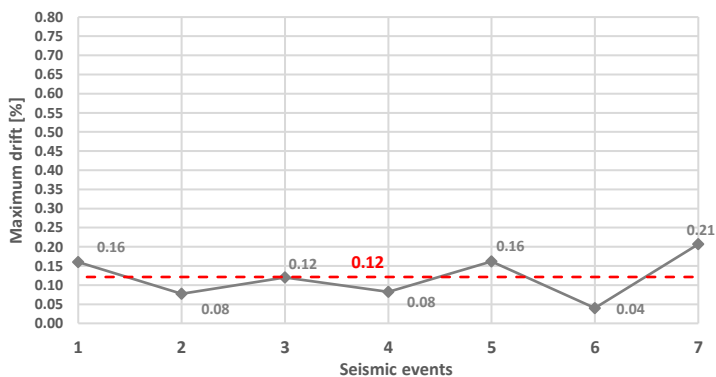


Figure VIII.34 - Maximum drifts achieved by the cladding panels.

The activation of the plastic hinges in the AdESA fuses and the controlled rocking of the cladding panels also allow for the limitation of seismic-induced loads in both principal directions, effectively limiting the maximum acceleration experienced by the roof diaphragm to 0.62 g (Figure VIII.35).

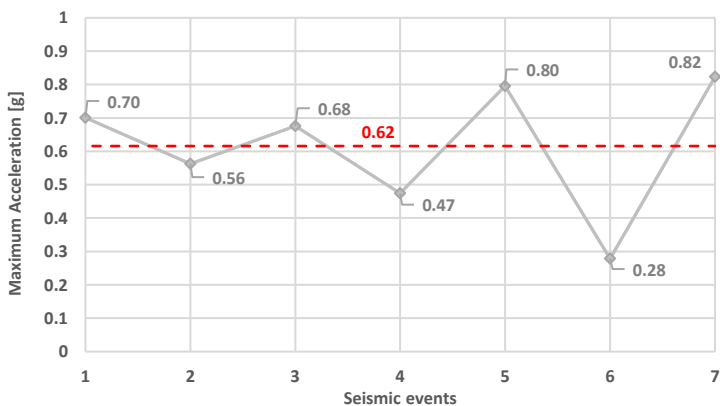


Figure VIII.35 - Maximum acceleration achieved by the centre of roof diaphragm.



## Stefano Cademartori

The existing precast concrete frame shows widespread activation of plastic hinges in the columns without reaching ultimate deformation in any seismic event, the average maximum inter-storey drift achieved by the existing RC frame is around 0.5% (Figure VIII.36).

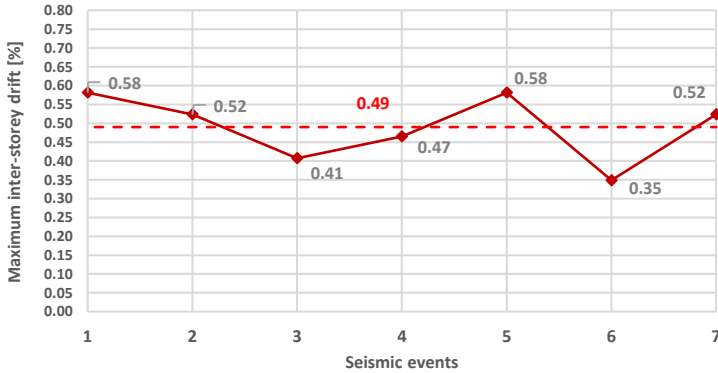


Figure VIII.36 - Maximum inter-storey drift achieved by the RC frame.

### 8.8. Lesson learned & partial re-engineering of the retrofit

The assembly of the entire AdESA system took 4-5 months, excluding the delay caused by the covid pandemic, while the installation of the hybrid transverse walls and the connection of the timber panels to the existing building took about 2 days with a team of 4 people and a light crane. The renovation cost, including the energy and structural shell, architectural finishes, construction site costs, preliminary works, contingencies, VAT and excluding technical costs, was approximately 390 €/m<sup>2</sup> of shell surface area (total shell surface of about 918m<sup>2</sup>). The cost breaks down in Figure VIII.37 shows: 30% of the total cost associated with the structural retrofit, about 30% with energy amelioration measures and finishes, and 40% with other construction expenses. The pre-installation off-site of the thermal insulation layer and of part of the finishes on the structural panels can further reduce the installation process.

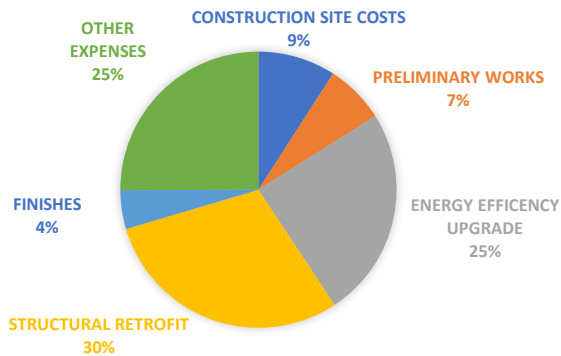


Figure VIII.37 - Synthetic construction cost breakdown. Other expenses includes construction site costs, preliminary works, contingencies, VAT and excluding technical costs.

The installation of the hybrid walls in the transverse direction (*Y direction*) represents the most expensive retrofitting work, accounting for approximately 58% of the total structural retrofit cost, while the longitudinal strengthening (*X direction*) account for only 12% of the total cost. The construction of the new roof diaphragm required 16% of the available resources for retrofitting, while the structural connections required the use of the remaining 14% of the resources (Figure VIII.38).

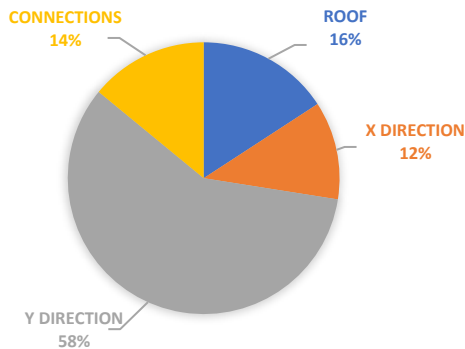


Figure VIII.38 - Percentage on structural retrofit cost (the intervention in the Y direction encompasses the hybrid steel-CLT walls and their sub structures; the intervention in the X direction includes costs for the mechanical couplers of the cladding panels)

The reduced number of micropiles considerably simplified the construction process and confirmed the suitability of the exoskeleton shell or extended/coupled shear walls. Furthermore, to the sake of the sustainability of the solution, the reduction of drilled piles results in a lower environmental impact and a reduction in construction time and cost compared to a traditional shear wall solution.

Beyond the theoretical conceptual design, the application of the proposed system to a real building allowed to address several construction issues, which resulted in a partial re-engineering of

the retrofit system. The need to account for the tolerances of the connecting system (by far the most relevant issue to be solved during construction), and the need to simplify the manufacturing and installation of the retrofit led to the development of an updated version of the AdESA system, which is being developed in a companion research, and which is based on the partial re-engineering of the connections of the exoskeleton to the building and to the foundations [242] [243].



Figure VIII.39 - Pictures of the prefabricated structural retrofit under erection. From [15].

The horizontal arrangement of the AdESA fuse strips may interfere with the possible disassembly and replacement of these elements following a severe seismic event, requiring the cutting of yielded components and the welding of new elements on site.

## **IX. Application of an adaptive exoskeleton to a post-World War II masonry building**

### **9.1. Introduction**

The second case study presented is the retrofitting of a residential building from the late 1950s, built in northern Italy in a medium-high seismicity area, erected using a structural typology that is common to many small to medium-sized residential buildings, characterised by the presence of a load-bearing masonry structure made of hollow clay bricks with horizontal holes bonded with cement based mortar [244] [245] [246]. Recent seismic events in northern Italy have highlighted the great seismic vulnerability of this widespread structural type, which is associated with the early collapse of the masonry walls and the brittle crushing of the hollow bricks caused by the concentration of earthquake-induced stresses and its inability to redistribute seismic loads once the ultimate capacity has been reached [246].

The initial section of the chapter describes the wooden exoskeleton as part of an integrated structural, energetic, and architectural renovation intervention carried out within the research project “SCC-Innovation hub and living lab network” financed by Regione Lombardia [247]. In the second section, the exoskeleton is *redesigned* by applying the design principles and processes described in Chapter VI, leading to the conception of an adaptive retrofit capable of further performance enhancement. In the final section of the chapter, several options for reengineering the connections at the base of the wooden panels are presented.

As stated in the introductory section of the research, the author's involvement in this case study is limited to the study of alternative numerical models for investigating the structural behaviour of coupled walls, also considering different structural schemes to those implemented.

## **9.2. Building description**

The analysed construction (Figure IX.1) is a small-medium size residential building, housing 4 apartments, representative of typical post-World War II social housing never renovated.



Figure IX.1 - View of the main façade before the intervention. Form [247]

The following is a summary of the building's condition prior to the renovation. Additional details are available in [247] and [248].

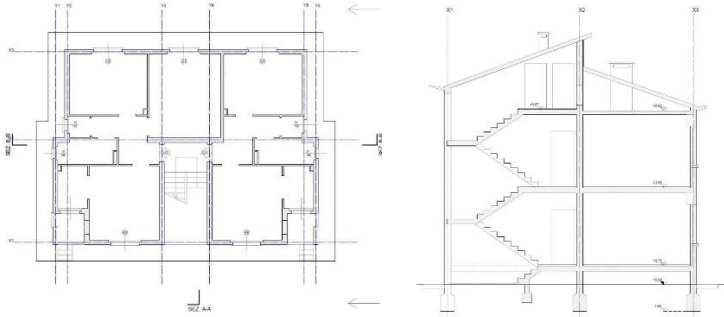


Figure IX.2 - On the left-side: plan of the building. On the right-side: building section A-A. From [248].

This social housing building, owned by the social housing owner ALER (Azienda Lombarda per l'Edilizia Residenziale), is in Prevalle in the province of Brescia in a moderate-high seismic zone ( $a_g = 0.158g$  [141], and climate zone E, HDD=2335). Built between 1958 and 1960 and designed solely for gravitational loads, it presents two floors above-ground, each housing a two-room flat and a three-room flat (Figure IX.2, right), plus an attic used for storage and cellars. The building is regular in plan and elevation, with a gross floor area per floor of approximately  $131m^2$ . The main façade is regular with an extension of 13.6 m while the rear one has an extension of 12.4 m; the side façades, with an extension of 10 m, feature a recess of approximately 0.60 m (Figure IX.2, left).

The structural system is composed of load-bearing masonry structure consisting of clay hollow bricks (each unit is  $245 \times 245 \times 120mm$ ) arranged with horizontal holes and bonded with cement-based mortar; at the corners between orthogonal

walls and at the end-segments of each masonry pier, the masonry is composed of solid bricks (Figure IX.3, Figure IX.4).

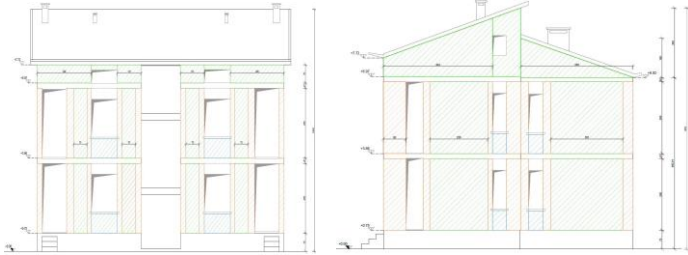


Figure IX.3 - Elevation schemes of the main facades, in which the hollow block masonry is depicted in green, the solid brick masonry in orange, and the horizontal walls with reduced thickness in blue. From [248].

The central reinforced concrete stairwell is supported by masonry walls erected using the same technique as the perimeter walls.

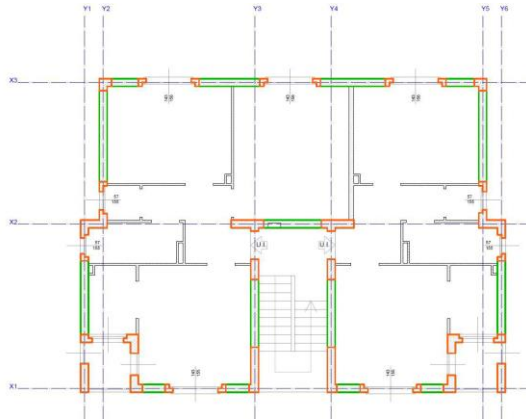


Figure IX.4 - Schematic building plan, in which hollow brickwork is outlined in green and solid brick in orange. From [248].

The existing slabs, made of clay block system, designed to support only gravity loads, are 0.20m thick bridging spans of



4.20m and 5.00m, with RC perimeter curbs placed above the masonry walls and RC main beam of approximately 0.43m bridging spans of 4.00 m. The two-roof pitches are mis-aligned and are composed of reinforced brick joists and hollow-core without extrados screed.

### **9.3. Assessment of the building in the as-is condition**

Before the renovation, the building presented several vulnerabilities associated with poor structural performances, poor energy efficiency, as well as poor architectural finishes and poor state of preservation. The construction materials are of poor quality and the structural elements are designed for basic performances against static loads only; the domestic plant system as well as the envelope are obsolete and unable to meet the users' needs, both in terms of functionality and in terms of energy efficiency and comfort.

From the structural point of view, the primary seismic vulnerability is related to the onset of local collapse mechanisms involving the out-of-plane overturning of the masonry walls, ineffectively constrained to the RC perimeter curbs. The elastic design spectrum of the site at life-safety limit state (LSLS) used for the analyses is reported in Figure IX.5.

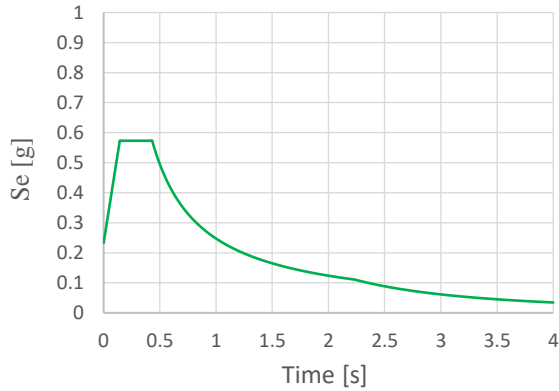


Figure IX.5 - Elastic design spectrum of the site at life-safety limit state (LSLS). From [141].

The vulnerability is associated to the overturning of the wall at the attic level (Figure IX.6), caused by the lack of a rigid roof diaphragm. The seismic safety index at LSLS equal to 0.12.

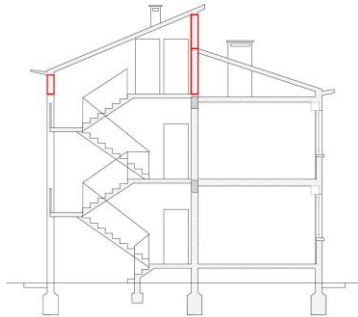


Figure IX.6 - Cross-section highlighting in red the most vulnerable masonry walls arranged in the longitudinal direction of the building. From [248].

The global seismic vulnerability of the building was investigated performing nonlinear static analyses of a 3D numerical model of the building (Figure IX.7, left), implemented in Midas Gen [194], assuming that the activation

of local collapse mechanisms was inhibited. This model was created by considering the geometric and sectional properties as well as the mechanical properties of the structural elements measured on-site.

The ultimate drift of the slender clay hollow brick masonry piers was limited to 0.4%, following the results of a companion research focused on the characterization of hollow clay masonry walls arranged with horizontal holes [246]. It is worth noting that such a value is quite lower than the maximum drift allowed by the Italian standard for slender walls [141] and accounts for the extremely low ductility and the brittle failure mechanism observed in the experimental campaign [245]. Furthermore, the experimental results showed the inability of the walls to withstand gravitational loads after the extensive damage to the pier base induced by the rocking motion, thereby highlighting the severe vulnerability of this masonry typology. The influence of the modelling assumption related to the ultimate drift amplitude on the building global behaviour was partly analysed in this research, whose results have been submitted for possible publication [246].

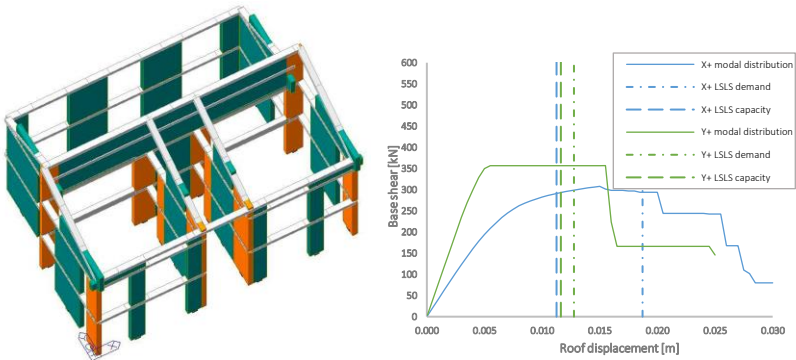


Figure IX.7 – On the left side: 3-D representation of the numeric model, extracted from the software. On the right side: capacity curves of the building in the as-is condition. In which the curve in the longitudinal direction X is represented by the continuous blue line, and that obtained in the transverse direction Y by the green continuous line. From [248].

Nonlinear static analyses showed the greatest vulnerability of the building in the longitudinal direction X (Figure 7, right). Upon inhibiting the local mechanisms, the global seismic vulnerability is associated with the activation of a soft-storey mechanism at the second level, caused by the widespread failure of the longitudinally arranged masonry piers subjected to flexural and shear stresses (Figure IX.8).

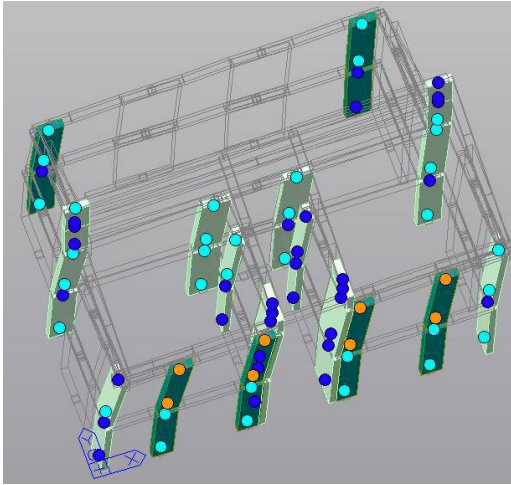


Figure IX.8 - Representation of the achievement of the ultimate drift for masonry piers at second level, highlighted by orange circles, extracted from the software. From [248].

These masonry elements exhibit a nearly fragile response to any potential failure mechanism compared to conventional solid bricks elements, with the additional risk of being unable to withstand gravitational loads following extensive damage at the pier base sections. Based on the described modelling assumptions, the building is also vulnerable with respect to global mechanisms, with a seismic safety index at LSL equal to 0.62 (Figure 7, left).

Concerning energy efficiency, the building exhibits major deficiencies typical of 1960s social housing constructions. The poor energy performance is due to the envelope obsolescence, all the external surfaces lack thermal insulation with quite relevant un-resolved thermal bridges. In addition, the central stairwell of the main facade is open toward the courtyard, substantially increasing the dispersing surfaces. The combination of these factors results in high energy

consumption, thus in a significant impact on the environment, besides being the source of users' discomfort. The energy performance of the building was evaluated using a detailed transient analysis conducted with a Trnsys® numerical simulation [247]. Starting with a 3D geometric model, the analysis considers the behaviour of the building, including the physical properties of the walls and the internal gains. The energy efficiency class before the intervention is B [249], the thermal transmittance of the masonry walls is  $0.964\text{W}/(\text{m}^2\text{K})$ , and the thermal transmittance of the windows is  $\lambda = 5.7\text{W}/(\text{m}^2\text{K})$ . The total annual thermal load of the building is 54kWh.

From an architectural standpoint, the building was in a precarious state of deterioration, and it required both aesthetic and functional renovations.

#### 9.4. Brief overview of the holistic intervention

The renovation of the building was accomplished by designing and implementing a shell layered exoskeleton simultaneously addressing the multiple structural, energy, and architectural deficiencies (Figure IX.9).

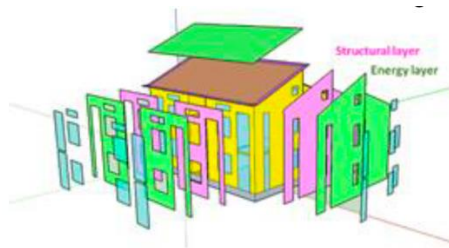


Figure IX.9 - Schematic representation of the components of the holistic intervention, in which the structural layer is coloured in purple and the energy layer in green. From [247].

The designed solution consists of an internal structural layer of CLT panels that improves the seismic behaviour of the building, an intermediate energy-efficient thermal insulation layer, an external finishing layer that improves the building's aesthetics, and a new plant distribution system consisting in the Fluxus-Ring system [247], installed without replacing the boiler and radiators and anchored to the structural envelope facilitating inspection from the outside.

As for the energy efficiency amelioration measures, an additional insulation coating layer (12cm of Rockwool) was fixed to the structural shell to reduce the thermal transmittance of the envelope to  $0.178\text{W}/(\text{m}^2\text{K})$  and limit thermal bridges. The installation of low-energy windows ( $\lambda = 2.6\text{W}/(\text{m}^2\text{K})$ ) completes the upgrades. These interventions resulted in a sensible reduction of total annual thermal load to  $15\text{kWh}$  with an energy savings of 72% (Figure IX.10). The energy rating shifted from Class F to Class B [249].

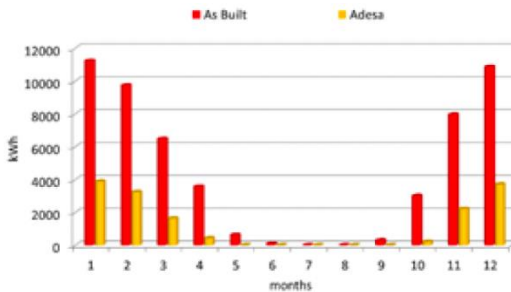


Figure IX.10 - Comparison of the energy performance of the building in the as-is and retrofitted states. From [247].

The introduction of the structural solution, described in the following paragraph, enables shifting from the seismic Class from F to A+ [250].

From the architectural standpoint, the façade was finished with a new coloured plaster while the windows were replaced and the staircase core was closed, increasing the comfort of the inhabitants, and reducing the need for thermal energy.

Detailed information on the integrated intervention is provided in [247], whilst in the following, focus is made on the sole structural retrofit.

## 9.5. Structural intervention

The primary structural components of the LRFS (Figure IX.11) encompass:

- the superstructure made of the wooden shell exoskeleton composed of CLT panels, the new plywood roof diaphragm the existing floors activating a diaphragm action and their mutual connections, including vertical dissipative couplers between adjacent panels;
- the new RC foundations;
- the exoskeleton-to-existing building as well as the exoskeleton-to-foundation connections.

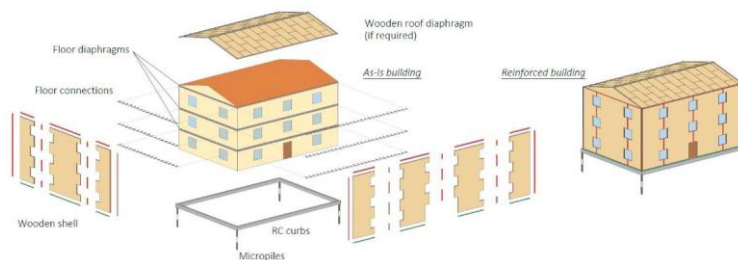


Figure IX.11 - Schematic representation of the components of the wooden exoskeleton. From [247].



During the design phase, the performance objectives of the retrofit were defined: elastic behaviour during moderate events and at LSLS and dissipative and re-centring behaviour for exceptional events. For severe earthquakes the activation of a global ductile mechanism for the existing building is expected with the preservation of its load-bearing capacity. To guarantee these performances, the following design targets were applied: limitation of the maximum inter-storey drift to 0.4% for seismic events at LSLS and yielding of the couplers between the vertically arranged structural panels for severe ones. The dissipation of seismic energy provided by the couplers limits the seismic loads and protects the integrity of the other elements and connections.



Figure IX.12 - Representations of the timber exoskeletons arranged along the main façades, in which the wooden elements are shaded in yellow and the Dywidag bars in purple. From [248]

The new foundation consists of a perimeter RC curb placed in adherence to the existing foundation to support the structural panels and transfer their actions to small-diameter, drilled RC piles driven 15m deep into the ground to support the tensile and compressive actions induced by the global seismic bending action acting on the retrofit.

The 10cm thick structural panels, consisting of 5 timber layers, conform to the shape of the existing openings (Figure IX.12) and are coupled by means of AdESA fuses (*type III, Section*

7.4.1) to ensure the ductility to retrofit and dissipation capacity (Figure IX.13).



Figure IX.13 - Images of AdESA fuses installed between CLT panels. From [247].

The shell is linked to the building floor slabs using  $\Phi 20/30\text{cm}$  stell dowels and two  $\Phi 12$  tie-rods per panel, fixed to the RC curbs. Each vertical panel is constrained to the new foundation by means of two g  $\Phi 18$  Gewi Dywidag steel bars, pre-installed off-site in 1m-deep holes drilled in the CLT panel, which transfer the bending moment of the retrofit to the foundation; the reduced length of the bars is due to technological limitations in panel processing. These re-centring elements, designed to remain in the elastic range, allow the containment of residual drift.

The shear resistance of the panels is guaranteed by the presence of two shear keys inserted at the base of the panel (Figure IX.14), consisting of  $\Phi 50$  tubular studs 3 mm thick welded to the plate nailed to the panel, inserted in special pockets made in the foundation and then filled with concrete.



Figure IX.14 - Images of the Structural connections between CLT panels and the foundation at their base. From [247].

The effectiveness of the intervention was assessed by performing nonlinear static analyses of a finite element model of the retrofitted building (Figure IX.15, left).

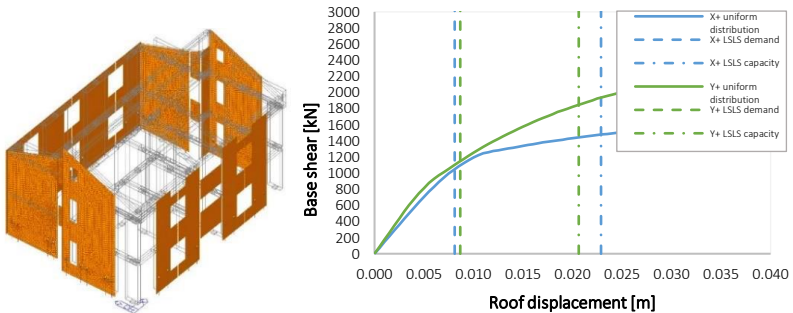


Figure IX.15 – On the left-side: 3-D finite element model of the retrofitted building featuring the shell exoskeleton. From [247]. On the right-side: Pushover curve of the retrofitted building. In which the curve in the longitudinal direction X is represented by the blue continuous line and that obtained in the transverse direction Y by the green continuous line. From [248].

The results demonstrate that the structure gains adequate stiffness and strength to limit displacement demand at LSLS below capacity. For this level of seismic intensity, yielding of

several dissipative fuses is observed, while the structural connections between the panels and the foundation and the CLT panels remain in the elastic range. Existing walls have a maximum inter-story drift of 0.12%, which is less than the experimentally determined and imposed maximum limit of 0.4%. Upon completion of the intervention, the seismic safety index is equal to 2.12 (Figure IX.15, right), corresponding to the seismic class A+.

## 9.6. Critical analysis of the structural intervention

Several scenarios and design hypotheses were analysed to evaluate the effectiveness of the design approach and of the adaptive exoskeletons as retrofit solutions for existing buildings. The models developed in Section 6.5 were adapted to reckon with the architectural constraint of the case study. Three configurations (Mesh A, B, and C) were first proportioned with hand calculation and with reference to the simplified models presented in Chapter VI (Section 6.5.3). Then, nonlinear time-history numerical analyses were carried out.

Based on the results of the hand calculation and on the observed drawbacks, a few corrective measures were considered, and the following cases were analysed:

- **Mesh A:** in this case, two isolated coupled walls as those presented in Sect. 6.5, are placed along the X1 alignment (Figure IX.16, a). Each wall is composed of two vertical CLT panels, with horizontal spandrel panels, with central vertical couplers. Hand calculation highlighted high foundation stresses due to the total resisting moment, and high stress in the panel-foundation connection.
- **Mesh B:** to reduce the stress due to the overturning moment, the two coupled walls were coupled (Figure IX.16, b).

- **Mesh C – Short bars (SB):** in this layout, Mesh B is supplemented with 1-meter Gewi bars rather than full-height bars (Figure IX.16, c). The contractor, also serving as the manufacturer of the CLT panels, declared the technical non-feasibility of full-height holes in the CLT panels at its production and processing plant.

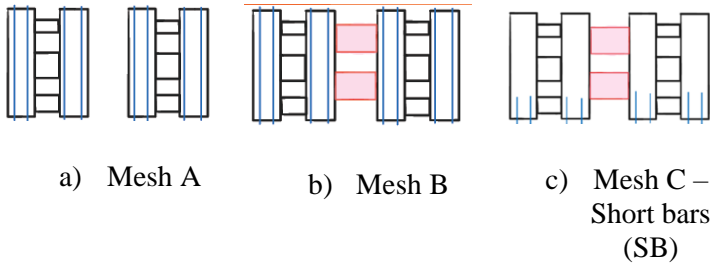


Figure IX.16 - Sketch of the layout analysed.

As per the performance objectives, the walls were required to behave elastically up to the design limit state (Life Safety Limit State - LSLS); the couplers would be activated beyond that limit.

Mesh A, B, C were subjected to a design ground motion (GM) (LSLS, whose associated accelerations correspond to the design one), an extraordinary GM (LSLS+, whose associated accelerations slightly exceed the design one), and a Collapse Limit State GM. (Figure IX.17) shows the design spectra for the selected site.

Due to the existing construction typology, with masonry blocks arranged with horizontal holes, the maximum design displacement was enforced as equal to 0.25% [246].

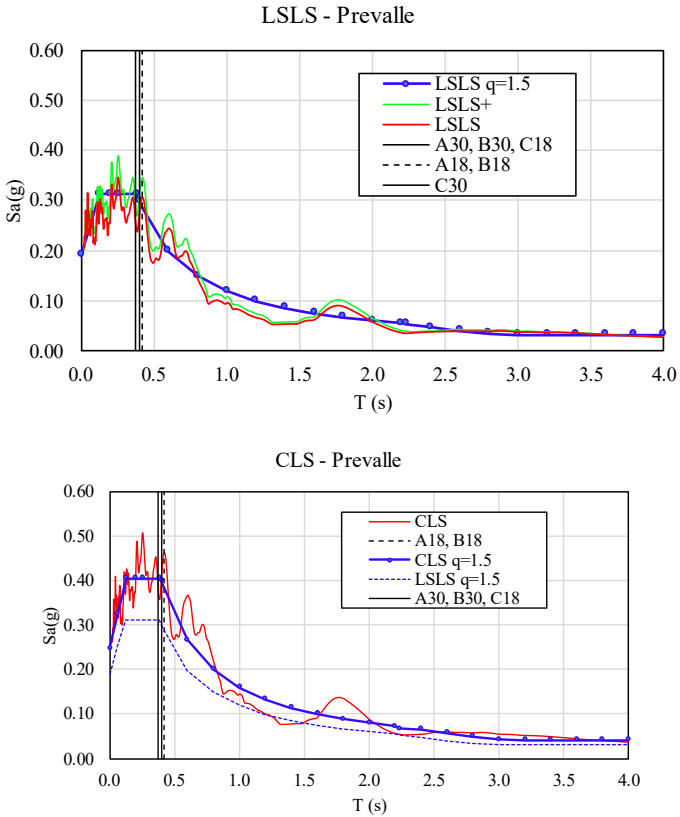


Figure IX.17 – Design spectra for the reference site: a) Life Safety Limit State, and b) Collapse Limit State. The elastic period of cases A and B are plotted with full and dashed black lines, respectively.

The main results are summarized in Table 6. The critical analysis of the results aims to open the discussion about the influence of technological aspects on the adaptive wall behaviour. An extension of the parametric analyses has to be made to further generalize and consolidate the discussion.

Table 6 - Overview of the analysed cases in the parametric analyses and summary of the main results.

| Case      | Mesh | $\Phi$ bars (mm) | GM    | $d_{TOP}$ (mm) | $\delta_{TOP}$ (%) | $d_V$ (mm) | $\sigma_{MAX,bar} / f_y$ |
|-----------|------|------------------|-------|----------------|--------------------|------------|--------------------------|
| C18-LSLS  | C    | 18               | LSLS  | 13.50          | 0.19               | 1.76       | 0.65                     |
| C18-LSLS+ | C    | 18               | LSLS+ | 18.05          | 0.26               | 2.35       | 0.87                     |
| C18-CLS   | C    | 18               | CLS   | 21.82          | 0.31               | 2.77       | 1.02                     |
| C30-LSLS  | C    | 30               | LSLS  | <b>17.26</b>   | 0.25               | 1.81       | 0.51                     |
| C30-LSLS+ | C    | 30               | LSLS+ | 19.98          | 0.29               | 2.29       | 0.58                     |
| C30-CLS   | C    | 30               | CLS   | 23.06          | 0.33               | 2.36       | 0.65                     |
| A18-LSLS  | A    | 18               | LSLS  | 12.20          | 0.18               | 2.99       | 0.16                     |
| A18-LSLS+ | A    | 18               | LSLS+ | 18.83          | 0.27               | 4.54       | 0.25                     |
| A18-CLS   | A    | 18               | CLS   | 21.37          | 0.31               | 5.16       | 0.28                     |
| A30-LSLS  | A    | 30               | LSLS  | <b>14.92</b>   | 0.21               | 3.06       | 0.15                     |
| A30-LSLS+ | A    | 30               | LSLS+ | <b>23.39</b>   | 0.34               | 4.69       | 0.24                     |
| A30-CLS   | A    | 30               | CLS   | <b>26.29</b>   | 0.38               | 5.21       | 0.26                     |
| B18-LSLS  | B    | 18               | LSLS  | 12.21          | 0.18               | 2.99       | 0.16                     |
| B18-LSLS+ | B    | 18               | LSLS+ | 18.61          | 0.27               | 4.48       | 0.24                     |
| B18-CLS   | B    | 18               | CLS   | 21.41          | 0.31               | 5.16       | 0.28                     |
| B30-LSLS  | B    | 30               | LSLS  | <b>14.93</b>   | 0.21               | 3.07       | 0.15                     |
| B30-LSLS+ | B    | 30               | LSLS+ | <b>23.28</b>   | 0.33               | 4.64       | 0.23                     |
| B30-CLS   | B    | 30               | CLS   | <b>26.05</b>   | 0.37               | 5.14       | 0.26                     |



Where:  $d_{TOP}$  is the maximum top displacement;  $\delta_{TOP}$  is the maximum drift;  $d_v$  is the vertical component of the retrofit displacement at the existing building floor level;  $\sigma_{MAX,bar}/f_y$  the stress rate in the steel bars.

The structure top drifts obtained in the non-linear time history analyses are plotted in Figure IX.18. The drift design target (0.25%) and the collapse limit target (0.40%) are satisfied at the design (LSLS) and collapse limit state (CLS) earthquakes, respectively. As for the LSLS (in which the walls behave elastically), a similar trend can be observed for both the cases with 18mm and 30mm bars. In these cases, Mesh C showed a higher displacement with respect to meshes B and A: the result may be associated to a higher acceleration associated to the mesh C (elastic period equal to about 0.37 s) which is stiffer than the meshes A and B (elastic period equal to about 0.40 s). When the non-linear range is reached (i.e., in the cases LSLS+ and CLS), Mesh C exhibits a lower maximum displacement; this may be associated with a higher energy dissipation enabled by the coupler's activation (Figure IX.21).

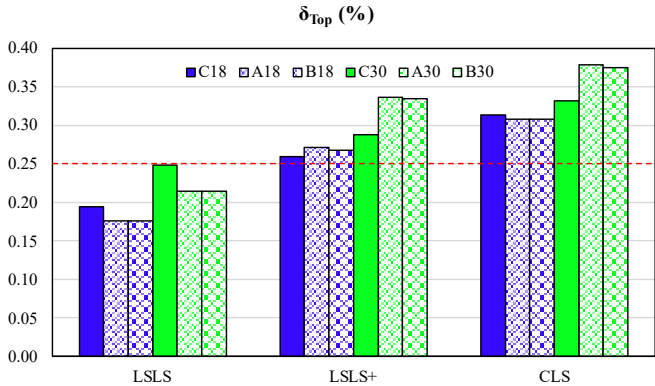


Figure IX.18 – Top drift over time for each analysed cases.

In Case A30-LSLS, set as the reference case, a maximum top displacement of 14.92 mm was recorded, corresponding to a 0.21% drift (lower than the drift target equal to 0.25%); the top displacement increases by 57% in case of an extraordinary seismic event (A-LSLS+), and by 77% in case of A-CLS ground motion, however, remaining quite low. In the analyses performed on Mesh B, a similar trend can be observed. The maximum displacement slightly reduces with respect to Mesh A as a result of the higher stiffness of Mesh B: despite the mass of Mesh B being double that of Mesh A, by coupling the two coupled walls, the overall stiffness more than doubles. In Mesh C, in the case of shorter bars (C-LSLS), the maximum top displacement increases by about 21% for the reasons previously discussed.

No residual displacement is recorded past the seismic event for Meshes A and B while Mesh C shows residual displacement equal to about 0.2 mm at the CLS which can be considered negligible for the reference case. Such a result is respectful of the “design for reparability” LCT principle and proves the recentring capacity of all systems, also in the case of shorter bars.

Further parametric analyses are being made to better evaluate the amount of residual displacement for different ground motions, wall layouts, and design targets.

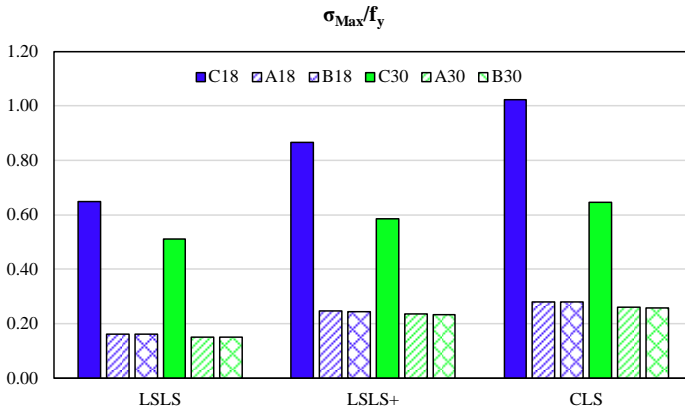


Figure IX.19 – Stress ratio of the vertical bars (fy=640 MPa).

To evaluate the compliance with the performance objectives for each considered scenario, the possible yielding of the bars was controlled. The maximum stress rate (maximum stress over the yielding stress  $f_y$  equal to 640 MPa) recorded in the bars is plotted in Figure IX.19. As can be observed the higher values are plotted in the cases of short bars (Mesh C); the result may be associated to a higher axial stiffness of such bars. Only in Mesh C at the CLS an external bar reaches the yielding value (stress rate equal to 1).

In Figure IX.20 the maximum vertical displacements recorded at the wall edges for each GM are plotted. Results show quite relevant vertical displacements. The vertical displacement is lower when short bars are adopted; the higher stiffness of short bars allow for lower vertical displacement of the walls. It is worth noting that the higher top displacement (i.e., higher drift) recorded at the LSLS for the cases C18 and C30 may be associated to a higher non-linear deformation at the wood panel base. In such cases the non-linear compression is about 1.5 times

that recorded in Meshes A and B. Based on these results, vertical tolerances should be added in the retrofit-to-existing building connections at the floor level, or the connections should be better located at the intersection of the floor level and the retrofit centroid axis.

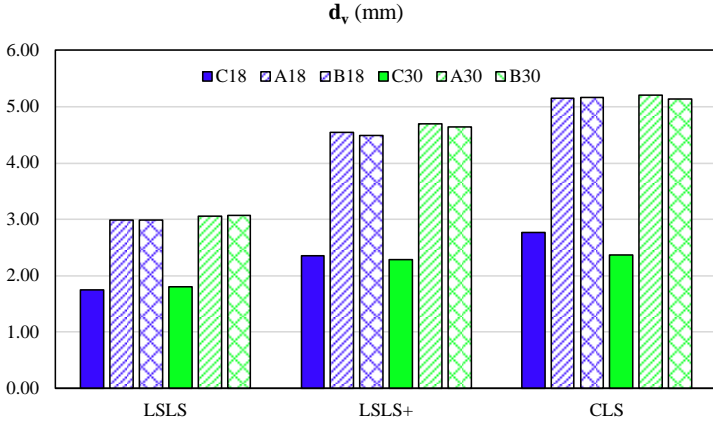


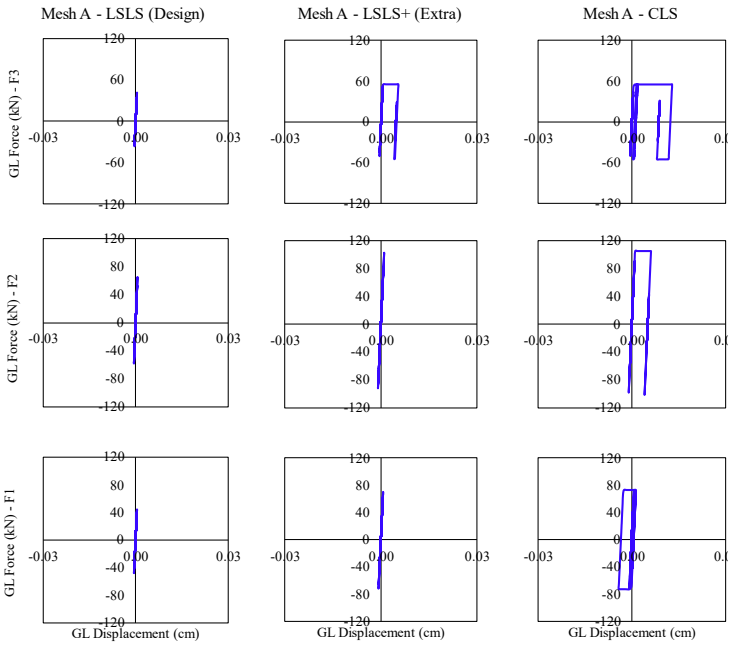
Figure IX.20 – Maximum vertical displacement recorded at the wall edges for each GM. Solid, ANSI31 and ANSI37 hatches indicate Meshes C, A, and B, respectively.

The force-displacement curves of the general links modelling the couplers are reported in Figure IX.21 (a) for Mesh A and in Figure IX.21 (b) for Mesh B and C. As expected, in Mesh A, all couplers remain elastic up to the design limit state (A - LSLS), while the third-floor coupler exhibit nonlinear behaviour when the ground motion slightly exceeds the design actions. All the couplers behave nonlinearly at the Collapse Limit State and dissipate energy. A similar trend can be observed for Mesh B when long bars are introduced. When short bars are considered in Mesh C (C - LSLS+), couplers behave nonlinearly also at the design limit state. In all cases, larger

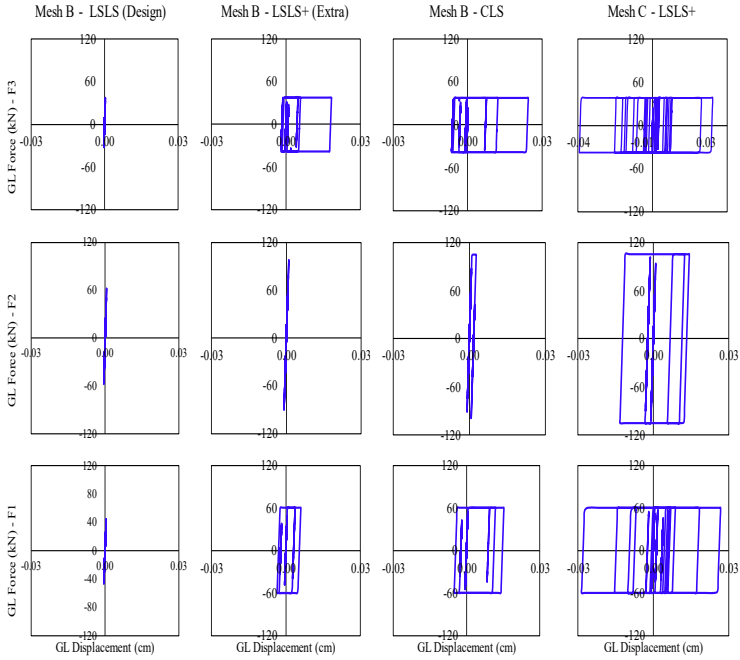
deformations accumulate in the couplers at the upper floor, as a result of the vibration mode of the coupled walls.

At foundation level, the shear loads can be transferred by means of shear keys, while the total resisting moment can be balanced through a couple of axial forces, where tensile actions are resisted by micropiles. In this case, it should be noted that coupled walls (Meshes B, and C) can benefit from a much greater lever arm than in the case of Mesh A, allowing a significant force reduction.

Based on the results it can be observed that a mindful evaluation of the structural details and technological aspects may play a fundamental role in the retrofit design.



a)



b)

Figure IX.21 – Non-linear deformation of the couplers at different floors (row) for different limit state (columns): a) for Mesh A, and b) for Mesh B and C.

Additional details are reported in .

## 9.7. Lessons learned and research needs

The completion of the intervention took approximately 6 months; the installation of the coupled shear walls and the connection of the timber panels to the existing building took about 150 days with a team of 3 people and a light crane. The renovation construction cost, including the energy amelioration measures (thermal coating and new distributive plant system) and the structural shell, architectural finishes, construction site costs, preliminary works, contingencies, VAT and excluding technical costs, was approximately 490 €/m<sup>2</sup> of shell surface area (total shell surface of about 600 m<sup>2</sup>). The cost breaks shows: 42% of the total cost associated with the structural retrofit, about 22% with energy amelioration measures and finishes, and 36% with other construction expenses.

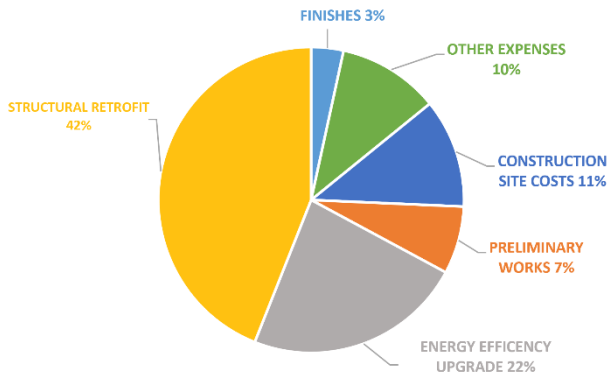


Figure IX.22 – Synthetic construction cost back down. Other expenses includes construction site costs, preliminarily works, contingencies, VAT and excluding technical costs.

The application of the analysed retrofit systems to a real building highlighted their major advantages, unveiled various construction and implementation limitations, as well as highlighted major research needs.



As mentioned in Chapter VIII, the partial re-engineering of the connections of the CLT panels to the foundations was needed to simplify installation, as well as to enhance structural performances. Several experimental tests [242] [243] demonstrated the criticalities associated with the connection of the steel base plate to the CLT panel using nails. The potential presence of hole-nail gaps, and the lack of contact between the panel and the base plate were shown to affect the behaviour of the retrofit system by reducing its stiffness. Connections of the exoskeleton to the existing building were also shown to require further engineering in order to better adapt to possible tolerances during constructions. For the extensive applications of these structural system more research on the connections is thus required.

In the construction stage, major advantages of the adoption of CLT based retrofit solution with respect to other construction technologies were observed. The exoskeleton was entirely prefabricated and partly assembled off-site, substantially reducing the assembly process and the construction time, with minimum disruption of the building functions. Through mindful proportioning of the components, particularly regarding the dimension for the panels, a light crane was sufficient to move the elements within the construction site, with major advantages in terms of construction time and costs. The wooden panels were easily adapted with simple construction site operations, such as manual carving sawing or drilling, to adapt to unforeseen peculiarities (such as unexpected small construction tolerances, or plant interferences).

The CLT exoskeleton was easily coupled on-site with the energy amelioration measures, such as the thermal insulation coating layers and the new external plant system. The great advantages of the CLT solutions, as opposed for example to

steel braced shear walls, are that they do not introduce thermal bridges, thanks to the remarkable insulation properties of the wooden panels, and they do offer a clean and even surface onto which insulation panels can be easily fixed. The pre-installation of thermal insulating elements on the CLT panels may reduce construction time even further.

With respect to adaptivity to future use of the building, wooden exoskeleton, particularly in the case of the shell exoskeletons extending over the building façades, can be easily complemented with plug-in modules attached to the structures, hosting new small living spaces or technical rooms. As for the end-of-life stage, relevant reduction of the demolition waste can be easily obtained by adopting connections that enable selective dismantling and by partial reuse-recycle of the components.

Concerning the structural retrofit scheme, the design procedure illustrated in Chapter VI was tested for the preliminary proportioning of the solution, as well as to further investigate the structural response for varying some design choices. The procedure was adapted to the particular geometry of the case study. The results of the numerical investigation showed the ability of the structural system to meet the severe performance objectives, appositely selected to account for the particularly brittle behavior associated with the peculiar masonry typology of the existing building, featuring bricks with horizontal holes.

## **X. Concluding remarks**

The ambitious UN and European targets in terms of sustainable development cannot be reached without reducing the substantial impacts associated with the built environment and the construction sector, through systematic renovation of the existing building stock. Despite this urgent need, to date, the renovation rate in the construction sector is very low (1.5%) due to the barriers and drawbacks of traditionally retrofitting strategies.

To overcome the major barriers and effectively renovate the existing building stock, a Life Cycle Thinking (LCT) approach must be addressed for the conceptual design of the renovation action. The LCT perspective emphasizes the need to shift to an integrated holistic renovation approach, addressing the multifaceted needs of the building and conjugating structural retrofit, architectural restyling, and energy efficiency measures.

Structural retrofit solutions must be conceived according to the enlarged concept of Life Cycle Structural Engineering (LCSE), thus considering LCT principles in all design phases together with a multi-criteria performance-based approach. Such an approach triggers a paradigm shift in how engineers would deal with existing building performances and needs, with relevant consequences in terms of operative choices, innovative solution sets, and societal challenges and demands.

In this context, in the last years, innovative retrofit solutions have been developed and studied. Among these, many studies proposed exoskeletons for an integrated renovation of existing buildings. Following the principles and guidelines of the LCT approach, this thesis investigates the potential benefits and limitations presented by the application of exoskeletons,

focusing on solutions that are effectively integrable with energy efficiency and architectural improvement measures. In this study, the performance of adaptive exoskeletons, a novel structural type able to adapt its behaviour as a function of seismic intensity, was specifically investigated, and a design method was proposed. In particular, the retrofitted building behaves elastically up to the design limit state (Life Safety Limit State - LSLS), while it exhibits a nonlinear behaviour beyond that limit thanks to specific and localized couplers located in the additional exoskeleton.

By localizing damage into few specific elements (couplers), the proposed system allows for reparability; while, by adopting a recentering system (post-tensioned bars), it avoids residual displacements. An example of couplers is the *AdESA fuse* was proposed in Chapter VII . These sacrificial elements, which can be easily integrated into the strengthening exoskeletons, may be conceived to behave as elastic couplers up to the design limit state and to exhibit a nonlinear behaviour beyond that limit. This allows for an energy dissipation and a ductile behaviour in case of an extra-ordinary earthquake. Experimental test results revealed the high reliability of these fuses, and the application on the real case study showed their ability to be manufactured and installed without the use of special manlabour.

Considering the limits of application of the solution, the adaptive exoskeleton perfectly suits those existing building characterized by ductile behaviour after the yielding point, while it may require particular attention in the definition of the design targets for those building with limited ductility (such as those discussed in Chapter IX featuring poor quality masonry). On the other hand the solution may be unsuitable for those existing buildings characterized by a brittle behavior; in such cases, adaptive system could only be implemented upon

completion of preliminary corrective interventions aimed at increasing ductility of some portions of the existing structure, and thus at controlling the collapse mechanism.

A design procedure was proposed to enable design professionals to proportion the retrofitting adaptive exoskeleton components based on established performance objectives and related design targets with reference to a simple static models. Parametric numerical analyses were performed to assess the effectiveness of the proportioning procedure, as well as to investigate the relevance of the design parameters, with a view to evaluate the potential benefit offered by adaptive exoskeleton for the retrofit of existing buildings. The parametric numerical analyses also allowed assessing the effectiveness of other exoskeleton configurations, thereby further investigating the relative influence of the adaptive shear wall components and of the design parameters. These preliminary parametric analyses showed that, according to the hypothesis adopted, the post-tension does not significantly affect the results when high diameter bars and/or high drift targets are imposed, and that high post-tension levels may lead to high nonlinear deformation at the wall toes and to the yielding of the post-tensioning bars, resulting in higher residual displacements. It is worth noting that more research is required to further investigate the structural solution and to extend the validity of the obtained results.

In the last two chapters, a critical analysis of two real integrated retrofit interventions was made. The analysis took into account the whole design process, which was carried out also addressing the design procedure presented in this thesis, as well as the construction site management and process, and it allowed to identify some critical issues. Such analysis led to the proposal of a partial re-engineering of some retrofit components, and to the identification of major research needs, especially aimed at

increasing applicability and feasibility of the proposed retrofit solution.

Among other, the critical analysis highlighted the need to deepen the study of the connection system. The first issue was connected to the tolerances of the connecting system, by far the most relevant problem to be solved during construction. In addition, the need to satisfy the LCT principles of easy assemblage, reparability or disassembly and replacement after a severe seismic event, and demountability at the end of life, led to a partial re-engineering of the CLT panel-foundation connections to simplify installation and deconstruction. Furthermore, experimental tests highlighted the criticalities associated with the nailed connection of the steel plate to the CLT panel base. The potential presence of hole-nail gaps and the lack of contact between the panel base and the steel plate were shown to affect the behaviour of the retrofit system by reducing its stiffness. The connections at the panels' base were also modified to take into account this important issue.

As for the case study building presented in Chapter IX, numerical analyses were also carried out, showing that the post-tension bar diameter and the displacement target significantly affect the structural behaviour of the system. In particular, for low displacement targets, post-tension and bar diameters of the system became more relevant in the global behavior evaluation. In this case, indeed, the post-tension allows for a higher control of the maximum drift; however, high stress levels of the post-tension may lead to high nonlinear deformation at the wall toes, which results in high residual displacements.

## References

- [1] S. Matthews, «fib Model Code 2020 and the life-cycle management of existing concrete structures,» fib, workshop online, 2020.
- [2] European Commission, “Piano D’azione Nazionale Sul Green Public Procurement (PANGPP). Criteri Ambientali Minimi per L’affidamento di Servizi di Progettazione e Lavori Per la Nuova Costruzione, Ristrutturazione e Manutenzione di Edifici Pubblici,» *European, commission. The European Construction Sector: A Global*, 2016.
- [3] A. Marini, P. Negro, C. Passoni, P. Riva, E. Romano e F. Taucer, «Technology Options for Earthquake Resistant, Eco-Efficient Buildings,» in *JRC Report EUR 26497 EN.; Report EUR 26497 EN. JRC87425*, Luxembourg, Publications Office of the European, 2014.
- [4] A. Vitali Roscini, O. Rapf e J. Kockat, «On the Way to a CLIMATE-NEUTRAL EUROPE. Contributions from the Building Sector to a,» BPIE Report, Brussels, Belgium, 2020.
- [5] J. Gantner, B. Wittstock, K. Lenz, M. Fischer e K. Sedlbauer, «EeBGuide Guidance Document–Part B: Buildings. Operational Guidance for Life Cycle Assessment Studies of the Energy Efficient Building Initiative,» FRAUNHOFER, 2012.
- [6] A. Belleri e A. Marini, «Does seismic risk affect the environmental impact of existing buildings?,» *Energy Build*, pp. 110, 149–158, 2016.

- [7] L. Freyrie, «Perché la Rigenerazione è necessaria,» MadeExpo, Milano, 2017.
- [8] F. Feroldi, «Sustainable renewal of the post WWII building stock through engineered double skin, allowing for structural retrofit, energy efficiency upgrade, architectural restyling and urban regeneration,» PhD Thesis, University of Brescia, 2014.
- [9] S. MAPI. [Online]. Available: <http://www.studiomapi.it/>. [Consultato il giorno 2022].
- [10] E. Union, «Roadmap 2050».
- [11] A. Caverzan, M. Lamperti Tornaghi e P. Negro, «Proceedings of SAFESUST Workshop: A Roadmap for the Improvement of Earthquake Resistance and Eco-Efficiency of Existing Buildings and Cities,» Publications Office of the European Union, Luxembourg, 2016.
- [12] A. Marini, C. Passoni, B. Belleri, F. Feroldi, M. Preti, M. Metelli, P. Riva, E. Giuriani e G. Plizzari, «Combining seismic retrofit with energy refurbishment for the sustainable renovation of RC buildings: a proof of concept,» *European Journal of Environmental and Civil Engineering*, 2017.
- [13] A. Marini, «Coupling energy refurbishment with structural strengthening in retrofit interventions,» Joint Research Centre, ISPRA, 2015.
- [14] UNEP/SETAC, «Greening the Economy through Life Cycle Thinking,» 2012.
- [15] J. Zanni, S. Cademartori, A. Marini, A. Belleri, C. Passoni, E. Giuriani, P. Riva, B. Angi, G. Brumana e A. Marchetti, «Integrated Deep Renovation of Existing Buildings with Prefabricated Shell Exoskeleton,» vol. Sustainability, 2021.



- [16] A. Marini, C. Passoni e A. Belleri, «Life cycle perspective in RC building integrated renovation,» *Procedia Structural Integrity*, vol. 11, pp. 28-35, 2018.
- [17] P. G. Lab, 2012.
- [18] C. Pan, H. Wang, S. Huang e H. Zhang, The Great East Japan Earthquake and tsunami aftermath: Preliminary assessment of carbon, vol. Tsunami events and lessons learned, Y. Kontar, V. Santiago-Fandino e T. Takahashi, A cura di, Netherlands: Springer, pp. 435-450.
- [19] C. Passoni, A. Marini, A. Belleri e C. Menna, «Redefining the concept of sustainable renovation of buildings: State of the art and an LCT-based design framework,» *Sustainable Cities and Society*, vol. 64, 2021.
- [20] U. Nations, «Transforming our world: The 2030 Agenda for Sustainable Development.,» Resolution adopted by the General Assembly on 25 September 2015, 2015.
- [21] BPIE, «Europe's buildings under the microscope: A country-by-country review of the energy performance of the buildings,» Brussel, 2011.
- [22] P. La Greca e G. Margani, «Seismic and energy renovation measures for sustainable cities: A critical analysis of the Italian scenario,» *Sustainability*, pp. 10, 254, 2018.
- [23] F. P-420, «Engineering Guideline for Incremental Seismic Rehabilitation,» Federal Emergency Management Agency, USA, 2009.
- [24] J. Zanni, S. Labò, C. Passoni, E. Casprini, A. Marini e A. e. A. Belleri, «Incremental integrated holistic rehabilitation: A new concept to boost a deep renovation of existing building

- stock,» in *CESB19 Central Europe Towards Sustainable Building 2019*, 2019.
- [25] E. P. Giuriani e A. Marini, «Wooden roof box structure for the anti-seismic strengthening of historical buildings,» *International Journal of Architectural Heritage*, vol. 2, n. 3, pp. 226-246, 2008.
- [26] E. P. Giuriani, A. Marini e M. Preti, «Thin folded shell for the renewal of existing wooden roofs,» *Journal of Architectural Heritage*, pp. 797-816, 2015.
- [27] C. Passoni, J. Guo, C. Christopoulos, A. Marini e P. Riva, «Design of dissipative and elastic high-strength exoskeleton solutions for sustainable seismic upgrades of existing RC buildings,» *Engineering structures*, n. 221, 2020.
- [28] Ecosism e s.r.l., «Genaile cappotto sismico».
- [29] SismaCoat.
- [30] s. Progetto, Resisto 5.9 il cappotto antisismico.
- [31] s. Wood Beton, «Rhnicros-wall: la corazza per la tua casa,» 2022.
- [32] G. Margani, G. Evola, C. Carola Tardo e E. Marino, «Energy, Seismic, and Architectural Renovation of RC Framed Buildings with Prefabricated Timber Panels,» *Sustainability*, vol. 12, 2020.
- [33] E. Commission e J. R. Centre, «Technology options for earthquake resistant, eco-efficient buildings in Europe: Research needs,» Publications Office of the European Union, European Union, 2014.

- [34] E. Commission, «Mapping Europe's earthquake risk».
- [35] E. CSEM, «Euro-Med Bulletin,» 2013.
- [36] K. Dol e M. Haffner, «Housing Statistics in the European Union 2010,» OTB Research Institute for the Build Environment, Delft University of Technology, Delft, 2010.
- [37] TABULA, «WebTool,» 2022.
- [38] Istat, «14° Censimento generale della popolazione e delle abitazioni,» 2001.
- [39] S. Hak, P. Morandi e G. Magenes, «Damage control of masonry infills in seismic design,» EUCENTRE, IUSS, Pavia, 2013.
- [40] G. Magenes e S. Pampanin, «Seismic response of gravity-load design frames with masonry infills,» 13th World Conference on Earthquake Engineering, Vancouver, 2004.
- [41] P. Ricci, V. Manfredi, F. De Luca e G. Verderame, «6th April 2009 L'Aquila earthquake, Italy: reinforce concrete building performance,» Bulletin of Earthquake Engineering, 2011, pp. 285-305.
- [42] F. Braga, V. Manfredi, A. Masi, A. Salvatori e M. Vona, «Performance of non structural elements in RC buildings during the L'Aquila, 2009 earthquake,» in *Bulletin of Earthquake Engineering*, 2011, pp. 307-324.
- [43] L. Decanini, D. Liberatore, L. Liberatore e L. Sorrentino, «Preliminary report on the 2012, May 20, Emilia Earthquake,» vol. vol.1, 2012.
- [44] G. Magenes, S. Bracchi, F. Graziotti, M. Mandirola, C. Manzini, P. Morandi, M. Palmieri, A. Penna, A. Rosti, M.

- Rota e M. Tondelli, «Preliminary damage survey to masonry structures after the May 2012 Emilia Earthquake,» vol. vol 1, 2012.
- [45] F. 454, «Designing for Earthquakes – A Manual for Architects,» Federal Emergency Management Agency, Washington, D.C., 2006.
- [46] C. Passoni, *Holistic renovation of existing RC buildings: a framework for possible integrated structural interventions*, Brescia: Università degli Studi di Brescia, PhD Thesis, 2016.
- [47] V. Bertero, «An Illustrated Introduction to Earthquake Engineering Principles – Simplicity, Symmetry, and Regularity,» National Information Service for Earthquake Engineering University of California, Berkeley, 1997.
- [48] T. Youd, J. Bardet e J. Bray, «Kocaeli, Turkey, earthquake of August 17, 1999 Reconnaissance Report,» Earthquake spectra, 2000.
- [49] S. C. Huang e M. Skokan, «Collapse of the Tungshing building during the 1999 Chi-Chi earthquake in Taiwan,» Proceedings of 7th U.S. National conference on earthquake engineering, Boston, 2002.
- [50] D. Marriott, S. Pampanin e D. Bull, «Improving the seismic performance of existing reinforced concrete buildings using advanced rocking wall solutions,» in *2007 NZSEE Conference*, 2007.
- [51] A. Giuffrè e C. Carocci, «Statica e dinamica delle costruzioni murarie storiche,» in *Le pietre da costruzione: il tufo calcareo e la pietra leccese*, Bari, 1993.
- [52] A. Marini, B. Belleri, C. Passoni, F. Feroldi e E. Giuriani, «In-plane capacity of existing post-WWII beam-and-clay

- block floor systems,» *Bulletin of Earthquake Engineering*, vol. 20, n. 2, pp. 1655-1682, 2022.
- [53] G. Magenes e G. Calvi, «In-plane seismic response of brick masonry walls,» *Earthquake Engineering & Structural Dynamics*, pp. 1091-1112, 1998.
- [54] C. Casapulla e D. D'Ayala, «In-plane collapse behaviour of masonry walls with frictional resistance and openings,» in *Structural Analysis of historic Construction*, Delhi, India, 2006.
- [55] G. Metelli, C. Beschi e P. Riva, «Cyclic behaviour of a column to foundation joint for concrete precast structures,» *European Journal of Environmental and Civil Engineering*, pp. 1297-1318, 2011.
- [56] G. Industriali, «Linee di indirizzo per interventi locali e globali su edifici industriali monopiano non progettati con criteri antisismici,» Gruppo di Lavoro Agibilità Sismica dei Capannoni, 2012.
- [57] M. Fischinger, M. Kramar e T. Isakovic, «Cyclic response of slender RC columns typical of precast industrial buildings,» *Bulletin of Earthquake Engineering*, pp. 512-534, 2008.
- [58] I. N. Psycharis e H. P. Mouzakis, «Shear resistance of pinned connections of precast members to monotonic and cyclic loading,» *Engineering Structures*, pp. 413-427, 2012.
- [59] D. A. Bournas, P. Negro e F. J. Molina, «Pseudodynamic tests on a full-scale 3-storey precast concrete building: Behavior of the mechanical connections and floor diaphragms,» *Engineering Structures*, 2013.
- [60] A. Belleri, E. Brunesi, R. Nascimbene, M. Pagani e P. Riva, «Seismic performance of precast industrial facilities following

- major earthquakes in the Italian territory,» *Journal of Performance of Constructed Facilities*, vol. 29, n. 5, 2015.
- [61] M. Rodríguez e J. Blandón, «Tests on a half-scale two-story seismic resisting precast concrete building,» *PCI Journal*, pp. 94-114, 2005.
- [62] A. Belleri e P. Riva, «Seismic performance and retrofit of precast grouted sleeve connections,» *PCI Journal*, pp. 97-109, 2012.
- [63] I. N. Psycharis e H. P. Mouzakis, «Assessment of the seismic design of precast frames with pinned connections from shaking table tests,» *Bulletin of Earthquake Engineering*, pp. 1795-1817, 2012.
- [64] A. Belleri, M. Torquati, R. Nascimbene e P. Riva, «Vulnerability assessment and retrofit solutions of precast industrial structures,» *Earthquakes and Structures An International Journal*, vol. 8, pp. 801-820, 2015.
- [65] V. Zanotti, F. Feroldi, A. Marini e E. Giuriani, «Recupero di edifici in c.a. del secondo dopoguerra: studio del comportamento dei solai esistenti in presenza di carichi orizzontali,» Technical Report, DICATAM, Università degli Studi di Brescia, 2014.
- [66] A. Marini, A. Belleri, C. Passoni e F. Feroldi, «In-plane capacity of existing post-WWII beam-and-clay block floor systems,» *Bulletin of Earthquake Engineering*, vol. 20, n. 2, pp. 1655-1683, 2022.
- [67] A. Marini, C. Passoni, P. Riva, P. Negro, E. Romano e F. Taucer, «Technology options for earthquake resistant, eco-efficient buildings in Europe: Research needs,» Publications Office of the European Union, Luxembourg, 2014.

- [68] F. Bulletin, «Seismic assessment and retrofit of rein-forced concrete buildings. State-of-art report,» vol. 24, International Federation for Structural Concrete, 2003.
- [69] M. Engindeniz, L. Kahn e A. Zureick, «Repair and Strengthening of Reinforced Concrete Beam-Column Joints: State of the Art,» *ACI structural journal*, vol. 102, 2005.
- [70] H. Kaplan e S. Yilmaz, *Earthquake-Resistant Structures - Design, Assessment and Rehabilitation*, 2012.
- [71] M. Corazao e A. Durrani, «Repair and Strengthening of Beam to Column Connections Subjected to Earthquake Loading,» Technical Report NCEER-89-0013, Buffalo, 1989.
- [72] A. Ghobarah, T. Aziz e A. Biddah, «Rehabilitation of reinforced concrete frame connections using corrugated steel jacketing,» *ACI Structural*, vol. 4, n. 3, p. 283–294, 1997.
- [73] C. Antonopoulos e T. Triantafillou, «Experimental investigation of FRP strengthened RC beam-column joints,» pp. 39-49, 2003.
- [74] G. Martinola, A. Meda, G. Plizzari e Z. Rinaldi, «An application of high performance fiber reinforced cementitious composites for R/C beams strengthening,» in *proceedings of FRAMCOS 6*, Catania, Italy, 2007.
- [75] C. Beschi, A. Meda e P. Riva, «Column and joint retrofitting with high performance fiber reinforced concrete jacketing,» *Journal of Earthquake Engineering*, vol. 15, n. 7, pp. 989-1014, 2011.
- [76] S. Raza, M. K. I. Khan, S. J. Menegon, H. Tsang e J. Wilson, «Strengthening and Repair of Reinforced Concrete Columns

- by Jacketing: State-of-the-Art Review,» *Sustainability*, n. 11, 2019.
- [77] C. Beschi, P. Riva e A. Meda, «Corner Beam-Column Joints Seismic Retrofitting With High Performance Fiber-Reinforced Concrete Jacketing,» in *Proceedings of 15 WCEE*, Lisbon, 2012.
- [78] F. B. No.24, «Seismic assessment and retrofit of rein-forced concrete buildings. State-of-art report,» *International Federation for Structural Concrete*, August 2003.
- [79] P. Riva, E. Perani e A. Belleri, «External R.C. Structural Walls for the Repair of Earthquake Damaged Buildings,» in *Sustainable Development Strategies for Constructions in Europe and China*, Roma, 2010.
- [80] A. Marini e A. Meda, «Retrofitting of RC shear walls by means of high performance jackets,» *Engineering Structures*, vol. 31, n. 12, pp. 3059-3064, 2009.
- [81] C. Facilitator, «Seismic Retrofitting Techniques for Existing RC buildings,» March 2019. [Online]. Available: <https://www.constrofacilitator.com/seismic-retrofitting-techniques-for-existing-rc-buildings/>.
- [82] S. Calvi. [Online]. Available: <https://www.studiocalvi.eu/it/progetti/progettazione-e-realizzazione/ospedali-mellino-mellini>.
- [83] M. Preti, N. Bettini e G. Plizzari, «Infill walls with sliding joints to limit infill- frame seismic interaction: large-scale experimental test,» *Journal of Earthquake Engineering*, n. 125, pp. 125-141, 2012.
- [84] M. Preti, L. Migliorati e E. Giuriani, «Experimental testing of engineered masonry infill walls for post-earthquake structural



- damage control,» *Bulletin of earthquake Engineering*, vol. 13, n. 7, pp. 2029-2049, 2015.
- [85] R. Langenbach, «From “Opus Craticium” to the “Chicago Frame”»: Earthquake-Resistant Traditional Construction,» *International Journal of Architectural Heritage: Conservation, Analysis and Restoration*, vol. 1, pp. 29-59, 2007.
- [86] M. Preti, V. Bolis e A. Stavridis, «Design of masonry infill walls with sliding joints for earthquake structural».
- [87] C. Christopoulos e A. Filiatrault, *Principles of Passive Supplemental Damping and Seismic Isolation*, Pavia: IUSS Press, 2006.
- [88] T. Soong e B. Spencer, «Supplemental energy dissipation: state-of-the-art and state- of-the practice,» *Engineering Structures*, 2002.
- [89] «ISAAC antisismica,» [Online]. Available: <https://isaacantisismica.com>. [Consultato il giorno September 2022].
- [90] G. Housner, L. Bergman, T. Caughey, A. Chassiakos, R. Claus, S. Masri, R. Skelton, T. Soong, B. Spencer e T. Yao, «Structural control: past, present, and future,» *ASCE*, vol. 9, n. 123, pp. 897-971, 1997.
- [91] «UNI EN 15129:2018».
- [92] I. Aiken, «Energy Dissipation Devices,» in *8NCEE*, 2006.
- [93] «Fip Mec,» [Online]. Available: <https://www.fipmec.it/en/products/anti-seismic-devices/>.

- [94] T. Trombetti e S. Silvestri, «Novel schemes for inserting dampers in shear-type systems based upon the mass proportional component of the Rayleigh damping matrix,» *Journal of Sound and Vibration*, vol. 3, n. 302, pp. 486-526, 2007.
- [95] H. Roh, G. Cimellaro e D. Lopez Garcia, «Seismic response of adjacent steel structures connected by passive device,» *Advances in Structural Engineering*, vol. 31, n. 14, pp. 499-517, 2011.
- [96] S. Labò, *Diagrid exoskeletons for the retrofit of RC buildings: Holistic sustainable solutions to renovate Post World War II RC buildings In a Life-Cycle Perspective*. Supervisor A. Marini., Bergamo: PhD thesis, University of Bergamo, 2021.
- [97] V. Ciampi, M. DeAngelis e F. Paolacci, «Design of yielding or friction-based dissipative bracings for seismic protection of buildings,» *Engineering Structures*, 175): 381-391, 1995., n. 175, pp. 381-391, 1995..
- [98] A. Benavent-Climen, «An energy-based method for seismic retrofit of existing frames using hysteretic dampers,» *Soil Dynamics and Earthquakes Engineering*, Vol. %1 di %231:1385-1396, 2011. , n. 31, pp. 1385-1396, 2011.
- [99] G. De Matteis, A. Formisano e F. Mazzolani, «An innovative methodology for seismic retrofitting of existing RC buildings by metal shear panels,» *Earthquake Engineering and Structural dynamics*, vol. 38, pp. 61-78, 2009.
- [100] D. Vian e M. Bruneau, «Steel Plate Shear Walls for Seismic Design and Retrofit of Building Structures,» Technical Report MCEER-05-0010, Buffalo, NY, 2005.

- [101] G. De Matteis, R. Landolfo e F. Mazzolani, «Seismic response of MR steel frames with low-yield steel shear panels,» *Engineering Structures*, vol. 25, pp. 155-168, 2003.
- [102] A. Giuffrè, *Sicurezza e conservazione dei centri storici in area sismica, il caso Ortigia*, Bari: Laterza, 1993.
- [103] A. Giuffrè e C. Carocci, *Codice di Pratica per la sicurezza e la conservazione del centro storico di Palermo*, Bari: Laterza, 1999.
- [104] E. Giuriani, *Consolidamento degli edifici storici*, Torino: UTET, pp. 350-351.
- [105] C. Modena, L. Binda e A. Anzani, «Investigation for the Design and Control of the Repair Intervention on Historical Stone Masonry Wall,» in *VII International Conference and Exhibition*, Edinburgh, 1997.
- [106] L. Binda, C. Modena, G. Baronio e S. Abbaneo, «Repair and investigation techniques for stone masonry walls,» in *Construction and Building Materials*, vol. 11, 1997, pp. 133-142.
- [107] L. Alexandros, S. Kouris, C. Thanasis e C. Triantafillou, «State-of-the-art on strengthening of masonry structures with textile reinforced mortar (TRM),» *Construction and building materials*, pp. 1221-1233, 2018.
- [108] L. Facconi, A. Conforti, F. Minelli e G. Plizzari, «Improving shear strength of unreinforced masonry walls by nano-reinforced fibrous mortar coating,» *Materials and Structures*, pp. 2557-2547, 2015.
- [109] M. Devaux e D. Redaelli, «Seismic retrofitting of masonry walls with thin UHPFRC layers,» 2016.

- [110] D. D'Ayala e E. Speranza, «Definition of collapse mechanisms and seismic vulnerability of historic masonry buildings,» *Earthquake Spectra*, Vol. %1 di %2D' Ayala D., Speranza E, n. 19, pp. 479-509, 2003.
- [111] V. Turnsek, S. Terceelj, P. Sheppard e M. Tomazevic, «The seismic resistance of masonry walls and buildings,» in *6th European conference on earthquake engineering*, Dubrovnik, 1978.
- [112] D. D'Ayala e E. Speranza, «An integrated procedure for the assessment of seismic vulnerability of historic buildings,» in *12th European conference on earthquake engineering*, London, 2002.
- [113] E. Giuriani e A. Marini, «Experiences from the Northern Italy 2004 earthquake: vulnerability assessment and strengthening of historic churches,» in *VI international conference on structural analysis of historical constructions SAHC 2008*, Bath, England, 2008.
- [114] M. Busselli, D. Cassol, A. Prada e I. Giongo, «Timber Based Integrated Techniques to Improve Energy Efficiency and Seismic Behaviour of Existing Masonry Buildings,» *MDPI Sustainability*, vol. 13, n. 10379, 2021.
- [115] D. Dizhur, M. Giaretton, I. Giongo e J. Ingham, «Seismic retrofit of masonry walls using timber strong-backs,» *SESOC Journal*, vol. 30, n. 2, 2017.
- [116] F. Smioldo, I. Paviani, I. Giongo, S. Zanon, R. Albatichi e M. Piazza, «An Integrated Approach to Improve Seismic and Energetic Behaviour of RC Framed Buildings Using Timber Panels,» *MDPI Sustainability*, vol. 13, n. 11304, 2021.
- [117] M. Indirli, M. Castellano, P. Clemente e A. Martelli, «Demo-application of Shape Memory Alloy devices: the

rehabilitation of the S. Giorgio Church Bell-Tower.»  
*Proceedings of SPIE*, 2001.

- [118] S. Pampin, «Controversial aspects in seismic assessment and retrofit of structures in modern times: understanding and implementing lessons from ancient heritage,» *BULLETIN OF THE NEW ZEALAND SOCIETY FOR EARTHQUAKE ENGINEERING*, vol. 39, n. 2, 2006.
- [119] S. Cademartori, A. Marini, A. Belleri e P. Riva, «Strengthening techniques for masonry buildings,» JRC Report, 2020.
- [120] M. Tomazevic, «Some aspects of structural strengthening of historic buildings in urban and rural nuclei against earthquakes,» *European Earthquake engineering*, n. 1, pp. 19-40, 1989.
- [121] D. D'Ayala, «Conservation principles and performance based strengthening of heritage buildings in post-event reconstruction,» *Geotechnical Geological Earthquake Engineering*, pp. 489-514, 2014.
- [122] A. Marini, E. Giuriani, A. Belleri e S. Cominelli, «Dowel connections securing roof-diaphragms to perimeter walls in historic masonry buildings and in-field testing for capacity assessment,» *Bulletin of Earthquake Engineering*, 2018.
- [123] E. Giuriani, Consolidamento degli edifici storici, Torino: UTET, 171-184.
- [124] P. Gelfi, E. Giuriani e A. Marini, «Stud shear connection design for composite concrete slab and wood beams,» *ASCE Journal of Structural Engineering*, n. 128, pp. 1544-1550, 2002.

- [125] P. Civile, Reluis, C. N. d. Ingegneri e ASSOBETON, «Linee di indirizzo per interventi locali e globali su edifici industriali monopiano non progettati con criteri antisismiciI,» 2012.
- [126] E. E. Agency, «Building renovation: where circular economy and climate meet,» 2022.
- [127] R. Castro e S. Denissof, [Re]modeler, M.tamorphoser, Paris: Le Moniteur, 2005.
- [128] M. Montuori, B. Angi e M. Botti, «EUTOPIA URABNA: la manutenzione ragionata dell'edilizia sociale,» in *Abitare il nuovo/abitare di nuovo ai tempi della crisi*, Napoli, CLEAN Edizioni, 2012.
- [129] V. van Altna, J. Meijboom e W. Tiessens, *The Image Project: New Tools for Neighbourhood Regeneration*, Delft: City of Delft, 2007.
- [130] B. Government, «Housing and Regeneration Act 2008,» [legislation.gov.uk](http://legislation.gov.uk), United Kingdom, 2008.
- [131] D. Czischke, «Urban Regeneration in Europe: The place of social housing in integrated urban policies,» CECODHAS Housing Europe, Bruxelles, 2009.
- [132] A. Masbouni, *Régénérer les grands ensembles*, Paris: Editions de la Villette, 2005.
- [133] R. Kronenburg, *Flexible: Architecture That Responds to Change*, London: Laurence King Publishing, 2007.
- [134] E. Zambelli, «Ristrutturazione e trasformazione del costruito,» *Il Sole 24 Ore*, Milano, 2004.
- [135] L. & Vassal, «Transformation de la Tour Bois le Prêtre,» 2011. [Online]. Available:

<http://www.lacatonvassal.com/?idp=56#>. [Consultato il giorno september 2022].

- [136] R. Di Giulio, «Sustainable roof-top extension: a pilot project in Florence (Italy),» in *International Conference Portugal SB10 - Sustainable Building Affordable to All*, Algarve (Portugal), 2010.
- [137] T. Takeuchi, K. Yasuda e M. Iwata, «Seismic Retrofitting using Energy Dissipation Facades,» in *ATC & SEI 2009 Conference on Improving the Seismic Performance of Existing Buildings and Other Structures*, San Francisco, 2009.
- [138] A. Soci e e. Al., «Relazione specialistica del progetto architettonico,» Brescia, 2019.
- [139] E. Commission, «Level(s): A guide to Europe’s new reporting framework for sustainable buildings.,» Produced with the support of Europe Regional Network – World Green Building Council, 2020.
- [140] L. Bragança, H. Koukkari, R. Landolfo, V. Ungureanu, E. Vesikari e O. Hechler, «Sustainability of Constructions— Summary Report of the Cooperative Activities of COST Action C25,» Tarxien, Malta, 2011., 2011..
- [141] M. d. I. e. d. Trasporti, DECRETO 17 gennaio 2018. Aggiornamento delle «Norme tecniche per le costruzioni», Roma: Gazzetta Ufficiale della Repubblica Italiana, 2018.
- [142] S. Pampanin, «Towards the practical implemetation of performance-based assessment and retrofit strategies for RC buildings. challenges and solutions.,» in *SMAR 2017 - Fourth Conference on Smart Monitoring, Assessment and Rehabilitation of Civil Structures*, Zurich, 2017.

- [143] S. V. 2. Committee, «Performance-based seismic engineering,» Association of California, Sacramento, 1995.
- [144] C. Passoni, S. Labò, A. Marini, A. Belleri e P. Riva, «Renovating the existing building stock: a Life Cycle Thinking Design Approach,» in *16th European Conference on Earthquake Engineering*, Thessaloniki, 2018.
- [145] G. Calvi, G. O'Reilly e G. Andreotti, «Towards a practical loss-based design approach and procedure,» *Earthquake Engineering & Structural Dynamics*, pp. 1-13, 2021.
- [146] C. Menna, L. Felicioni, P. Negro, A. Lupíšek, E. Romano, A. Prota e P. Hájek, «Review of methods for the combined assessment of seismic resilience and energy efficiency towards sustainable retrofitting of existing European buildings,» *Sustainable Cities and Society*, n. 77, 2022.
- [147] C. Passoni, M. Caruso, R. Pinho e R. Landolfo, «The Role of Life Cycle Structural Engineering in the Transition towards a Sustainable Building Renovation: Available Tools and Research Needs,» *Buildings*, vol. 12, n. 8, 2022.
- [148] W. Kam, S. Pampanin e D. Bull, «Selective weakening retrofit for existing R.C. structures - concept, validation and design example,» in *9th US National and 10th Canadian Conference on Earthquake Engineering: Reaching Beyond Borders*, Toronto, Canada, 2010.
- [149] G. Di Lorenzo, E. Colacurcio, A. Di Filippo, A. Formisano, A. Massimilla e R. Landolfo, «State-of-the-art on steel exoskeletons for seismic retrofit of existing RC building,» *International Journal of Earthquake Engineering*, 2020.



- [150] A. Marini, A. Belleri, C. Passoni, P. Riva e e. Al., «Coupling energy refurbishment with structural strengthening in retrofit interventions,» Joint Research Centre, ISPRA, 2015.
- [151] (JBDPA), «Standards for evaluation of seismic capacity and guidelines for seismic rehabilitation of existing reinforced concrete buildings,» 1977.
- [152] S. Labò, C. Passoni, A. Marini, A. Belleri, G. Camata, R. Riva e E. Spacone, «Diagrid solutions for a sustainable seismic, energy, and architectural upgrade of European RC buildings,» in *Proceedings of the XII International Conference on Structural Repair and Rehabilitation*, Porto, Portugal, 2016.
- [153] S. Labò, C. Passoni, A. Marini, A. Belleri, G. Camata, P. Riva e E. Spacone, «Prefabricated responsive diagrids for holistic renovation of existing mid-rise RC buildings,» in *COMPADYN 2017*, Rhodes Island, Greece, 2017.
- [154] 15129:2018, UNI EN.
- [155] F. P-2082, «NEHRP Recommended Seismic Provisions For New Buildings And Other Structures,» 2020.
- [156] S. Labò, C. Passoni, A. Marini e e. Al., «Design spectra for the preliminary design of elastic seismic retrofit solution from the outside,» in *COMPADYN 2019 - 7th ECCOMAS Thematic Conference on Computational Methods in Structural Dynamics and Earthquake Engineering*, Crete, Greece, 2019.
- [157] S. Labò, C. Passoni, C. Passoni, A. Marini e A. Belleri, «Design of diagrid exoskeletons for the retrofit of existing RC buildings,» *Engineering Structures*, n. 220, 2020.

- [158] R. C. G. M. Loonen, «Bio-inspired adaptive building skins,» in *Biotechnologies and Biomimetics for Civil Engineering*, Springer International Publishing, 2015, p. 115–134.
- [159] G. Granello, A. Palermo, S. Pampanin e S. ., v. d. L. J. Pei, «Pres-Lam Buildings: State-of-the-Art,» *Journal of Structural Engineering*, vol. 146, n. 6, 2020.
- [160] A. Barbosa, L. Rodrigues, A. Sinha, C. Higgins, R. Zimmerman, S. Breneman, S. Pei, J. van de Lindt, J. Berman e E. McDonnell, «Shake-Table Experimental Testing and Performance of Topped and Untopped Cross-Laminated Timber Diaphragms,» *Journal of Structural Engineering*, 2021.
- [161] H. Blomgren, S. Pei, Z. Zhibin Jin, J. Powers, J. Dolan, J. van de Lindt, A. Barbosa e D. Huang, «Full-Scale Shake Table Testing of Cross-Laminated Timber,» *Journal of Structural Engineering*, 2019.
- [162] M. Priestley, «Overview of the PRESSS research program,» vol. 36, n. 4, p. 50–57, 1991.
- [163] M. Priestley, S. Sritharan, J. Conley e S. Pampanin, «Preliminary results and conclusions from the PRESSS five-story precast concrete test building,» vol. 44, p. 42–67, 1999.
- [164] S. Pampanin, «Towards the “Ultimate Earthquake-Proof” Building: Development of an Integrated Low-Damage System,» in *Perspectives on European Earthquake Engineering and Seismology*, Atilla Ansal, 2014.
- [165] D. Marriott, S. Pampanin, B. D. e A. Palermo, «Dynamic testing of precast, post-tensioned rocking wall systems with alternative dissipating solutions,» *Bulletin of New Zealand*

*Society for Earthquake Engineering*, vol. 41, n. 2, p. 90–103, 2008.

- [166] D. Marriott, S. Pampanin e A. Palermo, «Quasi-static and pseudo-dynamic testing of unbonded post-tensioned rocking bridge piers with external replaceable dissipaters,» *Earthquake Engineering & Structural Dynamics*, vol. 38, n. 3, pp. 331-354, 2009.
- [167] J. Stanton, W. Stone e G. Cheok, «A hybrid reinforced precast frame for seismic regions,» *Precast/Prestressed Concrete Institute*, vol. 42, n. 2, pp. 20-32, 1997.
- [168] S. Sriharan, S. Aaleti, R. Henry, L. Kuang-Yen e T. Keh-Chyuan, «Precast concrete wall with end columns (PreWEC) for earthquake resistant design,» *Earthquake Engineering & Structural Dynamics*, vol. 44, pp. 2075-2092, 2015.
- [169] A. Palermo, S. Pampanin, A. Buchanan e M. Newcombe, «Seismic design of multi-storey buildings using Laminated Veneer Lumber (LVL),» in *Proceedings of New Zealand Society for Earthquake Engineering conference*, Wairakei, 2005.
- [170] A. Iqbal, S. Pampanin, A. Palermo e A. Buchanan, «Performance and design of LVL walls coupled with UFP dissipaters,» *Journal of Earthquake Engineering*, vol. 19, n. 3, pp. 383-409, 2015.
- [171] A. Iqbal, T. Smith, S. Pampanin, M. Fragiacommo, A. Palermo e A. Buchanan, «Experimental performance and structural analysis of plywood-coupled LVL walls,» *Journal of Earthquake Engineering*, vol. 142, n. 2, 2015.
- [172] L. Wiebe, C. Christopoulos e S. Pampanin, «Seismic response of self-centering base-rocking steel structures,» in *Ninth*

*Canadian Conference on Earthquake Engineering Ottawa*,  
Ottawa, Canada, 2007.

- [173] M. Eatherton, X. Ma, H. Krawinkler, D. Mar, S. Billington, J. Hajjar e G. G. Deierlein, «Design Concepts for Controlled Rocking of Self-Centering Steel-Braced Frames,» *Journal of Structural Engineering*, 2014.
- [174] N. 2006, «Appendix B: special provisions for the seismic design of ductile jointed precast concrete structural systems,» Concrete Standards, Wellington, New Zealand, 2006.
- [175] K. Kordani, «Estimation of seismic demand in post-tensioned rocking systems,» in *Pacific Conference on Earthquake Engineering 2019 i*, Auckland, 2019.
- [176] W. Kam, S. Pampanin, A. Palermo e A. Carr, «Self-centering structural systems with combination of hysteretic and viscous energy dissipations,» *Earthquake Engineering and Structural Dynamics*, n. 39, p. 1083–1108, 2010.
- [177] FEMA, «Recommended Future Issues and Research Needs: Identified During the Development of the 2020 NEHRP Recommended Seismic Provisions for New Buildings and Other Structures,» 2021.
- [178] M. Eatherton e J. Hajjar, «Hybrid simulation testing of a self-centering rocking steel braced frame system,» *Earthquake Engineering and Structural Dynamics*, vol. 43, p. 1725–1742, 2014.
- [179] G. Mavroeidis e A. Papageorgiou, «A mathematical representation of near-fault ground motions,» *Bulletin of the Seismological Society of America*, vol. 93, n. 3, p. 1099–1131, 2003.

- [180] B. Alavi e H. Krawinkler, «Behavior of moment-resisting frame structures subjected to near-fault ground motions,» *Earthquake Engineering and Structural Dynamics*, vol. 33, n. 6, pp. 687-706, 2004.
- [181] E. Kalkan e S. Kunnath, «Effects of fling step and forward directivity on seismic response of buildings,» *Earthquake Spectra*, vol. 22, n. 2, pp. 367-390, 2006.
- [182] M. Newcombe, D. D. Marriott, W. Kam, S. Pampanin e A. Buchanan, «Design of UFP-coupled post-tensioned timber shear walls,» in *Ninth Pacific Conference on Earthquake Engineering Building an Earthquake-Resilient Society*, Auckland, New Zealand, 2011.
- [183] A. Sandoli, M. Pinto, S. Pampanin e B. Calderoni, «Protezione sismica di edifici esistenti in c.a. mediante l'utilizzo di pareti lignee post-tese,» in *ANIDIS*, Pistoia, Italia, 2017.
- [184] M. Priestley, G. Calvi e M. Kowalsky, «Direct displacement-based design of structures. Proceedings of NZSEE Conference. New Zealand.,» in *NZSEE Conference*, New Zealand, 2007.
- [185] S. Cademartori, J. Zanni e A. Marini, «Report sull'edilizia residenziale di proprietà di ALER sita nell'ex Zona 2 delle province Brescia e Mantova,» 2019.
- [186] D. s.r.l., «Riquilificazione integrata strutturale, energetica ed architettonica,» 2022.
- [187] M. Jeleč, D. Varevac e V. Rajčić, «Cross-laminated timber (CLT) – a state of the art report,» *Gradevinar*, 2018.
- [188] T. Bogensperger, T. Thomas Moosbrugger e G. Silly, «Verification of CLT-plates under loads in plane,» in *World*

*Conference on Timber Engineering*, Riva del Garda, Italy, 2010.

- [189] Dywidag, «Gewi bars catalog,» [Online]. Available: <https://dywidag.com/technologies/reinforcement>. [Consultato il giorno 2022].
- [190] N. M. Newmark, C. P. Siess e I. M. Viest, «Tests and Analysis of Composite Beams with Incomplete Interaction,» *Proc. Society for Experimental Stress Analysis*, vol. 9, n. 1, 1951.
- [191] J. Kelly, R. Skinner e A. Heine, «Mechanisms of energy absorption in special devices for use in earthquake resistant structures,» *Bulletin of New Zealand Society for Earthquake Engineering*, vol. 5, n. 3, 1972.
- [192] D. Moroder, T. Smith, A. Dunbar, S. Pampanin e A. Buchanan, «Seismic testing of post-tensioned Pres-Lam core walls using cross laminated timber,» *Engineering Structures*, vol. 167, pp. 639-654, 2018.
- [193] L. Pozza, L. Benedetti, V. Tomei, B. Ferracuti, M. Zucconi e C. Mazzotti, «Cyclic response of CLT Post-Tensioned Walls: Experimental and numerical investigation,» *Construction and Building Materials*, vol. 38, 2021.
- [194] M. Structure, *midas Gen 2022*, 2022.
- [195] Z. Xu, A. Agrawal, W.-L. He e P. Tan, «Performance of passive energy dissipation systems during near-field ground motion type pulses,» *Engineering Structures*, vol. 29, n. 2, p. 224–236, 2007.
- [196] K. Yamamoto, K. Fujita e I. Takewaki, «Instantaneous earthquake input energy and sensitivity in base-isolated

building,» *The Structural Design of Tall and Special Buildings*, vol. 20, n. 6, p. 631–648, 2011.

- [197] D. Vafaei e R. Eskandari, «Seismic response of mega buckling-restrained braces subjected to fling-step and forward-directivity near-fault ground motions,» *The Structural Design of Tall and Special Buildings*, vol. 24, n. 9, p. 672–686, 2015.
- [198] Y. Ping, C. Cheng Fang, Y. Chen e M. Yam, «Seismic robustness of self-centering braced frames suffering tendon failure,» *Earthquake Engineering & Structural Dynamics*, vol. 50, n. 3, 2021.
- [199] E. Dimitrakopoulos e T. Paraskeva, «Dimensionless fragility curves for rocking response to near-fault excitations,» *Earthquake engineering & structural dynamics*, vol. 44, n. 12, pp. 2015–2033, 2015.
- [200] V. Bertero, S. Mahin e R. Herrera, «Seismic design implications of near-fault San Fernando earthquake records,» *Earthquake Engineering & Structural Dynamics*, vol. 6, n. 1, pp. 31–42, 1978.
- [201] J. Hall, T. Heaton, M. Halling e D. Wald, «Near-source ground motion and its effects on flexible buildings,» *Earthquake Spectra*, vol. 11, n. 4, p. 569–605, 1995.
- [202] M. Sasani e V. Bertero, «Importance of severe pulse-type ground motions in performance-based engineering: historical and critical review,» in *Twelfth World Conference on Earthquake Engineering*, Auckland, New Zealand, 2000.
- [203] N. Makris e C. Black, «Dimensional analysis of rigid-plastic and elastoplastic structures under pulse-type excitations,»

- Journal of Engineering Mechanics*, vol. 130, n. 9, p. 1006–1018, 2004.
- [204] K. Kojima e I. Takewaki, «Critical earthquake response of elastic-plastic structures under near-fault ground motions,» *Frontiers in Built Environment*, vol. 1, n. 12 -13, 2015.
- [205] G. Mavroeidis, G. Dong e A. Papageorgiou, «Near-fault ground motions, and the response of elastic and inelastic single-degree-freedom (SDOF) systems,» *Earthquake Engineering & Structural Dynamics*, vol. 33, n. 9, p. 1023–1049, 2004.
- [206] J. Bray e A. Rodriguez-Marek, «Characterization of forward-directivity ground motions in the near-fault region,» *Soil Dynamics and Earthquake Engineering*, vol. 24, n. 11, p. 815–828, 2004.
- [207] R. Rupakhety e R. Sigbjörnsson, «Can simple pulses adequately represent near-fault ground motions?,» *Journal of Earthquake Engineering*, vol. 15, n. 8, p. 1260–1272, 2011.
- [208] K. Kojima e I. Takewaki, «Closed-form critical earthquake response of elastic-plastic structures on compliant ground under near-fault ground motions,» *Frontiers in Built Environment*, vol. 2, n. 1 - 6, 2016.
- [209] R. Taniguchi, K. Kojima e I. Takewaki, «Critical response of 2DOF elastic-plastic building structures under double impulse as substitute of near-fault ground motion,» *Frontiers in Built Environment*, vol. 2, n. 2, 2016.
- [210] S. Coccia, M. Como e F. Di Carlo, «The Slender Rigid Block: Archetype for the Seismic Analysis of Masonry Structures,» *Journal of Earthquake Engineering*, 2022.



- [211] P. Gelfi, «SIMQKE\_GR».
- [212] A. Baird, A. Palermo e S. Pampanin, «Controlling seismic response using passive energy dissipating cladding connections,» in *NZSEE Conference*, Wellington, 2013.
- [213] T. Soong e G. Dargush, «Passive Energy Dissipation Systems in Structural Engineering,» Chichester, Wiley, 1997.
- [214] I. Aiken, «Energy Dissipation Devices,» in *100th Anniversary Earthquake Conference Commemorating the 1906 San Francisco Earthquake*, San Francisco, California, 2006.
- [215] A. Whittaker, V. Bertero, J. Alonso e C. Thompson, «Earthquake simulator testing of steel plate added damping and stiffness elements,» Earthquake Engineering Research Center, University of California, Berkeley, 1989.
- [216] A. Whittaker, V. Bertero, C. Thompson e L. Alonso, «Seismic testing of steel-plate energy dissipating devices,» *Earthquake Spectra*, vol. 7, n. 4, p. 563–604, 1991.
- [217] C. Xia e R. Hanson, «Influence of ADAS element parameters on building seismic response,» *Journal of Structural Engineering*, vol. 118, n. 7, p. 1903–1918, 1992.
- [218] E. Fierro e C. Perry, «San Francisco retrofit design using added damping and stiffness (ADAS) elements,» in *ATC-17-1 Seminar on Seismic Isolation, Passive Energy Dissipation and Active Control*, Redwood City, California, 1993.
- [219] I. Aiken, D. Nims, A. Whittaker e J. Kelly, «Testing of passive energy dissipation systems,» *Earthquake Spectra*, vol. 9, n. 3, 1993.
- [220] K. C. Tsai e C. P. Hong, «Steel triangular plate energy absorber for earthquake-resistant buildings,» in

*Constructional Steel Design: World Developments*, Elsevier Applied Science, 1992, pp. 529-540.

- [221] Di.Mo.Re., «Studio numerico del comportamento di connessione dissipativa standardizzata,» 2019.
- [222] J. Pinelli, J. Craig, B. Goodno e C. Hsu, «Passive control of building response using energy dissipating cladding connections,» *Earthquake Spectra*, vol. 9, n. 3, 1993.
- [223] R. Chan, «Experimental study of steel slit damper for passive energy dissipation,» *Engineering Structures*, vol. 30, 2008.
- [224] T. Karavasilis e A. Dimopoulos, «Seismic design and evaluation of a minimal-damage steel frame equipped with steel yielding devices and viscous dampers,» in *15 WCEE*, Lisboa, 2015.
- [225] P. Castaldo, «Passive Energy Dissipation Devices,» in *Integrated Seismic Design of Structures and Control Systems*, Switzerland: Springer International Publishing, 2014, p. Chapter II.
- [226] A. Wada, E. Saeki, T. Takeuchi e A. Watanabe, «Development of Unbonded Brace in Nippon Steel's Unbonded Braces (promotional document),» *Nippon Steel Corporation Building Construction and Urban Development Division*, p. 1–16, 1998.
- [227] T. Takeuchi, X. Chen e R. Matsui, «Seismic performance of controlled spine frames with energy-dissipating members,» *Journal of Constructional Steel Research*, vol. 114, pp. 51-65, 2015.
- [228] F. Sarti, T. Smith, A. Palermo, S. Pampanin, D. Bonardi e D. Carradine, «Experimental and analytical study of replaceable

- Buckling-Restrained Fused-type (BRF) mild steel dissipaters,» in *NZSEE Conference*, Wellington, 2013.
- [229] G. Rodger, C. Denmead, N. Leach, J. Chase e J. Mander, «Experimental development and analysis of a high force/volume extrusion damper,» in *NZSEE Conference*, 2006.
- [230] G. Rodgers, J. Chase, J. Mander, N. Leach e C. Denmead, «Experimental development, tradeoff analysis and design implementation of high force-to-volume damping technology,» *Bulletin of the New Zealand Society for Earthquake Engineering*, 2006.
- [231] G. Rodgers, J. Chase e J. Mander, «Repeatability and High-Speed Validation of Supplemental Lead-Extrusion Energy Dissipation Devices,» *Hindawi Advanced in Civil Engineering*, p. 13, 2019.
- [232] A. Pall, C. Marsh e P. Fazio, «Friction joints for seismic control of large panel structures,» *Journal of Prestressed Concrete Institute*, vol. 25, n. 6, pp. 38-61, 1980.
- [233] J. Butterworth e G. Clifton, «Performance of hierarchical friction dissipating joints in moment resisting steel frames.,» in *12th WCEE*, 2000.
- [234] A. Pall e C. Marsh, «Response of friction damped braced frames,» *Journal of the Structural Division*, vol. 108, pp. 1313-1323, 1982.
- [235] I. Aiken e J. Kelly, «Earthquake simulator testing and analytical studies of two energy absorbing systems for multistorey structures,» University of California, Berkeley, 1990.

- [236] F. Weber, G. Feltrin e O. Huth, «Guidelines for Structural Control,» SAMCO Final Report, 2006.
- [237] A. Sandoli, D. Moroder, S. Pampanin e B. Calderoni, «Simplified analytical models for coupled CLT walls,» in *World Conference on Timber Engineering*, Vienna, 2016.
- [238] J. Zanni, S. Cademartori, A. Marini, A. Belleri, E. Giuriani, P. Riva, B. Angi, G. Franchini, A. Marchetti, P. Odorizzi e G. Luitprandi, «Riqualificazione integrata e sostenibile di edifici esistenti con esoscheletri a guscio,» *New Horizons for Sustainable Architecture - Nuovi orizzonti per l'architettura sostenibile*, pp. 1596-1608, 2020.
- [239] B. Angi, A. Soci, B. Badiani, M. Battisti, M. Botti, R. Marmorì, A. Ghirardi, M. Buffoli, L. Capelli e S. Mlagari, «Relazione specialistica del progetto architettonico,» 2019.
- [240] A. Belleri, F. Cornali, C. Passoni, A. Marini e P. Riva, «Evaluation of out-of-plane seismic performance of column-to-column precast concrete cladding panels in one-storey industrial buildings,» *Earthquake Engineering and Structural Dynamics*, vol. 4, n. 2, pp. 397-417, 2017.
- [241] RELUIS, «REXEL v 3.5,» 2022.
- [242] L. Gaspari, «Riqualificazione integrata di edifici mediante esoscheletri a guscio in legno: reingegnerizzazione delle connessioni in ottica LCT,» Dalmine, 2022.
- [243] E. Giuriani, A. Marini, J. Zanni e M. Bosio, «Report prova a flessione nel piano su pareti in XLAM dotate di connessioni rigide in fondazione,» SCC, Innovation Hub & Living Lab Network, 2022.

- [244] N. Canal, «Resistenza meccanica di blocchi forati a fori orizzontali,» *Consorzio POROTON Italia*, 2006.
- [245] F. Messali, G. Metelli e G. Plizzari, «Experimental results on the retrofitting of hollow brick masonry walls with reinforced high performance mortar coatings,» *Construction and Building Materials*, pp. 619-630, 2017.
- [246] S. Labò e A. Marini, «In-plane flexural behavior of hollow brick masonry walls with horizontal holes,» *Engineering Structures*, vol. 8, n. 273, 2022.
- [247] J. Zanni, S. Castelli, M. Bosio, C. Passoni, S. Labò, A. Marini, A. Belleri, E. Giuriani, G. Brumana, C. Abrami, S. Santini, G. Venturelli e A. Marchetti, «Application of CLT prefabricated exoskeleton for an integrated renovation of existing buildings and continuous structural monitoring,» in *XIX ANIDIS Conference, Seismic Engineering in Italy*, Torino, 2022.
- [248] E. Giuriani, A. Marini e J. Zanni, «Intervento di riqualificazione architettonica, sismica ed energetica dell'edificio di proprietà aler sito a Prevalle (BS) in via zanardelli 1,» 2021.
- [249] n. 6. Decreto Legge 4 giugno 2013, *4 giugno 2013, n. 63*, Roma.
- [250] M. d. i. e. d. trasporti, *Decreto Ministeriale numero 58 del 28/02/2017*.
- [251] B. Calderoni, C. E. e L. P., «La vulnerabilità sismica degli edifici esistenti in c.a. progettati per soli carichi verticali,» in *XVI CTE Conference*, Parma, 2006.
- [252] B. Calderoni, A. Sandoli e L. Migliaccio, «Valutazione della vulnerabilità sismica degli edifici in c.a. progettati per soli

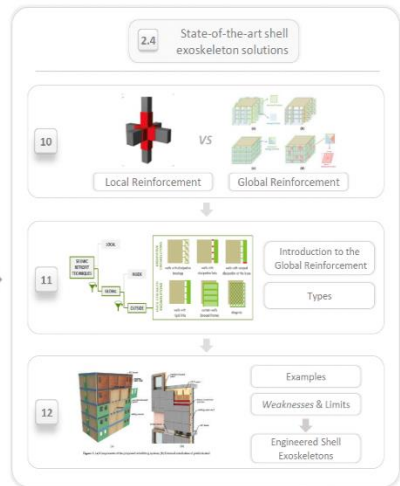
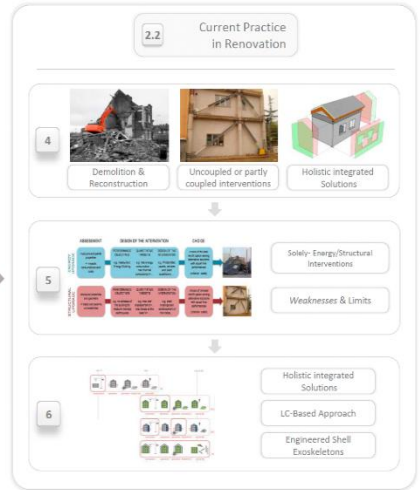
carichi verticali mediante una procedura semplificata.» Iuss Press, Pavia, 2015.

- [253] S. Labò, *Diagrid exoskeleton for the retrofit of RC buildings*. Supervisor A. Marini., Bergamo: PhD thesis, University of Bergamo, 2021.

## Appendix A

This appendix contains some graphic representations of the main contents of the different chapters and the organisation of the manuscript. The contributions and insights described in the text are highlighted in green.

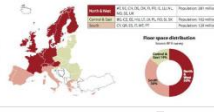


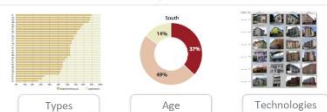





# Stefano Cademartori


**3.2 Introduction + EU Building**

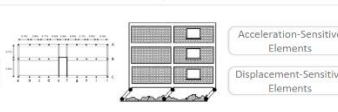
13  Introduction

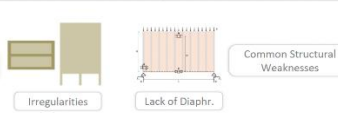
14  Types Age Technologies

15  Seismic Vulnerability of the Existing Building Stock

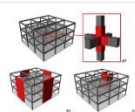
**3.3 Main Structural Vulnerabilities**


16  RC + Infills Masonry Precast RC

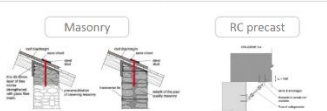
17  Acceleration-Sensitive Elements Displacement-Sensitive Elements

18  Irregularities Lack of Diaphragms Common Structural Weaknesses


**4.2 Introduction + Overview Traditional Interventions**


19  Global vs Local Solutions


20  RC

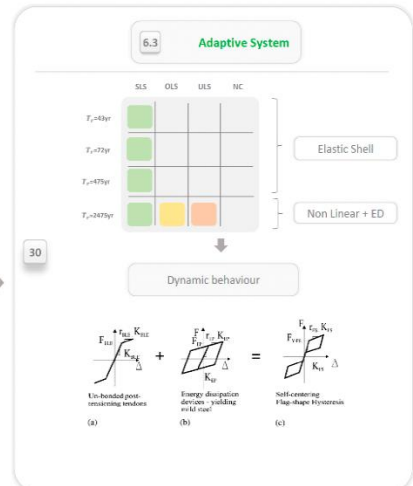
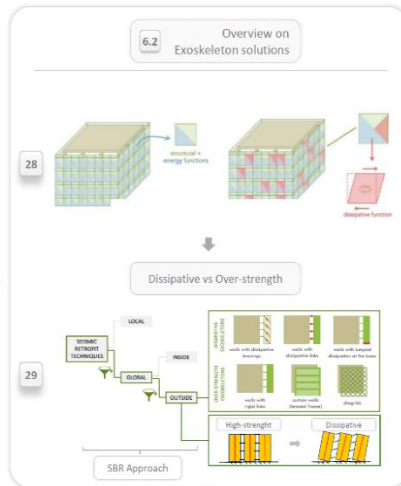
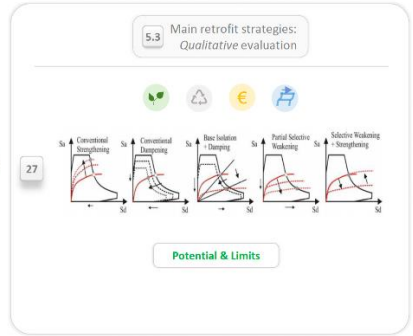
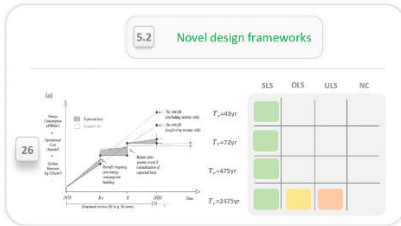
21  Masonry RC precast

**4.4 Integrated Retrofit Interventions + Examples**

22  Types

23  Examples

24  Holistic & Integrated Solutions AdESA System



**6.4 Conceptual Design**

Vertical Arrangement

Horizontal Arrangement

31

**Structural Design procedure**

Elastic range

Nonlinear range

32

**6.5 Numerical Analyses**

NLTHs

Case studies

33

**Analysis of results**

34

**7.2 Brief overview on PEDDs**

Displacement-Proportional

35

**7.4 AdESA fuse**

Mild Steel Plates

Config. I

Config. II

Config. III

37

**Experimental Tests**

38

**7.3 Analysis from Life-Cycle Eng. Persp.**

36

8.2 Building Description

39

8.3 Structural Deficiencies

40

Displacement direction

Model A

Model B

Model C

8.4 Conceptual design of The exoskeleton

41

AdESA Structure AdESA Energy

- Max. Interstorey drift  $\leq 0.5\%$
- Limited Seismic Actions  $\rightarrow$  Elastic Behaviour
- + Energy Dissipation

8.5 Structural Concept of Retrofit

42

$d_{target}$   $F_1 \rightarrow$   $d_{target}$   $F \rightarrow$

$T$   $R$   $C$   $T$   $\delta$   $F$   $C$

Description of the Holistic Intervention

43

AdESA fuse

# Stefano Cademartori

## 9.2 Building Description

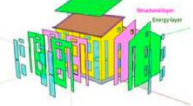
44



Clay hollow bricks arranged with horizontal holes & cement-based mortar

## 9.4 Overview of the Holistic Intervention

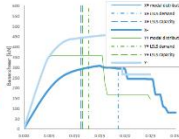
46



- Structure
- Energy
- Architecture

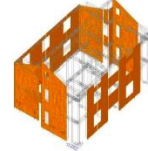
## 9.3 Structural Deficiencies

45



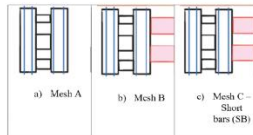
## 9.5 Structural Intervention

47



## 9.6 Critical analysis

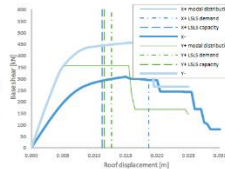
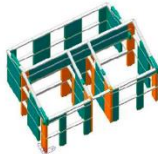
48



Adaptive exoskeleton

## 9.7 Re-engineering of the connection

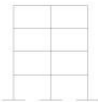
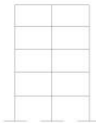


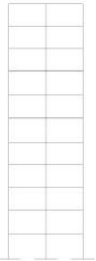
49



## Appendix B

### - Reference geometry of post WWII RC building

Table 7 - Reference features of the post WWII RC buildings. From [96].

|   |   |   |   |   |
|---|---|---|---|---|
|  |  |  |  |  |
| $m_j = 451 \text{ kN/g}$  | $m_j = 800 \text{ kN/g}$  | $m_j = 1000 \text{ kN/g}$   | $m_j = 800 \text{ kN/g}$  | $m_j = 800 \text{ kN/g}$  |
| $k_j = 24 \text{ kN/mm}$  | $k_j = 24 \text{ kN/mm}$  | $k_j = 24 \text{ kN/mm}$  | $k_j = 14 \text{ kN/mm}$  | $k_j = 7.9 \text{ kN/mm}$   |
| $T_j = 0.86 \text{ s}$  | $T_j = 1.15 \text{ s}$  | $T_j = 1.28 \text{ s}$  | $T_j = 1.5 \text{ s}$   | $T_j = 2.00 \text{ s}$  |
| $N = 4 \text{ (floors)}$  | $N = 5 \text{ (floors)}$  | $N = 7 \text{ (floors)}$  | $N = 8 \text{ (floors)}$  | $N = 11 \text{ (floors)}$   |

### - Structural design of the adaptive exoskeletons

In accordance with the design procedure outlined in the Section 6.4, starting with the definition of the SDOF response curve of the building in the as-is condition, the following steps are carried out.

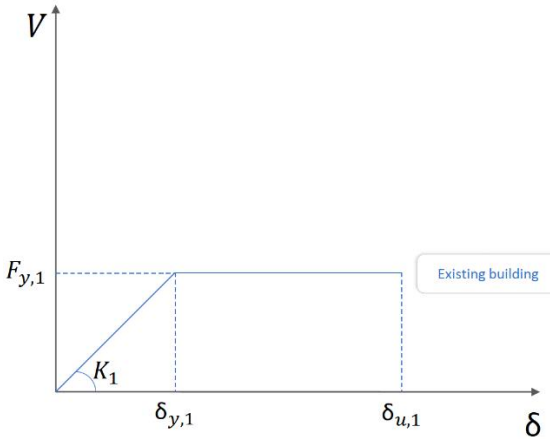


Figure 0.1 – Response curve of the existing building.

The yielding displacement  $\delta_{y,1}$  corresponds to the achievement a drift associated to limited damage to structural and non-structural elements, whereas the ultimate displacement  $\delta_{u,1}$  correspond to a 1% building drift [251] [252]. For this case study, characterised by a limited yielding displacement, the target elastic displacement  $\delta_{d,Elast.}$  correspond to a 0.5% building drift ().

$$\delta_{y,1} = \frac{F_{y,1}}{K_1} = \frac{1219kN}{73.81 \text{ kN/mm}} = \mathbf{16.5mm}$$

$$\delta_{d,Elast.} = 0.5\% H = 0.5\% 9.5m = \mathbf{47.5mm}$$

Consequentially, the target *elastic damage parameter*  $\mu_{Elast.}$  is equal to.

$$\mu_{Elast.} = \frac{\delta_{d,Elast.}}{\delta_{y,1}} = \frac{47.5mm}{16.5mm} = \mathbf{2.88}$$

Assuming the location of the building in a medium-high seismicity zone,  $a_g = 0.233g$  [141], the elastic design spectrum at life-safety limit state (LSLS) adopted is as follows ().

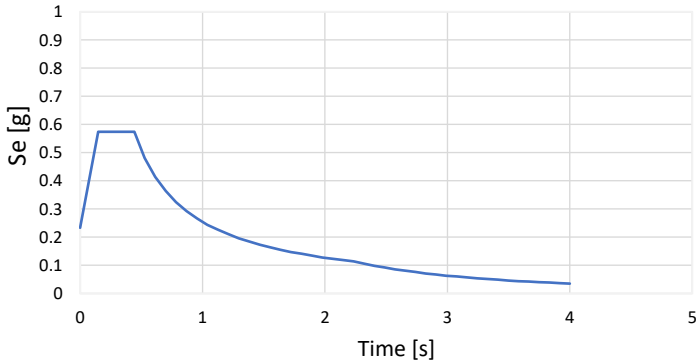


Figure 0.2 - Elastic design spectrum of the site at life-safety limit state (LSLS). From [141].

The site spectral acceleration  $Se(T_1)$  obtained is approximately.

$$Se(T_1) = 0.31g$$

Accordingly, the strength parameter  $\eta$ :

$$\eta = \frac{F_{y,1}}{[m_1 Se(T_1)]} = \frac{1219kN}{[11180 \frac{kN}{g} 0.31g]} \cong \mathbf{0.35}$$

The *stiffness ratio*  $\tilde{\lambda}$  obtained by the design spectra in relation to target *elastic damage parameter*  $\mu_{Elas}$ . is approximately 0.63 ().



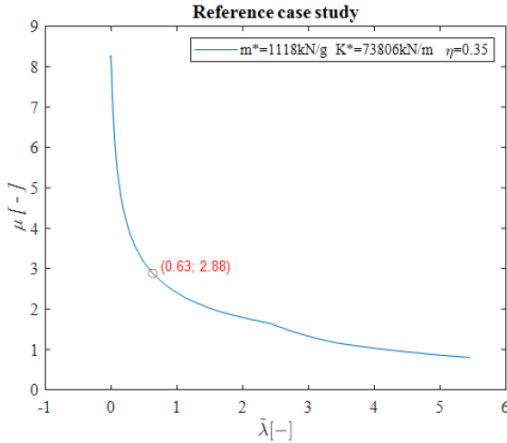


Figure 0.3 - Design spectra of the reference case study building obtained for a *strength parameter*  $\eta$  equal to 2.88.

*Minimum equivalent elastic stiffness of the retrofit* ( $k_2$ ) is calculated by multiplying the *stiffness ratio*  $\tilde{\lambda}$  by the initial elastic stiffness of the existing structure ( $k_1$ ):

$$k_2 = \tilde{\lambda} k_1 = 0.63 \cdot 73.81 \frac{\text{kN}}{\text{mm}} = 46.5 \frac{\text{kN}}{\text{mm}}$$

The minimum required total stiffness ( $k_{tot,min}$ ) for the retrofitted system:

$$k_{tot,min} = k_1 + k_2 = (73.81 + 46.5) \frac{\text{kN}}{\text{mm}} = 120.3 \frac{\text{kN}}{\text{mm}}$$

As a result, the *fundamental Period Retrofitted System* ( $T_{1,retrofitted}$ ):

$$T_{1,retrofitted} = 2 \pi \sqrt{\frac{1.1 m_1}{k_{tot,min}}} = 2 \pi \sqrt{\frac{1.1 \cdot 11180 \frac{\text{kN}}{\text{g}}}{120.3 \frac{\text{kN}}{\text{mm}}}} = 0.64\text{s}$$

The *Minimum required base shear for the retrofit* ( $V_{Rd,min.}$ ) defined according to the site elastic spectrum:

$$\begin{aligned} V_{Rd,min.} &= 1.1 W_1 Se(T_{1,retrofitted}) - F_{y,l} \\ &= 1.1 \cdot 11180 \frac{\text{kN}}{\text{g}} \cdot 0.377\text{g} - 1219\text{kN} = 3417\text{kN} \end{aligned}$$

Consequently, the *minimum required global resistant moment* ( $M_{Rd,min.}$ ):

$$M_{Rd,min.} = V_{Rd,min.} \frac{2}{3} H = 3417\text{kN} \frac{2}{3} 9.5\text{m} = 21641\text{kNm}$$

After defining the characteristics of the exoskeleton in the elastic range, the *target displacement* of the existing building in the nonlinear range  $\delta_{d,Nonlin.}$  is determined with reference to the Near-Collapse Limit State (NCLS):

$$\delta_{d,Nonlin.} = 0.8\% H = 0.8\% \cdot 9.5\text{m} = 76\text{mm}$$

The *Nonlinear ductility demand*  $\mu_{Nonlin.}$  for existing building is accordingly:

$$\mu_{Nonlin.} = \frac{\delta_{d,Nonlin.}}{\delta_{d,Elast.}} = \frac{76\text{mm}}{47.5\text{mm}} = 1.6$$

The existing building's equivalent viscous damping ( $\xi_{Exist.Build.}$ ) is conservatively defined as 40% of the 5% conventional elastic damping:

$$\xi_{Exist.Build.} = 40\% \xi_{el.} = 0.4 \cdot 5\% = 2\%$$

The equivalent viscous damping of the shell exoskeleton ( $\xi_{exosk.}$ ) is defined assuming a coefficient  $\beta_{CB}$  equal to 0.45:

$$\xi_{Exosk.} = \xi_{el} + \xi_{hys} = 2\% + \frac{2 \beta_{CB} (\mu_{Nonlin.} - 1)}{\pi \mu_{Nonlin.} (1 + r(\mu_{Nonlin.} - 1))}$$

$$= 2\% + \frac{2 \cdot 0.45 \cdot (1.6-1)}{\pi \cdot 1.6 \cdot (1+0.06(1.6-1))} = \mathbf{12.37\%}$$

It follows that the equivalent viscous damping ratio for the retrofitted system ( $\xi_{Retrofitted}$ ) is:

$$\begin{aligned} \xi_{Retrofitted} &= \frac{V_{Rd,min.}}{V_{Rd,min.} + F_{1,y}} \xi_{Esosk.} + \frac{F_{1,y}}{V_{Rd,min.} + F_{1,y}} \xi_{Exist.Build.} \\ &= \frac{3417kN}{3417kN + 1219kN} 2\% + \frac{1219kN}{3417kN + 1219kN} 12.37\% = \mathbf{11.38\%} \end{aligned}$$

The effective period of the retrofitted system ( $T_{eff,Retrofitted}$ ) is calculated utilising the design displacement spectra of the site at NCLS () [54], dampened by introducing the equivalent viscous damping ratio ( $\xi_{Retrofitted}$ ) previously calculated.

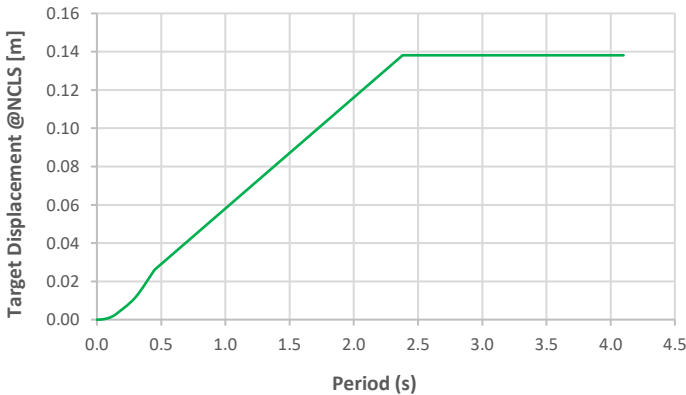


Figure 0.4 - Dampened displacement design spectrum of the site at near-collapse limit state (NCLS). From [141].

$$T_{eff,Retrofitted} = \mathbf{1.31s}$$

The *minimum base shear required* ( $V_{Rd,min.,DBDR}$ ), defined by applying the *Displacement Based Design Retrofit* approach:

$$V_{Rd,min.,DBDR} = 4 \pi^2 \frac{1.1 m_1}{T_{eff,Retrofitted}^2} \delta_{d,Nonlin.} \cdot F_{1,y}$$

$$= 4 \pi^2 \frac{1.1 \cdot 11180 \frac{kN}{g}}{T_{eff,Retrofitted}^2} 76mm - 1219kN = 978kN$$

$$< V_{Rd,min.} = 3417kN$$

The adaptive exoskeleton designed meets the structural requirements, compliance with elastic performance requirements determines the resistance and elastic stiffness of the retrofit.

## - Design of the case studies

This section of the appendix contains the description of the process for the technological design of the configurations in the Section 6.5, divided between representative models of the vertical and horizontal structural arrangement of adaptive exoskeletons, erected using *commercial-sized CLT panels* for the structural panels and *Dywidag GEWI steel bars* for the re-centring bars.

The material mechanical properties are to the same for all solutions and are listed below:

- Structural Panels: *Five-layers cross-laminated timber (CLT) panels* with a total thickness of 100mm, C24 class.  
Assuming that the base cross section of the panels consists of 3 layers of 20mm fibres oriented in the main

direction and 2 layers oriented in the orthogonal direction, the mechanical properties defined in the scientific literature [187] and reduced by the Standard's safety factors and multiplied by the corrective coefficient accounting for the service conditions [141] are as follows.

The design compression resistance ( $f_{cd,CLT}$ ):

$$f_{cd,CLT} = f_{c,0,k} \frac{K_{mod}}{\gamma_{M0}} \frac{60mm}{100mm} \frac{1}{\gamma_{Rd}} = 21MPa \frac{1.1}{1.45} \frac{60mm}{100mm} \frac{1}{1.1}$$

$$f_{cd,CLT} \cong \mathbf{8.69MPa}$$

where:

- $K_{mod}$  is the correction coefficient that considers the effect on resistance parameters of both load duration and moisture of the timber, equal to 1.1.
- $\gamma_{M0}$  is the partial safety factor relative to the material; equal to 1.45.
- $\gamma_{Rd}$  is the overstrength factor, equal to 1.1.

The design shear strength ( $f_{vd,CLT}$ ) of these CLT panels under in-plane loads is defined according to formulations available in the literature regarding resistance to torsion failure [188]:

$$f_{vd,CLT} = \mathbf{2.5MPa} \frac{K_{mod}}{\gamma_{M0}} = 2.5MPa \frac{1.1}{1.45} = \mathbf{1.9MPa}$$

Orthotropy of the CLT material is assumed. Accordingly, axial and tangential moduli of elasticity are introduced.

General  
Material ID: 1 Name: Legno

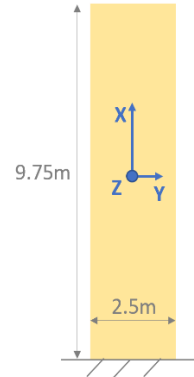
Elasticity Data  
Type of Design: User Defined  
User Defined  
Standard: None  
DB:   
Product:   
Concrete  
Standard:   
Code:   
DB:

Type of Material  
 Isotropic  Orthotropic

User Defined

|                         | Local-x    | Local-y    | Local-z    |                   |
|-------------------------|------------|------------|------------|-------------------|
| Modulus of Elasticity : | 4.4000e+03 | 6.6000e+03 | 8.0000e+03 | N/mm <sup>2</sup> |
| Thermal Coefficient :   | 0.0000e+00 | 0.0000e+00 | 0.0000e+00 | 1/[F]             |

|                   | Local-xy   | Local-xz   | Local-yz   |                   |
|-------------------|------------|------------|------------|-------------------|
| Shear Modulus :   | 4.7500e+02 | 4.7500e+02 | 4.7500e+02 | N/mm <sup>2</sup> |
| Poisson's Ratio : | 0          | 0          | 0          |                   |



- *Dywidag Gewi Plus S670/800* steel bars [189]. The mechanical properties of the material are as follows:
  - Conventional yield strength ( $f_{0,2k}$ ) :

$$f_{0,2k} = 670\text{MPa}$$

- Design yield strength ( $f_{yd}$ ):

$$f_{yd} = 645\text{MPa}$$

- Ultimate tensile strength ( $f_{tk}$ ):

$$f_{tk} = 800\text{MPa}$$

- Elasticity modulus of the steel ( $E_s$ ):

$$E_s = 210000\text{MPa}$$

- Diameter of the bars ( $\Phi$ ):

$$\Phi = 30\text{mm}$$

- Resistant area of bars ( $A_s$ ):

$$A_s = 707mm^2$$

This diameter was chosen as to limit the maximum compression in the CLT section and to enable the application of the post-tensioning action without using heavy tools.

The design procedure main steps are described in Section 6.4, i the design principles defined in Section 5.3 for the different structural performance points.

- **Vertical structural arrangement**

**A) Configuration A: CLT coupled rocking walls with post-tensioned steel bars ( ).**

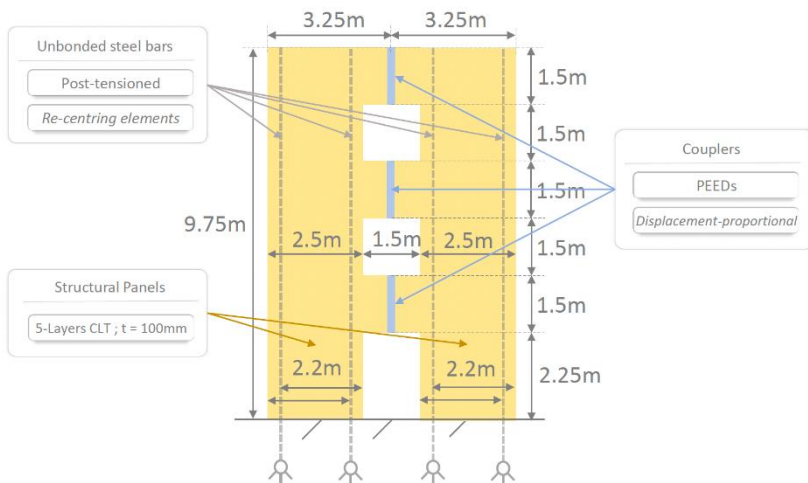


Figure 0.5 - Conceptual representation and synthetic description of the *configuration A*.

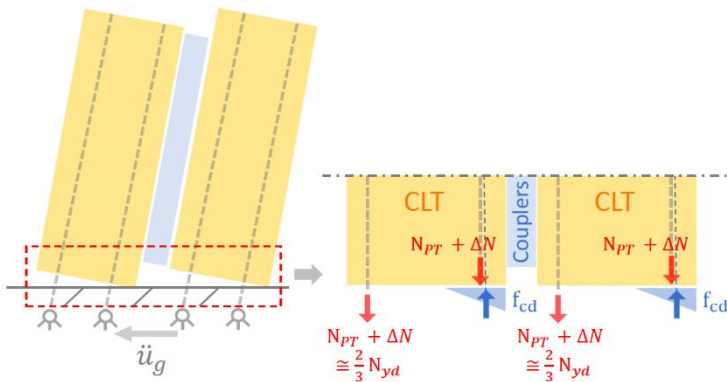
The re-centering system, consisting of steel bars placed inside the panels, constrained at the top of the vertical panels and hinged to the foundation, only withstands tensile actions. The design

length of the bars ( $L_d$ ) is assumed to be equal to the height of the wall:

$$L_d = 9.75\text{m}$$

Listed below are the sequential steps for dimensioning the solution based on the various performance points specified in Paragraph 6.4.

1. *First performance point - Couplers yielding*



The first step is the definition of axial load at the base section of each CLT panels provided by the post-tensioning ( $N_{PT}$ ) and elastic deformation of bars ( $\Delta N$ ), and gravity loads ( $N_g$ ). In order to ensure proper behaviour of the re-centring system, it was decided to limit the maximum action in each steel bar ( $N_{P-T} + \Delta N$ ) below the yielding action ( $N_{yd}$ ). **In particular:**

$$N_{PT} + \Delta N \cong \frac{2}{3} N_{yd}$$



$$N_{PT} + \Delta N = \frac{2}{3} f_{yd} A_s = \frac{2}{3} 645 \text{MPa} 707 \text{mm}^2 \cong \mathbf{305.5 \text{kN}}$$

Since the wall drift at this point is a design choice (= 0.5%), the increase in axial load in the bars due to elastic deformation of the retrofit ( $\Delta N$ ), which depends on their axial deformation ( $\epsilon_s$ ), reads as follow:

$$\epsilon_s = \frac{\sqrt{(0.5\% L_d)^2 + L_d^2}}{L_d} = \mathbf{0.00125\%}$$

$$\begin{aligned} \rightarrow \Delta N &= E_s A_s \epsilon_s = 210000 \text{MPa} 707 \text{mm}^2 0.00125\% \\ &\cong \mathbf{185.5 \text{kN}} \end{aligned}$$

Accordingly, the design post-tensioning load for each steel bar is:

$$\rightarrow N_{PT} = 305.5 \text{kN} - 185.5 \text{kN} \cong \mathbf{120 \text{kN}}$$

The gravity load carried by the panel is exclusively associated with its own weight, approximately equal to:

$$N_g \cong H_{tot} t_{CLT} B_{CLT} \gamma_{CLT}$$

$$N_g = 9.75 \text{m} 0.1 \text{m} 2.5 \text{m} 4.2 \frac{\text{kN}}{\text{m}^3} \cong \mathbf{10.2 \text{kN}}$$

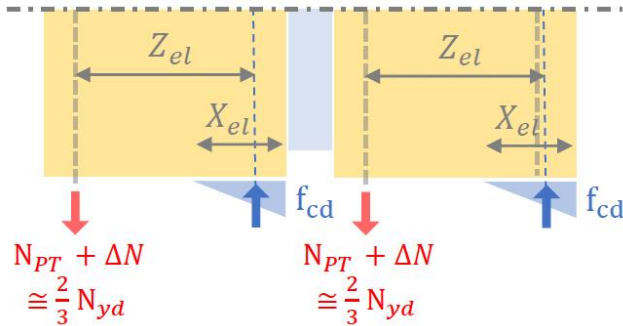
The resistant moment provided by the post-tensioning of the steel bars and their elastic deformation ( $M_{PT}$ ) and by gravity loads ( $M_N$ ) can be calculated as follows:

- Definition of the extension of the compressed portion of the CLT base section ( $X_{el}$ ):

$$\frac{1}{2} f_{cd} t_{CLT} X_{el} = n^\circ \text{ barre } (N_{P-T} + \Delta N) + N_g$$

$$\rightarrow X_{el} = \frac{n^{\circ} \text{ barre } (N_{P-T} + \Delta N) + N_g}{\frac{1}{2} f_{cd} t_{CLT}} = \frac{2 (305.5 \text{ kN}) + 10.2 \text{ kN}}{\frac{1}{2} 8.69 \text{ MPa } 100 \text{ mm}} = \mathbf{1.4 \text{ m}}$$

- Simplified definition of the resistant moment ensured by each panel:



$$M_{PT} + M_N \cong (N_{PT} + \Delta N) Z_{el}$$

$$\rightarrow M_{PT} + M_N = 305.5 \text{ kN } 1.73 \text{ m} = \mathbf{528.5 \text{ kNm}}$$

where  $Z_{el}$  is the lever arm between the centroid axis of the bar (in red) and the centre of pressure in the timber section.

- The resistant moment provided by coupling effect ( $M_S$ ) is defined assuming the yielding of the couplers:

$$M_S = \beta_{CB} M_{tot,R} = \beta_{CB} [n^{\circ} \text{ panels}(M_{PT} + M_N) + M_S]$$

$$\rightarrow M_S = \frac{\beta_{CB}}{(1-\beta_{CB})} n^{\circ} \text{ panels}(M_{PT} + M_N)$$

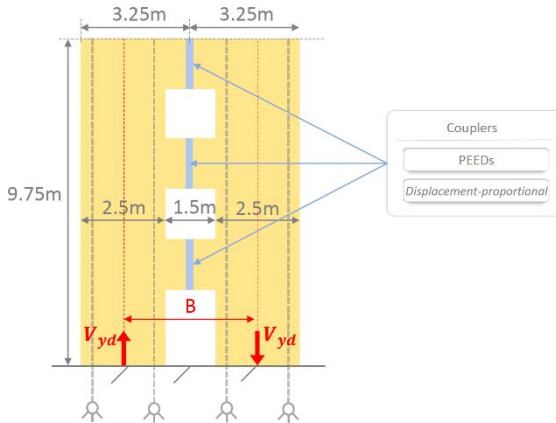
$$\rightarrow M_S = \frac{0.45}{(1-0.45)} 2 \cdot 528.5 \text{ kNm} \cong \mathbf{864.8 \text{ kNm}}$$

As a design choice, the coupling effect resisting contribution was limited to 0.45 the total resisting moment

to potentially guarantee the re-centring behaviour. Consequently, the coefficient  $\lambda$  that represents:

$$\lambda = \frac{n^{\circ} \text{ panels } (M_{PT} + M_N)}{M_S} = \frac{2 \cdot 528.5 \text{ kNm}}{864.8 \text{ kNm}} = \mathbf{1.22}$$

- Definition of the shear yielding force ( $V_{yd}$ ) of the vertical couplers:



The coupling moment ( $M_S$ ) can be assumed to be equal to the product of the shear yielding force ( $V_{yd}$ ) and the distance between the centroid of the vertical panels ( $B$ ):

$$M_S = V_{yd} B$$

$$V_{yd} = \frac{M_S}{B} = \frac{864.8 \text{ kNm}}{4 \text{ m}} \cong \mathbf{216.2 \text{ kN}}$$

Each of the three verticals stripes of couplers has a shear yielding force ( $V_{yd,i}$ ) equal to:

$$V_{yd,i} = \frac{V_{yd}}{3} = \frac{216.2 \text{ kN}}{3} \cong \mathbf{72 \text{ kN}}$$

- The total resistant moment of the adaptive coupled shear walls is equal to:

$$M_{tot,R} = n^{\circ} \text{ panels } ( M_{PT} + M_N ) + M_S$$

$$\rightarrow M_{tot,R} = 2 \cdot 528.5 \text{ kNm} + 864.8 \text{ kNm} \cong \mathbf{1921.8 \text{ kNm}}$$

- The elastic base shear resistance of the coupled shear walls is equal to:

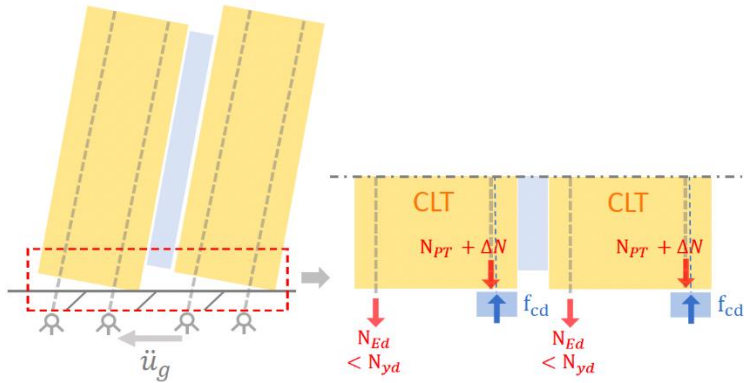
$$F_{el,2} = \frac{M_{tot,R}}{\frac{2}{3}H} = \frac{1921.8 \text{ kNm}}{\frac{2}{3} \cdot 9.75 \text{ m}} \cong \mathbf{295.7 \text{ kN}}$$

The ratio between the average compression in the most stressed panel ( $\sigma_{el}$ ) and the compressive strength of the CLT ( $f_{cd}$ ):

$$\frac{\sigma_{el}}{f_{cd}} = \frac{N_g + 2(N_{P-T} + \Delta N) + V_{yd}}{B_{CLT} \cdot t_{CLT}} \cdot \frac{1}{f_{cd}}$$

$$\rightarrow \frac{\sigma_u}{f_{cd}} = \frac{(10.2 + 2(120 + 185.5) + 216.2) \text{ kN}}{2.5 \text{ m} \cdot 0.1 \text{ m}} \cdot \frac{1}{8.69 \text{ MPa}} = 0.38 < 0.5$$

### 3. Third performance point – Re-centring system yielding



Also at this performance point, calculating the ultimate overturning resistant moment offered by the system requires the specification of various contributions:

$$M_{u,2} = n^{\circ} \text{ panels } ( M_{yd} + M_N ) + M_S$$

where:

- **n° panels** = number of vertical structural panels = 2
- **$M_{u,2}$**  = Ultimate overturning resistant moment
- **$M_{yd}$**  = Resistant moment provided by the yielding of post-tensioning steel bars ( $N_{yd}$ )

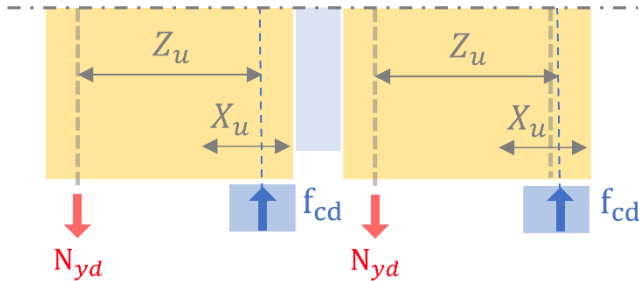
Definition of the extension of the base's compressed section ( $X_u$ ):

$$f_{cd} t_{CLT} X_u = (N_{PT} + \Delta N) + N_{yd} + N_g$$

$$\rightarrow X_u = \frac{(N_{PT} + \Delta N) + N_{yd} + N_g}{f_{cd} t_{CLT}} = \frac{305.5kN + 456kN + 10.2kN}{8.69MPa \cdot 100mm} \cong 0.89m$$

At this point, the steel bar in the compressed zone only contributes by increasing the axial load at the wall's base ( $N_{PT} + \Delta N$ ), while the other bar yields ( $N_{yd}$ ).

- Simplified definition of the resistant moment ensured by each panel:



$$M_{yd} + M_N \cong N_{yd} Z_u$$

$$\rightarrow M_{yd} + M_N = 456\text{kN} \cdot 1.76\text{m} \cong \mathbf{802.5\text{ kNm}}$$

where  $Z_u$  is the distance between the centroid axis of the stretched bar (in red) and the centre of compressions in the timber section.

- The ultimate overturning resistant moment of the coupled rocking walls is equal to:

$$M_{u,2} = n^\circ \text{ panels } ( M_{yd} + M_N ) + M_S$$

$$\rightarrow M_{u,2} = 2 \cdot 802.5\text{kNm} + 864.8\text{kNm} \cong \mathbf{2470\text{kNm}}$$

- The ultimate base shear resistance of the coupled rocking walls is equal to:

$$F_{u,2} = \frac{M_{u,2}}{\frac{2}{3}H} = \frac{2470kNm}{\frac{2}{3} \cdot 9.75m} \cong \mathbf{380kN}$$

The ratio between the base shear defined at the first performance point ( $F_{el,2}$ ) and the ultimate shear ( $F_{u,2}$ ):

$$\frac{F_{u,2}}{F_{el,2}} = \frac{380kN}{295.7kN} = \mathbf{1.285} < \mathbf{1.3}$$

The ratio between the maximum mean compression in the most stressed panel ( $\sigma_u$ ) and the compressive strength of the CLT ( $f_{cd}$ ):

$$\frac{\sigma_u}{f_{cd}} = \frac{N_{yd} + N_g + N_{PT} + \Delta N + V_{yd}}{B_{CLT} t_{CLT}} \frac{1}{f_{cd}}$$

$$\rightarrow \frac{\sigma_u}{f_{cd}} = \frac{(456+10.2+120+185.5+216.2)kN}{2.5m \cdot 0.1m} \frac{1}{8.69MPa} = \mathbf{0.45} < \mathbf{0.5}$$

The maximum tangential stress ( $\tau_{max,ED}$ ) in Timber panels is less than the resistance provided by CLT panels ( $f_{vd,CLT}$ ):

$$\tau_{max,Ed} = 1.5 \frac{F_{u,2}}{n^{\circ} \text{ panels}} \frac{1}{t_{CLT} B_{CLT}} = 1.5 \frac{308kN}{2} \frac{1}{100mm \cdot 2500mm} \cong \mathbf{0.93MPa} < \mathbf{1.9MPa}$$

$$\rightarrow \tau_{max} < f_{vd,CLT}$$

**B) Configuration B:** *CLT coupled rocking walls with non-post-tensioned steel bars* ( ).

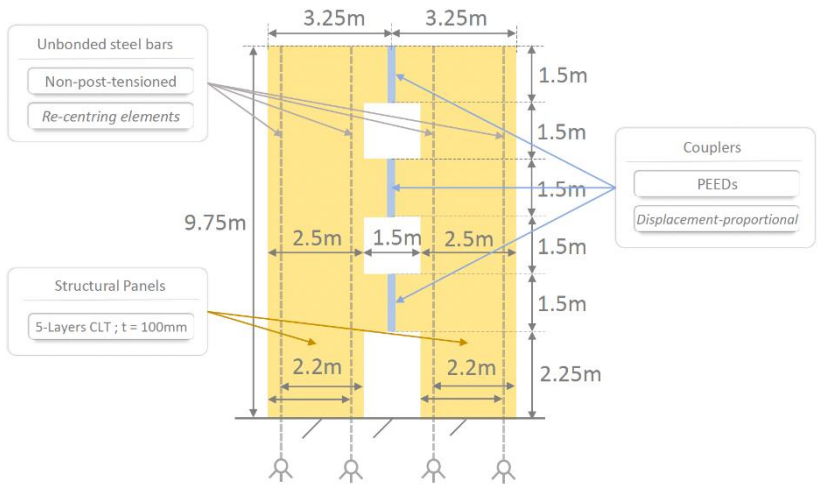


Figure 0.6 - Conceptual representation and synthetic description of the *configuration B*.

This solution has the same geometry and properties as configuration A, with the exception that the vertical steel bars lack post-tensioning.

**C) Configuration C:** *CLT coupled rocking walls with post-tensioned steel bars and sacrificial fuse toes* ( ).



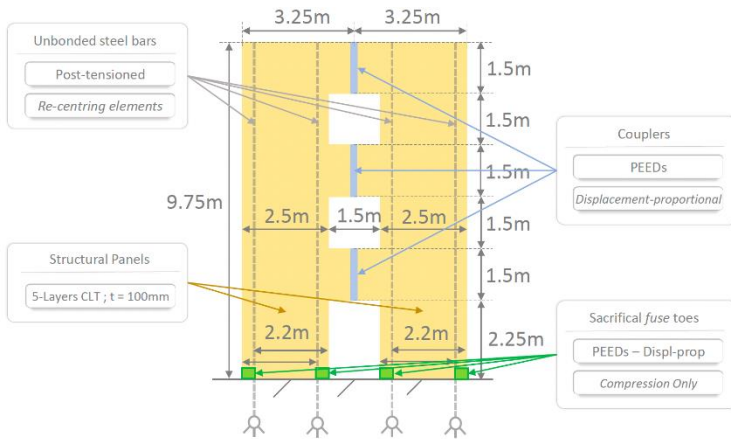
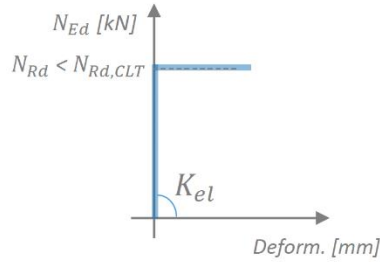


Figure 0.7 - Conceptual representation and synthetic description of the *configuration C*.

The only difference between this configuration and configuration A is the presence of sacrificial fuse elements at the base corners. This section analyses these replaceable devices from a theoretical and non-technical perspective.

These devices are conceptually designed to react only when compressed and exhibit a lower compressive strength than the CLT section to which they are in contact, thereby preserving their integrity and concentrating damage. At this stage of the research, also these dissipative devices are also conceptually represented by a rigid-plastic constitutive model:



**D) Configuration D:** CLT coupled rocking walls with non-post-tensioned steel bars and sacrificial fuse toes ().

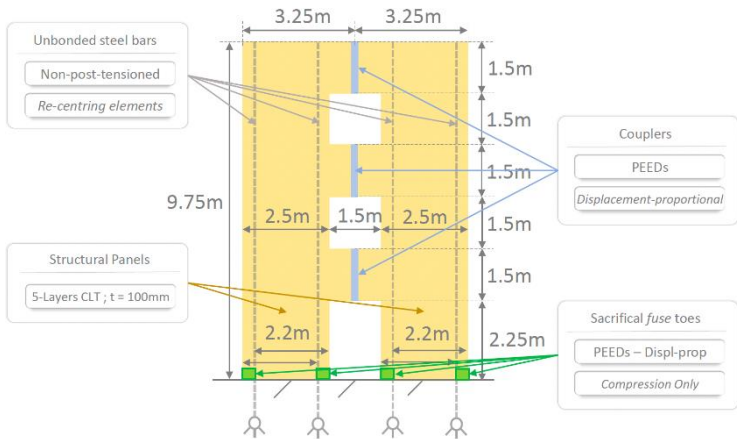


Figure 0.8 - Conceptual representation and synthetic description of the *configuration D*.

This configuration was created to evaluate the effect of post-tensioning load on system response. This solution has the same geometry and properties as configuration C, with the exception that the passive vertical steel bars are adopted.

**E) Configuration E:** CLT coupled rocking walls with post-tensioned steel bars and Steel end-columns ( ).

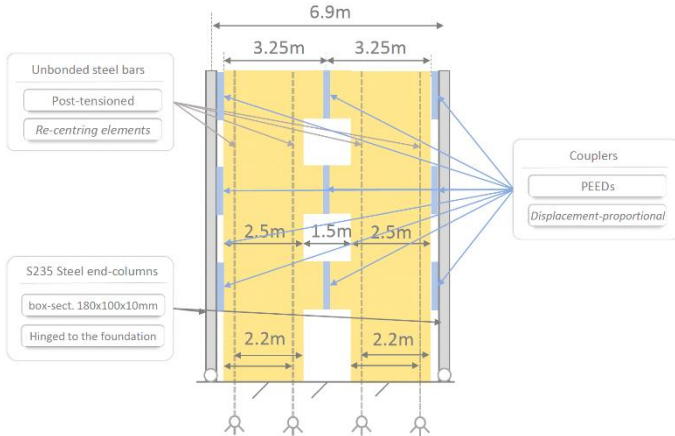


Figure 0.9 - Conceptual representation and synthetic description of the *configuration E*.

The mechanical properties of the S235 steel are as follows:

- Characteristic yield strength ( $f_{y,k}$ ) :

$$f_{y,k} = 235\text{MPa}$$

- Design yield strength ( $f_{y,d}$ ):

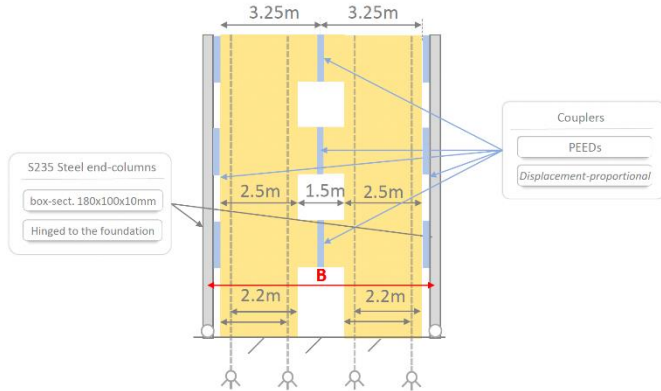
$$f_{y,d} = \frac{f_{y,k}}{1.05} = 223.8\text{MPa}$$

- Elasticity modulus of the steel ( $E_s$ ):

$$E_s = 210000\text{MPa}$$

1. First performance point - Couplers yielding

Definition of the design shear yielding force ( $V_{yd}$ ) of the vertical couplers.



The coupling moment ( $M_S$ ) can be assumed to be equal to the product of the design shear yielding force ( $V_{yd}$ ) and the distance between the centroid of the steel end-columns ( $B$ ):

$$M_S = V_{yd} B = 864.8 \text{ kNm} ; B \cong 6.9 \text{ m}$$

$$V_{yd} = \frac{M_S}{B} = \frac{864.8 \text{ kNm}}{6.9 \text{ m}} \cong 125 \text{ kN}$$

The total resistance offered by the inner couplers between CLT panels is identical to that of the more external couplers. The Design shear yielding force for each of the 3 vertical rows of couplers between CLT panels and steel end-columns:

$$V_{yd,i} = \frac{V_{yd}}{3} = \frac{125 \text{ kN}}{3} \cong 41.5 \text{ kN}$$

**F) Configuration F:** CLT coupled rocking walls with non-post-tensioned steel bars and Steel end-columns ( ).

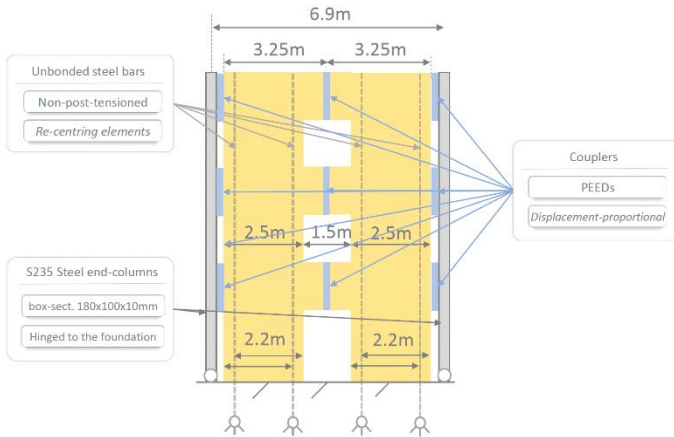


Figure 0.10 - Conceptual representation and synthetic description of the *configuration F*.

As for the previous cases, this configuration was created solely to evaluate the effect of post-tensioning load on system response. This solution has the same geometry and properties as configuration E, with the exception that the vertical steel bars are devoid of post-tensioning.

- **Horizontal structural arrangement**

**G) Configuration G:** *CLT shear-walls with post-tensioned steel bars and horizontal couplers located between the structural panels of the ground and first floors ().*

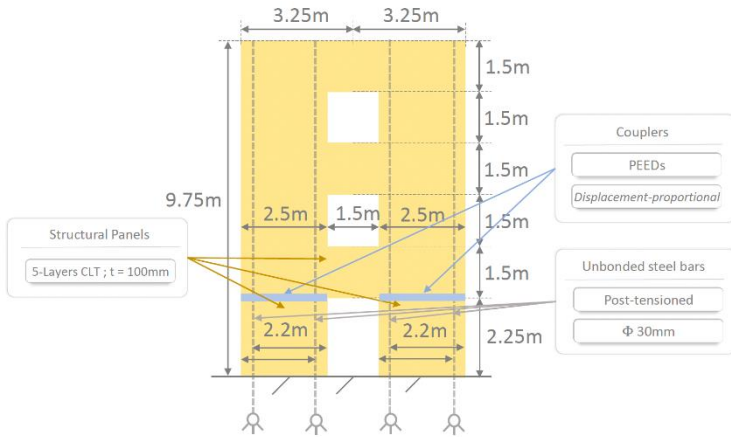


Figure 0.11 - Conceptual representation and synthetic description of the configuration G.

### 1. First performance point - Couplers yielding

When the first performance point is reached, yielding of the horizontal couplers occurs, thereby limiting the shear forces transferred from the overlaying structural portion. For the sake of simplicity, it is assumed that the base shear of the system is equal to the resisting shear offered by the PEEDs. In order to compare the dynamic behaviour of the alternative configurations, the same maximum elastic resistance is imposed to all of them:

$$F_{el,2} = F_{y,2} = F_{u,2} = 295.7\text{kN}$$

The resulting moment at the base of the timber panels is equal to:

$$M_{Ed} = F_{el,2} H \cong 295.7\text{kN} \cdot 3\text{m} = 887.1\text{kNm}$$

Assuming the sectional characteristics and post-tensioning load to be the same as defined for configuration A, the total resisting moment provided by the steel bars ( $M_{PT}$ ) and gravity loads ( $M_N$ ) is equal to:

$$M_{PT} + M_N = 1057\text{kNm} > M_{Ed} = 887.1\text{kNm}$$

Such a moment is sufficiently large as to inhibit rocking activation.

**H) Configuration H:** *CLT shear-walls with non-post-tensioned steel bars and horizontal couplers located between the structural panels of the ground and first floors ()*.

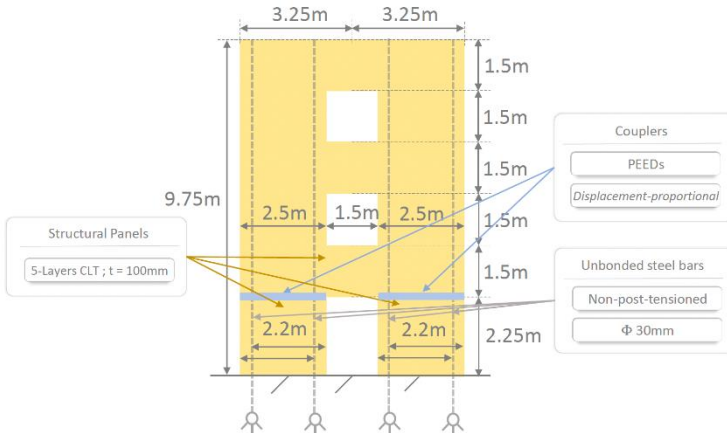


Figure 0.12 - Conceptual representation and synthetic description of the configuration H.

As for the previous cases, this configuration was created solely to evaluate the effect of post-tensioning load on

system response. This solution has the same geometry and properties as configuration G, with the exception that the vertical steel bars are devoid of post-tensioning.

## Appendix C

This appendix contains a description of the design process for the prototypes of Section 7.4.1 which were manufactured using structural steel [141].

### I. First specimen: welded steel plates in S275

The moment and shear resistance offered by the individual steel plate is calculated assuming that the plastic hinges are activated at its ends, close to the weld lines, and that the vertical extension of the elements is approximately 1.5 times their thickness, equal to 12mm ( ).

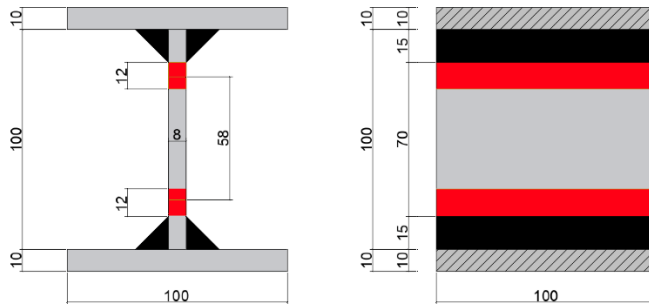


Figure 0.1 - Sectional view of the device, in which the steel sections are coloured in grey, the welds lines in black, and the plastic hinges in red.

It follows that the distance between the centres of the plastic hinges is about:

$$L_p = 58mm$$



The plate sections are bending class 1, so it can be assumed that they achieve complete yielding ().

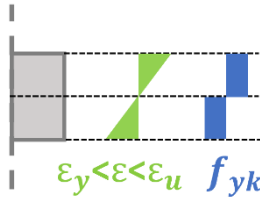


Figure 0.2 - Conceptual representation of the complete sectional yielding.

The following mechanical properties are considered for structural steel S275 elements less than 40 mm thick:

$$f_{yk} = 275\text{MPa} ; f_{tk} = 430\text{MPa} ; E_s = 210000\text{MPa}$$

The yielding moment ( $M_y$ ) provided by plastic hinges is computed using the steel's characteristic yield stress ( $f_{yk}$ ):

$$M_y = f_{yk} W_{el}$$

$$W_{el} = (L_s \frac{t_s}{2}) \frac{1}{2} \frac{2}{3} t = (100\text{mm} \frac{8\text{mm}}{2}) \frac{1}{2} \frac{2}{3} 8\text{mm} \cong 1066\text{mm}^2$$

$$\rightarrow M_y = 275\text{MPa} \cdot 1066 \text{ mm}^2 = \mathbf{0.293\text{kNm}}$$

The resulting yield shear resistance ( $V_y$ ) associated:

$$V_y = \frac{2 M_y}{l} ; l = \mathbf{70\text{mm}}$$

$$\rightarrow V_y = \frac{2 \cdot 0.293\text{kNm}}{70\text{mm}} \cong \mathbf{8.4\text{kN}}$$

The plastic moment ( $M_p$ ) provided by plastic hinges is computed using the steel's characteristic yield stress ( $f_{yk}$ ):

$$M_p = f_{yk} W_p$$

$$W_p = L_s \left(\frac{t_s}{2}\right)^2 = 100\text{mm} \left(\frac{8\text{mm}}{2}\right)^2 = 1600 \text{ mm}^2$$

$$\rightarrow M_p = 275\text{MPa} \cdot 1600 \text{ mm}^2 = \mathbf{0.44\text{kNm}}$$

The resulting plastic shear resistance ( $V_p$ ) associated:

$$V_p = \frac{2 M_p}{L_p} ; L_p = \mathbf{58\text{mm}}$$

$$\rightarrow V_p = \frac{2 \cdot 0.44\text{kNm}}{58\text{mm}} \cong \mathbf{15.2\text{kN}}$$

The ultimate moment ( $M_u$ ) provided by plastic hinges is computed using the steel's characteristic ultimate tensile stress ( $f_{tk}$ ):

$$M_u = f_{tk} W_p = 430\text{MPa} \cdot 1600 \text{ mm}^2 = \mathbf{0.688\text{kNm}}$$

The resulting plastic shear resistance ( $V_u$ ) associated:

$$V_u = \frac{2 M_u}{L_p} ; L_p = \mathbf{58\text{mm}}$$

$$\rightarrow V_u = \frac{2 \cdot 0.688\text{kNm}}{58\text{mm}} \cong \mathbf{23.7\text{kN}}$$

## II. Second specimen: welded steel plates in S355

This second configuration, referred to for simplicity as *configuration II*, present the same geometric properties as the previous configuration (*configuration I*) () except for the structural steel used, which is S355.

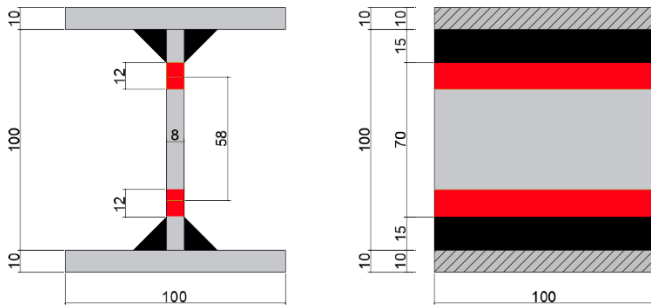


Figure 0.3 - Sectional view of the device, in which the steel sections are coloured in grey, the welds lines in black, and the plastic hinges in red.

The following mechanical properties are considered for structural steel S355 elements less than 40 mm thick:

$$f_{yk} = 355\text{MPa} ; f_{tk} = 510\text{MPa} ; E_s = 210000\text{MPa}$$

The yielding moment ( $M_y$ ) provided by plastic hinges is computed using the steel's characteristic yield stress ( $f_{yk}$ ):

$$M_y = f_{yk} W_{el}$$

$$W_{el} = \left( L_s \frac{t_s}{2} \right) \frac{1}{2} \frac{2}{3} t = \left( 100\text{mm} \frac{8\text{mm}}{2} \right) \frac{1}{2} \frac{2}{3} 8\text{mm} \cong 1066\text{mm}^2$$

$$\rightarrow M_y = 355\text{MPa} \cdot 1066 \text{ mm}^2 = \mathbf{0.378\text{kNm}}$$

The resulting yield shear resistance ( $V_y$ ) associated:

$$V_y = \frac{2 M_y}{l} ; l = 70mm$$

$$\rightarrow V_y = \frac{2 \cdot 0.378kNm}{70mm} \cong 10.8kN$$

The plastic moment ( $M_p$ ) provided by plastic hinges is computed using the steel's characteristic yield stress ( $f_{yk}$ ):

$$M_p = f_{yk} W_p$$

$$W_p = L_s \left(\frac{t_s}{2}\right)^2 = 100mm \left(\frac{8mm}{2}\right)^2 = 1600 mm^2$$

$$\rightarrow M_p = 355MPa \cdot 1600 mm^2 = 0.568kNm$$

The resulting plastic shear resistance ( $V_p$ ) associated:

$$V_p = \frac{2 M_p}{L_p} ; L_p = 58mm$$

$$\rightarrow V_p = \frac{2 \cdot 0.58kNm}{58mm} \cong 19.58kN$$

The ultimate moment ( $M_u$ ) provided by plastic hinges is computed using the steel's characteristic ultimate tensile stress ( $f_{tk}$ ):

$$M_u = f_{tk} W_p = 510MPa \cdot 1600 mm^2 = 0.816kNm$$

The resulting plastic shear resistance ( $V_u$ ) associated:

$$V_u = \frac{2 M_u}{L_p} ; L_p = 58mm$$

$$\rightarrow V_u = \frac{2 \cdot 0.816kNm}{58mm} \cong 28.1kN$$

The maximum stresses perpendicular to the weld line axis results in:

$$t_{\perp} = \frac{V_u}{2} \frac{1}{L_s H_W} = \frac{28.1kN}{2} \frac{1}{100mm \cdot 15mm} \cong 9.4MPa$$

$$n_{\perp} = \frac{M_u}{t} \frac{1}{L_s H_W} = \frac{0.816kNm}{8mm} \frac{1}{100mm \cdot 15mm} \cong 68MPa$$

$$\sqrt{n_{\perp}^2 + t_{\perp}^2} = \sqrt{9.4^2 MPa + 68^2 MPa} \cong 69MPa < 0.7 f_{yd}$$

$$|n_{\perp}| + |t_{\perp}| = 9.4 + 68 = 77.4MPa < 0.85 f_{yd}$$

### III. *Third specimen: welded steel plates in S275 with reduced sections showing sharp edges*

The moment and shear resistance offered by the individual steel plate is calculated assuming that the plastic hinges are activated in correspondence of the section reduced by the slits ().

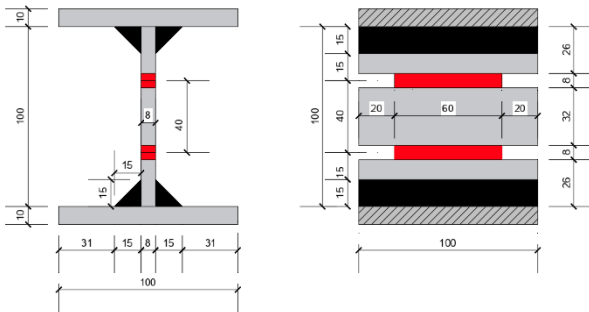


Figure 0.4 - Sectional view of the device, in which the steel sections are coloured in grey, the welds lines in black, and the plastic hinges in red.

It follows that the distance between the centres of the plastic hinges is about:

$$L_p = 40mm$$

The plate sections are bending class 1, so it can be assumed that they achieve complete yielding. The following mechanical

properties are considered for structural steel S275 elements less than 40 mm thick:

$$f_{yk} = 275\text{MPa} ; f_{tk} = 430\text{MPa} ; E_s = 210000\text{MPa}$$

The yielding moment ( $M_y$ ) provided by plastic hinges is computed using the steel's characteristic yield stress ( $f_{yk}$ ):

$$M_y = f_{yk} W_{el}$$

$$W_{el} = (L_s \frac{t_s}{2}) \frac{1}{2} \frac{2}{3} t = (60\text{mm} \frac{8\text{mm}}{2}) \frac{1}{2} \frac{2}{3} 8\text{mm} \cong 640\text{mm}^2$$

$$\rightarrow M_y = 275\text{MPa} \cdot 640\text{mm}^2 = \mathbf{0.176\text{kNm}}$$

The resulting yield shear resistance ( $V_y$ ) associated:

$$V_y = \frac{2 M_y}{l} ; l = \mathbf{48\text{mm}}$$

$$\rightarrow V_y = \frac{2 \cdot 0.176\text{kNm}}{48\text{mm}} \cong \mathbf{7.3\text{kN}}$$

The plastic moment ( $M_p$ ) provided by plastic hinges is computed using the steel's characteristic yield stress ( $f_{yk}$ ):

$$M_p = f_{yk} W_p$$

$$W_p = L_s (\frac{t_s}{2})^2 = 60\text{mm} (\frac{8\text{mm}}{2})^2 = 960 \text{mm}^2$$

$$\rightarrow M_p = 275\text{MPa} \cdot 960 \text{mm}^2 = \mathbf{0.264\text{kNm}}$$

The resulting plastic shear resistance ( $V_p$ ) associated:

$$V_p = \frac{2 M_p}{L_p} ; L_p = \mathbf{40\text{mm}}$$

$$\rightarrow V_p = \frac{2 \cdot 0.264\text{kNm}}{40\text{mm}} \cong \mathbf{13.2\text{kN}}$$

The ultimate moment ( $M_u$ ) provided by plastic hinges is computed using the steel's characteristic ultimate tensile stress ( $f_{tk}$ ):

$$M_u = f_{tk} W_p = 430\text{MPa } 960 \text{ mm}^2 = \mathbf{0.41\text{kNm}}$$

The resulting plastic shear resistance ( $V_u$ ) associated:

$$V_u = \frac{2 M_u}{L_p} ; L_p = \mathbf{40\text{mm}}$$

$$\rightarrow V_u = \frac{2 \cdot 0.41\text{kNm}}{40\text{mm}} \cong \mathbf{20.6\text{kN}}$$

The maximum stresses perpendicular to the weld line axis results in:

$$t_{\perp} = \frac{V_u}{2} \frac{1}{L_s H_W} = \frac{20.6\text{kN}}{2} \frac{1}{100\text{mm } 15\text{mm}} \cong \mathbf{6.9\text{MPa}}$$

$$n_{\perp} = \frac{M_u}{t} \frac{1}{L_s H_W} = \frac{0.41\text{kNm}}{8\text{mm}} \frac{1}{100\text{mm } 15\text{mm}} \cong \mathbf{35\text{MPa}}$$

$$\sqrt{n_{\perp}^2 + t_{\perp}^2} = \sqrt{6.9^2\text{MPa} + 35^2\text{MPa}} \cong \mathbf{36\text{MPa} < 0.7 f_{yd}}$$

$$|n_{\perp}| + |t_{\perp}| = 6.9 + 35 = \mathbf{42\text{MPa} < 0.85 f_{yd}}$$

#### IV. Fourth specimen: welded steel plates in S355 with reduced sections showing rounded edges

The fourth configuration was derived from the second (*configuration II*) by introducing slits with rounded edges ( ) that reduce the resistant sections by localising the activation of plastic hinges.

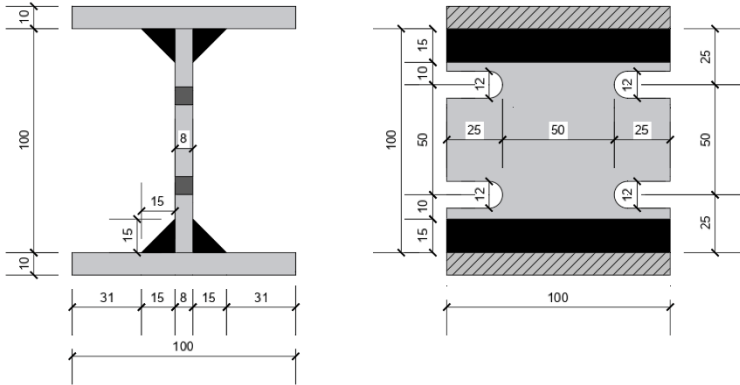


Figure 0.5 - On the left-side: sectional view of the device, in which the steel sections are coloured in grey and the welds in black. On the right-side: side view of the device.

It follows that the distance between the centres of the plastic hinges is about:

$$L_p = 50mm$$

The plate sections are bending class 1, so it can be assumed that they achieve complete yielding. The following mechanical properties are considered for structural steel S275 elements less than 40 mm thick:

$$f_{yk} = 355MPa ; f_{tk} = 510MPa ; E_s = 210000MPa$$

The yielding moment ( $M_y$ ) provided by plastic hinges is computed using the steel's characteristic yield stress ( $f_{yk}$ ):



$$M_y = f_{yk} W_{el}$$

$$W_{el} = \left( L_s \frac{t_s}{2} \right) \frac{1}{2} \frac{2}{3} t = \left( 50\text{mm} \frac{8\text{mm}}{2} \right) \frac{1}{2} \frac{2}{3} 8\text{mm} \cong 533\text{mm}^2$$

$$\rightarrow M_y = 355\text{MPa} \cdot 533\text{mm}^2 = \mathbf{0.189\text{kNm}}$$

The resulting yield shear resistance ( $V_y$ ) associated:

$$V_y = \frac{2 M_y}{l} ; l = \mathbf{50\text{mm}}$$

$$\rightarrow V_y = \frac{2 \cdot 0.189\text{kNm}}{50\text{mm}} \cong \mathbf{7.6\text{kN}}$$

The plastic moment ( $M_p$ ) provided by plastic hinges is computed using the steel's characteristic yield stress ( $f_{yk}$ ):

$$M_p = f_{yk} W_p$$

$$W_p = L_s \left( \frac{t_s}{2} \right)^2 = 50\text{mm} \left( \frac{8\text{mm}}{2} \right)^2 = 800 \text{mm}^2$$

$$\rightarrow M_p = 355\text{MPa} \cdot 800 \text{mm}^2 = \mathbf{0.284\text{kNm}}$$

The resulting plastic shear resistance ( $V_p$ ) associated:

$$V_p = \frac{2 M_p}{L_p} ; L_p = \mathbf{50\text{mm}}$$

$$\rightarrow V_p = \frac{2 \cdot 0.284\text{kNm}}{50\text{mm}} \cong \mathbf{11.4\text{kN}}$$

The ultimate moment ( $M_u$ ) provided by plastic hinges is computed using the steel's characteristic ultimate tensile stress ( $f_{tk}$ ):

$$M_u = f_{tk} W_p = 510\text{MPa} \cdot 800 \text{mm}^2 = \mathbf{0.408\text{kNm}}$$

The resulting plastic shear resistance ( $V_u$ ) associated:

$$V_u = \frac{2 M_u}{L_p} ; L_p = 50mm$$

$$\rightarrow V_u = \frac{2 \cdot 0.408kNm}{50mm} \cong 16.3kN$$

The maximum stresses perpendicular to the weld line axis results in:

$$t_{\perp} = \frac{V_u}{2} \frac{1}{L_s H_W} = \frac{16.3kN}{2} \frac{1}{100mm \cdot 15mm} \cong 5.5MPa$$

$$n_{\perp} = \frac{M_u}{t} \frac{1}{L_s H_W} = \frac{0.408kN}{8mm} \frac{1}{100mm \cdot 15mm} \cong 34MPa$$

$$\sqrt{n_{\perp}^2 + t_{\perp}^2} = \sqrt{5.5^2 MPa + 34^2 MPa} \cong 35MPa < 0.7 f_{yd}$$

$$|n_{\perp}| + |t_{\perp}| = 5.5 + 34 = 39.5MPa < 0.85 f_{yd}$$

**V. Fifth specimen: device consisting of H-beam sections made of S355 structural steel**

The moment and shear resistance offered by the individual steel web is calculated assuming that the plastic hinges are activated at its ends, close to the root radius sections, and that the vertical extension of the elements is approximately 1.5 times their thickness, equal to 9mm ( ).

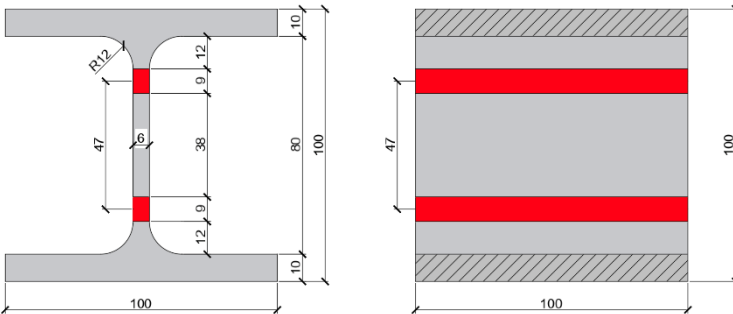


Figure 0.6 - Sectional view of the device, in which the steel sections are coloured in grey, the welds lines in black, and the plastic hinges in red.

It follows that the distance between the centres of the plastic hinges is about:

$$L_p = 47mm$$

The plate sections are bending class 1, so it can be assumed that they achieve complete yielding.

In contrast to other configurations that refer to normative requirements for the definition of resistant stresses, it was decided for this one to use the mechanical properties defined by the direct tensile test of a dog-bone shaped specimen from the web of the HEB100 beam with which the prototype specimen tested in the laboratory was made ( ).

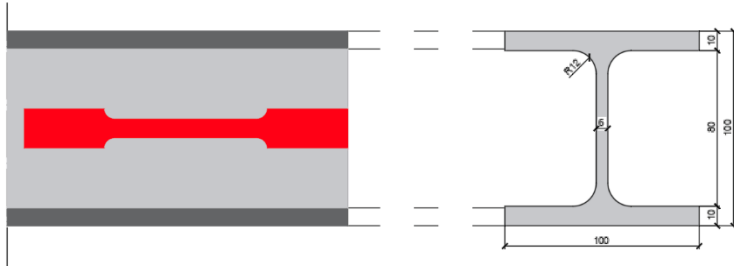


Figure 0.7 – Position of the dog-bone shaped specimen from the web of the HEB100.

The following mechanical properties obtained from the experimental test are considered for this configuration:

$$f_y = 390.5\text{MPa} ; f_t = 550\text{MPa} ; E_s = 210000\text{MPa}$$

The yielding moment ( $M_y$ ) provided by plastic hinges is computed using the experimental steel's yield stress ( $f_y$ ):

$$M_y = f_y W_{el}$$

$$W_{el} = \left( L_s \frac{t_s}{2} \right) \frac{1}{2} \frac{2}{3} t = \left( 100\text{mm} \frac{6\text{mm}}{2} \right) \frac{1}{2} \frac{2}{3} 6\text{mm} \cong 600 \text{ mm}^2$$

$$\rightarrow M_y = 390.5\text{MPa} \cdot 600\text{mm}^2 = \mathbf{0.234\text{kNm}}$$

The resulting yield shear resistance ( $V_y$ ) associated:

$$V_y = \frac{2 M_y}{l} ; l = \mathbf{56\text{mm}}$$

$$\rightarrow V_y = \frac{2 \cdot 0.234\text{kNm}}{56\text{mm}} \cong \mathbf{8.4\text{kN}}$$

The plastic moment ( $M_p$ ) provided by plastic hinges is computed using the real steel's yield stress ( $f_y$ ):

$$M_p = f_y W_p$$

Stefano Cademartori

$$\mathbf{W_p} = L_s \left(\frac{t_s}{2}\right)^2 = 100\text{mm} \left(\frac{6\text{mm}}{2}\right)^2 = 900 \text{ mm}^2$$

$$\rightarrow \mathbf{M_p} = 390.5\text{MPa} \cdot 900 \text{ mm}^2 = \mathbf{0.35\text{kNm}}$$

The resulting plastic shear resistance ( $V_p$ ) associated:

$$\mathbf{V_p} = \frac{2 M_p}{L_p} ; L_p = \mathbf{47\text{mm}}$$

$$\rightarrow \mathbf{V_p} = \frac{2 \cdot 0.35\text{kNm}}{47\text{mm}} \cong \mathbf{14.95\text{kN}}$$

The ultimate moment ( $M_u$ ) provided by plastic hinges is computed using the real steel's ultimate tensile stress ( $f_t$ ):

$$\mathbf{M_u} = f_t \mathbf{W_p} = 550\text{MPa} \cdot 900 \text{ mm}^2 = \mathbf{0.495\text{kNm}}$$

The resulting plastic shear resistance ( $V_u$ ) associated:

$$\mathbf{V_u} = \frac{2 M_u}{L_p} ; L_p = \mathbf{47\text{mm}}$$

$$\rightarrow \mathbf{V_u} = \frac{2 \cdot 0.495\text{kNm}}{47\text{mm}} \cong \mathbf{21\text{kN}}$$

## Appendix D

### - *Structural connection between RC cladding panels and frame*

The cladding panels were conceived as non-structural elements, but they can significantly affect the seismic response of the structure, both in terms of resistance and displacement capacity. Furthermore, the failure of the structural connections between these elements and the resulting collapse or out-of-plane overturning represents a vulnerability for the building that cannot be ignored. For this reason, the connections between these elements at their various levels were investigated. These connections were studied based on the available construction documents, as well as on the findings of the on-site inspections and the scientific literature related to the connections for prefabricated infill panels [240].

Each vertical panel is supported by four connections, two at the intermediate level and two at the roof level; these connections consist of an anchor steel channel profile arranged horizontally on the beams or on the corbels of the columns, another steel channel profile arranged vertically on the internal side of the infill panel, a bayonet arranged horizontally with the head inserted into the panel's channel profile and the opposite end fixed by a bolt to the other steel profile (**Figure VIII.10**).

Although all the connections are of the same type, it has been observed that their length and stiffness vary depending on the structural element to which they are linked; therefore, three types of connections have been distinguished, and their stiffness and strength have been calculated ().

Table 8 - Rc-frame-to-cladding panel connection resistance ( $V$ ) and elastic rotational stiffnesses ( $K$ ), calculated according to [240].

| Connection Type                                  | Length [cm] | $K_{\theta 1}$ [kNm] | $K_{\theta 2}$ [kNm] | $K_c$ [kN/mm] | $V_u=(M_1+M_2)/L$ [kN] | $V_{Rd}$ [kN] |
|--|-------------|----------------------|----------------------|---------------|------------------------|---------------|
| 1 - Cladding panels - Intermediate RC beams      | 2           | 1800.75              | 41.14                | 1676.8        | 20.9                   | 7.3           |
| 2 - Cladding panels - Roof-level RC beams        | 14          | 257.25               | 17.65                | 5.81          | 3.0                    | 7.3           |
| 3- Cladding panels – Intermediate column corbels | 12          | 300.13               | 20.60                | 9.23          | 3.5                    | 7.3           |

In the numerical models, these connections are represented as nonlinear general-links. For each connection type, the elastic stiffness of the link in the horizontal direction parallel to the plane of the panels was computed, as well as the shear resistance offered by the connection, i.e. the force that causes the channel profile failure and the bayonet to fall out.

For *type 1* connection, it has been observed that the resistant shear  $V_{Rd}$  is less than the ultimate shear that can be activated by a flexural mechanism  $V_u = (M_1+M_2) / L$ ; consequently, an elasto-fragile () type connection with ultimate resistance equal to  $V_{Rd}$  is implemented.

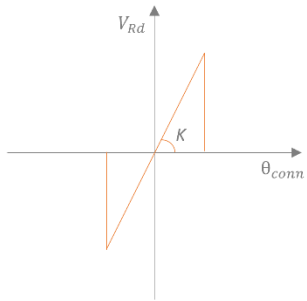


Figure 0.1 - Elasto-fragile model for type 1 connections.

For *type 2* and *3* connections, however,  $V_{Rd}$  is greater than  $V_u$ , so an elasto-plastic model ( $\square$ ), associated with the bayonets, is implemented with ultimate resistance equal to  $V_u$ .

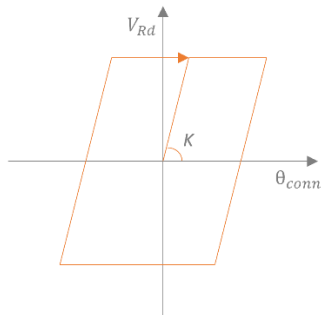


Figure 0.2 - Elasto-plastic model for type 2 and 3 connections



- *Numerical model of the retrofitted building*

Below is a description of the additional elements introduced into the numerical model, *mesh C* (), of the retrofitted building.

*Structural elements of the existing building:*

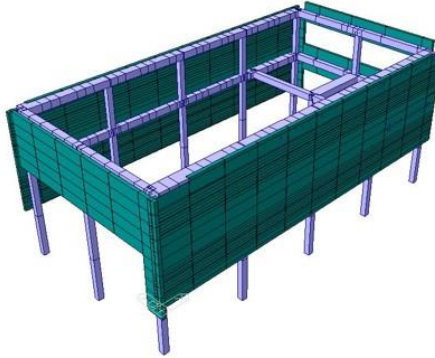


Figure 0.3 - 3D representation of the numerical model of the pre-existing building, mesh C, extracted from the software, in which the RC frame is shown in grey and the vertical cladding panels in green. From [15].

- *Intermediate RC slab*: this element was modelled with elastic plate elements to simulate its in-plane stiffness, which is provided by the cast-in-place structural section. Its own weight and the loads bearing on it were evenly distributed across the beams present.
- *Precast RC cladding panels*: modelled as one-dimension beam-elements and connected to the building through rigid links to avoid their out-of-plane overturning, and non-linear general-link to simulate the influence of the existing connections between panels and beams/columns as well as the new dowel connections. These panels are only supported on the 12cm thick layer above the existing RC foundation

curbs; their rocking behaviour and shear-sliding kinematics are simulated by the series of rigid-plastic vertical general-links placed at their base ( ) at intervals of 4cm with an axial resistance of 48kN each, adopting the same modelling principles applied in the Chapter VI.



Figure 0.4 - FEM modelling to simulate the rocking and sliding shear behaviour at the base of precast panels using general-links.

- RC foundation pockets are modelled as interlocks at the base of the pillars, placed 3m below the ground level to simplify the representation of their deformability.

### ***Structural elements of the AdESA shell exoskeleton:***

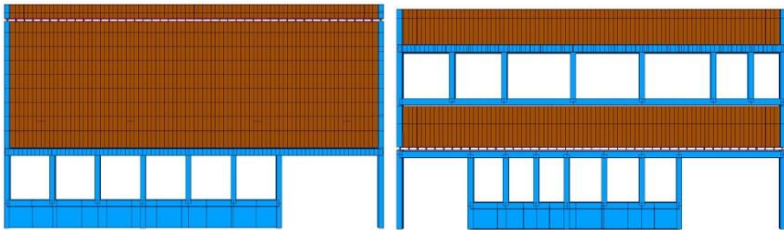


Figure 0.5 - On the left-side: view of the hybrid retrofitting wall of the northern façade. On the right-side: view of the hybrid retrofitting wall of the southern façade. In which the steel frames are shown in blue and the CLT panels in brown. From [15].

- *S355 steel frames*: these elements were modelled as elastic 1-dimension beam-elements in order to record the resistance demand and elastic deformations induced by seismic events.

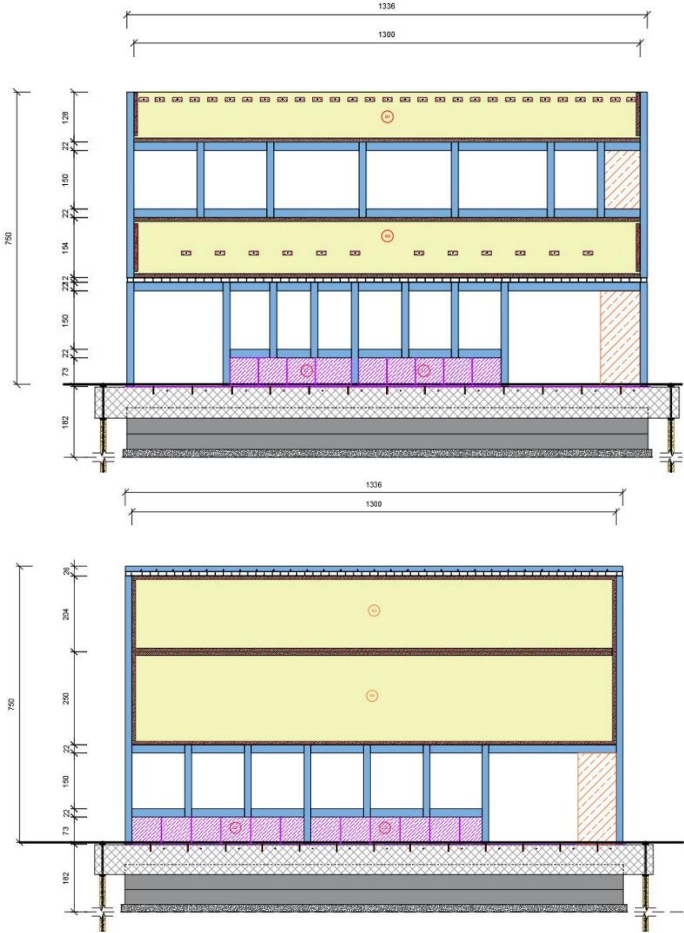


Figure 0.6 - On the top: Representation of the hybrid north wall. On the bottom: Representation of the hybrid south wall. In which steel frames are shown in blue, purple for the base steel plate, and CLT panels in yellow. From [15].

- *CLT panels*: modelled as elastic 2-dimensions plate-elements with the dimensions and stiffnesses of the timber panels. These horizontally arranged panels present commercial dimensions of approximately 13m in length and variable width, up to a maximum of 2.5m. These panels present the same mechanical properties of the structural CLT panels used to dimensioning the case study models examined in the Paragraph 6.5.3, reported in . The main mechanical characteristics are listed below.

Design compression resistance ( $f_{cd,CLT}$ ):

$$f_{cd,CLT} = f_{c,0,k} \frac{K_{mod}}{\gamma_{M0}} \frac{60mm}{100mm} \frac{1}{\gamma_{Rd}} = 21MPa \frac{1.1}{1.45} \frac{60mm}{100mm} \frac{1}{1.1}$$

$$f_{cd,CLT} \cong \mathbf{8.69MPa}$$

Design shear strength ( $f_{vd,CLT}$ ):

$$f_{vd,CLT} = 2.5MPa \frac{K_{mod}}{\gamma_{M0}} = 2.5MPa \frac{1.1}{1.45} = \mathbf{1.9MPa}$$

Out-of-plane bending resistance ( $M_{Rd,CLT}$ ):

$$M_{Rd,CLT} = \frac{f_{md}}{J_{eff}} \frac{t_{CLT}}{2} = \frac{18.2MPa}{6.6 \cdot 10^7 mm^4} \frac{100mm}{2} = \mathbf{24 KNm /m}$$

where:

- $f_{md}$  is the design bending strength of the CLT panels.

$$f_{md} = f_{mk} \frac{K_{mod}}{\gamma_{M0}} = 24MPa \frac{1.1}{1.45} = \mathbf{18.2MPa}$$

- $J_{eff}$  is the rotational inertia of the effective section considering 1m-wide panel.

$$J_{\text{eff}} = 6.6 \cdot 10^7 \text{ mm}^4$$

- $t_{\text{CLT}} / 2$  corresponds to half the thickness of the panel.

$$\frac{t_{\text{CLT}}}{2} = \frac{100\text{mm}}{2} = 50\text{mm}$$

- *AdESA fuses*: modelled as S275 steel plates with a bilinear elasto-plastic hysteretic model ().

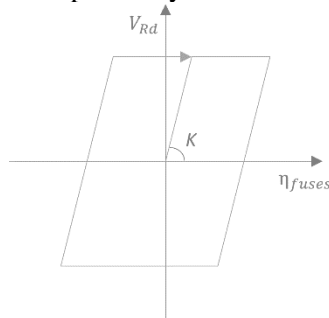


Figure 0.7 - Elasto-plastic model for AdESA fuses.

The elastic stiffness of the 100x100x10mm steel plates is self-calculated by the software based on the end constraints and the mechanical and sectional characteristics of the elements, while that of the second section is close to zero; the flexural resistance  $M_{Rd}$  is 0.42 kNm and a shear resistance  $V_{Rd}$  of about 15kN.

- *New RC curbs*: modelled using elastic beam elements with the sectional and mechanical characteristics of the reinforced concrete element (C25/30), 30x80cm. The end drilled piles were modelled as fixed restraints in the vertical direction, while the metal dowels  $\Phi 22/80\text{cm}$  connecting the new foundations with the existing

foundations were modelled as elastic-links with a stiffness of 72.7kN/mm.

- *Steel connections* between hybrid wall-roof diaphragm, between cladding hybrid wall-intermediate slab and between hybrid wall-RC foundation: structural connections made of steel dowels, represented by elastic links with calibrated stiffness based on the number of connections, in order to define the resistance demand induced by the earthquake, subsequently compared with their shear-resistance and elastic stiffness were defined according to the formulation reported in the scientific literature [124]. The connections between hybrid walls-roof diaphragm are comprised of dowels  $\Phi 22/38\text{cm}$  made of S355 steel, with a design shear resistance of 21.3kN and a stiffness of 12.7kN/mm, while the connections with the existing foundation,  $\Phi 22/85\text{cm}$  made of S355 steel, with a resistance of 48.1kN. The S355 steel dowels connecting the additional retrofit wall with the intermediate slab,  $\Phi 22/50\text{cm}$ , exhibit a shear-resistance of 21.2kN and a stiffness of 17kN/mm.
- *Mechanical coupling elements*: These elements placed along the longitudinal facades, made of S355 steel, were modelled by introducing general links between adjacent cladding panels and the (8+8)  $\Phi 20$  dowels made of S355 steel ( $\cdot$ ). The strength and stiffness of the dowels are designed to serve as the *weakest link* in the mechanical connection. When their maximum resistant shear is reached, for seismic events with an intensity greater than the predetermined threshold, these ductile elements yield, permitting the relative sliding of the

adjacent panels and the activation of the rocking behavior, while maintaining the remaining components in the elastic range.

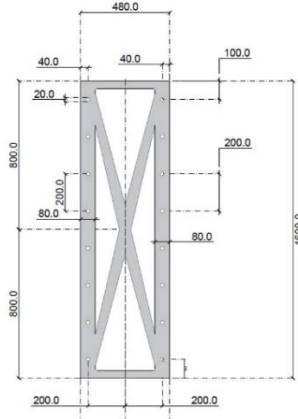


Figure 0.8 - representation of the mechanical coupling elements. From [15].

These structural connections, defined in terms of strength and stiffness using a bilinear elasto-plastic hysteretic model ( $\bullet$ ), were calibrated according to the properties of the steel dowels and the connected layers.

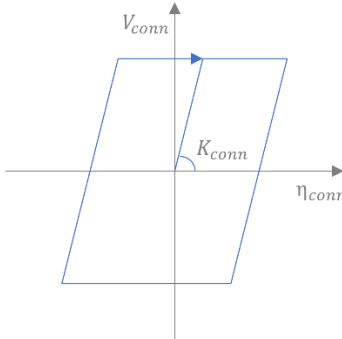


Figure 0.9 - bilinear elasto-plastic hysteretic model of the general-links introduced to simulate the new mechanical coupling connections between adjacent cladding panels and the steel dowels.

The design shear resistance ( $V_{conn}$ ) of each row of dowels were defined equal to 130kN, while the elastic stiffness ( $K_{conn}$ ) equal to 123.4kN/mm.

- *Steel connections* between vertical cladding panels-roof diaphragm, between cladding panels-foundation and between vertical panels-intermediate slab: these connections, made of steel dowels, are represented by elastic links with calibrated stiffness based on the number of the adopted connections, in order to define the resistance demand induced by the earthquake. Their shear-resistance and elastic stiffness were defined according to the formulation reported in the scientific literature [124].

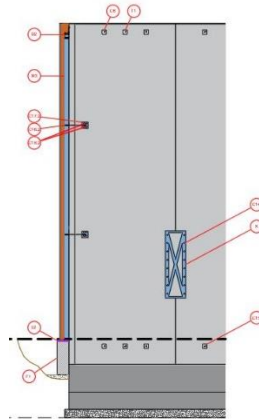


Figure 0.10 - Detail of longitudinal elevations. From [15].

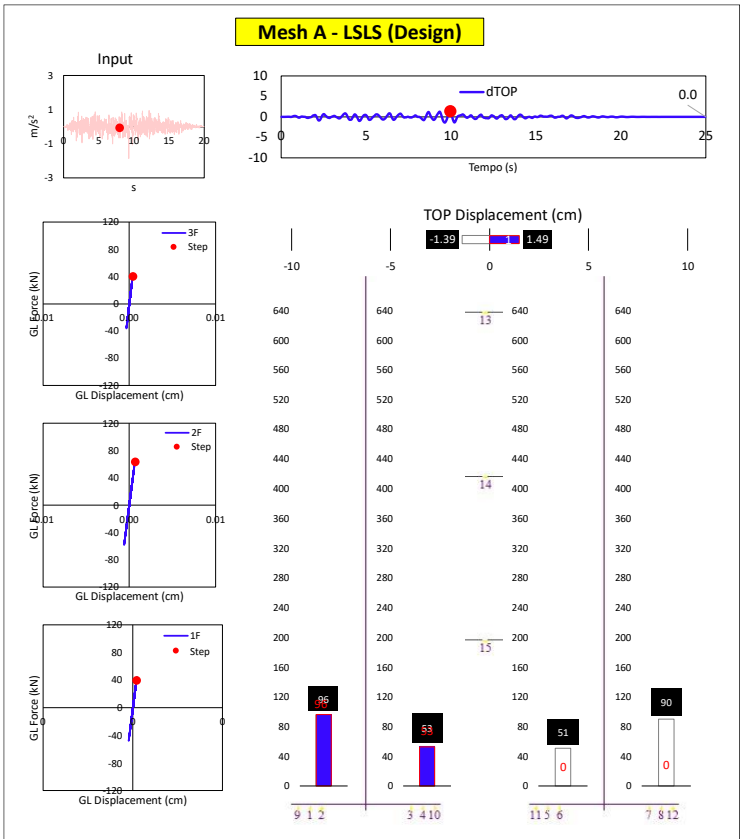
The connections between cladding panels-roof diaphragm are made of 2 dowels  $\Phi 20$  made of S355 steel, with a design shear resistance of 39.7kN and a stiffness of 444kN/mm, while the connections with the existing foundation, 3 dowels  $\Phi 22$  made of S355 steel,



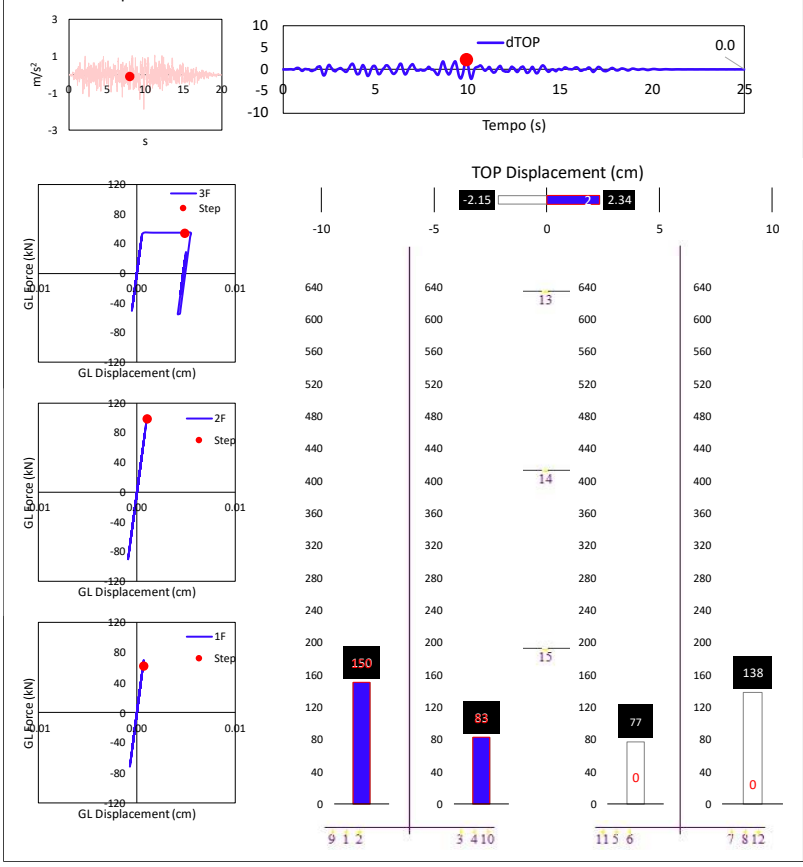
with a resistance of 48.1kN and a stiffness of 548kN/mm. The 26 steel dowels connecting the external panels with the intermediate slab, made of S355 steel  $\Phi 20$  bars, exhibit a shear-resistance of 24.5kN and a stiffness of 72kN/mm.

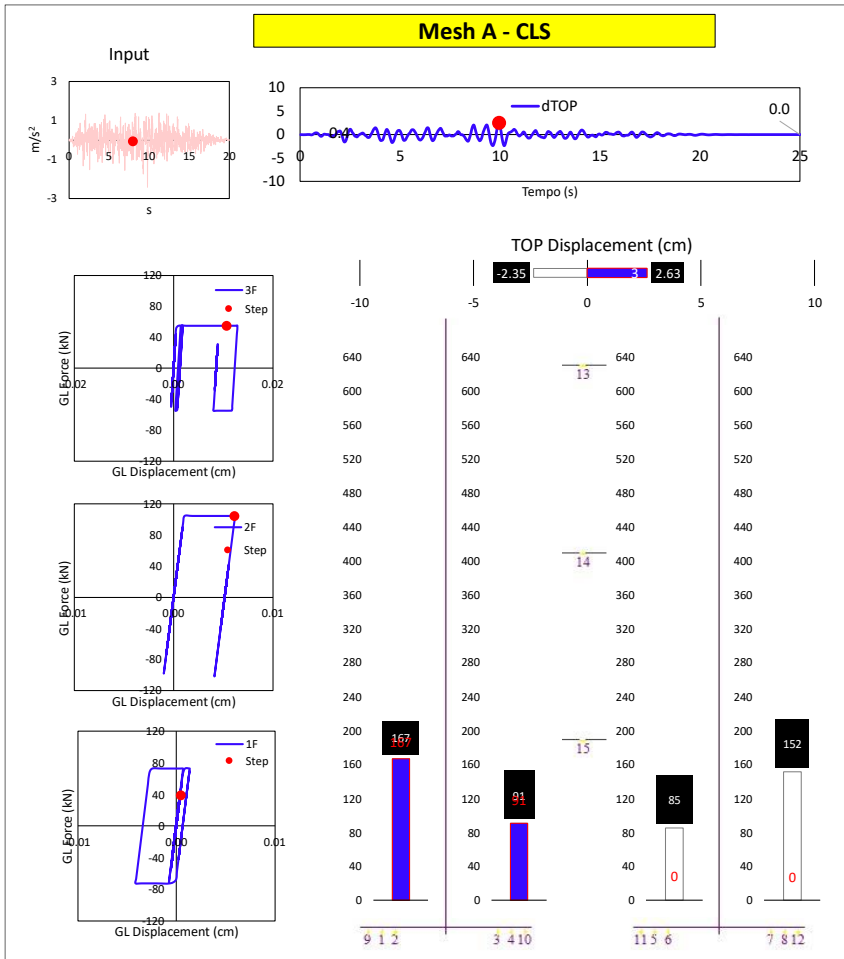
## Appendix E

Example of some significant cases. Relevant parameters of the analysed cases at the step in which the maximum top displacement was experienced. The step of the analysis is marked with a red dot. At the top, on the left, the seismic input and on the right the top displacement over time are presented; the residual displacement is indicated. On the left the force-displacement curves of the *general links* introduced to model the couplers are reported. On the right the top displacement and the forces in the bars are plotted; in the blue bars, the values refer to the considered step, while in the grey bars, the maximum value is plotted.

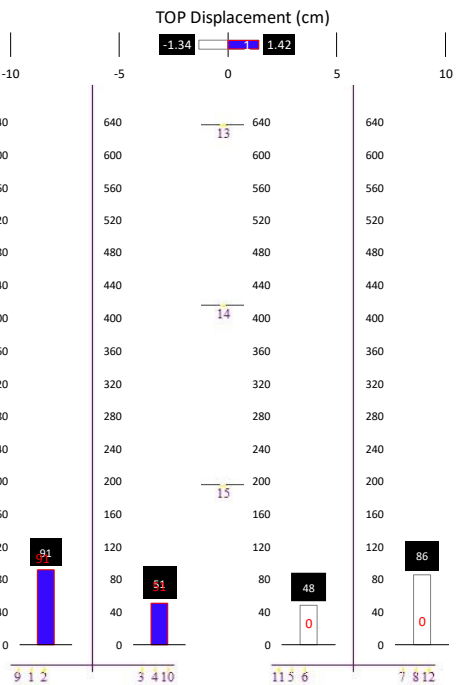
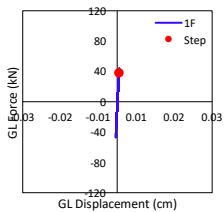
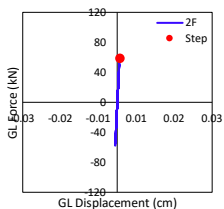
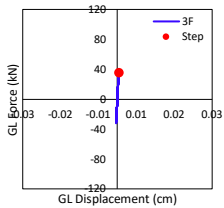
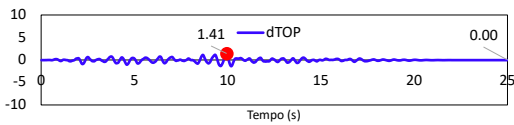
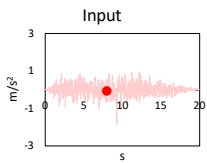


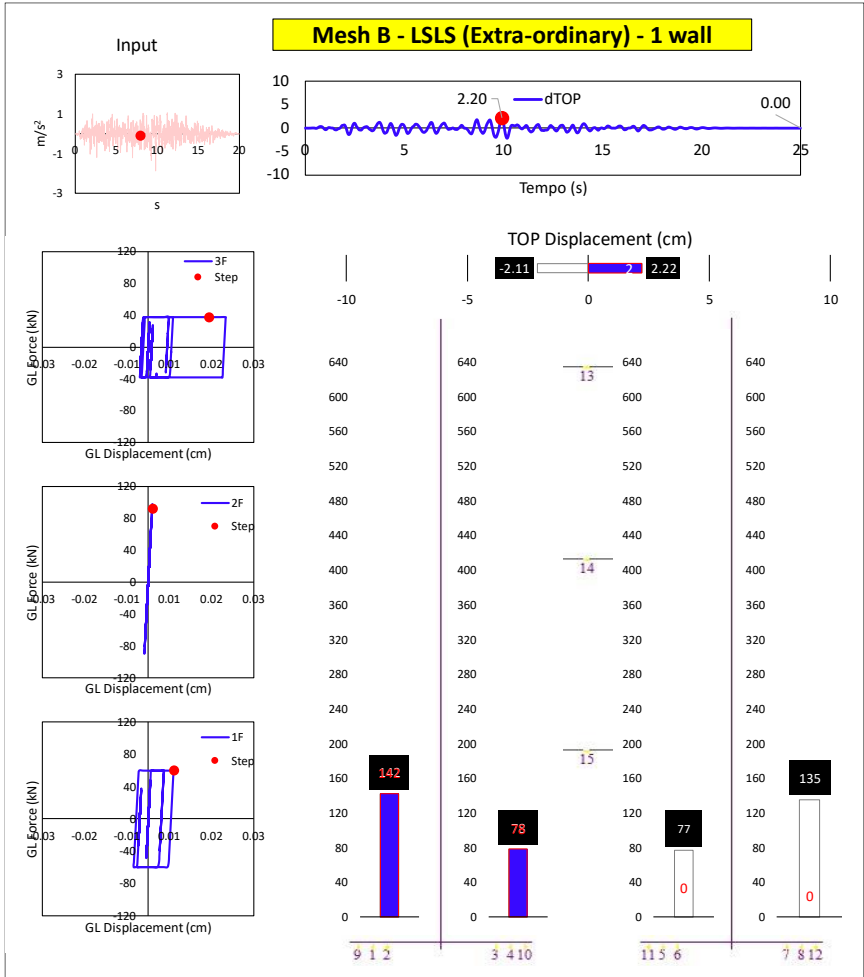
**Mesh A - LSLS (Extra-ordinary)**





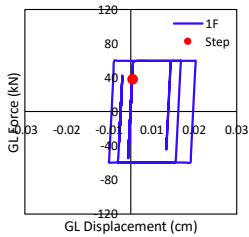
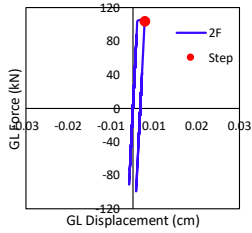
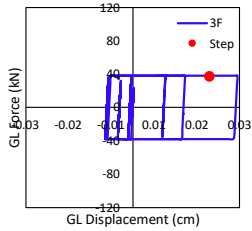
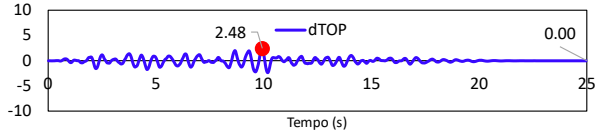
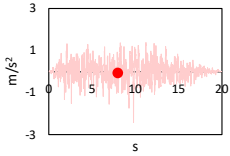
**Mesh B - LSL (Design) - 1 wall**



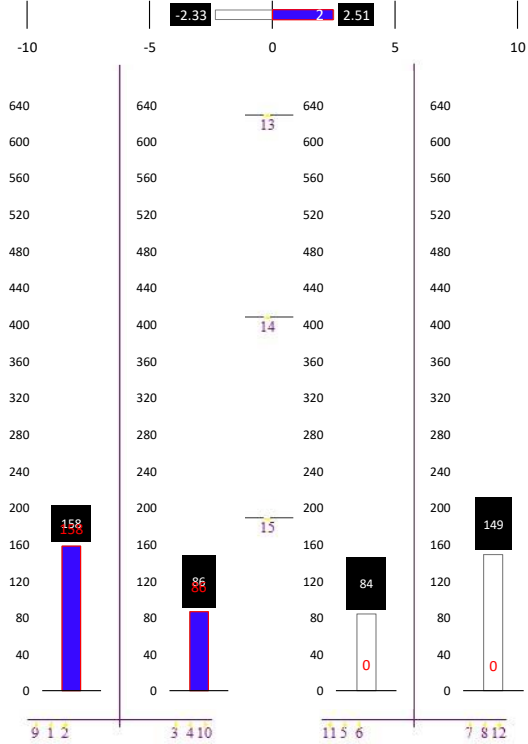


## Mesh B - CLS - 1 wall

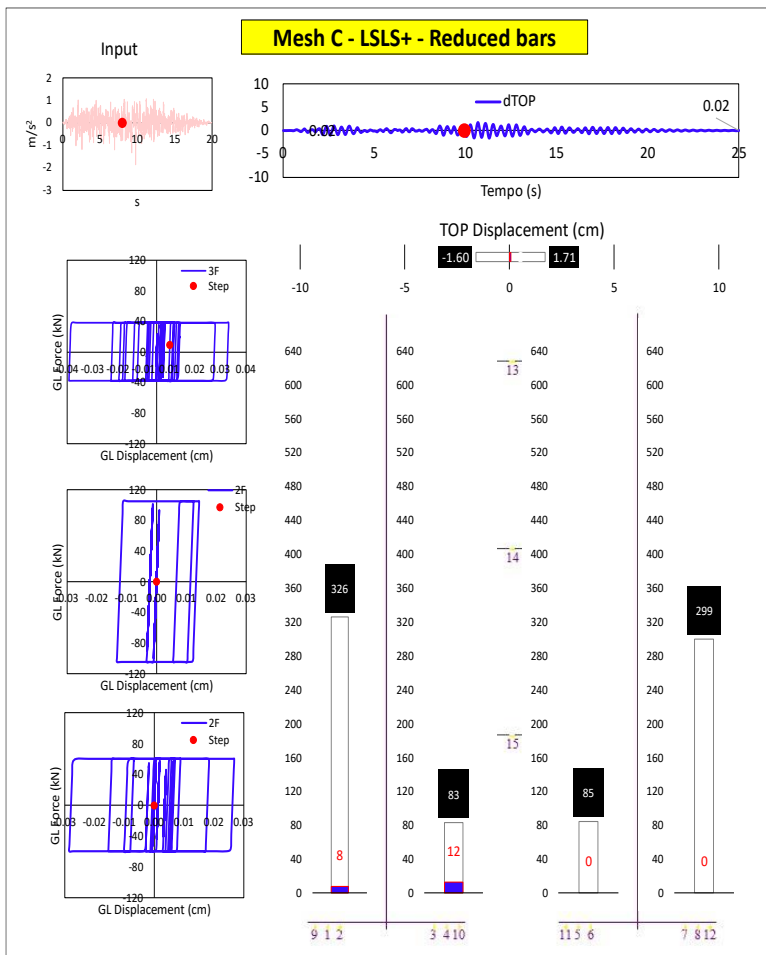
Input



TOP Displacement (cm)





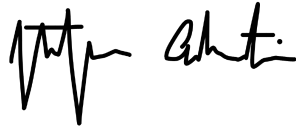


## *Acknowledgements*

My special thanks go to my supervisor Prof. Alessandra Marini and co-supervisor Eng. Simone Labò for their crucial role in the realization of this work. I would also like to thank the Structural Engineering research group at the University of Bergamo for their support and the many lessons they have taught me over the years.

Prof. Ezio Giuriani, an important inspiration both from a professional and human perspective, deserves special thanks.

Finally, I would like to extend a grateful and heartfelt thank you to my family, who has always supported me without reservation.  
*Thank you very much.*

A handwritten signature in black ink, consisting of two distinct parts. The first part is a stylized, somewhat abstract scribble of lines, and the second part is a more legible, cursive signature that appears to be 'A. Marini'.